

**In Vivo Studies of Normal and Abnormal Development
of the Anterior Chamber of Children Eye using Hand-
held Spectral Domain Optical Coherence Tomography**

Thesis submitted for the degree of

Doctor of Philosophy

at the University of Leicester

By

Budor S A Edawaji MBChB, MSc

Department of Cardiovascular Sciences

Ulverscroft Eye Unit

University of Leicester

January 2019

Abstract

In Vivo Studies of Normal and Abnormal Development of the Anterior Chamber of Children Eye using Hand-held Spectral Domain Optical Coherence Tomography

Budor S A Edawaji

Background: In-vivo postnatal normative development of the anterior chamber of the eye of children has not been investigated. The availability of a portable hand-held non-invasive optical coherence tomography (HH-OCT) can facilitate such investigations. However, HH-OCT application in imaging the anterior chamber has not been optimised and validated for imaging the anterior chamber of the eye. This study aims to test the feasibility and reproducibility of HH-OCT for imaging the anterior chamber and investigates the normal and abnormal postnatal development of the anterior chamber of children.

Methods: HH-OCT was used for imaging the anterior chamber of healthy children and children with congenital glaucoma, prematurity, nystagmus and anterior segment abnormalities. HH-OCT feasibility and reproducibility were tested in healthy children and children with nystagmus and congenital glaucoma < 6 years of age. The normal development of anterior chamber was investigated in 265 children. The abnormal development of the anterior chamber of children with congenital glaucoma and prematurity was compared to age-matched controls.

Results: We showed that HH-OCT has 89% feasibility, excellent repeatability and reproducibility in imaging the anterior chamber of children with ICC of > 0.9 for anterior chamber angle width measurements. We found that normal development of the anterior chamber is non-linear and occurs rapidly during the first year of age and reaches maturity by the age of 5 years. This study showed that females have smaller anterior chamber measurements compared to males and an association of anterior chamber development to the myopic shift during emmetropisation.

Children with congenital glaucoma had significantly wider anterior chamber angle and greater anterior chamber width compared to age-matched controls. Premature born children had delayed development of anterior chamber compared to age-matched controls. HH-OCT is a useful method for assessing the anterior chamber of children with anterior segment abnormalities.

Conclusions: This thesis presents in-vivo measurements of the anterior chamber of healthy children and children with anterior chamber pathology using HH-OCT, for the first time, with excellent feasibility and repeatability. HH-OCT is a useful method for evaluating the development of anterior chamber of children.

Acknowledgements

I am grateful to the God for the good health and wellbeing that were necessary to complete this thesis (Alhamdulillah).

I would like to offer my special thanks to my great supervisors, Prof Irene Gottlob and Dr Frank Proudlock for giving me the opportunity to fulfil my dream in completing a PhD study. I have been through so many obstacles that made me think that my dream would never be true. However, here I am, in the final stage writing my acknowledgements.

Prof Gottlob was a wonderful supervisor who has encouraged and supported me to improve and show my research abilities and talents. Dr Proudlock has been so kind to share his knowledges in data analysis and statistical programming. I learnt from him many valuable skills.

I would like to express my very great appreciation to the wonderful team of the Ulverscroft Eye Unit, at University of Leicester for their assistance in data collection including the recruitment of participants, technical support and friendly advice. I would like to thank Miss Sonal Shah for her help with data analysis.

My special thanks are extended to the children and their parents who took part in my studies. This thesis would not have been possible without their help.

I am grateful for the assistance given by my husband Faraj, who was a wonderful supporter. I am particularly grateful to my little kids (Mohamed and Taqwa) for being in my life and supporting me spiritually. Last but not the least, I would like to thank my family for supporting me in my life in general.

Table of Contents

<i>Abstract</i>	<i>i</i>
<i>Acknowledgements</i>	<i>ii</i>
<i>Table of Contents</i>	<i>iii</i>
<i>List of Tables</i>	<i>xii</i>
<i>List of Figures</i>	<i>xvi</i>
<i>Abbreviations</i>	<i>xxi</i>
<i>Overview of the thesis</i>	<i>1</i>
1. <i>Chapter one: Introduction and literature reviews</i>	<i>3</i>
1.1 <i>Anatomy and development of anterior segment of the eye</i>	<i>3</i>
1.1.1 Anatomy of anterior segment of the eye.....	<i>3</i>
1.1.2 Normal development of anterior chamber.....	<i>9</i>
1.1.3 Abnormal development of anterior chamber.....	<i>13</i>
1.1.4 Congenital ocular diseases.....	<i>17</i>
1.1.5 Nystagmus.....	<i>22</i>
1.1.6 Ocular diseases associated with prematurity:	<i>23</i>
1.2 <i>Imaging of the eye by optical coherence tomography (OCT)</i>	<i>24</i>
1.2.1 Technology of optical coherence tomography	<i>25</i>
1.2.2 Types of optical coherence tomography (OCT)	<i>25</i>

1.2.3	Development and history of optical coherence tomography	27
1.2.4	Hand-held spectral domain optical coherence tomography (HH-OCT)	30
1.2.5	Anterior segment optical coherence tomography (AS-OCT)	31
1.3	Literature review of the application of anterior segment OCT	34
1.3.1	Application of OCT in visualising the cornea.....	34
1.3.2	Application of AS-OCT in measurements of the anterior chamber	38
1.3.3	The impact of accommodation and illumination on anterior chamber measurements....	58
1.4	Gaps in the research literature	60
1.4.1	Aims of the thesis.....	61
1.4.2	Outline of chapters covering the main aims	62
2.	<i>Chapter two: General methods.....</i>	63
2.1	Ethical approval	63
2.2	Study design	63
2.3	Recruitment of participants.....	64
2.3.1	Healthy participants.....	64
2.3.2	Premature born children.....	64
2.3.3	Participants with ocular pathology	65
2.4	Steps in data collection	67
2.4.1	Medical History	67
2.4.2	Clinical examination	67

2.5 Imaging of anterior segment using HH-OCT.....	72
2.5.1 Acquisition of anterior segment image using HH-OCT.....	72
2.5.2 Optimising the HH OCT protocol for imaging the anterior segment of the eye	75
2.5.3 Optimisation of scanning environment	83
2.6 HH-OCT images analysis	85
2.6.1 Programming of anterior chamber image analysis.....	85
2.7 Normal distribution of data.....	94
2.8 Statistical analysis.....	97
2.8.1 Reproducibility of HH-OCT	97
2.8.2 Development of anterior chamber	98
2.8.3 Power calculation and sample size	98
2.9 Discussion of the problems that were encountered in this study:.....	100
3. <i>Chapter three: Feasibility and Reproducibility of Anterior Chamber Angle Measurements in Children Using Hand-held Spectral Domain Optical Coherence Tomography</i>	101
3.1 Introduction	101
3.2 Methods.....	104
3.2.1 Participants	104
3.2.2 OCT imaging and analysis.....	104
3.2.3 Feasibility analysis.....	105
3.2.4 Quantitative measurements of anterior chamber	105

3.2.5	Reproducibility of HH-OCT measurements	107
3.2.6	Statistical analysis	109
3.3	Results	110
3.3.1	Feasibility	110
3.3.2	Reproducibility of HH-OCT	111
3.3.3	Intraobserver and interobserver variability of landmark identification	111
3.3.4	Intraobserver and interobserver (same image) reproducibility of anterior chamber measurements.	113
3.3.5	Test retest (repeated images) reproducibility of the anterior chamber measurements.	120
3.4	Discussion	123
3.4.1	Feasibility	123
3.4.2	Landmark identification: intra-observer and inter-observer variability of the same image	124
3.4.3	Reproducibility of anterior chamber measurements.....	124
3.4.4	Illumination	126
3.4.5	Limitations of HH-OCT.....	127
3.4.6	Summary	128
4.	<i>Chapter four: Postnatal Anterior Chamber Development: An In Vivo Quantitative Study Using High Resolution Hand-held Optical Coherence Tomography</i>	129
4.1	Introduction	129
4.1.1	Anterior chamber biometry in adults	129
4.1.2	Importance of anterior chamber biometry.....	130

4.1.3	Ocular biometry in children	130
4.1.4	Gaps in the research literature	132
4.2	Methods.....	133
4.2.1	Participants	133
4.2.2	Clinical examination	133
4.2.3	HH-OCT imaging	134
4.2.4	HH-OCT image analysis	134
4.2.5	Statistical analysis.	135
4.3	Results	136
4.3.1	Subjects	136
4.3.2	Refraction data	137
4.3.3	Non-quantitative inspection of anterior chamber development	137
4.3.4	Quantitative measurements of anterior chamber development	140
4.3.5	Anterior chamber development	147
4.3.6	The impact of predictor factors on anterior chamber development.....	151
4.4	Discussion	159
4.4.1	Anterior chamber development	159
4.4.2	Comparison between ocular biometry in children and adults.....	163
4.4.3	Gender variation of anterior chamber development	163
4.4.4	Association of refraction variation and eye biometry	164

4.4.5	Clinical impact of understanding the normal development of anterior chamber	165
4.4.6	Limitations of study.....	167
4.4.7	Summary	168
5.	<i>Chapter five: Novel In Vivo Morphometric Measurements of Anterior Chamber in Children with Congenital Glaucoma Using Hand Held Spectral Domain Optical Coherence Tomography</i>	169
5.1	Introduction	169
5.1.1	Primary congenital glaucoma (PCG).....	169
5.1.2	The pathology of primary congenital glaucoma	172
5.1.3	Genetic and molecular mechanism of congenital glaucoma	172
5.1.4	Anterior chamber morphometry of congenital glaucoma and research gaps.....	174
5.1.5	Research aims and questions.....	175
5.2	Methods.....	176
5.2.1	Patients and controls	176
5.2.2	History and clinical examination.....	177
5.2.3	OCT imaging and analysis.....	178
5.2.4	Statistical analysis	179
5.3	Results	181
5.3.1	Morphology of anterior chamber in congenital glaucoma	181
5.3.2	Measurements of anterior chamber in congenital glaucoma	182
5.3.3	Development of anterior chamber in congenital glaucoma	188

5.3.4	Correlation between IOP and central corneal thickness in congenital glaucoma	195
5.4	Discussion	196
5.4.1	Development of anterior chamber angle in congenital glaucoma	196
5.4.2	The role of ocular biometry in the management of congenital glaucoma.	198
5.4.3	Central corneal thickness (CCT) in congenital glaucoma	199
5.4.4	Limitations of study.....	200
5.4.5	Possible applications of HH-OCT and future studies of congenital glaucoma	200
5.4.6	Summary	202
6.	<i>Chapter six: Development of Anterior Chamber of Premature Born Children....</i>	203
6.1	Introduction	203
6.1.1	Ocular abnormalities of prematurity	203
6.1.2	Anterior chamber of premature children	204
6.2	Methods.....	204
6.2.1	Subjects.....	204
6.2.2	Image analysis	207
6.2.3	Statistical analysis.	209
6.3	Results	210
6.3.1	Development of anterior chamber in premature born children.....	210
6.4	Discussion	226
6.4.1	Ocular development of premature children	226

6.4.2	Central corneal thickness in premature and full-term children.....	227
6.4.3	Anterior chamber angle in premature and full-term children.....	228
6.4.4	Nasal temporal asymmetry	229
6.4.5	Importance of this study	230
6.4.6	Limitations of study.....	230
6.4.7	Summary	231
7.	<i>Chapter seven: Clinical Exploration of Congenital Anterior Segment Abnormalities Using HH-OCT</i>	232
7.1	Introduction	232
7.2	Methods:.....	232
7.3	Results	233
7.3.1	Aniridia	235
7.3.2	Peters anomaly	236
7.3.3	Axenfeld Rieger syndrome	238
7.3.4	Sturge Weber Syndrome.....	240
7.4	Discussion	242
7.4.1	Summary	242
8.	<i>Chapter eight: General Conclusions and Future Studies</i>	243
8.1	General conclusions	243
8.2	Summary of the significance of findings.....	247

8.3	Recommendations of future studies	249
9.	<i>Chapter nine: Appendix.....</i>	253
9.1	Appendix of chapter 5.....	253
9.1.1	Congenital glaucoma surgical management	253
9.2	Examples of steps of statistical analysis	256
9.2.1	Calculating the mean value and 95 % confidence and prediction intervals	256
9.2.2	Comparing the difference of two groups.....	257
9.3	Examples of information leaflets and consent forms	261
9.4	Awards and Conferences.....	274
9.4.1	Award	274
9.4.2	Conferences	274
10.	<i>Chapter ten: Bibliography</i>	275

List of Tables

Table 1-1: Classification of glaucoma.....	13
Table 1-2: Examples of commercially available time domain optical coherence tomography.....	28
Table 1-3: Examples of commercially available Fourier domain optical coherence tomography (FD-OCT).	29
Table 1-4: Comparison between different methods of visualizing the anterior chamber.....	32
Table 1-5: The percentage of identification of scleral spur in various studies using different anterior segment OCT devices.	45
Table 1-6: Summary of publications comparing the identification of scleral spur and Schwalbe's line using Fourier domain optical coherence tomography (FD-OCT) devices.....	46
Table 1-7: List of literature of measurements of anterior chamber angle based on identification of scleral spur using anterior segment optical coherence tomography.....	52
Table 1-8: Summary of literature of trabecular meshwork measurements using optical coherence tomography.	55
Table 2-1: Sample size of healthy participants categorised by ethnicity	63
Table 2-2 : Sample size of recruited patients.	65
Table 2-3: Different volumetric dimensions that were tested using HH-OCT comparing the speed and quality of different numbers of B-scans.	77
Table 2-4: The outcome of using different protocols of B-scans and A-scans for imaging the anterior chamber angle of the eye.....	78
Table 3-1: Percentage of successful HH-OCT anterior chamber images among different age groups of healthy participants.	110
Table 3-2: The intraobserver and interobserver agreement of identification of landmarks of healthy children, nystagmus and congenital glaucoma groups.	112

Table 3-3: Intraobserver and interobserver assessment of anterior chamber angle measurements of the same image.....	118
Table 3-4: The results of test retest repeatability and reproducibility of HH-OCT anterior chamber angle measurement of images obtained in the same examination day and analysed by the same observer.....	121
Table 3-5: The results of test retest repeatability and reproducibility of HH-OCT anterior chamber width, limbal distances and pupil diamter measurement of images obtained in the same examination day and analysed by the same observer.....	122
Table 4-1: Demography of healthy participants categorized by age group.	136
Table 4-2: Demography of the HH-OCT measurements per eye and angle.....	137
Table 4-3: Established normative measurements of the anterior chamber width and central corneal thickness categorised by different age group.....	141
Table 4-4: Established normative measurements of nasal and temporal anterior chamber angle measurements categorised by different age group.	142
Table 4-5: Rate of growth of the anterior chamber measurements per year	146
Table 4-6: The correlation of the development of each anterior chamber measurement with gender, eye and angle variation after controlling the effect of age.	152
Table 4-7: First order partial correlation between anterior chamber measurements and spherical power.	157
Table 5-1: Demography of congenital glaucoma and control groups.	177
Table 5-2: Demography of HH-OCT images analysed per eye and per angle in congenital glaucoma and control groups.....	179
Table 5-3: The mean and 95% prediction interval of nasal and temporal Schwalbe's line angle opening distance in children with congenital glaucoma and age-matched healthy controls.	183

Table 5-4: The mean and 95% prediction interval of nasal and temporal Schwalbe's line trabecular iris surface area (SL-TISA) in children with congenital glaucoma and age-matched healthy controls.	184
Table 5-5: The mean and 95% prediction interval of anterior chamber width (ACW) and central corneal thickness (CCT) measurements in children with congenital glaucoma and age-matched healthy controls.....	185
Table 5-6: The rate of development of anterior chamber width (SS-SS-D and SL-SL-D) and central corneal thickness (CCT) measurements in children with congenital glaucoma and age-matched healthy controls per year.	186
Table 5-7: The rate of development of temporal and nasal anterior chamber angle measurements in children with congenital glaucoma and age-matched healthy controls.....	187
Table 5-8: The difference of the anterior chamber angle measurements between children with congenital glaucoma and age-matched controls at different ages.....	191
Table 5-9: The difference of the anterior chamber width and central corneal thickness measurements between children with congenital glaucoma and age-matched controls at different ages.	194
Table 6-1: Clinical information of premature born children.	206
Table 6-2: The mean and 95% prediction intervals of anterior chamber width and central corneal thickness measurements in premature and full-term born children.....	211
Table 6-3: The mean and 95% prediction interval of temporal and nasal anterior chamber angle measurements per age in premature and full-term born children.....	212
Table 6-4 : Difference between premature and full-term born children in anterior chamber width and central corneal thickness at different ages.	221
Table 6-5: The rate of change of anterior chamber width and central corneal thickness measurements in premature and full-term born children.	222
Table 6-6: Difference between premature and full-term born children at different ages in temporal and nasal anterior chamber angle measurements.	224

Table 6-7: The rate of growth of temporal and nasal anterior chamber angle measurements in premature and full-term born children per year.	225
Table 7-1: Clinical information of the patients with congenital abnormalities of anterior segment...	234
Table 9-1: Demography of congenital glaucoma patients	254

List of Figures

Figure 1-1: Optical coherence tomography (OCT) image of anterior chamber obtained by Visante TD-OCT.....	6
Figure 1-2: Structure of anterior chamber angle.....	7
Figure 1-3: Development of anterior chamber angle after birth and its configuration in adulthood described by Anderson et al (1981).	11
Figure 1-4: Emmetropisation and refraction error.	12
Figure 1-5: Difference between open angle and closed angle glaucoma.	15
Figure 1-6: Features of Axenfeld Rieger anomaly.	19
Figure 1-7: Comparison of optical coherence tomography (OCT) image and histology of retina.	24
Figure 1-8: Hand held C2300 Envisu SD-OCT.	30
Figure 1-9: Measurements of the cornea by OCT.....	34
Figure 1-10. Anterior chamber images of differnt OCT technology.	39
Figure 1-11: Schematic and OCT images of the iridocorneal angle measurements derived from identification of scleral spur.....	49
Figure 1-12: Schematic images of the anterior chamber measurements derived from Schwalbe's line.	50
Figure 2-1: Steps of diagnosis of albinism and idiopathic infantile nystagmus	66
Figure 2-2: Methods of visual acuity measurements.....	68
Figure 2-3: Refraction examination using Plusoptix.	69
Figure 2-4: Eye movement direction	70
Figure 2-5: Cover test technique.....	71

Figure 2-6: Retina stuctures in funduscopy examination	71
Figure 2-7: Anterior segment lens of hand-held optical coherence tomography.....	73
Figure 2-8: Acquisition of scans of the eyes of children using HH-OCT	73
Figure 2-9: Acquisition of anterior segment images using HH-OCT.	74
Figure 2-10: Different dimensions of B-scans obtained by HH-OCT.....	79
Figure 2-11: Different HH-OCT volumetric scans showing the pupil	80
Figure 2-12: Individual B-scans at the centre of pupil consists of 3000 A-scans	80
Figure 2-13: Individual B-scans at the centre of pupil consisting of different numbers of A-scans.	81
Figure 2-14: HH-OCT individual B-scan at the centre of pupil showing the anterior chamber.	82
Figure 2-15: Optimisation of scanning environment.....	84
Figure 2-16: The measurement of central corneal thickness by HH-OCT.	86
Figure 2-17: Example of the anterior chamber angle analysis using ImageJ macro.	89
Figure 2-18: HH-OCT B-scan showing anterior chambers measurement	90
Figure 2-19: HH-OCT B-scan showing anterior chambers angle measurements	90
Figure 2-20: HH-OCT image showing anterior chambers angle measurements based on identification of Schwalbe's line.	91
Figure 2-21: HH-OCT image showing limbal distance measurements.....	92
Figure 2-22: Example of data in Excel sheet template.....	93
Figure 2-23: Example of the histogram and P-P plot of anterior chamber data.....	95
Figure 2-24: Example of Q-Q plot of normal distribution	96
Figure 2-25: Example of calculation of achieved power of used sample size using G Power software. 99	

Figure 3-1:Criteria of good quality anterior chamber image.....	105
Figure 3-2: Summary of anterior chamber measurements using HH-OCT image.....	107
Figure 3-3: HH-OCT B-scan of the anterior chamber of 4 year old female with congenital glaucoma.	113
Figure 3-4: The intraobserver and interobserver coefficient of variation (COV) and interclass correlation coefficient (ICC) of anterior chamber angle measurements.	115
Figure 3-5: Comparison between the Bland Altman plot of intraobserver and interobserver assessment of Schwalbe's line trabecular iris surface area (SL-TISA) in healthy children and congenital glaucoma.	116
Figure 3-6: Comparison between the Bland Altman plot of intraobserver and interobserver assessment of scleral spur angle opening distance (SS-AOD), in healthy children and congenital glaucoma.	117
Figure 4-1: Development of the eye from birth up to age of 20 years using magnetic resonance imaging.	131
Figure 4-2: Anterior segment OCT images at different ages ranging between 2 days and 16 years of age.	139
Figure 4-3: Scatter plots showing the development of anterior chamber width and central corneal thickness.	143
Figure 4-4: Scatter plots showing the development of nasal and temporal anterior chamber angle measurements.	144
Figure 4-5: The rate of changes of the anterior chamber measurement per age.....	145
Figure 4-6: Polynomial plots comparing the development of nasal and temporal anterior chamber angle measurements.....	149
Figure 4-7: Polynomial plots comparing the development of anterior chamber angle of males and females.	153
Figure 4-8: Polynomial plots comparing the development of the anterior chamber width and central corneal thickness of males and females.	155

Figure 4-9: Correlation between anterior chamber measurements, postmenstrual age and spherical equivalent.....	158
Figure 4-10: Comparison of HH-OCT image and histology of anterior chamber angle.	160
Figure 4-11: Schematic illustration of the postnatal development of anterior chamber.	162
Figure 5-1: Steps of the diagnosis and management of congenital glaucoma.	171
Figure 5-2: HH-OCT images of the anterior chamber of a 3 year old, female with congenital glaucoma compared to age-matched healthy female child.	181
Figure 5-3: Fractional polynomial curve fit comparing the angle measurements of children with congenital glaucoma and age-matched controls from the age of 3 months up to 10 years old.	190
Figure 5-4: Fractional polynomial curve fit comparing the anterior chamber width (SS-SS-D &SL-SL-D) and central corneal thickness (CCT) in children with congenital glaucoma and age-matched controls from the of 3 months up to 10 years old.	193
Figure 6-1: HH-OCT images of the anterior chamber of a premature child.....	208
Figure 6-2: Individual anterior chamber width and central corneal thickness measurements of premature children with regards to mean and 95% prediction intervals of the development of anterior chamber of healthy full-term born children.....	213
Figure 6-3: Individual anterior chamber angle measurements of premature children with regards to mean and 95% prediction intervals of the development of nasal and temporal anterior chamber angle of healthy full-term born children.....	215
Figure 6-4: Polynomial curve fit comparing the development of anterior chamber width and central cornea thickness of premature and full-term born children.	216
Figure 6.5: Polynomial curve fit comparing the development of nasal and temporal angles of premature and full-term born children.	218
Figure 7-1: HH-OCT images of the anterior chamber of left eye of a known case of aniridia.....	235
Figure 7-2: HH-OCT images of the anterior chamber, in three children with Peters' anomaly.	237

Figure 7-3: HH-OCT images of the anterior chamber of an 11 year old Asian male diagnosed with Axenfeld Rieger syndrome.....	238
Figure 7-4: HH-OCT images of the anterior chamber of a 4 year old male with confirmed diagnosis of Axenfeld Rieger syndrome.....	239
Figure 7-5: HH-OCT images of the anterior chamber of 8 month old Caucasian male diagnosed with Sturge Weber Syndrome.....	241
Figure 8-1: HH-OCT image of the anterior chamber angle showing the trabecular meshwork.....	249
Figure 8-2: HH-OCT images comparing between the a) healthy iris of a 4 year old child, b) the iris of an age-matched child with congenital glaucoma and c) the iris of healthy new-born child.....	251

Abbreviations

AC	Anterior chamber
ACA	Anterior chamber angle
ACD	Anterior chamber depth
ACV	Anterior chamber volume
ACW	Anterior chamber width
AL	Axial length
AOD	Angle opening distance
AS-OCT	Anterior segment optical coherence tomography
BCVA	Best corrected visual acuity
BE	Both eyes
CCT	Central corneal thickness
CD	Corneal diameter
CH	Corneal hysteresis
CI	95% confidence interval
COV	Coefficient of variation
F	Female
FD-OCT	Fourier domain optical coherence tomography
GA	Gestational age
HD	High definition
HH-OCT	Hand held optical coherence tomography
ICC	Interclass correlation coefficient
ID	Identification
IIN	Idiopathic infantile nystagmus
IOL	Intraocular lens
IOP	Intraocular pressure
L-Dopa	Dihydroxy phenylalanine
OS	Left eye
LogMar	Logarithm of the minimum angle of resolution
LOV	Level of agreement
LV	Lenticular vault
M	Male
MRI	Magnetic resonance imaging
n	Sample size
Ns	Not significant
OC	Ocular albinism
OCA	Oculo-cutaneous albinism
OCT	Optical coherence tomography
ORA	Ocular response analyser
PD	Pupil diameter

PI	95% prediction interval
PL	Preferential looking
PMA	Postmenstrual age
OD	Right eye
RE	Refractive error
ROP	Retinopathy of prematurity
SD	Standard deviation
SD-OCT	Spectral domain optical coherence tomography
SE	Standard error
SL	Schwalbe's line
SL-AOD	Schwalbe's line angle opening distance
SL-AOD500	Schwalbe's Line Angle Opening Distance 500µm From SL
SL-LD	Schwalbe's line limbal distance
SL-SL-D	Nasal Schwalbe's line to temporal Schwalbe's line distance
SL-TISA	Schwalbe's line trabecular iris surface area
SS	Scleral spur
SS-AOD	Scleral spur angle opening distance
SS-LD	Scleral spur limbal distance
SS-OCT	Swept source optical coherence tomography
SS-SS-D	Nasal scleral spur to temporal scleral spur distance
TD-OCT	Time domain optical coherence tomography
TISA	Trabecular iris surface area
TM	Trabecular meshwork
TML	Trabecular meshwork length
UBM	Ultrasound biomicroscopy
VA	Visual acuity
VEGF	Vascular endothelial growth factor

Overview of the thesis

This thesis involved obtaining in vivo quantitative measurements of the anterior chamber of children's eyes at different ages using high resolution hand-held optical coherence tomography (HH-OCT). Comparing the changes of anterior chamber measurements with increasing age can provide information about how and when the anterior chamber develops and reaches maturity normally. Comparing the development of the anterior chamber of healthy children with children who have abnormal anterior chamber development such as, congenital glaucoma can provide valuable information. This will help:

- To understand the normative development of anterior chamber of human eye from birth, during childhood and up to adult life.
- To establish normative morphometric data of anterior chamber in children
- To highlight the pathological development of the anterior chamber that is associated with ocular diseases in children through comparing the anterior chamber measurements of healthy and known ocular diseases in children such as congenital glaucoma.
- To explore the development of the anterior chamber of premature born children.

The first part of chapter one covers overview of ocular anatomy, development of anterior chamber, the common ocular disease affecting the children and the principle of optical coherence tomography. The second part of chapter one addresses the literature review of the application of OCT in imaging the anterior segment; what has been achieved to date and what information gaps are yet to be investigated. The third part includes a list of the general research questions and the aims of this thesis.

Chapter two describes the general methods including details about the criteria of participants, the imaging protocol used for OCT, analysis programmes of OCT images, statistical analysis and the practical difficulties of the project.

Chapter three presents the feasibility and reproducibility of hand held spectral domain optical coherence in imaging the anterior chamber of children younger than 6 years of age

and explored the best accurate and reproducible measurements to better describe the anterior chamber development

Chapter four reports the findings of normative development of anterior chamber in children.

Chapter five compares the anterior chamber development in children diagnosed with congenital glaucoma and age-matched healthy controls up to 10 years of age

Chapter six compares the anterior chamber development in premature and age-matched full-term born children up to 6 years of age

Chapter seven presents clinical use of HH-OCT in visualising the congenital abnormality of the anterior chamber in children

Chapter eight presents a summary of the thesis findings and recommendations of future studies.

Chapter nine shows appendix.

Chapter ten lists the bibliography.

1. Chapter one: Introduction and literature reviews

1.1 Anatomy and development of anterior segment of the eye

1.1.1 Anatomy of anterior segment of the eye

The anterior segment refers to all structures that lie in front of the vitreous. It includes the cornea, iris, ciliary body, lens and both the anterior and posterior chambers. The anterior chamber is the space between cornea and iris. The posterior chamber is a space between the iris, ciliary processes and suspensory ligaments of the lens. Both chambers are filled with aqueous humour.

1.1.1.1 Cornea

This is the transparent avascular anterior structure of the eye. In adults, the cornea has an optical power of approximately 43 dioptres. The corneal diameter is about 11.50 mm (11.86 mm in children (Puvanachandra and Lyons, 2009)). The corneal thickness ranges from 0.5 to 0.6 mm in the center and from 0.6 to 0.8 mm at the periphery. Histologically, the cornea consists of five layers (Ehlers and Hjortdal, 2005), which are:

1. **Corneal epithelial:** a non-keratinized stratified squamous epithelium, which is easily regenerated. This layer is covered by a thin film of tears.
2. **Bowman's layer:** a tough subepithelial basement membrane composed of collagen; about 8 to 14 μm in thickness.
3. **Stroma:** a thick, transparent middle layer, rich in regularly arranged collagen fibers. There are about 200 ($\sim 500 \mu\text{m}$ thick) parallel layers of mainly type I collagen fibrils.
4. **Descemet's membrane:** a thin basement membrane of corneal endothelium. The thickness ranges between about 3 μm at birth to 4 -10 μm in adults. The termination of Descemet's membrane at the corneoscleral junction is called Schwalbe's line, which represents an important anatomical landmark (this will be mentioned frequently in this thesis).

5. **Corneal endothelium:** a simple cuboidal non-regenerating cell layer, about 5 μm thick, which is responsible for regulating fluid and solutes (electrolytes and nutrients) transport between the aqueous and corneal stroma.

1.1.1.2 Iris

Iris is the thin, circular coloured structure of the eye that controls the diameter and size of the pupil to optimize the amount of light reaching the retina. The iris is divided by the collarette into two major regions: 1) the pupillary part around the pupil, and 2) the ciliary part that extends to the iris root at the ciliary body. The collarette is the thickest region of the iris, where the sphincter muscle and dilator muscle overlap separating the pupillary portion from the ciliary portion. On the anterior surface of iris, there are series of openings called the Crypts of Fuchs on the either side of the collarette. On the posterior surface, there are series of fine radial folds extending from the pupillary margin to the collarette which called the radial contraction folds of Schwalbe. Histologically (Clinicalgate, 2015), the iris consists of the following layers:

1. Anterior limiting layer
2. Stroma, the front pigmented fibro-vascular layer
3. Iris sphincter and dilator papillae muscles which control the pupil size.
4. Anterior pigment myo-epithelium
5. Posterior pigmented epithelial cells, which restricts the light passing through the iris to the retina.

The various pigmented colour typically range between brown, hazel, green, grey, or blue. The light color of the iris is due to a lack of melanin pigmentation.

1.1.1.3 Anterior chamber (AC):

This is the space between the corneal endothelium anteriorly and the iris and lens vault posteriorly (Figure 1-1). AC is filled with aqueous humour. The normal anterior chamber depth (ACD) of the eye ranges between 2.5mm to 3.5mm (Nongpiur et al., 2011a).

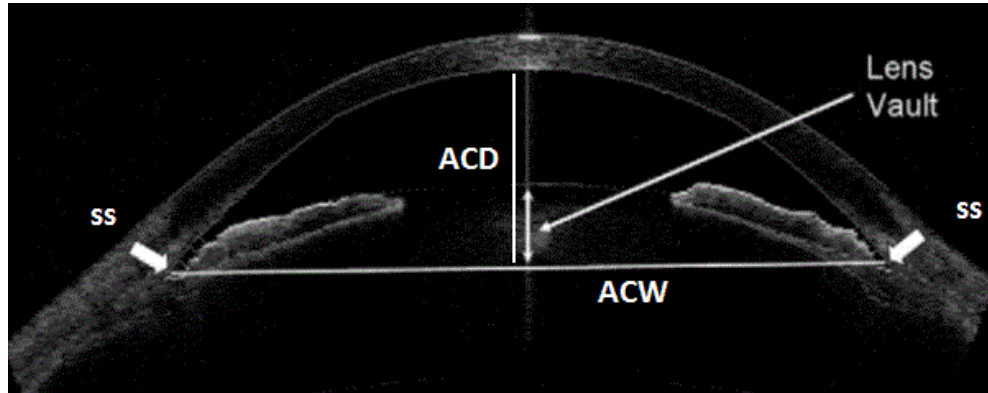


Figure 1-1: Optical coherence tomography (OCT) image of anterior chamber obtained by Visante TD-OCT.

The image shows the measurement of anterior chamber depth (ACD), anterior chamber width (ACW) and lens vault (LV) (Nongpiur et al., 2011a). The anterior chamber width is the linear distance between scleral spur (SS). The ACD is measured as the distance between the corneal endothelium and the crystalline lens vault. The lens vault is the perpendicular distance between the anterior pole of crystalline lens and the horizontal line joining the two scleral spurs. Schwalbe's line (SL) cannot be identified using time domain optical coherence tomography (TD-OCT).

1.1.1.4 Aqueous humour

This is a transparent fluid secreted from the epithelium of the ciliary process and flows from the posterior chamber to the anterior chamber through the pupil. The majority of fluid drains through the trabecular meshwork (TM) to Schlemm's canal and then to the episcleral veins. A small degree of the drainage of aqueous humour (5-10%) occurs through the uveo-scleral pathway. The aqueous humour maintains the eye shape, intraocular pressure (IOP), refraction index and provides nutrients and immunoglobulin to the avascular structure of cornea. Impaired drainage of aqueous humour leads to an increase in the IOP due to accumulation of aqueous humour inside the eye (Silverthorn et al., 2016).

1.1.1.5 Scleral spur (SS)

This is an inward protrusion of the sclera at the junction of the sclera to the ciliary body. It appears as a change in the curvature of the corneoscleral-aqueous interface and it forms the posterior end of the trabecular meshwork (Figure 1-1 and 1-2). SS is used as an anatomical landmark in the assessment of the anterior chamber angle either by gonioscopy, ultrasound bio-microscopy (UBM) or using optical coherence tomography (OCT).

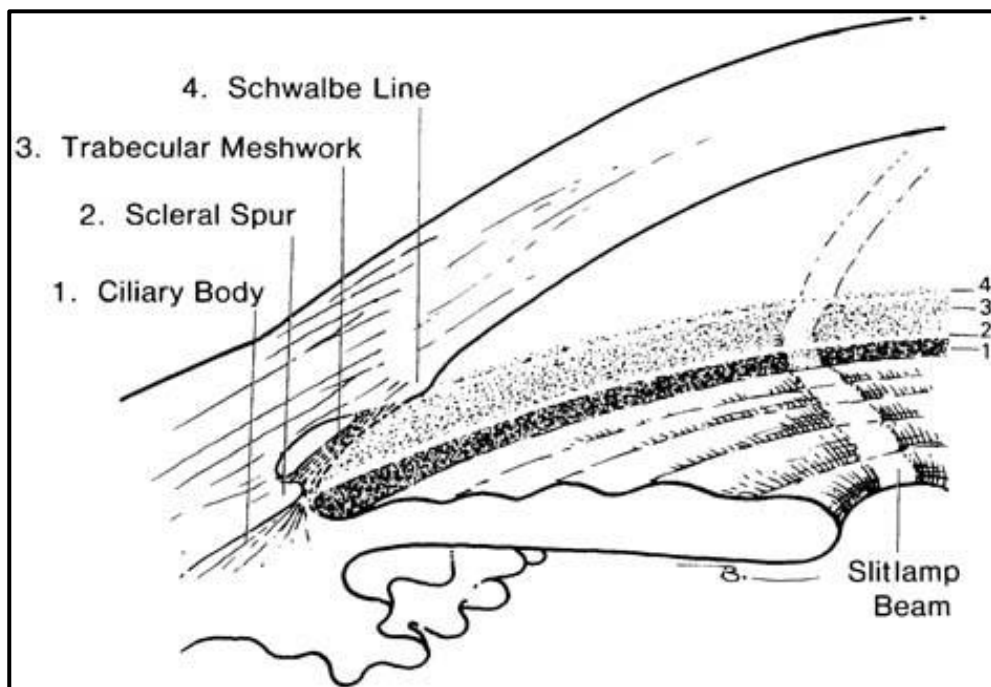


*Figure 1-2: Structure of anterior chamber angle.
The images shows the anatomical position of Schwalbe's line (SL), trabecular meshwork (TM) and scleral spur (SS) (Phat, 2016).*

1.1.1.6 Schwalbe's line (SL)

Schwalbe's line represents the termination of Descemet's membrane of the cornea at the inner corneoscleral junction (Figure 1-2).

1.1.1.7 Trabecular meshwork (TM)

Trabecular meshwork is a spongy pigmented pore-like structure that extends from Schwalbe's line anteriorly to the scleral spur posteriorly (Figure 1-2), surrounding the circumference of the anterior chamber. It allows aqueous humour to drain into Schlemm's canal. The TM contains of three differentiated layers.

(1) The uveal meshwork, which is the outer layer, exposed to anterior chamber, formed by prolongation of connective tissue of the iris and ciliary body stroma and totally covered by endothelial cells. This layer has large intercellular spaces that allow passive aqueous humor outflow.

(2) The corneoscleral meshwork, the intermediate layer, characterized by the presence of lamellae covered by endothelium like cells standing on a basal membrane. It has narrower intercellular spaces which are responsible for the increase in aqueous flow resistance.

(3) The juxta-canalicular or cribriform meshwork, the inner layer. It is in direct contact with the inner wall of endothelial cells of Schlemm's canal. It is formed by cells embedded in a dense extracellular matrix. It has narrow intercellular spaces, which constitute the major resistance to the aqueous outflow (Llobet et al., 2003).

TM length has been approximately estimated as a 500 µm anterior to SS, using ultrasound bio-microscopy (UBM) image (Pavlin et al., 1992, Ishikawa et al., 2000), because Schwalbe's line cannot be seen using UBM and TD-OCT.

1.1.1.8 Schlemm's canal

The trabecular meshwork covers the scleral sulcus to form a circular channel known as Schlemm's canal. The aqueous humour drains from the anterior chamber into the anterior ciliary veins through Schlemm's canal, which transfers approximately 2-3 microliters of aqueous humor per minute (Johnson and Kamm, 1983).

1.1.2 Normal development of anterior chamber

1.1.2.1 Intrauterine development

The eyes are developed from several layers including:

- (A) The surface ectoderm, which forms the lens, corneal epithelium and eyelid.
- (B) The neuro-epithelium, which forms the retina, ciliary body, iris, and optic nerves.
- (C) The extracellular mesenchyme, that consists of the neural crest and mesoderm, and gives rise to the sclera, cornea, blood vessels, muscles, and vitreous (Barishak, 1992).

The eyes begin to develop as a pair of optic vesicles. These vesicles derive as diverticula at the third week of pregnancy from the lateral aspects of forebrain. The formation of optic vesicles begins by outgrowth and protrusion of the optic sulci. The neural tube closes at the end of the fourth week and forms the optic vesicles. The optic vesicles then form the optic cups. The outer layer of the cups forms the retinal pigment epithelium and the inner layer form the retina. The middle layer develops into the ciliary body and iris. At the same time, the lens placode is formed from a part of ectoderm which thickens and then separates to form the lens vesicle at the open end of the optic cup. When the optic vesicles make contact with surface ectoderm, further development is induced involving the entrance of blood vessels through the choroid fissure; a groove at the bottom of the optic vesicles.

Reme et al (1981) studied the development of the normal eye by visualising the ocular tissues of foetuses under light and electron microscopy. The major growth phases of the human eye were described as following; the main separation into corneoscleral and ciliary iris region occur by the 15th week of fetal life. By the 22nd week, a differentiation into definitive structures becomes visible and after the 6th month more specialization of tissues appears (Reme and Depinay, 1981).

1.1.2.2 Genetic control of eye development

Eye development is controlled by the paired box protein (*PAX-6*), a transcription factor. It is also called aniridia type II protein (AN2). It is considered the master regulator of the development of the eye and brain. *PAX6* gene mutations cause abnormal development of the eyes seen in diseases such as aniridia and Peter's anomaly. Other genes that play an important role in the eye development include: *CYP1B1*, *LTBP*, *PITX2* and *FOXC1* (Suri et al., 2009)

1.1.2.3 Mechanism of anterior chamber development

The physiological mechanism of the entire eye development is still unclear. Anterior chamber development is suggested due to cell death and /or resorption. Previous studies on rat (Reme et al., 1983) and cat (Richardson et al., 1985) anterior chambers reported macrophage infiltration and marked cellular necrosis of the anterior chamber during postnatal life. In contrast, studies on human tissue reported a decline in numbers and density of cells at the irido-corneal angle and trabecular meshwork with presence of macrophage-like cells from the 15th to the 27th fetal weeks. However, no evidence of cell necrosis has been detected (Meghpara et al., 2008, Mcmenamin, 1991, Mcmenamin, 1989). This contradicts cell death and /or resorption theory and suggests that formation of intra-trabecular space results from cellular differentiation and reorganization.

1.1.2.4 Postnatal development of anterior chamber.

1.1.2.4.1 Postnatal maturation of anterior chamber

Reme et al (1981) found that the anterior chamber angle reaches the configuration of the adult eye by 1 to 4 years after birth and the final cellular and extracellular maturation of trabecular meshwork is achieved by 1 to 8 years of age (Reme and Depinay, 1981). In the same year, Anderson described the normal development of the anterior chamber angle through histological examination of 40 eyes of children (age ranged from 20 weeks gestational age to 5 years of postnatal age) under light and electron microscope. Anderson (1981) reported that, at birth the posterior part of the trabecular meshwork is embedded in the corneoscleral junction and overlapped by the ciliary process and the iris (Figure 1-3).

The iris is curved forward. Shortly after birth, the ciliary muscles and process slide posteriorly, in relation to the cornea and sclera. The iris recesses behind the scleral spur, exposing the TM in the anterior chamber. The ciliary processes eventually extend into the peripheral iris, lie side by side to the ciliary muscle. As a consequence, the anterior chamber angle is widening (Anderson, 1981).

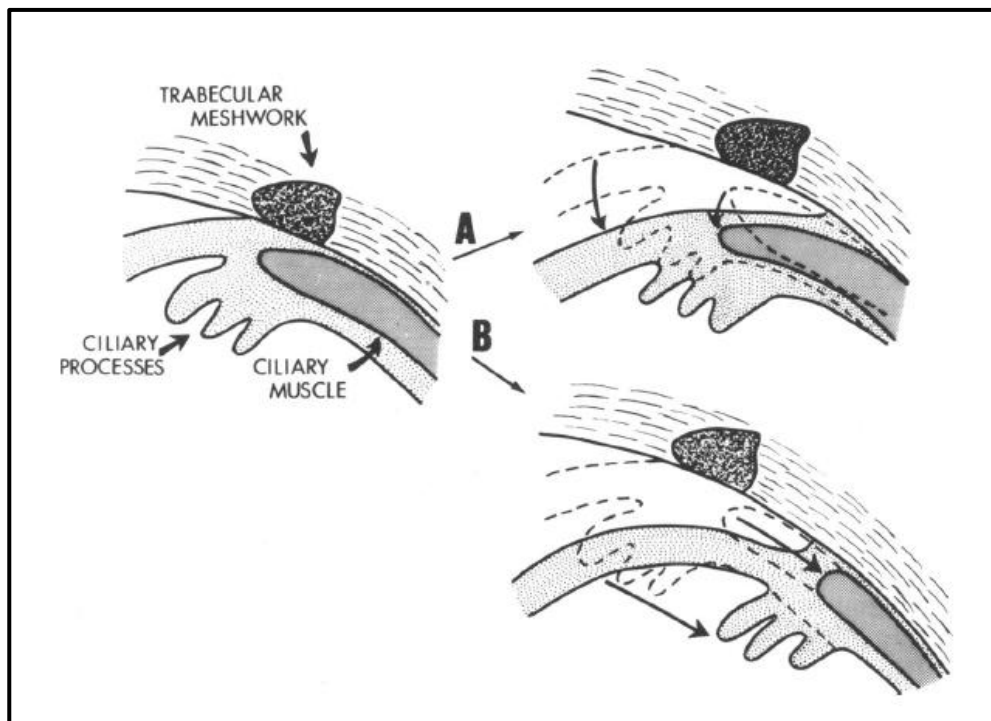


Figure 1-3: Development of anterior chamber angle after birth and its configuration in adulthood described by Anderson et al (1981).

In the newborn, the TM is covered by the iris. A) The ciliary process and ciliary muscles slide backwards, resulting in anterior chamber angle widening with increasing age. Then, B) The ciliary process and ciliary muscle further slide backward and lie side by side at the peripheral iris behind the scleral spur in the final modelling. This process exposes the TM to the anterior chamber.

The histological studies of the development of the anterior chamber relied on a small sample size. They were also performed in-vitro using dead and chemically manipulated tissues. Availability of non-invasive techniques such as optical coherence tomography (OCT), with potential of visualisation and quantitative measurements of the anterior chamber of children, can now more readily provide data with much large sample sizes to perform in-vivo studies of the development of the anterior chamber. This is the main focus of this thesis.

1.1.2.4.2 Emmetropisation

Emmetropisation is a physiological process that matches axial length and optical power of the cornea and lens (Brown et al., 1999). This phenomena is well known to happen rapidly during the first 12 months of age and is associated with increase in axial length (AL) and anterior chamber depth (ACD) (Pennie et al., 2001). It changes the eye from oblate to prolate shape (Ishii et al., 2011, Munro et al., 2015). During emmetropisation, the focus point of the parallel light rays, shift from behind the retina, with the growing eye, to eventually focus on the retina. The infinity becomes the far point of the eye (Figure 1-4). Emmetropisation is associated with thinning and flattening of the lens and cornea, resulting in reduction of the refractive power of both cornea and lens (Mutti et al., 2005). The later causes a shift from myopia to hypermetropia and balances the myopic shift of the growing AL. The largest reduction in spherical refractive power is attributed to a reduced lenticular thickness (Zadnik et al., 1995). The range of emmetropic eye is defined as the interval between ± 0.5 Dioptrre (Atchison et al., 2005).

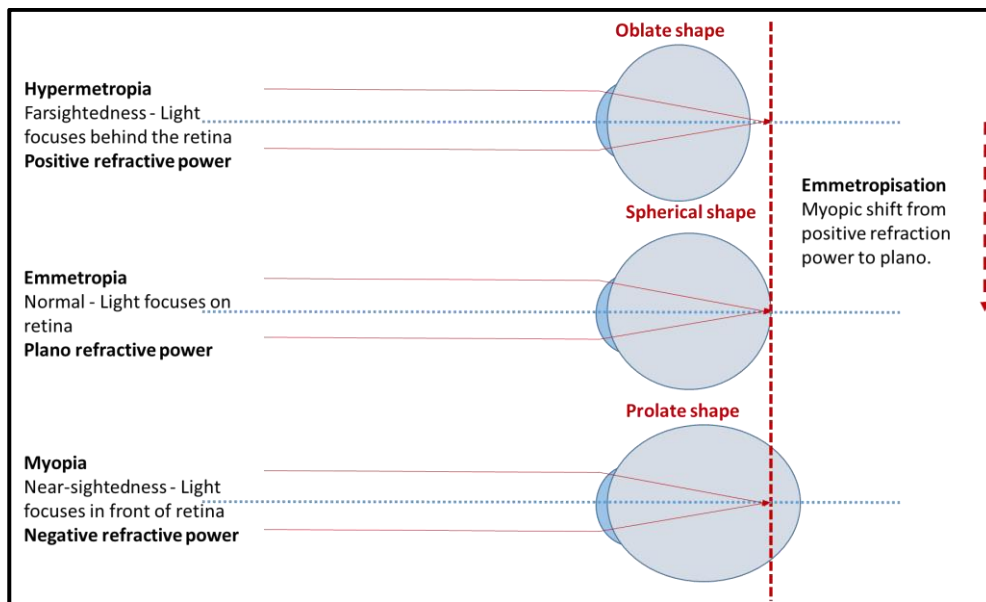


Figure 1-4: Emmetropisation and refraction error.

The image illustrates the physiological process of emmetropisation with age, which involves myopic shift from a positive refractive power to plano. It is associated with an increase in anteroposterior diameter of eye (axial length) till the light focuses on the retina. Longer axial length is associated with pathological myopia, where light focuses in front of the retina.

1.1.3 Abnormal development of anterior chamber

Failure of normal development of the eye can either be associated with developmental abnormalities of other organs (syndromes) or can be limited only to eye. Abnormal development of the anterior chamber results in glaucoma. In general, glaucoma refers to progressive cupping of optic disc that is associated with increased intraocular pressure (IOP). High IOP results from accumulation of aqueous humour due to disturbance of its drainage and outflow (Weinreb and Khaw, 2004). Glaucoma can be congenital developing from birth or occurs at an older age. The classification of glaucoma is summarised in table (1-1).

Table 1-1: Classification of glaucoma

Criteria of classification		
1	Absence or presence of causative factor	Primary Secondary
2	Speed of onset	Acute Chronic
3	Anatomy of anterior chamber angle	Closed Opened
4	Late onset	Adulthood Childhood
4	Age of onset	At birth or before birth
	Early onset (Congenital)	Infantile: Birth until 3 years of life
		Juvenile: 3 years to adulthood
5	Level of IOP	High IOP Normal tension (normal IOP)

1.1.3.1 Late onset glaucoma

This type of glaucoma can develop later on in life during childhood and adulthood and has different pathology and mechanism to congenital glaucoma. It is classified according to the anatomy of anterior chamber into open and closed angle glaucoma (Figure 1-5). The late onset glaucoma results from either obstruction of anterior chamber angle (angle closure

glaucoma) or defect in the draining function of trabecular meshwork (open angle glaucoma) (Weinreb and Khaw, 2004).

1.1.3.1.1 Angle closure glaucoma (ACG)

It is usually associated with sudden high rise in the intraocular pressure that results from mechanical outflow obstruction of aqueous humour (pupillary block). Pupillary block is caused by narrowing or complete closure of the anterior chamber angle due to contact between the iris and trabecular meshwork. Such a prolonged contact may gradually damage the trabecular meshwork causing synechiae formation, which subsequently leads to permanent obstruction of aqueous outflow. ACG prevalence is higher in old age, female, Chinese, African, Caribbean and ethnicity (Cheng et al., 2014). Angle closure glaucoma in children is suggested to have different underlying pathology instead of pupillary block (Ritch et al., 2003). This pathology involves structural and developmental defects such as plateau iris syndrome (Belovay et al., 2015), retinopathy of prematurity (Suzuki et al., 2005), uveitis (Heinz et al., 2007) and Marfan's syndrome. Closed angle glaucoma occurs suddenly and the patient complains of a red eye with severe pain. It is urgently treated by laser iridotomy to open the blockage (Sun et al., 2017).

1.1.3.1.2 Primary open angle glaucoma (POAG)

This is painless, asymptomatic condition that develops gradually over time and only gives manifestation when it is in advanced stages. The anterior chamber angle structurally is open while the aqueous drainage is impaired.

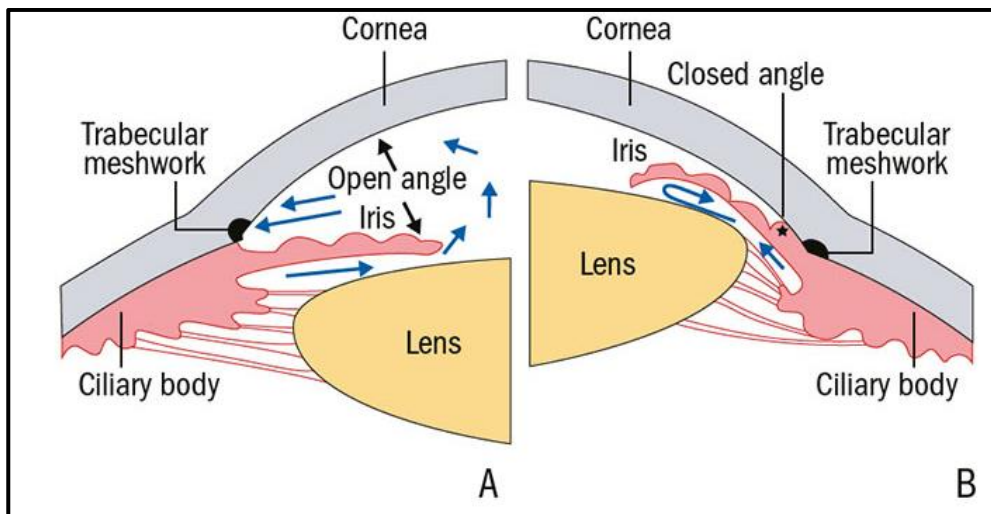


Figure 1-5: Difference between open angle and closed angle glaucoma.

Schematic representation of anterior chamber shows the mechanism of open and closed angle glaucoma. A) In open angle glaucoma, the anterior chamber angle is opened, the trabecular meshwork is exposed to aqueous humour but functionally is impaired. B) In angle closure glaucoma, the anterior chamber is closed and the flow of aqueous humour is obstructed by the direct contact of iris to trabecular meshwork (Optician online, 2018).

1.1.3.2 Early onset congenital glaucoma

Congenital glaucoma is attributed to abnormal development of the trabecular meshwork and anterior chamber angle that prevent adequate aqueous humour outflow (Tamm, 2011). The exact etiology of congenital glaucoma is still unknown. Congenital glaucoma is classified according to association with other ocular or systemic abnormalities into:

- a. Primary congenital glaucoma (PCG)

PCG affects about 1 per 10,000 births, is more common in males (65%) and bilateral in 70% of affected children. It occurs at birth or within the first few years of life. It is usually not associated with ocular malformation or systemic anomalies. Most cases are sporadic but inheritance can be autosomal recessive. Further details about the pathogenesis of PCG is addressed in chapter 5.

Clinical changes in PCG include:

- a) A rise in intraocular pressure, an IOP greater than 21 mm Hg.
- b) Enlargement of eyeball (buphthalmos)

- c) Increased corneal diameter (increased horizontal corneal diameter \geq 11 mm within the first year of life).
- d) Deep anterior chamber.
- e) Endothelial edema.
- f) Opacification of the cornea with rupture of Descemet's membrane (Haab's striae).
- g) Thinning of the anterior sclera and iris atrophy.
- h) The posterior segment remains normal except for a progressive glaucomatous optic atrophy.
- i) Visual acuity may be reduced and/or visual fields may be restricted. In untreated cases, blindness invariably occurs.

b. Secondary congenital glaucoma (SCG)

Secondary congenital glaucoma occurs in presence of ocular developmental anomalies or systemic anomalies and has the same manifestation of PCG. SCG includes:

- i. SCG to congenital ocular diseases
 - 1. Anterior segment dysgenesis syndromes:
 - a. Peters' anomaly
 - b. Axenfeld Rieger (A-R) anomaly.
 - 2. Coloboma
 - 3. Aniridia.
 - 4. Micro-cornea.
 - 5. Congenital cataract.
- ii. SCG associated with systemic syndromes.

1.1.3.3 Genetic and molecular mechanism of congenital glaucoma

Genetic studies have so far detected more than 20 mutant genes associated with glaucoma development (Souzeau, 2018). *CYP1B1*, *LTBP2* (autosomal recessive) and *TEK* (autosomal dominant) genes are associated with primary congenital glaucoma (Lewis et al., 2017).

Mutation in *PAX6*, *MYCO*, *PITX2*, *OPTN*, *CAV1*, *OPTC*, *ANGPT1*, *NTF4*, *FBNI*, *ASPH*, *ADAMTS10*, *ADAMTS17*, *WDR36* and *FOXC1* are also associated with different forms of congenital glaucoma (Fuchshofer et al., 2009, Gencik et al., 1980, Yang et al., 2017, Reis et al., 2015, Chang et al., 2015, Anderson et al., 1996).

1.1.4 Congenital ocular diseases

1.1.4.1 Anterior segment dysgenesis (ASD)

The anterior segment dysgenesis is a heterogeneous group of disorders that are inherited in an autosomal dominant manner. It presents by abnormal ocular structures and associated with systemic defects. Glaucoma is a common ocular problem herein. Some cases of primary congenital glaucoma (PCG) are not easy to distinguish clinically from some of the anterior segment dysgenesis syndromes. ASD appear to be phenotypically and genotypically distinct from PCG. These syndromes include:

1.1.4.1.1 Peters' anomaly

This is a specific type of abnormal development of the mesenchymal layers of the anterior segment leading to incomplete separation of the cornea from the iris or the lens. It affects 3 to 6 individuals per 100,000 and is bilateral in 80% cases (Pomella and Wagner, 1998). The cause of Peters' anomaly is unknown. However, mutations in the *FOXC1*, *PAX6*, *PITX2*, or *CYP1B1* gene has been associated with Peters' anomaly.

There is central corneal opacity (leukoma), which varies in size and intensity from a small, faint streak to a large, white cloudy area that covers the front surface of the eye and causes blurred vision (Bhandari et al., 2011). The anterior chamber is shallow with synechiae between the iris and cornea (Eugene Chang, 2014).. 50% of Peters' anomaly is associated with low vision early in life because the corneal opacification causes blockage of the central visual axis which subsequently lead to lack of visual stimulation, and amblyopia can develop. Peters' anomaly is often associated with strabismus, glaucoma, cataract, and microphthalmia. It is also associated with delayed mental development and dwarfism.

There are three types of Peter's anomaly (Lesnik Oberstein et al., 1993):

1. Type I iridocorneal: characterized by an incomplete separation of the cornea and iris and mild to moderate corneal opacity.
2. Type II lenticulo-corneal: characterized by an incomplete separation of the cornea and lens and severe corneal opacity that may involve the entire cornea.
3. Type III Peters plus syndrome: the corneal lenticular adhesion is associated with systemic disorders.

1.1.4.1.2 Axenfeld Rieger (A-R) syndrome

It is a common form of anterior segment dysgenesis that is associated with systemic structural anomalies (Tumer and Bach-Holm, 2009). It is inherited as an autosomal dominant pattern due to genetic mutation of *PITX2*, *PAX6* and *FOXC1* (Reis et al., 2012). The ocular manifestation include an opaque ring around the cornea known as posterior embryotoxon, hypoplasia of the iris, focal iris atrophy, and ectropion uveae (Figure 1-6) (Volkmann et al., 2011). The systemic defects include maxillary dental hypoplasia and thin upper lip. Pituitary anomalies, cardiac disease, oculo-cutaneous albinism and redundant peri-umbilical skin are also features. The iris is commonly adhered to the prominent Schwalbe's line (posterior embryotoxon). 50% of the patients have glaucoma. The A-R anomaly is always bilateral, but it might be asymmetric between the eyes (Chang et al., 2012).

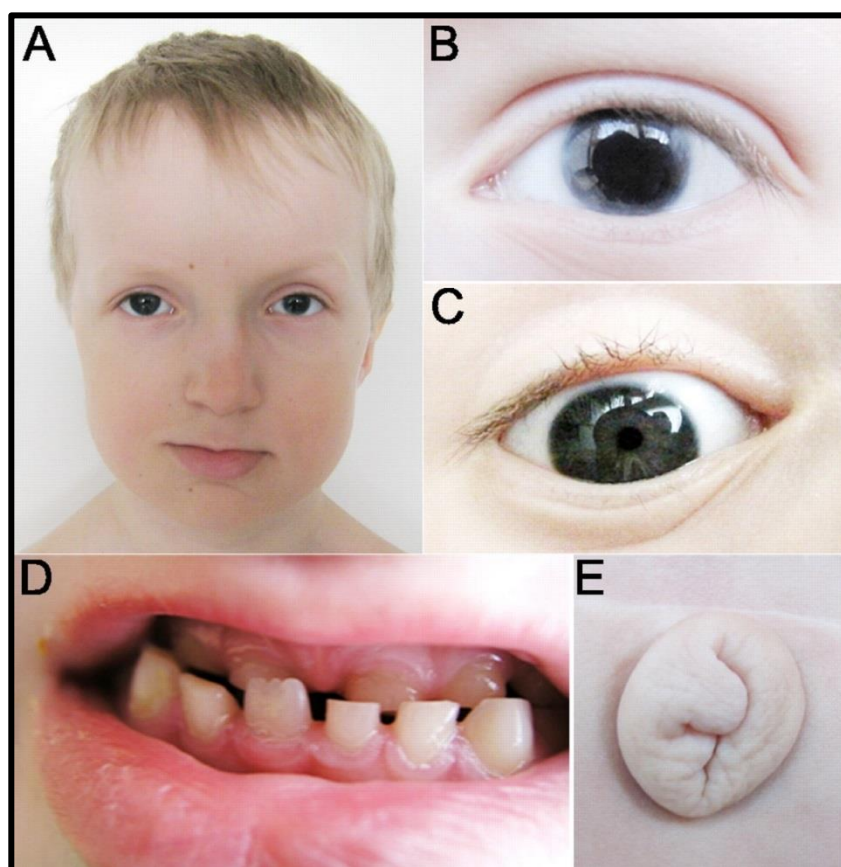


*Figure 1-6: Features of Axenfeld Rieger anomaly.
A) Facial features of thin upper lip, and broad nasal bridge, (B) Left eye with iris atrophy, (C) The pupil is not central. (D) Defect of teeth including dental dysplasia and maxillary hypoplasia, (E) Redundant periumbilical skin (Volkmann et al., 2011).*

1.1.4.2 Coloboma

Coloboma develops due to the failure of closure of the choroidal fissure during early stages of eye development. It is associated with a mutation in the *PAX2* gene. It can appear as a keyhole shaped defect of the iris (Yüksel and Karaer, 2013). Several parts of the eye such as the iris (most common), eyelids, lens zonules, cornea, ciliary body, choroid, retina or optic disc can be affected. It can be unilateral or bilateral. The vision can be normal or severely affected depending on the size of the defect. Coloboma (Munoz de Escalona Rojas et al., 2016) might be associated with microphthalmia, or glaucoma, nystagmus, scotoma, or strabismus.

1.1.4.3 Aniridia

Aniridia is a complete or partial iris hypoplasia. It is usually bilateral and associated with foveal hypoplasia. Paired box gene 6 (*PAX6*) mutation is the major cause of the classic aniridia phenotype (Dubey et al., 2015). *CYP1B1* mutations are also reported to associate with severe form of glaucoma, corneal opacification and aniridia (Alzuhairy et al., 2015). The common ocular findings associated with *PAX6* mutations are iris hypoplasia (Hingorani et al., 2012), nystagmus, cataract, glaucoma, corneal opacification and optic nerve hypoplasia. Aniridia can also occur in association with kidney nephroblastoma (Wilms tumor) and genitourinary anomalies (Orawiec et al., 2010, Schneider et al., 1996). The uncommon association of aniridia with intellectual disability and cerebellar ataxia (Gillespie syndrome) is also reported (Defreyn et al., 2007). Aniridia inheritance is mainly autosomal dominant in *PAX6* mutations, sporadic or rarely autosomal recessive such as in Gillespie syndrome.

1.1.4.4 Microcornea

Microcornea is defined by a corneal diameter less than 10 mm. It can be associated with glaucoma and congenital cataracts, sclerocornea, and corneal plana. It also can be a feature of systemic syndromes.

1.1.4.5 Congenital cataract

Cataract is an opacification of crystalline lens. Congenital cataract occurs at birth and affects about 15 per 10,000 children. The cataract may be unilateral or bilateral. 30% of congenital cataracts are associated with congenital rubella (Arnold, 1995). Twenty-nine genes have been identified to be associated with congenital cataracts (Huang and He, 2010). Congenital cataract can be associated with microcornea or iris coloboma. Affected children may also have autism, abnormal lower incisors, bifid uvula, or inguinal hernia. Cataract is diagnosed by an absent red reflex (Wan and VanderVeen, 2015) Deprivation amblyopia, nystagmus, and strabismus are complication of congenital cataract. The risk of amblyopia is very high if cataract is not removed surgically before the age of 10 weeks (Birch et al., 2009). Cataract is considered the most common treatable cause of blindness in childhood (Pi et al., 2012). However, cataract extraction is also associated with a risk of secondary glaucoma (Birch et al., 2009). Implantation of intraocular lens (IOL) is debatable. There is less tendency to implant IOLs after congenital cataract extraction due to the limited information about and normal and abnormal eye growth. However, a preference of IOL implantation in children over 2 years old has increased (Chan et al., 2012).

1.1.4.6 Congenital glaucoma associated with Sturge Weber syndrome

Sturge Weber syndrome (SWS) is a sporadic syndrome due to a somatic mutation in the *GNAQ* gene (Huang et al., 2017). It affects 1 per 50,000 live births and manifests in infancy and early childhood. SWS has a classic triad of port-wine stain (facial cutaneous venous dilation), ocular abnormalities and leptomeningeal capillary-venous malformation. Children commonly have epilepsy, headache, mental retardation and developmental delay. The most common ocular defect associated with SWS is glaucoma, which is unilateral in up to 70% of affected children (Akhter and Salim, 2014). Other ocular defects include presence of vascular abnormality of choroid, retina, sclera eyelid, conjunctiva and ciliary body (Mantelli et al., 2016). The exact mechanism of glaucoma is unknown. Developmental anomaly of the anterior chamber angle and elevated episcleral venous pressure are suggested to cause aqueous outflow obstruction and an increase the IOP

(Phelps, 1978). The anterior chamber angle in SWS has the same clinical and histopathological features of primary congenital glaucoma (Akhter and Salim, 2014).

1.1.5 Nystagmus

This is a repetitive, involuntary, to-and-fro oscillation of the eyes. It can be congenital or acquired and the movement can be horizontal, vertical, torsional or multiplanar (Serra and Leigh, 2002). According to etiology, nystagmus is classified into:

- 1) **Nystagmus associated with other ocular diseases:** This type accounts for 80 to 90% of childhood nystagmus that appears in the first two to three months of life. It occurs as bilateral, conjugate, horizontal movements that disappears during sleep. This type of nystagmus is associated with albinism and anterior segment dysgenesis. Presence of corneal opacities, cataracts, retinopathy of prematurity can also impair the visual development and results in nystagmus.
- 2) **Idiopathic infantile nystagmus:** This type is inherited in either X-linked, autosomal recessive, autosomal dominant form or is most frequently sporadic. The X-linked infantile nystagmus is associated with mutation in the *FRMD7* gene (AlMoallem et al., 2015, Tarpey et al., 2006) which affects the development of the retina (Thomas et al., 2014). It affects infants at two months who clinically have normal eyes and normal developmental milestones. Most affected patients have good visual acuity (Thomas et al., 2008) and are diagnosed only by exclusion of other neurological and ocular abnormalities (Zahn, 1978).
- 3) **Neurological nystagmus:** It is associated with space-occupying lesions, metabolic diseases, neurodegenerative disorders and trauma.

As mentioned above, the anterior segment dysgenesis is commonly associated with nystagmus. Clinical examination of the anterior segment of the eyes with nystagmus is difficult. Affected children with suspected anterior segment dysgenesis are often sedated and examined under general anesthesia. HH-OCT can provide the opportunity to image the anterior segment of children with nystagmus without sedation.

1.1.6 Ocular diseases associated with prematurity:

Premature born children usually have underdeveloped eyes at birth and are at high risk of ocular diseases. Exposure of eye to extra uterine environment before complete maturation and specialisation of ocular structure enhances unwanted changes that modify the normal ocular development. Therefore, premature born children become more susceptible to ocular problems. There is increased risk of retinopathy of prematurity, refractive error particularly myopia, strabismus, amblyopia and glaucoma. All these problems can cause impaired vision and blindness.

1.1.6.1 Retinopathy of prematurity (ROP)

Premature born babies, born before the 37 weeks gestation, are often kept in neonatal care unit and given oxygen to promote the development of premature lungs. Retinopathy of prematurity (ROP) affects premature babies who receive oxygen therapy. Normally, the growth of retinal vessels is stimulated by vascular endothelial growth factor (VEGF) (Aiello, 1996). If the immature retina is exposed to high oxygen, the vessels stop growing. Excessive oxygen causes vaso-obliteration in the immature retina. When the retina becomes ischemic, the released VEGF stimulates the arterial venous shunts and neovascularization. However, a recent review by Kandasamy and colleagues has questioned the role of VEGF in neovascularization, after reporting reduced VEGF level in premature children two months after birth (Kandasamy et al., 2017). The abnormal disorganized growth of retinal blood vessels may easily bleed and heal by scarring. Traction of the developed scarring may cause retinal detachment, the leading cause of visual loss and blindness in prematurity. ROP is also associated with increased risk of refractive error, amblyopia, strabismus and even glaucoma. ROP incidence inversely correlates with birth weight and gestational age.

1.2 Imaging of the eye by optical coherence tomography (OCT)

Optical coherence tomography (OCT) is a non-invasive optical imaging technique that can generate detailed images of ocular structures (Huang et al., 1991) and has the capability to capture a micrometre resolution image. The OCT produces high resolution cross-sectional topographic layers of tissues that mimics to some extent the histological structure (Figure 1-7).

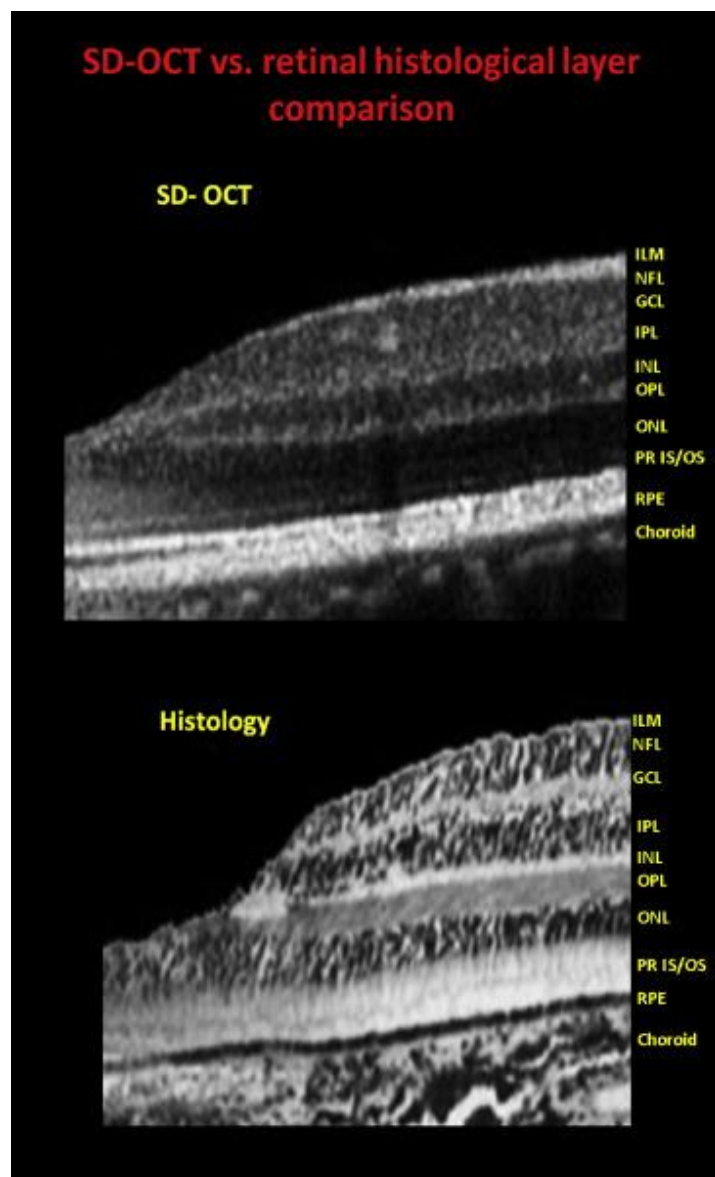


Figure 1-7: Comparison of optical coherence tomography (OCT) image and histology of retina.

The OCT generates retinal images that can show the different histological layers of the retina (Murthy et al., 2016).

1.2.1 Technology of optical coherence tomography

The technology of optical coherence tomography (OCT) involves measuring the different degrees of optical back-reflected light after directing a low-coherence (high-bandwidth near infrared) light beam onto the tissue of interest (Huang et al., 1991). The light in an OCT device is divided into two arms, a sample arm (light directed to the tissue) and a reference arm (light is reflected back from a mirror). The light directed to the tissue is absorbed variably by the layers, scattered and reflected back. The combination of reflected light from the sample arm and from the reference arm produces an interference pattern, which is transformed into a reflectivity profile by the photodetector (Huang, 2009).

Areas of the sample that reflect back a lot of light will create greater interference than areas that reflect back less light. When the paths taken by all of the interfering waves vary by less than the coherence length, the wave interference will be strong. Any light that is outside the short coherence length will not interfere (Fujimoto et al., 2000). The image formed from this reflectivity profile is called an A-scan. The A scan contains information about the location and spatial dimensions of the scanned structures. Lateral combination of a series of these axial depth scans (A-scans) gives rise to a cross-sectional tomography (B-scan). The scanning speed is measured by the number of A-scans acquired per second. A three dimensional (3D) image is produced from multiple B scans.

1.2.2 Types of optical coherence tomography (OCT)

Based on the above technology principles, two OCT platforms have been developed (Schmitt, 1999): **(A) time domain OCT** and **(B) Fourier domain OCT**.

1.2.2.1 Time domain optical coherence tomography (TD-OCT)

TD-OCT is the first-generation system of OCT, which uses a broadband light source containing a moveable reference mirror that moves for each A-scan to allow scanning of each depth position in the image. This limits the speed of scanning to a range of 1 to 5 mm/s.

1.2.2.2 Fourier domain optical coherence tomography (FD-OCT)

FD-OCT is a new-generation system that is based on spectral analysis of interferometric signals as a function of wave length. This technology uses a Fourier transformation algorithm of the spectral interferogram to produce an A-scan and has a fixed reference mirror to measure the depth. This results in better signal-to-noise ratio, faster sweeps and faster image acquisition, with better quality compared to the TD-OCT. There are two types of FD-OCT:

1.2.2.2.1 Spectral domain optical coherence tomography (SD-OCT)

SD-OCT uses a broadband light source along with an interferometer, a spectrometer to record spectral fringe patterns and a line-scan camera.

1.2.2.2.2 Swept source optical coherence tomography (SS-OCT)

SS-OCT uses a wavelength-swept laser as the light source that sweeps back and forth across a range of wavelengths. SS-OCT has a single detector with a high speed analog-to-digital (A/D) converter that enables deep tissue penetration, high imaging speeds, long imaging range and Doppler OCT flow analysis compared to SD-OCT technology.

1.2.3 Development and history of optical coherence tomography

The first study of ocular use of OCT was published in 1991 and presented quantitative measurements of retinal thickness (Huang et al., 1991). In 1994, Izatt et al presented the first use of TD-OCT as a diagnostic technique in imaging the anterior segment of human eye. This OCT version has a superluminescent diode light of 830nm wave length, which has enabled the visualization of corneal thickness, corneal epithelium, anterior chamber depth, iris thickness and dense nuclear cataracts of lens (Izatt et al., 1994). The first commercially available TD-OCT was the Stratus TD-OCT 3000 (Carl Zeiss Meditec) in 1995, used for posterior segment imaging. Since then, the OCT technology has rapidly advanced. Radhakrishnan et al (2001) has described the first use of SD-OCT for anterior segment imaging. The SD-OCT has a light source of 1310 nm wave length, which allows better penetration in the scattering tissues like sclera and iris. Therefore, better visualization of morphological details of deep structures like anterior chamber angle is possible. (Radhakrishnan et al., 2001). Nowadays, OCT has become a prominent clinical standard that is widely used for the diagnosis and follow up of ocular diseases.

In the mid-2000s, two anterior segment OCT (AS-OCT) devices became commercially available for anterior segment imaging based on TD- OCT technology (Table 1-2). In 2007, four SD-OCT devices that can be used for posterior and anterior segment imaging, have been presented on the market: Cirrus HD-OCT (Carl Zeiss Meditec), Spectralis OCT (Heidelberg), Spectralis HRA+OCT (Heidelberg) and RTVue-100 (Optovue). The criteria of these different devices is described in table 1-3. The first commercially available SS-OCT is the Casia OCT SS-1000 (Tomey Corporation, Nagoya, Japan) in 2008. This advanced device provides an OCT image of the whole anterior segment.

In a comparison study between Spectralis SD-OCT and Topcon Atlantis DRI OCT-1 SS-OCT in imaging posterior staphyloma (pathological posterior outpouching of the wall of the eye) in highly myopic eyes, the SS-OCT technology of Topcon provided superior imaging capabilities to the Spectralis. Topcon Atlantis OCT has better delineation of the choroid and better visualization of retino-choroidal structures (Lim et al., 2014). Wong et al reported that HD Cirrus SD-OCT provides higher resolution images than Visante TD-OCT (Wong et al., 2009). Marion et al reported excellent reproducibility and agreement

between two spectral domain optical coherence tomography devices (Spectralis and Cirrus SD-OCTs) for anterior chamber angle measurements (Marion et al., 2015). Marion et al suggest possible interchangeability between SD-OCT devices.

The aforementioned devices are based on head and chin fixation. Therefore, their clinical application is limited to cooperative patients, which are usually old enough to follow the examiner's instructions. Many attempts to scan children using the Stratus TD-OCT (Skarmoutsos et al., 2006) and Cirrus SD-OCT (Querques et al., 2008) have previously been reported for children over five years old. However, there were difficulties with the children's cooperation and positioning on the fixed chin table-mounted OCT scanner. Hand held OCT (HH-OCT) was designed to facilitate the imaging of paediatric patients.

Table 1-2: Examples of commercially available time domain optical coherence tomography.

Time domain optical coherence tomography	
Visante OCT (Carl Zeiss Meditec, Dublin, CA)	Slit-lamp OCT (Heidelberg Engineering, Germany)
First used 2005	First used 2006
Has a superluminescent diode wave length 1310 nm	Has a superluminescent diode wave length 1310 nm
2000 A scan /sec	200 A scans/sec
18 µm axial resolution	10 to 25 µm axial resolution
Axial scan depth is 6mm	Axial scan depth is 7mm
It has semi-automated built in software for quantitative analysis of anterior chamber angle (ACA)	It was designed at the University of Lubeck, Germany by Hoerauf et al with wavelength of 830 nm. Then modified with a super-luminescent diode at 1310 nm
Uses internal fixation	Uses external fixation

Table 1-3: Examples of commercially available Fourier domain optical coherence tomography (FD-OCT).

Spectral domain optical coherence tomography (SD-OCT) devices			Swept source optical coherence tomography (SS-OCT) devices	
Cirrus HD-OCT (Carl Zeiss Meditec, Dublin, CA)	RTVue FD-OCT (Optovue, Fremont, CA)	Spectralis AS-OCT (Heidelberg Engineering, Heidelberg, Germany)	CASIA SS-1000 OCT (Tomey Corporation, Nagoya, Japan)	DRI OCT Triton, SS-OCT(Topcon, Tokyo, Japan)
First used 2007	First used 2006	Approved by FDA in 2012	First used 2008	First used 2015
Superluminescent diode wave length 840 nm	Superluminescent diode wave length 830 nm	Superluminescent diode with a peak wavelength of 870 nm	Swept-source laser 1310 nm wave length	Swept-source laser 1050 nm wave length
27000 A-scans /sec	26000 A-scans /sec	40000 A-scans /sec	30000 A-scans/sec	100000 A-Scans/sec
5 µm axial resolution, 15 lateral resolution and 6mm deep	5 µm axial resolution, 15 lateral resolution and 6mm deep	7 µm axial resolution. The only SD-OCT with TruTrack active eye tracking	10 µm axial resolution, 30 µm transverse resolution and 6mm deep	-
ImageJ software is used for image analysis	Provided with software that can measure anterior chamber parameters	Built in software for measurement of ACA based on manual placement of scleral spur	Built in software for measurement of ACA based on manual placement of scleral spur	-

TD-OCT = Time domain optical coherence tomography, FD-OCT = Fourier domain optical coherence tomography, SD-OCT =Spectral domain optical coherence tomography, SS-OCT = swept source optical coherence tomography. ACA = Anterior chamber angle. AS = anterior segment. HD = high definition.

1.2.4 Hand-held spectral domain optical coherence tomography (HH-OCT)

The hand-held SD-OCT (Leica Microsystem Ltd) became available in 2007. It has a hand piece that can be positioned at any angle for scanning. It allows portable scanning of patients from premature infants up to adults, seated or supine, awake or under anaesthesia (Figure 1-8).



Figure 1-8: Hand held C2300 Envisu SD-OCT.

The hand-held probe (1.6 kg) is connected through a 1.3 meter fiberoptic cable to a movable cart housing the SD-OCT with a computer. It has a superluminescent diode light source that generates light with a wave length of 840nm (which is shorter than the usual wave length used in anterior segment OCT). HH-OCT produces a high resolution image with axial resolution of 3.3 μ m resolution (2.4 μ m in tissue) and a 3.4 mm scan depth (2.5 mm in tissue). The lens, attached to the hand-held probe, is removable. There are different lenses, available for imaging the posterior and the anterior segments of the eye.

HH-OCT has enabled high resolution ophthalmic imaging of children's retinae. HH-OCT was used in imaging the retina of full term infants under sedation with general anaesthesia (Scott et al., 2009) and the retina of a baby with shaken baby syndrome (Muni et al., 2010). HH-OCT was also successfully used in scanning the fovea of normal children and infants of different ages without sedation (Gerth et al., 2009, Lee et al., 2015) and premature neonates (Maldonado et al., 2010). HH-OCT has also been successfully applied in studying the foveal morphology in children with infantile nystagmus (Lee et al., 2013b), the optic nerve development in healthy children (Patel et al., 2016) and aiding the diagnosis of children with anterior segment dysgenesis (Pilat et al., 2017).

Folgar et al has compared the lateral and axial measurement of 8 types of SD-OCT devices including HH-OCT and reported that HH-OCT has low variability and high reproducibility. This implies that the hand instability of a human operator does not introduce significant additional errors while holding the hand-held probe (Folgar et al., 2014).

1.2.5 Anterior segment optical coherence tomography (AS-OCT)

The gold standard for visualizing the anterior chamber of the eye is gonioscopy. However, gonioscopy only provides a qualitative assessment. Unlike ultrasound biomicroscopy (UBM) or OCT which can provide quantitative measurements of the anterior segment. The main advantages and disadvantages of each method are illustrated in table 1-4. OCT is a non-contact method that has the least risk and the ability to provide excellent qualitative and quantitative assessments of the anterior segment of the eye.

Table 1-4: Comparison between different methods of visualizing the anterior chamber.

Gonioscopy	Ultrasound bio-microscopy	Optical coherence tomography
The current gold standard for anterior chamber angle assessment since 1899 (Dellaporta, 1975)	First use of UBM (Pavlin et al., 1992)	First use of OCT for imaging anterior segment (Izatt et al., 1994)
It should be performed in a relatively dark room and sitting position	Supine position	Sitting position
Qualitative assessment	Qualitative and quantitative assessments	Qualitative and quantitative assessments
Subjective measurements	Objective measurements	Objective measurements
Invasive procedure, where the lens is in direct contact with the eye	Invasive procedure, with a water bath needed to image the eye	No direct contact with the eye
The angle morphology is prone to change due to pressure of the gonio-lens with potential risk of errors. The position of lens and illumination intensity affects the assessments	The angle morphology is prone to change due to pressure of the UBM probe and potential risk of errors due to illumination intensity	Potential of errors due to illumination intensity
Cannot visualize structures posterior to iris. It used mainly for visualising the iridocorneal angle	It can visualize structures posterior to the iris such as the ciliary body, lens zonules and anterior choroid	It cannot visualize structures posterior to iris but it can produce detailed images of retina
It has substantial inter-observer variability (Friedman and He, 2008)	Generally, it had poor intra-observer and inter-observer reproducibility in angle measurements (Tello et al., 1994, Urbak et al., 1998)	Excellent intra-grader but moderate inter-grader reproducibility of anterior chamber measurements using Visante AS. OCT (Maram et al., 2015b)

Information obtained from (Tello et al., 1994, Urbak et al., 1998, Pavlin et al., 1992, Izatt et al., 1994, Maram et al., 2015b) (Dellaporta, 1975).

Qin et al detected a high correlation between RTVue FD-OCT and gonioscopy in measurement of anterior chamber angle width (Qin et al., 2013). Sakata and colleagues compared Visante TD-OCT and gonioscopy and found that Visante was more sensitive in detecting anterior chamber angle closure than gonioscopy. The Visante AS-OCT detected greater closed anterior chamber angles than gonioscopy, particularly in the superior and inferior quadrants (Sakata et al., 2008a).

In a comparison study between gonioscopy and UBM, Barkana et al showed high agreement between gonioscopy and UBM (Barkana et al., 2007), while Narayanaswamy et al reported overestimation of angle width by gonioscopy compared to UBM (Narayanaswamy et al., 2004).

Similar to UBM, AS-OCT provides quantitative anterior chamber angle measurements. AS-OCT was capable in detecting the presence of narrow anterior chamber angles better than gonioscopy (Radhakrishnan et al., 2005a). In fact, AS OCT was easier to use and did not require contact with the eye.

Imaging of the anterior segment of children using these aforementioned methods is difficult to perform. El Shakankiri et al have reported that UBM is a valuable tool for evaluating the anterior segment of paediatric patients. However UBM requires examination of children under anaesthesia (El Shakankiri et al., 2009). The Visante TD-OCT has been used for evaluating the abnormal structures of anterior segment of paediatric patients. However, the images acquisitions of young children were challenging and difficult (Cauduro et al., 2012).

HH-OCT is a child-friendly device and has the advantage of a flexible movement of hand-held probe, which can easily positioned to scan the eyes of the young children without sedation. The focus of this thesis is to apply the HH-OCT for imaging of the anterior segment of the children.

1.3 Literature review of the application of anterior segment OCT

Anterior segment OCT has been widely used in adults to establish normative quantitative data and to understand the pathology of underlying developmental abnormalities of the cornea, anterior chamber angle structures and iris.

1.3.1 Application of OCT in visualising the cornea

1.3.1.1 Normative data of the cornea

The quantitative measurements of the cornea (Figure 1-9) includes:

1. Central corneal thickness (CCT)
2. Anterior corneal curvature (ACC)
3. Posterior corneal curvature (PCC)
4. Posterior corneal arc length (PCAL)

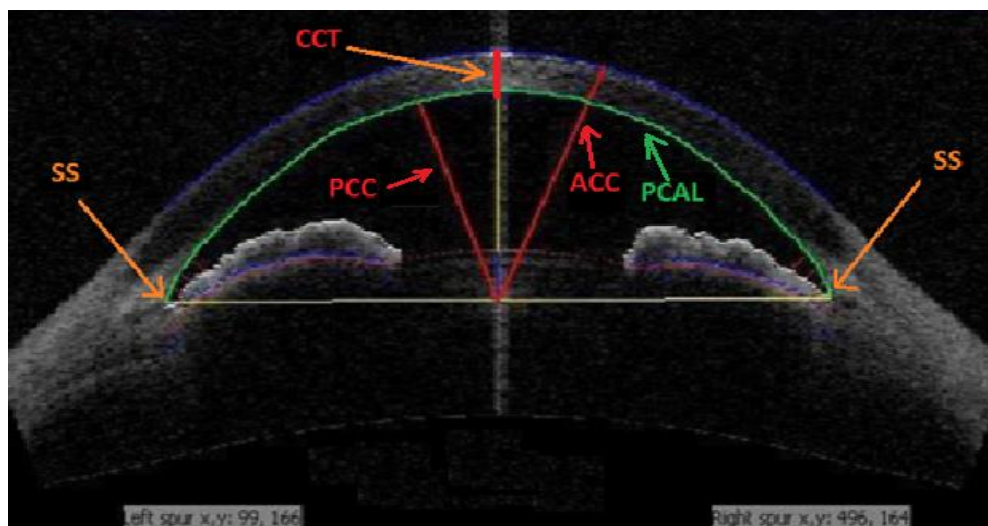


Figure 1-9: Measurements of the cornea by OCT.

A Visante TD-OCT image of the anterior chamber with illustrated anterior chamber landmark and the corneal measurements (Ang et al., 2012) is shown. SS = scleral spur, ACC = anterior corneal curvature, PCC = posterior corneal curvature and PCAL= posterior corneal arc length. PCAL is the distance between scleral spurs on the posterior border of cornea. The parameters were calculated automatically using ZAAP software (The Zhongshan Angle Assessment Program [Guangzhou, China]), following manual identification of the scleral spur.

In a study of 50 eyes, Li et al measured the mean central corneal thickness using both SL-OCT (Heidelberg Engineering, Heidelberg, Germany) and Visante OCT (Carl Zeiss Meditec, Dublin, CA). The CCT measurements were reliable and showed comparable agreement with ultrasound pachymetry (Li et al., 2008). This was in accordance with the findings of other studies that reported the CCT of $533 \pm 53 \mu\text{m}$ (Mueller et al., 2010) and $581 \pm 48 \mu\text{m}$ using SL-OCT and $568 \pm 61 \mu\text{m}$ using the Visante-OCT (Wirbelauer et al., 2009, Viestenz et al., 2009).

Using Visante AS-OCT, Ang et al presented a normative database of the corneal measurements of healthy Indian adults (> 40 years old). These measurements include a mean CCT of $561.4 \pm 34.1 \mu\text{m}$, a mean PCAL of $13.85 \pm 0.54 \text{ mm}$, a mean ACC of $7.17 \pm 0.35 \text{ mm}$, a mean PCC of $6.45 \pm 0.35 \text{ mm}$ and a mean anterior chamber depth (ACD) of $2.72 \pm 0.37 \text{ mm}$. This study suggested the posterior corneal arc length as a novel anterior segment parameter that can be used to estimate the ACD owing to the positive and strong correlation between PCAL and ACD independent of sex and age (Ang et al., 2012). The PCAL was higher in Indian compared to Chinese ethnicity. However, this still needs to be confirmed in a larger study (Yuen et al., 2010).

Yoo et al found thinner CCT in normal tension glaucoma compared to primary open angle glaucoma (POAG) and normal controls (Yoo et al., 2011). The CCT was reported to play an important role in the measurement of intra-ocular pressure (IOP) (Brandt et al., 2001, Uva et al., 2011).

The above findings were based on using the TD-OCT with a wavelength of 1310 nm. Using RTVue, a SD-OCT device with a wave length of 830nm, it was possible to measure the central epithelial thickness of cornea, which was $53.4 \pm 2.7 \mu\text{m}$. The central epithelial thickness was constant compared to the paracentral corneal epithelial thickness and nasal and temporal limbal epithelial thickness. The nasal and temporal limbal epithelial thickness became thinner with increasing age. In contrast, there was no effect of age on limbal epithelial thickness at the superior and inferior quadrants (Yang et al., 2014).

1.3.1.2 Development of central corneal thickness

1.3.1.2.1 Development of central corneal thickness in adults

The association between CCT and aging has been widely investigated. Schuster and colleagues reported an increase in CCT with age among adults of working age using AS-OCT (Schuster et al., 2016). While no significant change in CCT with age was detected in a sample of 4698 participants (aged 35 to 74 years), using pachymetry (Hoffmann et al., 2013). In contrast, in a recent longitudinal study that included 758 controls and 58 glaucomatous patients (mean age 59.9 ± 9.2 years), CCT was reported to decrease with age using pachymetry. The rate of CCT reduction was greater in glaucoma patients compared to controls (Mwanza et al., 2018). Previous longitudinally design publications have detected similar findings in adult age group using pachymetry (Choudhari et al., 2013, Hashemi et al., 2016).

1.3.1.2.2 Development of central corneal thickness in children

CCT was reported to decrease with age after birth and reach an adult thickness by age of 3 years (Ehlers et al., 1976). Higher CCT is reported in male (626.70 ± 67.46 µm) compared to female (577.45 ± 45.50 µm) new-borns using a pachymetry (Ferreira and Tavares, 2017).

1.3.1.3 Central corneal thickness in congenital glaucoma

Even with controlled IOP, glaucoma patients had thicker CCT compared to controls (Amini et al., 2012). CCT is higher in congenital glaucoma compared to age-matched healthy controls before treatment due to corneal oedema and reduced to a normal value postoperatively (Paletta Guedes et al., 2016). A thicker cornea is suggested to be associated with higher IOP measurements (Prost and Oleszczynska-Prost, 2005).

1.3.1.4 Application of AS-OCT in visualising congenital corneal abnormalities

Majander et al has observed three distinct phenotypes of congenital corneal opacity among seven children (age ranges between 2 days to 2.5 years) using Casia SS-OCT (Majander et al., 2012). These phenotypes are: **(a) type 1 Peters' anomaly** of iridocorneal adhesion **(b) type 2 Peters anomaly** of lenticulo-corneal adhesion, and **(c) congenital corneal staphyloma** with complete corneal adhesion. It was possible to assess the characterization of defects into mild, moderate and severe. This study has proved that AS-OCT is a valuable non-invasive method in the diagnosis and follow up of paediatric patients (Majander et al., 2012).

1.3.2 Application of AS-OCT in measurements of the anterior chamber

The TD-OCT has lower resolution compared to SD-OCT. However, the light source of TD-OCT (1310 nm) enables the imaging of the entire anterior chamber in one image (Figure 1-10A). Therefore, TD-OCT is widely used in measuring the anterior chamber. The SD-OCT cannot produce an image showing the entire depth of anterior chamber (Figure 1-10C), because the light source of SD-OCT devices (wavelength of 840nm) has a scanning depth of less than 3.5 mm. However, using an adapted external lens with the Cirrus SD-OCT, it was possible to obtain an image showing the entire anterior chamber (Figure 1-10D) (Tun et al., 2017) . SD-OCT can provide precise information about small areas of the anterior chamber such as anterior chamber angle because of its high resolution and better tissue penetration capabilities. The CASIA SS-OCT has a scanning depth of 6 mm because it has a light source of 1310 nm wavelength. Hence, high resolution image of entire anterior chamber is achievable using the SS-OCT technology (Figure 1-10B).

The various anterior chamber parameters measured by AS-OCT are:

- 1. The anterior chamber width (ACW);** the linear distance between the two angle recesses or scleral spurs (Figure 1-1).
- 2. The anterior chamber depth (ACD);** defined as a distance between the inner margin of the cornea and the anterior wall of lens (Figure 1-1).
- 3. Anterior chamber area (ACA).** The anterior chamber area (ACA) can be defined as the cross-sectional area of anterior segment bounded by the corneal endothelium, the anterior surface of iris, and the anterior surface of lens (within the pupil) (Wu et al., 2011)(Leung and Weinreb, 2011).
- 4. Anterior chamber volume (ACV).** Anterior chamber volume (ACV) is calculated by drawing a vertical axis through the midpoint of anterior chamber area and rotating the ACA 360° around this vertical axis (Wu et al., 2011)
- 5. Crystalline lens vault:** This is the perpendicular distance between the anterior pole of crystalline lens and the horizontal line joining the two scleral spurs on horizontal AS-OCT (Figure 1-1).
- 6. Anterior chamber (irido-corneal) angle (ACA) measurements.** These measurements reflect the width of the anterior chamber angle.

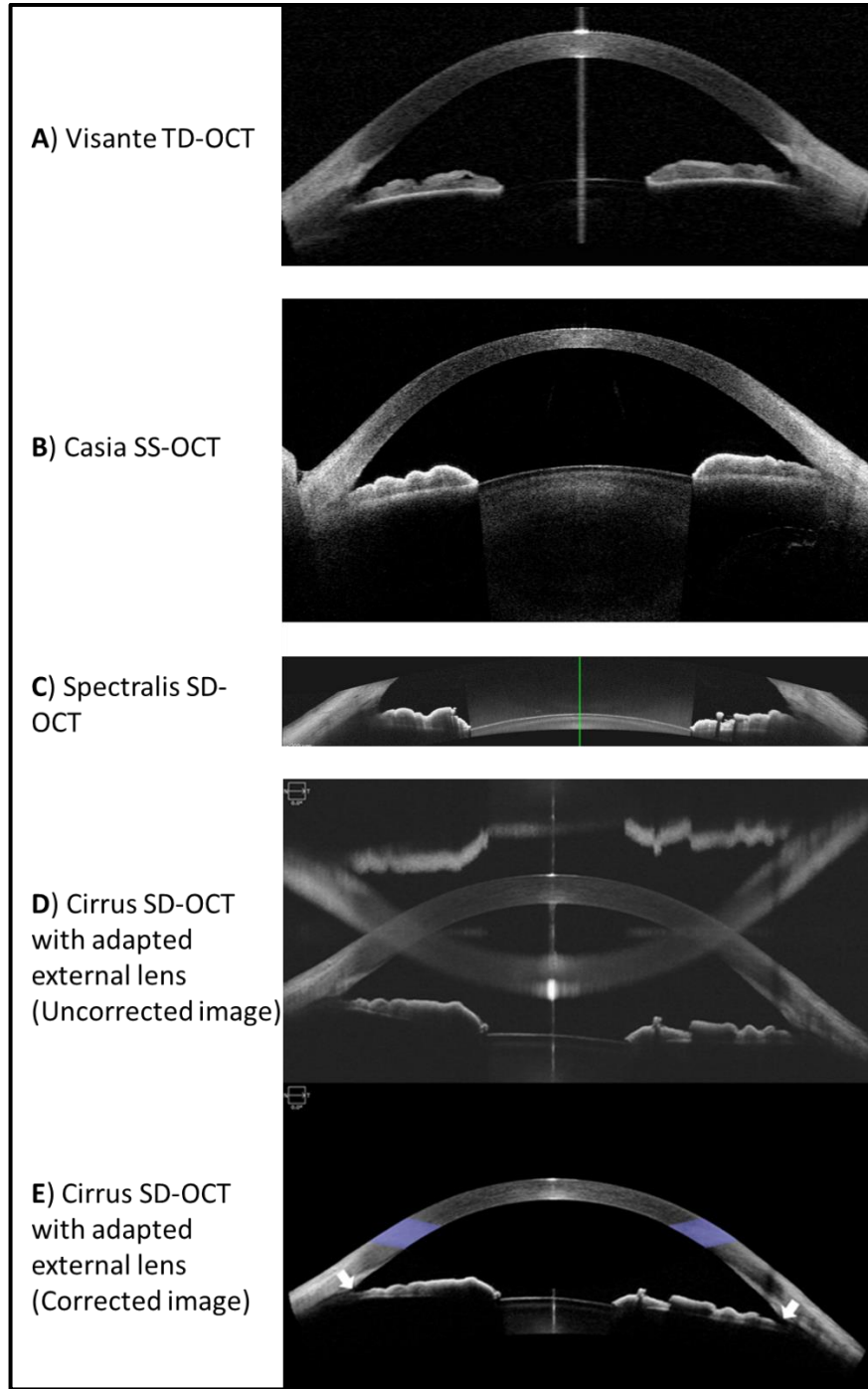


Figure 1-10. Anterior chamber images of different OCT technology.

A) TD-OCT image shows the whole anterior chamber. B) SS-OCT image shows the whole anterior chamber in one image with better resolution and quick capturing. C) SD-OCT image showing that SD-OCT can produce better resolution image but has a scanning depth of less than 3 mm, which partially showing the anterior chamber. D) An image obtained by Cirrus SD-OCT adapted with external lens. The external lens has enabled capturing of whole anterior chamber. (E) Post imaging correction of the Cirrus SD-OCT is performed to adjust the image and eliminate the reflection of cornea (Xu et al., 2017, Tun et al., 2017).

1.3.2.1 Anterior chamber width (ACW)

Kohnen et al have reported that ACW can represent accurate measurements of the anterior chamber compared to corneal diameter, measured with instruments such as the Orbscan & IOL Master (Kohnen et al., 2006). Goldsmith et al presented for the first time quantitative measurement of anterior chamber using the prototype of Visante TD-OCT that was developed specifically for anterior segment imaging (Goldsmith et al., 2005b). Goldsmith and co-authors reported an ACD of 2.99 ± 0.323 mm, ACW of 12.53 ± 0.47 mm and LV of 0.39 ± 0.27 mm among 40 eyes of 20 normal adult volunteers. This study showed that ACW value is bigger than the mean corneal diameter of 11.78 ± 0.57 μm and questioned whether corneal diameter is an accurate indicator of anterior chamber biometry. In a study of 270 eyes of 148 subjects over 18 years old using Visante, Huang et al reported the mean ACW of 11.58 ± 0.37 mm (Huang et al., 2015b), which is similar to the corneal diameter value reported by Goldsmith. This implies that other factors such as age, gender, and ethnicity play a role on the measurement of ACW. Yan and colleagues have found that vertical ACW is anatomically larger compared to horizontal ACW and postulated that the shape of the anterior chamber is an erect ellipse (Yan et al., 2010).

1.3.2.2 Anterior chamber depth (ACD)

Clinically, the ACD is usually measured by either the IOL Master or Pentacam. These devices have been approved as accurate methods for ACD measurement (Dinc et al., 2010, Sayed and Alsamman, 2015) and showed excellent agreements (*Fernandez-Vigo et al., 2015a, Utine et al., 2009*). Fernandez-Vigo et al studied 1006 Caucasians (aged 18 to 84 years) and reported a mean ACD of 3.30 ± 0.42 mm (range 2.13 - 4.50 mm) using the IOL Master and 3.35 ± 0.43 mm (range 2.07 - 4.63mm) using the Pentacam. Sng et al found similar ACD values in the adult Asian population (1543 subjects) with mean ACD of 3.24 ± 0.35 mm using IOL Master (Sng et al., 2012). Rufer et al reported smaller ACD values among 390 healthy Caucasian subjects using Orbscan II compared to IOL Master. This study also reported a linear decrease in ACD with age, about 0.58mm over a period of 50 years (Rufer et al., 2010).

1.3.2.3 Anterior chamber area and volume

Wu et al studied the relation between the risk of closed angle and anterior chamber area (ACA), volume (ACV) and depth (ACD) among 1922 subjects using Visante TD-OCT. Wu and co-authors reported mean ACA of 20.1mm^2 (range $10.4\text{-}33.6\text{ mm}^2$) and the mean ACV of 134.8 mm^3 (range, $56.6\text{-}242.1\text{mm}^3$). Small ACA and ACV were independently associated with presence of narrow anterior chamber angles. The authors proposed the optimal cut-off point for the detection of the eyes with narrow angles at 17.9 mm^2 for ACA (AUC: 0.877; 95% CI, 0.856 - 0.899) and 116.0 mm^3 for ACV (AUC: 0.877; 95% CI, 0.855-0.898). The ACA and ACV showed a stronger association with narrow angles in women compared to men. In a similar study, Huang et al has reported that females have smaller anterior chamber areas and volumes in addition to narrow anterior chamber. This may explain why females have higher risk of closure angle glaucoma compared to males (Huang et al., 2015a). Wang *et al* reported a significant difference in the anterior chamber volume in eyes with normal, deep and shallow anterior chambers and a significant difference in the ACV in eyes before and after iridotomy (a surgical incision of iris to facilitate aqueous humour drainage from posterior to anterior chamber) (Wang et al., 2007). Wang and colleagues studied four different ethnicity; American Caucasians, American Chinese, southern and northern mainland Chinese and reported that Chinese had significantly smaller ACA and ACV and smaller ACA/ACV ratio compared to Caucasians. The ACA and the ACV decreased with advanced age in both Chinese and Caucasians. The Chinese females, unlike females of other ethnicity, had smaller ACA/ACV than that of males (Wang et al., 2012).

1.3.2.4 Lens parameters

Nongpiur et al measured Lens vault thickness (LV) in 102 Chinese with angle closure and 176 normal controls, using Visante AS-OCT, and found a significantly greater lens vault thickness in angle closure glaucoma compared to healthy controls (Nongpiur et al., 2011b). The mean lens vault thickness is $901 \pm 265\text{ }\mu\text{m}$ in angle closure verse $316 \pm 272\text{ }\mu\text{m}$ in controls ($p <0.001$). In addition, healthy women have significantly greater LV compared to men ($379.07\text{ }\mu\text{m}$ vs. $260.09\text{ }\mu\text{m}$ respectively; $p <0.001$) and lens vault increases with age (Nongpiur et al., 2011b). Nongpiur and colleagues have proposed for the first time the lens

vault (LV) as a potential novel indicator of angle closure. It was suggested that the increased lens thickness pushes the peripheral iris against the trabecular meshwork which subsequently imposes contact between ciliary iris and trabecular meshwork. In the same time, the irido-lenticular contact causes pupillary block. Hence, obstructing both the flow of aqueous humour from posterior to anterior chamber and through the trabecular meshwork. Yan et al presented a mean ACD of 3.50 ± 0.37 mm and LV of 0.11 ± 0.023 mm using slit lamp AS-OCT and reported an increase in the crystalline lens anterior pole by approximately 11 μm per year (Yan et al., 2010).

1.3.2.5 Anterior chamber (iridocorneal) angle

The quantitative anterior chamber angle biometry was measured for the first time using UBM based on manual identification of scleral spur (Pavlin et al., 1992). TD-OCT produces similar anterior chamber image to the UBM with better resolution. Therefore, the manual detection of the scleral spur is applied in the analysis of TD-OCT image. The TM histologically extend from SS to SL. Due to the fact that neither the SL nor the TM is visible on UBM or TD-OCT, the TM length (TML) is estimated based on identification of SS, as 500 μm to 750 μm anterior to SS (Bald et al., 2012)(Tian et al., 2011). SD-OCT produces high quality images where the visualization of Schwalbe's line is possible (Wylegala et al., 2009, Wong et al., 2009, Asrani et al., 2008)(Chen et al., 2018). The ability of identification of the SL enables the measurement of actual TML.

1.3.2.5.1 Visualization of scleral spur

The scleral spur is identified as a point of the junction of the reflective sclera to the less reflective ciliary body (Sakata et al., 2008b). Cumba et al identified the SS as an inward protrusion of the sclera at the inner corneo-scleral junction which represents the change in the curvature of corneo-scleral aqueous interface (Cumba et al., 2012, Sakata et al., 2008c). Usui et al marked the scleral spur as the most posterior end of the trabecular meshwork on the posterior corneo-scleral-aqueous interface (Usui et al., 2011). Many publications reported that the identification of SS is sometimes difficult and often undetectable in the images obtained by TD-OCT (Sakata et al., 2008c, Liu et al., 2010).

In addition, many papers reported that the visualisation of scleral spur is also not always possible on SD-OCT images (Cheung et al., 2011a, Nongpiur et al., 2011a). The light source, of 830-nm wave length, of the SD-OCT system limits the clear visualisation of the anterior chamber angle structure, due to the backscattering properties of the anterior portion of the sclera to the OCT light (Hoerauf et al., 2002a). In order to allow a better light penetration and visualization of angle structure, the OCT devices, specifically designed for anterior segment imaging (including TD-OCT and SS-OCT), have a light source of 1310 nm wave length (Hoerauf et al., 2002a, Hoerauf et al., 2002b). The SD-OCT, used for anterior segment imaging, with a light source of 840 nm wave length, has weak penetration capability at the angle area. This system has a disadvantage of drop-off in signal intensity

with depth, which makes the contrast at angle area very low. Quek et al suggested that increasing the width of image to include both angles and apply post acquisition image processing can be a possible solution of the attenuated details of the scleral spur (Quek et al., 2012b).

The SS-OCT has a high scanning speed, higher sensitivity and less signal drop-off properties compared to the SD-OCT system. This allows better visualization of anterior chamber. The CASIA SS-OCT, has enabled the identification of SS in up to 99 % of acquired images (Tun et al., 2013b, Cumba et al., 2012, Usui et al., 2011). Summary of literatures about identification of scleral spur using different OCT devices is shown in table 1-5.

Table 1-5: The percentage of identification of scleral spur in various studies using different anterior segment OCT devices.

Authors and year	Identification of scleral spur %	OCT device
Sakata et al (2008)	72%	Visante TD-OCT (Carl Zeiss Meditec, Inc.)
Wong et al (2009)	78.9%	Cirrus HD OCT (Carl Zeiss Meditec Inc.) with 60 D lens
Narayanaswamy et al (2010)	75%	Visante TD-OCT
Cheung et al (2011)	85%	Cirrus HD-OCT
Cumba et al (2012)	99%	Casia SS-1000 OCT (Tomey, Nagoya, Japan)
Quek et al (2012)	82%	Cirrus HD-OCT
	66%	IVue (Optovue, Inc)
Qin et al (2013)	81%	RTVue (Optovue, Inc)
Tun et al (2013)	99.7%	Casia SS-1000 OCT
McKee et al (2013)	95 to 100 %	Casia SS-1000 OCT
	50 to 95 %	Casia SS-1000 OCT
Tay et al (2015)	45%	Spectralis OCT (Heidelberg, Germany)
	84.8%	Visante TD-OCT

1.3.2.5.2 Visualization of Schwalbe's line (SL)

The Schwalbe's line visibility has been reported to range between 44 % up to 100 % using SD-OCT and SS-OCT technology (Wong et al., 2009). Summary of the studies that compared between the identification of Schwalbe's line and scleral spur is shown in table 1-6.

Table 1-6: Summary of publications comparing the identification of scleral spur and Schwalbe's line using Fourier domain optical coherence tomography (FD-OCT) devices.

Authors and year	Identification of SS	Identification of SL	OCT machine
Tun et al (2013)	99.70%	98.80%	Casia SS-OCT.
Quek et al (2012)	82%	77%	Cirrus HD-OCT
	66%	74.50%	IVue SD-OCT
Wong et al (2009)	78.90%	93.30%	Cirrus SD-OCT With 60 D lens
Cheung et al (2011)	85%	95%	Cirrus SD-OCT
Qin et al (2013)	80.80%	97.70%	RTVue SD-OCT

SS = scleral spur , SL = Schwalbe's line TD-OCT = Time domain optical coherence tomography, FD-OCT = Fourier domain optical coherence tomography, SD-OCT = Spectral domain optical coherence tomography, SS-OCT = Swept source optical coherence tomography, ACA = Anterior chamber angle, and HD = high definition.

The visibility of SL was better than SS using Cirrus HD-OCT; that was adapted for anterior segment (Cheung et al., 2011a, Wong et al., 2009). Cheung et al has recommended the use of Schwalbe's line as a new landmark for the anterior chamber angle measurements instead of SS. Cheung and colleagues have reported a strong correlation of SL parameters with gonioscopy grading in closed anterior chamber angles (Cheung et al., 2011a). Qin et al reported better visualization of SL using RTVue (Optovue Inc, Fremont, CA, USA) and found high correlation between the angle measurement derived from SL and gonioscopy (Qin et al., 2013).

Many studies suggested that the visibility of angle landmarks depends on the type of OCT device. A study comparing Cirrus to IVue SD-OCT found that IVue provided better visualization of SL than Cirrus. In contrast, Cirrus provided images with clearer SS than SL (Quek et al., 2012b). In this study, Quek et al has identified SS in 66% and SL in 74.5% in

IVue OCT images. While SS was identified in 82% and SL was identified in 77% of total images of Cirrus OCT. This discrepancy is suggested to result from the differences of image quality of the two OCT systems and the subjective interpretation of images between observers. Kiernan et al reported that inter-device comparison is not practical, due to the different scanning software of the commercially available OCT systems (Kiernan et al., 2010).

1.3.2.5.3 Agreement between different OCT devices in anterior chamber angle measurements

Leung et al compared the anterior chamber angles measurements obtained by two TD-OCT and reported poor agreements between Visante OCT and Slit lamp OCT. The difference between these two machines for trabecular iris angle degree (TIA) was detected within 28° in 95% of observations. This indicated that different TD-OCT system measurements are not interchangeable (Leung et al., 2008). In contrast, Wylegala and colleagues reported a high correlation and no statistical difference between angle measurements based on identification of scleral spur obtained by Visante TD-OCT and RTVue-100 SD-OCT (Wylegala et al., 2009). Marion et al reported excellent inter-instrument, intra-instrument, intra-observer and inter-observer reproducibility in a study comparing the Spectralis and Cirrus OCTs, the two SD-OCT devices. This suggests possible interchangeability of the measurements obtained by different SD-OCT devices (Marion et al., 2015).

1.3.2.5.4 Anterior chamber angle measurements derived from scleral spur

Anterior chamber angle measurements based on identification of scleral spur are shown in (Figure 1-11) and include:

1) Angle opening distance (AOD) is the perpendicular distance between trabecular meshwork and iris, which represent angle width and provides a clue whether the TM is exposed to anterior chamber. Small AOD indicates closed angle, with the TM is covered by iris. This causes partial or complete reduction of aqueous humour drainage. AOD is

measured at specific distances (500 µm or 750 µm) anterior to the scleral spur (Pavlin et al., 1992). The 500 or 750 µm represents the estimated length of trabecular meshwork (TM) which extend from SS anteriorly to SL. Narayanaswamy et al reported that AOD at 750 µm is the most useful parameter for angle measurement (Narayanaswamy et al., 2010a).

2) Angle recess area (ARA): Ishikawa et al defined the ARA as the area bordered by the anterior iris surface, corneal endothelium, and a line perpendicular to the corneal endothelium that is drawn to the iris surface from a point 750 µm anterior to the scleral spur (Ishikawa et al., 1999).

3) Trabecular-iris angle degree (TIA): is the angle formed from angle recess to a point 500 µm from the scleral spur and perpendicular on the surface of iris. Low reproducibility of TIA is reported because it depends on manual placement of both the scleral spur and iris angle recess. The angle recess visibility is also subjective to the high quality of image which is not usually achievable (Pavlin et al., 1991).

4) Trabecular iris surface area (TISA): is the area bounded anteriorly by AOD; posteriorly by a line drawn from the scleral wall to the opposing iris; superiorly by the inner corneo-scleral wall; inferiorly by the iris surface. TISA is either measured at 500 and 750 µm (Figure 1.11) anterior to SS. This parameter was proposed to be more accurate than ARA because it excludes the non-filtering region behind the scleral spur (Radhakrishnan et al., 2005b).

5) Trabecular iris contact length (TICL): is used in case of closed iridocorneal angle. It is defined as the linear distance of iris contact with the corneo-scleral surface beginning at scleral spur and extending anteriorly in an anatomically apposed or closed angle (Radhakrishnan et al., 2005a).

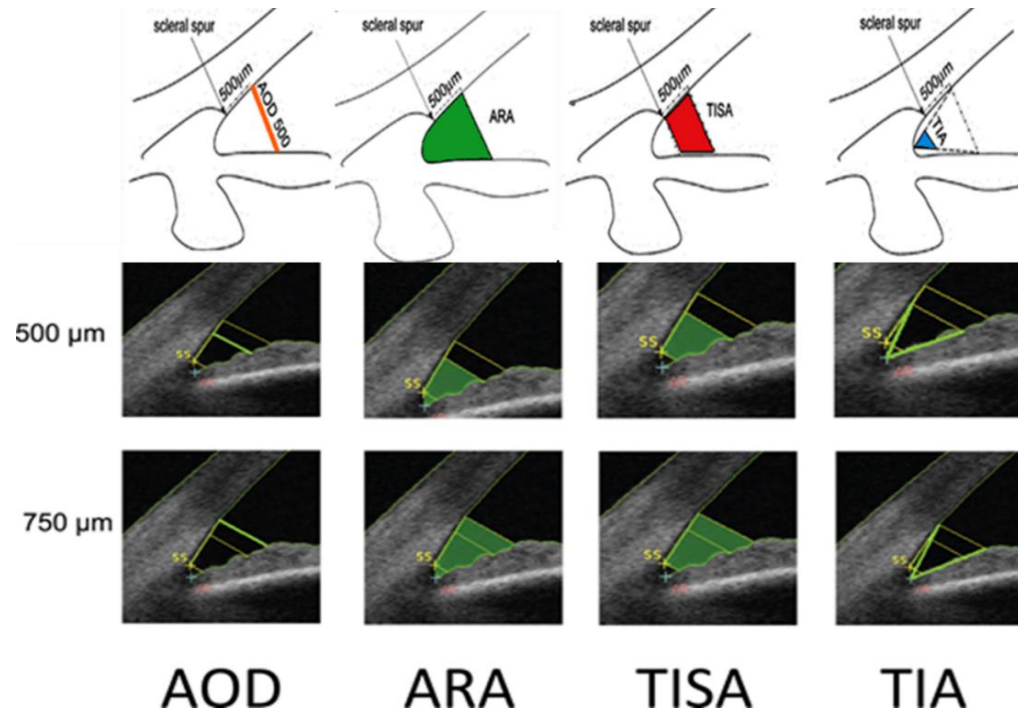


Figure 1-1: Schematic and OCT images of the iridocorneal angle measurements derived from identification of scleral spur.

Images are modified from (Sanchez-Parra et al., 2015). AOD = angle opening distance at 500 and 750 μm anterior to scleral spur. TISA= trabecular iris surface area 500 and 750 μm anterior to scleral spur. AOD is defined as the length of a line drawn perpendicular to the cornea anterior to the SS and ending on the anterior surface of the iris. TISA is the area bordered centrally by the AOD line, anteriorly by the posterior corneoscleral-aqueous interface, and posteriorly by the anterior surface of the iris. The peripheral border is a line segment starting at the SS perpendicular to the corneoscleral-aqueous interface and ending on the anterior surface of the iris (Cumba et al., 2012). and angle recess area (ARA) 500 anterior to scleral spur. Trabecular-iris angle degree (TIA) is the angle formed from angle recess to points 500 μm from the scleral spur.

1.3.2.5.5 Anterior chamber angle measurements derived from Schwalbe's line

These measurements include:

- 1) **Schwalbe's line angle opening distance (SL-AOD).** SL-AOD is defined as the distance from the SL to the anterior iris surface, perpendicular to the corneal endothelial surface (Figure 1-12).
- 2) **Schwalbe's line trabecular iris space area (SL-TISA).** SL-TISA is defined as the area between the SL-AOD, a line drawn along the trabecular meshwork at 500 µm posterior to the SL, perpendicular to the plane of the inner scleral wall, iris surface and the inner corneo-scleral wall (Figure 1-12).. SL-TISA reflects the area of TM exposed to anterior chamber where the aqueous humour drain into Schlemm's canal. When the iris occludes the angle the SL-TISA become smaller and SL-AOD becomes shorter. This indicates closed angle which is a risk factor of angle closure glaucoma.

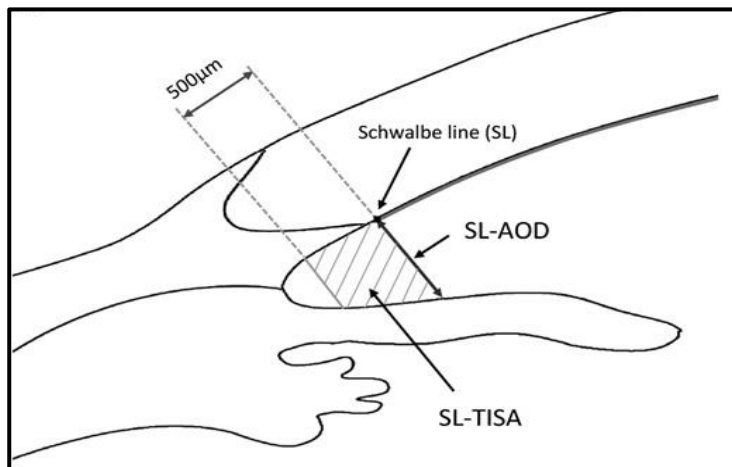


Figure 1-12: Schematic images of the anterior chamber measurements derived from Schwalbe's line.

A) The image shows the measurements of Schwalbe's line angle opening distance (SL-AOD) and SL-trabecular iris space area (SL-TISA) as described by (Cheung et al., 2011b).

1.3.2.5.6 Normative values of anterior chamber angle measurements

Anterior chamber angle measurements based on identification of SS are well documented in literatures. Table 1-7 shows examples of the angle opening distance (AOD) and trabecular iris surface area (TISA) measurements using OCT devices. Leung et al reported good agreement between Visante and SL-OCT in measuring AOD and TISA. The temporal angle AOD and TISA are wider compared to the angle measurements of nasal quadrants (Leung et al., 2008). A negative correlation between angle width and age particularly the superior angle quadrant is shown (Rufer et al., 2010).

Table 1-7: List of literature of measurements of anterior chamber angle based on identification of scleral spur using anterior segment optical coherence tomography.

Authors and year	OCT device	AOD 500	TISA	TIA
Leung et al (2008)	Visante (Carl Zeiss Meditec, Dublin, CA)	Nasal 527 ± 249 , Temporal $572 \pm 275\mu\text{m}$	Nasal $0.180 \pm 0.091\text{mm}^2$ Temporal $0.193 \pm 0.102\text{mm}^2$	Nasal 38.1 ± 12.3 Temporal $39.6 \pm 13.2^\circ$
	SL-OCT (Heidelberg, Germany)	Nasal $534 \pm 234 \mu\text{m}$. Temporal $628 \pm 254 \mu\text{m}$	Nasal $0.191 \pm 0.089 \text{ mm}^2$. Temporal $0.217 \pm 0.093 \text{ mm}^2$	Nasal $37.8 \pm 10.1^\circ$ Temporal $40.6 \pm 10.7^\circ$
Amerasinghe et al (2009)	Visante (Carl Zeiss Meditec, Dublin, CA)	Nasal $0.274\text{mm} \pm 0.131\text{mm}$	Nasal $0.111 \pm 0.049\text{mm}$.	
		Temporal $0.266 \pm 0.138\text{mm}$	Temporal $0.103 \pm 0.049\text{mm}$.	
Cheung et al (2011)	Cirrus SD-OCT (Carl Zeiss Meditec, Dublin, CA), mounted with 60 D lens	$0.25 \pm 0.15\text{mm}$ (ranging from 0 to 0.64 mm)	$0.086 \pm 0.054 \text{ mm}^2$ (ranging from 0 to 0.242 mm^2)	

AOD 500 = angle opening distance 500 anterior to scleral spur. TISA =trabecular iris surface area, TIA= trabecular iris angle degree. (Leung et al., 2008) (Amerasinghe et al., 2009a) (Cheung et al., 2011a).

1.3.2.5.7 Angle opening distance (SL-AOD) and trabecular iris surface area (SL-TISA) based on identification of Schwalbe` line.

Cheung et al introduced these new parameters based on identification of Schwalbe's line (Cheung et al., 2011a).The eyes of 47 females and 26 males (mean age = 60.6 years old)were scanned using Cirrus SDOCT. Only 117 images of good quality were included in the results. The mean SL-AOD was 0.25 (0.15) mm (ranging from 0.0 to 0.64 mm). The mean SL-TISA500 was 0.086 (0.054mm²) (ranging from 0.0 to 0.242mm²). SS-to-SL distance was 0.67 (0.13) mm (ranging from 0.39 to 1.23 mm). They were significantly correlated with the measurements based on the identification of scleral spur (SS-AOD and TISA parameters) and with gonioscopic grading. The SL-TISA results were similar to the SS based TISA values of other literatures (Leung et al., 2008) (Amerasinghe et al., 2009a). While the AOD had different values in these papers, which generally ranging from 0.0 to 0.64 mm. This suggested that TISA was a more accurate indicator of angle width than the AOD. The AOD may not truly reflect the anterior chamber angle (ACA), because the iris curvature plays an important role in determining the angle width. Sng et al studied the iris curvature, thickness and area using AS-OCT in adults. The iris thickness did not change with ageing while the (forward) iris curvature and iris area were reported to increase with age. This is associated with the narrowing of the anterior chamber angle (Sng et al., 2013).

1.3.2.5.8 Visualization of trabecular meshwork

As mentioned above, identification of trabecular meshwork was not possible in the UBM and TD-OCT images. Therefore, it is estimated as 500μm up to 750 μm anterior to the detectable SS. (Pavlin et al., 1992, Ishikawa et al., 2000). With the development of SD-OCT, Wong et al (2009) have identified and measured trabecular meshwork for the first time. Cirrus HD-OCT adapted with 60 D lens has enabled the visibility of TM in 62.2% of images of 45 Chinese adults (Wong et al., 2009). Table 1-8 summarises the literature with respect to measuring trabecular meshwork. Usui et al measured the TM in adults, using Casia-1000 SS-OCT (Tomey, Nagoya, Japan) (age 29-81y) and presented mean TM length of $466.9 \pm 60.7 \mu\text{m}$ and mean TM area of $0.067 \pm 0.058 \mu\text{m}^2$ This agreed with the findings of a cross-sectional study of 1006 Caucasian healthy subjects using RTVue SD-OCT (Fernandez-Vigo et al., 2015b). Where the TM was visible in 91% of eyes and the mean TM length was

496.99 ± 92.77 μm (range, 275-800). TM thickness was 174.16 ± 28.14 μm (range, 100-276 μm) and TM area was 0.069 ± 0.031 μm^2 (range, 0.023-0.133 μm^2).

In another study, using also Casia 1000 SS-OCT, Tun et al measured the TM in the four quadrants and reported that a TM length ranged between 554-1054 μm among 160 Chinese subjects. The inferior quadrant TM length was the widest compared to other quadrants. The average TM width was significantly shorter in closed-angle than open-angle eyes. Although, there was no significant association between TM width and angle parameters, this study suggests that the length of trabecular meshwork may play an important role as a predisposing factor in glaucoma (Tun et al., 2013b). The TM length value in this study is wide compared to the other previous studies. The difference in ethnicity and age could be the reason of this variability.

Chen et al studied the TM length in different ethnic groups using Cirrus SD-OCT and reported wide TM length of 836 ± 131 μm . Although, the TM length was not significantly associated with ethnicity, the African was observed to have shorter TM. This has postulated a possible reason of the increased risk of Africans to closure angle glaucoma (Chen et al., 2015). Both these studies had small sample group compared to *Fernandez Vigo et al* study.

Table 1-1: Summary of literature of trabecular meshwork measurements using optical coherence tomography.

Authors	Parameters	OCT machine	Findings
Fernandez-Vigo et al (2015)	Trabecular meshwork (TM) length, thickness and area	RTVue SD-OCT 1006 Caucasian healthy subjects (18 and 85 years)	TM was identified in 91.1% of the total eyes studied, The mean TM length was $496.99 \pm 92.77 \mu\text{m}$ (range, 275–800 μm) The TM thickness was $174.16 \pm 28.14 \mu\text{m}$ (Range, 100–276 μm) The TM area was $0.069 \pm 0.031 \text{ mm}^2$ (range, 0.023–0.133 mm^2)
Chen et al (2015)	Trabecular meshwork height	Cirrus SD-OCT	The mean TM height was $836 \pm 131 \mu\text{m}$ The TM height was not associated with ethnicity
Tun et al (2013)	TM length in four quadrants	Casia 1000 SS-OCT (Tomey, Nagoya, Japan) 160 Chinese subjects	TM length was $779 \pm 98 \mu\text{m}$ (range, 554–1054 μm) The inferior quadrant TM was the widest compared to other quadrants The average TM width was significantly shorter in closed-angle than open-angle eyes
Usui et al (2011)	The first study using OCT for measuring TM area	Casia 1000 swept SS-OCT	The mean TM length was $466.9 \pm 60.7 \mu\text{m}$. The TM area was $0.067 \pm 0.058 \text{ mm}^2$

1.3.2.6 The association between the anterior chamber measurement, age, gender, and ethnicity

Many studies have detected a correlation between anterior chamber measurements and increasing age in adults (Xu et al., 2008, Nongpiur et al., 2010b, Huang et al., 2015b). Nongpiur and colleagues have detected reduction in anterior chamber width with increasing age. Similar to ACW, anterior chamber depths (ACD) also decreased with increasing age (Rufer et al., 2010, O'Donnell et al., 2011, Orucoglu et al., 2015). Using linear regression, ACD is predicted to decrease by 10.4 µm/year (Fernandez-Vigo et al., 2015a), 11.9 µm/year (Sun et al., 2012), 11.5 µm/year (Rufer et al., 2010), 15 µm/year (Sng et al., 2012), 171m/year (Yan et al., 2010) and 9 µm/year (Xu et al., 2008). The variations in these publications are likely due to different age groups, ethnicity and different instruments used in these studies. Chinese ethnicity and old age is associated with shorter ACW and shallower ACD. Similarly, greater ACD in men than in women is shown (Cui et al., 2014, He et al., 2008). Chinese females have narrower anterior chamber measurements (ACD, ACW, ACA area and ACV), narrower anterior chamber angle, higher iris curvature, larger lens vault compared to males (Huang et al., 2015b). Using Visante TD-OCT to study the anterior chamber of 1465 Chinese subjects, Nongpiur et al reported shorter ACW in women compared to men and suggested that smaller anterior chamber width may be an indicator of narrow angle (Nongpiur et al., 2010a).

The aforementioned studies enrolled adults and provided data about Chinese ethnicity only. There is limited information about Caucasian anterior chamber. More importantly, there is no information about anterior chamber measurements in the paediatric age groups.

1.3.2.6.1 Anterior chamber angle width of different gender

In a study of 2985 Chinese participants using a slit lamp TD-OCT(Heidelberg Engineering, Heidelberg, Germany), Xu et al have connected the presence of narrow anterior chamber angle with small optic disc, short body stature, thicker central corneal thickness and risk of chronic angle closure glaucoma (Xu et al., 2008).

Amerasinghe *et al* studied the angle width of 239 right eyes of Malay people (aged 40 to 80 years) in Singapore (Amerasinghe et al., 2009a). Using Visante AS OCT, they reported that women had a smaller mean AOD500 than men; both nasally (0.255 vs. 0.293 mm, respectively; $p = 0.026$) and temporally (0.245 vs. 0.286 mm, respectively; $p = 0.023$). The mean ACD was smaller in women than in men (2.71 vs 2.87 mm, respectively; $p = 0.001$). The mean TISA-500 was smaller in women in the nasal quadrant only (0.104 vs. 0.117 mm, respectively; $P=0.035$). Multiple linear regressions showed that axial length and ACD were significantly associated with AOD-500 and TISA-500 both nasally and temporally. The AOD-500 was more highly correlated with clinical gonioscopic assessment of angle width than TISA-500.

1.3.2.7 Anterior chamber measurements in glaucoma

Closed angle glaucoma is associated with presence of shallow anterior chamber and shorter anterior chamber width (Nongpiur et al., 2010b), increased lens thickness (Nongpiur et al., 2011b), thicker iris and narrow anterior chamber angle (Wang et al., 2010). ACV is smaller by 25% in primary acute angle closure (PACG) patients compared to healthy controls (Congdon et al., 1997).

To the best of our knowledge, there have been no previous studies about using of OCT for quantitative measurements of the anterior chamber angle of congenital glaucoma in paediatric age group. The focus of this thesis is to use HH-OCT to measure the changes of anterior chamber associated with congenital glaucoma.

1.3.3 The impact of accommodation and illumination on anterior chamber measurements

1.3.3.1 Accommodation

Accommodation is the physiological process that enables the eye to adjust the refractive state in order to see objects clearly at different distances.

Helmholtz's theory (1867) is still the most accepted theory of accommodation. It describes different biometric changes during the accommodation reflex which includes constriction of the pupil, increase in the thickness of the lens which becomes round with increase in the curvature of the anterior and posterior pole. These changes are attributed to the contraction of ciliary muscle and are associated with increase in the refractive power of elastic lens. Coleman (1986), proposed that the contraction of the ciliary muscles increases the vitreous pressure which in turn has a hydraulic effect on the posterior pole of the lens. Therefore, there is minimal change of the posterior pole of the lens. This hydraulic theory was contradicted by Martin and colleagues in favour of Helmholtz's theory (Martin et al., 2005).

Using AS-OCT, it was reported that a 0.3 mm forward movement of anterior pole of lens is associated with 10 dioptre increase in refractive power of the lens (Baikoff et al., 2004). Using UBM, Kaluzny et al reported that the movement of anterior pole varies, depending on refraction state of eye. It moves forward by 0.14 ± 0.14 mm in emmetropic eyes, 0.071 ± 0.13 mm in myopic eyes, and 0.242 ± 0.16 mm in hyperopic eyes (Kaluzny, 2007).

In recent study using AS-OCT, Farouk and associates have detected that the backward and the forward movement of the posterior and anterior poles of the lens are nearly equal (Farouk et al., 2015). This finding agreed with the capsular theory and contradict the hydraulitic theory of Coleman.

1.3.3.2 Effect of illumination on anterior chamber width

The pupil of the eye constricts when the illumination changes from dim to bright light and vice versa. This physiological process occurs to minimise the amount of light entering the

eye Leung *et al* studied the effect of illumination on angle width among 55 Chinese patients (37 open angles and 18 narrow angles) subjects using Visante AS-OCT(Leung et al., 2007). First the participants were adapted to the dark for about 1 minute, and then the room light was turned on with intensity of 368 lux. They found that the AOD500 and TISA500 measured in light were significantly greater than those measured in the dark for both open and narrow angle groups. The average of dark to light AOD difference and TISA difference were 180 μ m and 0.073 mm² respectively. This was in an agreement with the finding of other studies using Spectralis AS-OCT (Masoodi et al., 2014), UBM (Woo et al., 1999) or Visante (Hirose et al., 2013). The ACD and lens thickness were higher in photopic compared to mesopic conditions (Koktekir et al., 2014). Dacosta *et al* reported that the ACD is not influenced by ambient lighting conditions while the pupil diameter (PD) increased and the angle width decreased significantly in scotopic conditions (Dacosta et al., 2008).

Accommodation and illumination can affect the anterior chamber morphology.

Therefore, it is essential to control and take into account the influence of the accommodation and illumination in any study of anterior chamber biometry.

1.4 Gaps in the research literature

This thesis focuses on three research areas in the literature which have not been studied before. These research areas are:

Firstly, the application of anterior segment optical coherence tomography (AS-OCT) in imaging the anterior chamber of children has not been widely investigated. It is difficult to stabilise eye, head and body movements of children without intervention with sedation, particularly children younger than 5 years old. HH-OCT was successfully used for visualization of fovea as previously mentioned. It has helped to achieve a rapid scanning of the fovea of young children in few seconds without sedation. However, HH-OCT application in imaging the anterior segment structures, particularly the anterior chamber angle has not been systematically studied yet.

Secondly, the availability of a non-invasive technique for imaging the anterior chamber of children can help to investigate the *in vivo* postnatal normal development of the anterior chamber

Thirdly, the availability of a non-invasive technique for imaging the anterior chamber of children can help to understand the pathological change of the anterior chamber associated with diseases such as congenital glaucoma, prematurity and anterior segment dysgenesis.

In this thesis, we evaluated the applicability of hand-held SD-OCT in imaging the anterior chamber of children without sedation. The first area of investigation was to assess the feasibility and reliability of HH-OCT for imaging the anterior segment in children (chapter 3). In the second part, we investigated the normal development of anterior chamber in children (chapter 4). In the third part, we explored the pathological changes of anterior chamber associated with congenital glaucoma (chapter 5), prematurity (chapter 6) and anterior segment dysgenesis (chapter 7).

1.4.1 Aims of the thesis

Chapter 3 (feasibility and reliability of HH-OCT for anterior chamber measurements)

1. To investigate the feasibility of HH-OCT for anterior chamber imaging in children.
2. To investigate the reproducibility of anterior chamber landmarks identification and measurements in children using HH-OCT.
3. To identify the best accurate angle landmarks and measurements to study the morphometric development of anterior chamber angle.

Chapter 4 (normal changes of anterior chamber measurements)

4. To establish normative database (mean and 95% prediction intervals) of anterior chamber measurement in children since birth and to investigate the postnatal normative development of the anterior chamber.

Chapters 5 to 7 (changes in anterior chamber associated with pathology)

5. To compare the development of the anterior chamber in congenital glaucoma and age-matched healthy children
6. To determine whether the premature born children have abnormal anterior chamber development compared to age-matched full term born children.
7. To perform an exploratory study of the possible clinical use of HH-OCT in congenital abnormalities of the anterior segment such as Peters' anomaly, aniridia and Axenfeld-Rieger syndrome.

1.4.2 Outline of chapters covering the main aims

The design of imaging protocol is discussed in chapter 2 of general methods.

Chapter 3 addresses aims 1, 2 and 3 and has a title of “Feasibility and reproducibility of anterior chamber measurements in children using of HH-OCT”.

Chapter 4 addresses aim 4 and has the title of “Postnatal anterior chamber development: an *in-vivo* quantitative study using high resolution hand-held optical coherence tomography”.

Chapter 5 addresses aim 5 and has the title of “Novel *in-vivo* morphometric measurements of anterior chamber in children with congenital glaucoma using hand held spectral domain optical coherence tomography”.

Chapter 6 addresses aim 6 and has the title of “Development of anterior chamber of premature born children”.

Chapter 7 addresses aim 7 and has the title of “clinical exploration of congenital anterior segment abnormalities using HH-OCT. It presents HH-OCT images of congenital abnormalities of anterior segment.

Chapter 8 covers the general conclusion with the significance of findings and the future studies.

2. Chapter two: General methods

2.1 Ethical approval

This study followed the tenants of Declaration of Helsinki. Ethical approval was obtained by the local ethics committee. Ethics were obtained prior to commencing the trial for testing the designed imaging protocol.

2.2 Study design

Data collection involved recruitment of healthy children and children with ocular diseases. The study was performed over the period of 2.5 years using cross sectional prospective cohort design. The majority of participants are Caucasians including white British, Indian, white North African. Percentages of ethnicity are summarised in table 2-1

Table 2-1: Sample size of healthy participants categorised by ethnicity

Ethnicity	Percentage
White European	64%
White North African	15%
Indian	17%
Others	5%

(*) *Others include mixed ethnicity and Afro-Caribbean.*

2.3 Recruitment of participants

2.3.1 Healthy participants

The age of healthy subjects ranged from birth and 45 years of age. New-born children were recruited from the Maternity Unit of Leicester Royal Infirmary. Older children were recruited from different Leicester city nurseries, schools as well as general children clinic at Leicester Royal Infirmary. Adult participants were invited friends, students and staff of the University of Leicester. The exclusion criteria of healthy participants were presence of any ocular, neurological abnormalities on examination, any family history of ocular or neurological abnormalities, or any history of eye surgery, trauma or medication that can affects the eyes physiology such as steroids or dilating eye drops. Participants with refractive error of more than +/-3 dioptre were excluded.

In this study, we recruited total of 353 participants; 292 children aged from 2 days up to 16 years of age and 59 adults above the age of 18 years. Those include the participants that we failed to scan or have bad quality images, which were only included in the feasibility study. The cohort of included participants to answer each research question was described in each chapter.

2.3.2 Premature born children

Premature born children were recruited from Neonatal unit and Orthoptic clinic in Leicester royal Infirmary during their follow up appointment. Complete details about the cohort and criteria of this group is described in chapter 6.

2.3.3 Participants with ocular pathology

The cohort of the patients is detailed in each relevant chapter. Those patients included children diagnosed with:

1. Nystagmus such as albinism and idiopathic infantile nystagmus.
2. Congenital glaucoma including primary congenital glaucoma and secondary congenital glaucoma to Sturge Weber syndrome.
3. Congenital abnormalities of anterior segment including aniridia, Peters' anomaly and Axenfield Rieger syndrome.

The total sample size of patients is summarised in table 2-2. The clinical criteria of the diagnosis of albinism and idiopathic infantile nystagmus are shown in the flow chart (Figure 2-1). Details of the clinical features of congenital glaucoma and congenital abnormalities of anterior segment are discussed in chapter 1 section 1.1.3 and further information is described in chapter 5. Details of the clinical features of the congenital abnormalities of anterior segment are discussed in chapter 1 section 1.1.4 and further information is described in chapter 7.

Table 2-2 : Sample size of recruited patients.

Diagnosis	Number	Age range
Premature born children	17	28 weeks gestational age - 6 years
Idiopathic infantile nystagmus	9	7 months - 6 years
Albinism	9	15 days - 6 years
Congenital glaucoma	33	2 months - 10 years
Aniridia	1	1.8 years
Peters' Anomaly	3	8 months - 7 years
Axenfield Rieger Syndrome	2	4 - 11 years
Sturge Weber syndrome	4	8 months - 8 years

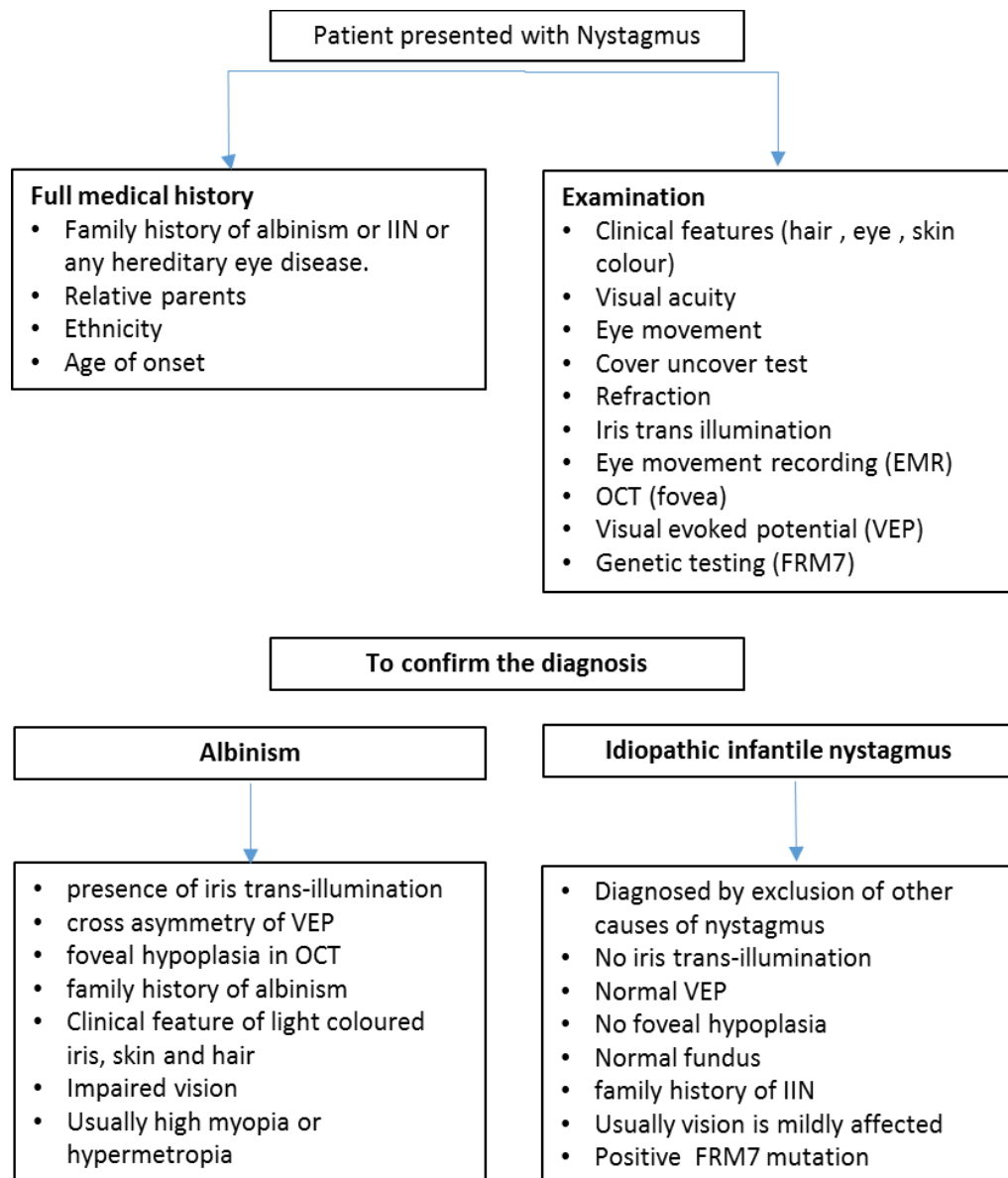


Figure 2-1: Steps of diagnosis of albinism and idiopathic infantile nystagmus

2.4 Steps in data collection

The parents of healthy children and the children were approached for invitation to participate in this study. The study information leaflet was initially explained. A considerable time was given for the parents and children to decide whether to enrol in this study or no, with option to withdraw at any time. With the willingness to participate, the medical history was initially obtained from healthy participants to verify the inclusion and exclusion criteria.

All children's parents or guardians and adults gave their informed consents prior to the examination. Older co-operative children gave assents. In case of patients with ocular diseases, the patient's clinical information was collected from their recent medical notes. After they gave their consent. (Examples of information leaflet and consent form are supplied in appendix).

2.4.1 Medical History

The parents were asked about the gestational age of children. Children born before 37 weeks gestational age were included in the premature group. Any child who had one of the exclusion criteria of healthy participant was excluded from the study.

2.4.2 Clinical examination

All the included healthy participants were examined for visual acuity, refraction and ocular motility. The slit-lamp and funduscopic examination was undertaken if required. The patient's clinical examination was collected from their notes

2.4.2.1 Visual acuity

Newborns and infant's visual acuity (VA) was tested using preferential looking Teller acuity cards (Figure 2-2). The examiner held the card in front of the child and judge by the look of the child if they could see the grating lines. If so, the next card with smaller grating lines would be presented in turns till the examiner could not judge the reaction of the child and therefore record the last seen card as the child's VA.

Younger cooperative children were assessed by log-MAR Kay acuity cards. In this test the child points at the picture that he can see from a distance using the picture card he was given to hold.

LogMAR EDTRS chart was used for older children and adults. They were asked to read the letters from a distance of 4 meters, under monocular and binocular condition, starting from the top largest letter and going gradually down to the bottom's smallest letter line (Figure 2-2).

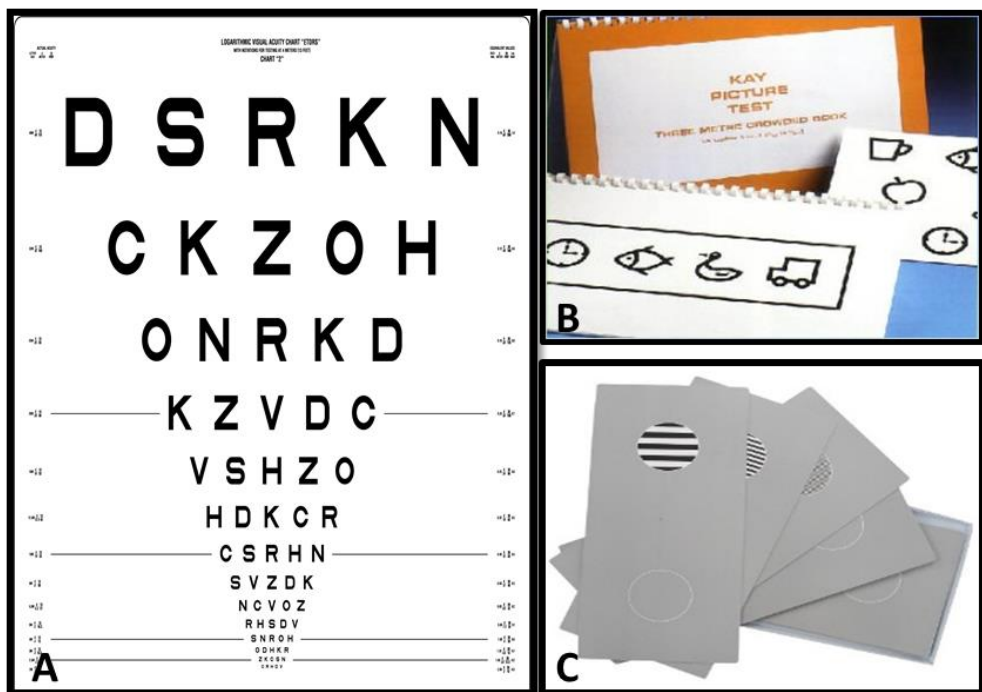


*Figure 2-2: Methods of visual acuity measurements
A) LogMar chart. B) Kay acuity cards. C) Preferential looking Teller acuity cards.*

2.4.2.2 Refraction

Healthy children were examined by a mobile paediatric auto-refractor (Plusoptix A12C, Germany) (Figure 2-3A). It produces gross rapid measurement of refraction without cycloplegic eye drop administration. The device was held about one metre in front of the child face. The child is attracted to look at a smiley face with a funny sound of the device. The reading of both eyes (binocular) is recorded automatically (Figure 2-3C). If the child had a reading for more than +/-2 Dioptrre, the child is referred for further refraction

examination with a recommendation of cycloplegic refraction. Plusoptix has been reported to be highly sensitive in detecting anisometropia, myopia and astigmatism compared to cycloplegic retinoscopy (Paff et al., 2010). It is also proved to be good for detecting cylindrical power without cycloplegia (Ayse et al., 2011). However, Plusoptix was found to overestimate the spherical power of myopia and underestimate the spherical power of hyperopia in children, when used without cycloplegia (dilated pupil) (Paff et al., 2010, Peterseim et al., 2014). Plusoptix is considered a good screening device that can save precious chair time.

The refraction data of patients was collected from the notes of patients at the closest time to scanning using HH-OCT. Usually refraction by optometrist was done on the same day of OCT examination. Children can be measured starting at 6 months of age. We tried to record refraction of younger children and it was successful with some children of 3 months old.

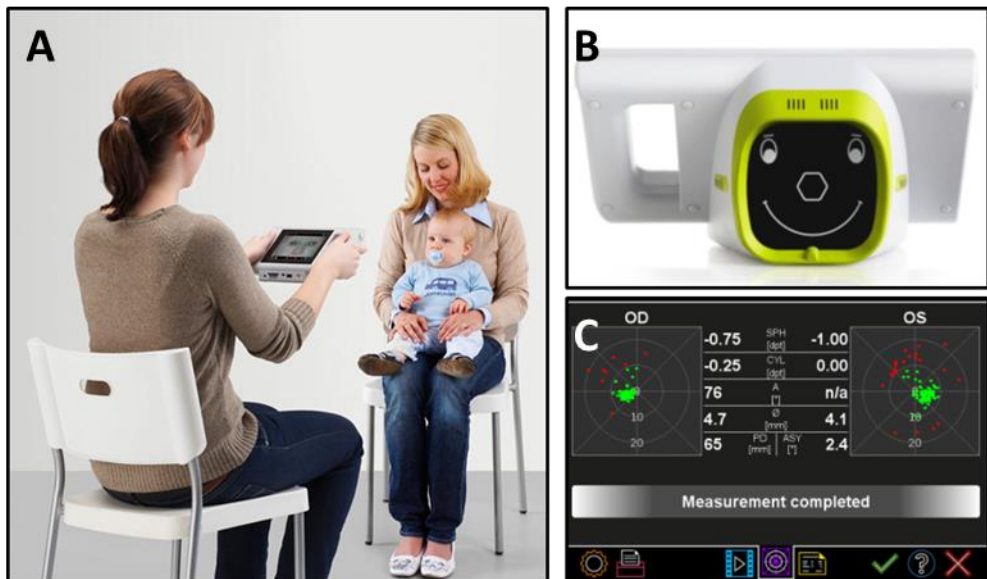


Figure 2-3: Refraction examination using Plusoptix.

A) The Plusoptix auto-refractor device is held about one metre in front of the child face image obtained from the device catalog. B) The child is attracted to look at a smiley face with a funny sound of the device. C) The reading of both eyes (binocular) is recorded automatically.

2.4.2.3 Eye movement and cover test.

Ocular motility was tested by asking the participants to look in different directions of gaze (Figure 2-4) following the movement of an object held in the examiner's hand. This tests the ocular motility of the eye muscles while the participant's head movement is fixed.

To test any deviation in one eye (squint), one eye was covered while the fixation of other eye was tested by looking at far (4 metre) and near distance (33 cm). These tests were used to detect any squint (Figure 2-5), restricted movement or latent nystagmus of eye as well as to assess the direction and intensity of nystagmus.

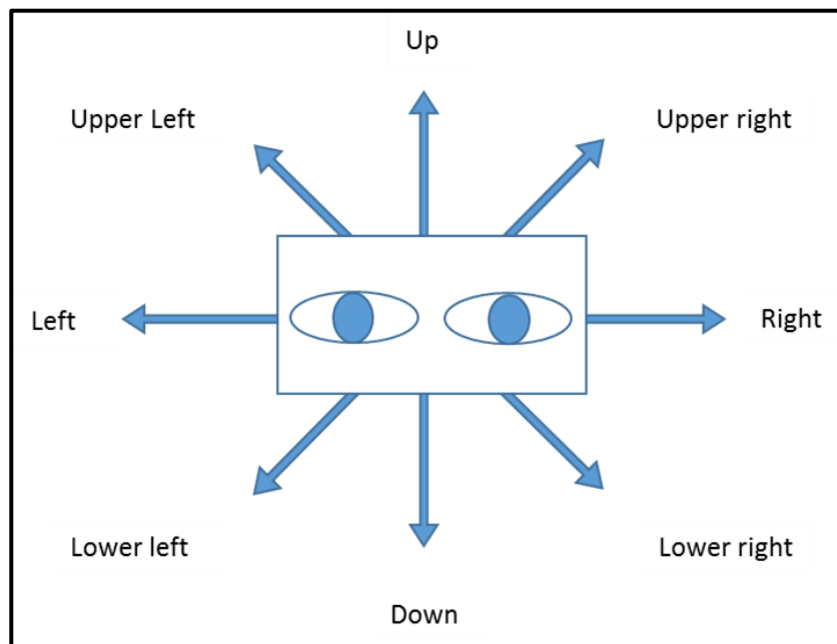


Figure 2-4: Eye movement direction

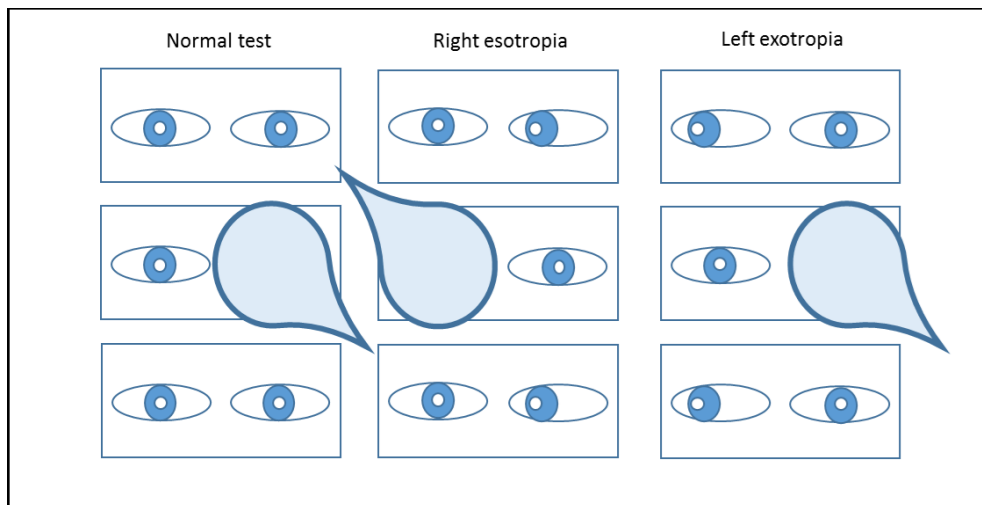


Figure 2-5: Cover test technique

2.4.2.4 Slit lamp biomicroscopy and fundus examination

If we suspected any abnormality of either the anterior segment or the posterior segment of eye, direct visualisation of anterior segment structures with slit-lamp biomicroscopy or examination of retina by funduscopy was performed (Figure 2-6). Any participant with detected abnormality was referred for further investigation and was excluded from the study.

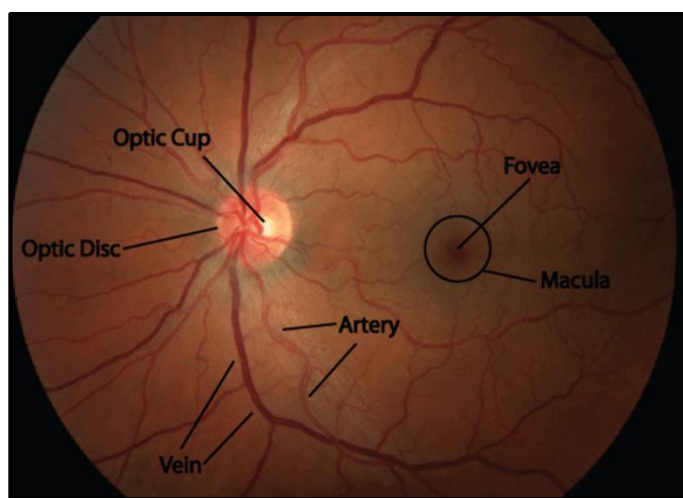


Figure 2-6: Retina stuctures in funduscopy examination

Image of normal fundus obtained during funduscopy examination taken from (StanfordMedine25, 2018).

2.5 Imaging of anterior segment using HH-OCT

2.5.1 Acquisition of anterior segment image using HH-OCT

The anterior segment structure was scanned by the Envisu C-Class HH-OCT system (Leica Microsystems Ltd) described in section 1.3.4). This was done by mounting the 25 mm diameter anterior segment lens on the hand-held probe (Figure 2-7). Both the reference arm and the software of HH-OCT were set for anterior segment imaging. The probe was held about 1 cm in front of the participant's eye (Figure 2-8). The examiner adjusts the probe towards and away from the eye until a clear en face volumetric image appears on the screen at left side window (showing pupil and iris) and a cut section (B scan) appeared on the right side (Figure 2-9). Initially, during the design of this study, it was necessary to optimize a protocol for better visualisation of anterior chamber (details is described below). The B scan shows a cut section of cornea and by moving the probe closer and slightly right or left, different anterior chamber structures can be seen, including iris, pupil, peripheral cornea, anterior pole of lens and most importantly the anterior chamber angle (Figure 2.9). If the probe is too close the image inverts upside down. Unlike other AS-OCT e.g Visante (TD-OCT) or Casia (SS-OCT) (Figure 1-26), HH-OCT has only 2.5 mm (in tissue) scanning depth which does not allow the visualisation of the whole anterior segment in one image. For this reason, we designed a protocol where 2 scans were obtained, one showing the cornea and the other showing the anterior chamber.



*Figure 2-7: Anterior segment lens of hand-held optical coherence tomography
A) Hand-held OCT. B) 25 mm anterior segment lens. C) 25 mm lens mounted in the hand-held probe.*



*Figure 2-8: Acquisition of scans of the eyes of children using HH-OCT
The examiner holds the HH-OCT probe about 1 cm in front of the child's eye and move it slightly towards and away from the eye until a clear en face volumetric image appears on the OCT screen. A) Children younger than 6 months were scanned in supine position. B) Older children were scanned in sitting position.*

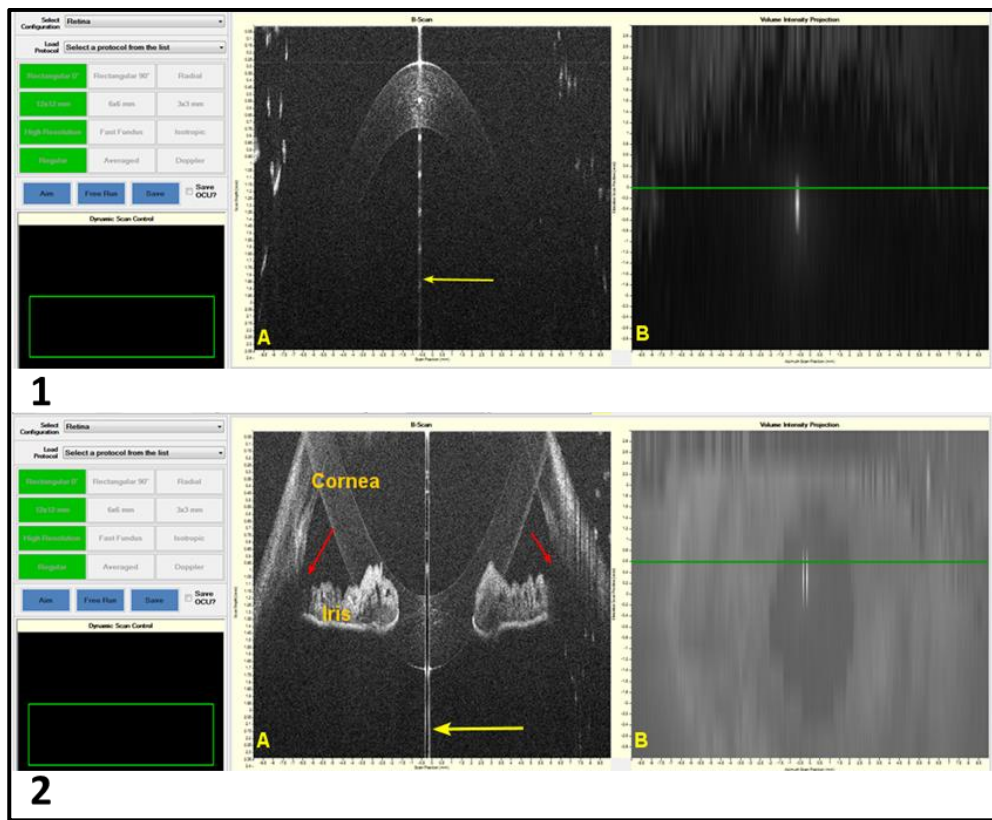


Figure 2-9: Acquisition of anterior segment images using HH-OCT.

- 1) An HH-OCT scan of cornea, where: 1A) is a B scan showing the central cornea, and 1B) An en face image of the cornea. The green line marks the B scan that is shown in right screen.
- 2) An HH-OCT scan of anterior chamber, where: 2A) is a B scan showing nasal and temporal anterior chamber angle, iris, reflection of cornea, margin of cornea and anterior pole of lens, and 2B) is an en face image shows iris, pupil. Green line mark the B scan that is shown in right screen.

2.5.2 Optimising the HH OCT protocol for imaging the anterior segment of the eye

The OCT volumetric scan consists of multiple B-scans. Each B scan is formed from sequences of A-scans. The vertical resolution of the volumetric scan is determined by the number of B-scans. The image quality is determined by the density of A-scans. The image quality can be improved by increasing the number of A-scans per B scan but high density of B-scans slows down the scanning speed. Therefore, reducing the number of B scans and increasing the number of A-scans can provide volumetric scan with optimal capturing time and high quality. An individual B-scan at the centre of pupil is sufficient to horizontally visualise the nasal and temporal angle together in one image.

The quality and the speed of scanning time are also affected by the dimension of volumetric scan. The smaller the width of image, the higher the density of A-scans per B scan. The smaller the height of image, the higher the density of B-scans, the quick the image capturing time. Capturing the two angles in one image requires a dimension of scan to be larger than the average corneal diameter of 12 mm. Therefore, adjusting the volumetric scan dimension can improve both the quality of image and scanning time.

We tested different protocols for anterior segment scanning to find the best protocol that produces good quality image of anterior chamber angle and enables optimal scanning speed that is sufficient to overcome the difficulty in keeping the eyes fixed or the rapid eye movement in pathological condition such as nystagmus.

2.5.2.1 Methods

We scanned both eyes of 5 healthy participants and 3 patients. These included two healthy children and three healthy adults (age; 5 months, 7, 28, 29, and 33 years) and a 2 year old female identified with megalocornea (corneal diameter >13 mm), a 3 month old female diagnosed with congenital glaucoma and a 5 year old albino with nystagmus. They were all scanned to compare different protocols of HH-OCT.

Initially, protocols of different dimensions (Table 2-3) were assessed for the best suitable width and height of the horizontal volumetric scan. These protocols had the following criteria:

1. They showed both anterior chamber angles together across the centre of pupil.
2. The centre was detected by the reflection of light seen in the central individual B-scan. Secondly, in order to get images with good quality and minimum scanning time, different selection of B-scans and A-scans were tested (Table 2-4). The scans were evaluated by exporting the OCT images into ImageJ, where a specific OCT reader plugin is used to open the images (further details of the image analysis was discussed next in the image analysis section)

2.5.2.2 Results

Summary of speed of capturing the scans and the quality of images are presented in tables 2-3 and 2-4. Examples of the obtained images of different dimensions are shown in (Figure 2-10). The 12 mm width showed only one angle per image. The images of 16, 18 and 20 mm width showed both angles. Although capturing both angles using the 16 mm image was possible, the 18 mm image was easier to capture. The scan height of 6 mm enabled visualisation of the entire pupil and had high density of B-scans than the scan of 8 and 12 mm height (Table 2-3). Reducing the number B scans (Figure 2-11) enabled quick capturing of volumetric scan (Table 2-3) without affecting the image quality (Table 2-4 and Figure 2-12). Increasing the number of A-scans per B-scan enabled improvement in the quality of image (Figure 2-13).

Table 2-3: Different volumetric dimensions that were tested using HH-OCT comparing the speed and quality of different numbers of B-scans.

Dimension of image	number of A-scans per B-scan	B-scan density per height	Number of B-scans = 33		Number of B-scans = 11	
			Speed	A-scan density	Speed	A-scan density
20 mm width × 6 mm height	3000	500	3.08 sec	1.65	0.96 sec	0.55
18 mm width × 12 mm height	3000	250	3.08 sec	1.83	0.96 sec	0.61
18 mm width × 8 mm height	3000	375	3.08 sec	1.83	0.96 sec	0.61
18 mm width × 6 mm height	3000	500	3.08 sec	1.83	0.96 sec	0.61
16 mm width × 12 mm height	3000	250	3.08 sec	2.06	0.96 sec	0.68
16 mm width × 8 mm height	3000	375	3.08 sec	2.06	0.96 sec	0.68
12 mm width × 8 mm height	3000	375	3.08 sec	2.75	0.96 sec	0.91

A total 14 scans were obtained per participant. The density of B-scans increases by reducing the height. The speed of scan increases by reducing the number of B-scans. The density of A-scans decreases by increasing the width of image.

Table 2-4: The outcome of using different protocols of B-scans and A-scans for imaging the anterior chamber angle of the eye.

18mm width x 6mm height / Horizontal			
Number B scans	Number of A scans per B scan	Duration of Scanning	Comments on the duration of obtaining the scans and quality of images
11	500	0.18 sec	Too rapid/very bad quality
	1000	0.33 sec	Too rapid/ bad quality
	2000	0.65 sec	Rapid/ average quality
	2500	0.80 sec	Optimal/ average quality
	3000	0.96 sec	Optimal/ very good quality
	4000	1.27 sec	Slow/ very good quality
22	500	0.38 sec	Too rapid/ very bad quality
	1000	0.70 sec	Optima/ bad quality
	2000	1.36 sec	Optimal/ average quality
	2500	1.96 sec	Too slow/ average quality
	3000	2.02 sec	Too slow/ good quality
	500	0.58 sec	Too rapid/very bad quality
33	1000	1.08 sec	Optimal/ bad quality
	2000	2.08 sec	Slow/ average quality
	2500	2,58 sec	Too slow/ very good quality
	3000	3.08 sec	Too slow/ very good quality

A total 16 scans were obtained per participant. The highlighted protocol was selected as the best suitable protocol to perform the scanning.

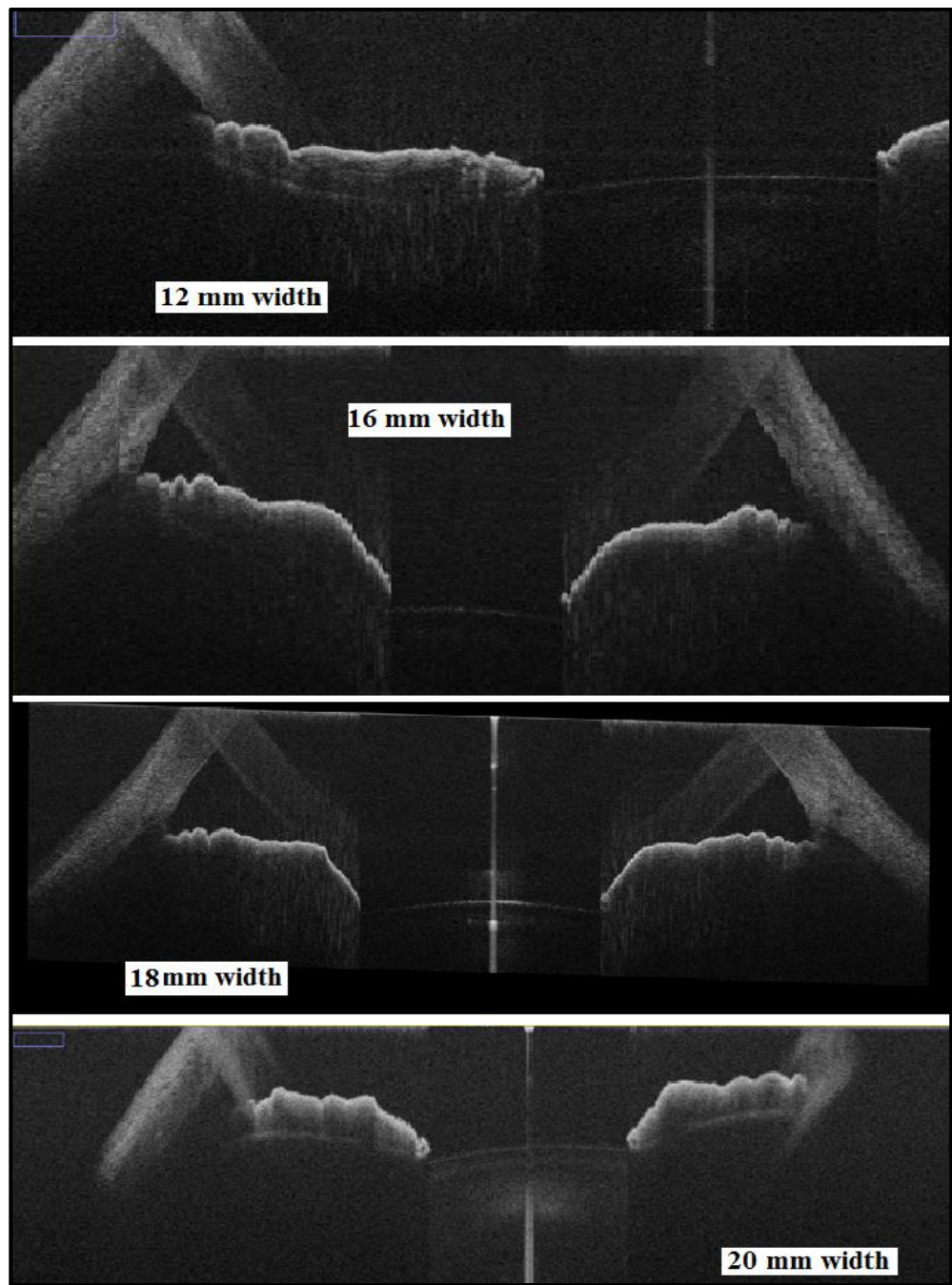


*Figure 2-10: Different dimensions of B-scans obtained by HH-OCT.
The 12 mm width showed only one angle per image. The images of 16, 18 ad 20 mm width showed both angles. Although capturing both angles using the 16 mm image was possible, the 18 mm image was easier to capture.*

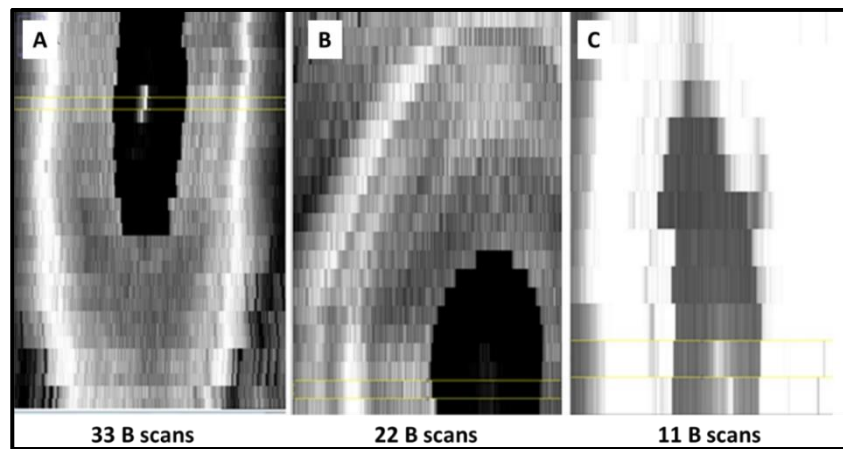


Figure 2-11: Different HH-OCT volumetric scans showing the pupil consists of different number of B-scans. (A) The scan has a dimension of 18 mm width, 6mm height, 33 B scans and 3000 A-scans per B-scan. B) The scan has a dimension of 16 mm width, 6 mm height, 22 B-scans and 3000 A-scans per B-scan. C) The scan has a dimension of 18 mm width, 6mm height, 11 B-scans and 3000 A-scans. The yellow lines indicate the selected B-scan that will be analysed.

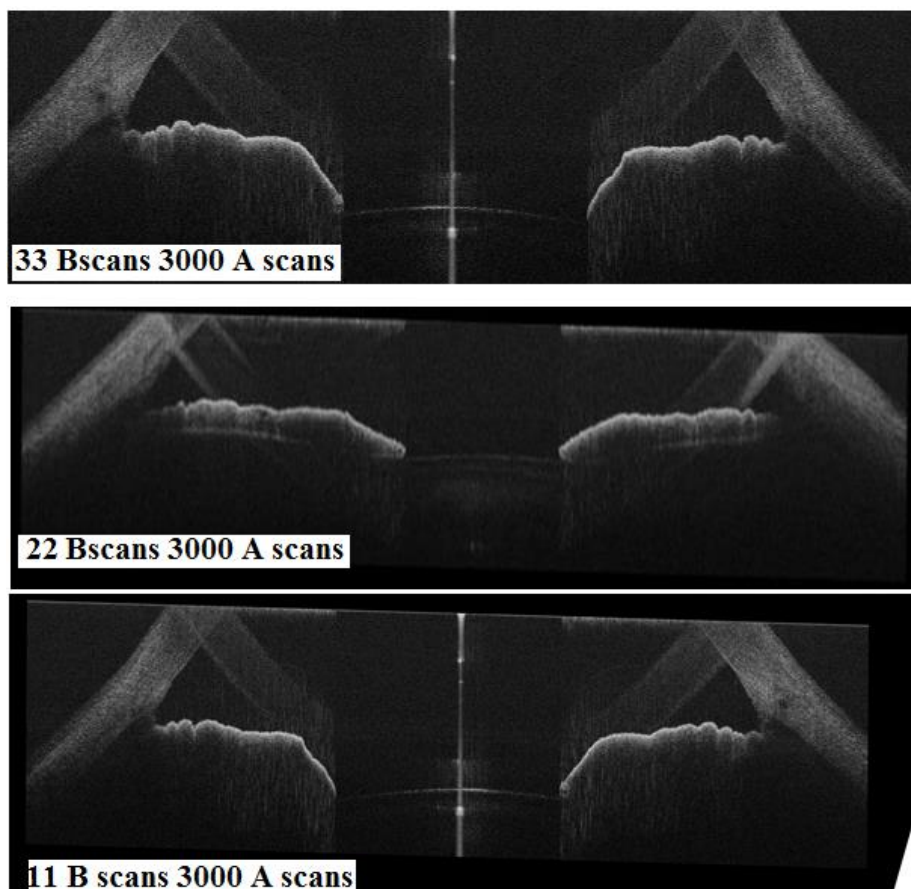


Figure 2-12: Individual B-scans at the centre of pupil consists of 3000 A-scans. Each B-scan was selected from different number of B-scans of each protocol (33, 22 and 11 B-scans). No difference in the image quality is shown but the scanning speed was faster with reducing the number of B-scans.

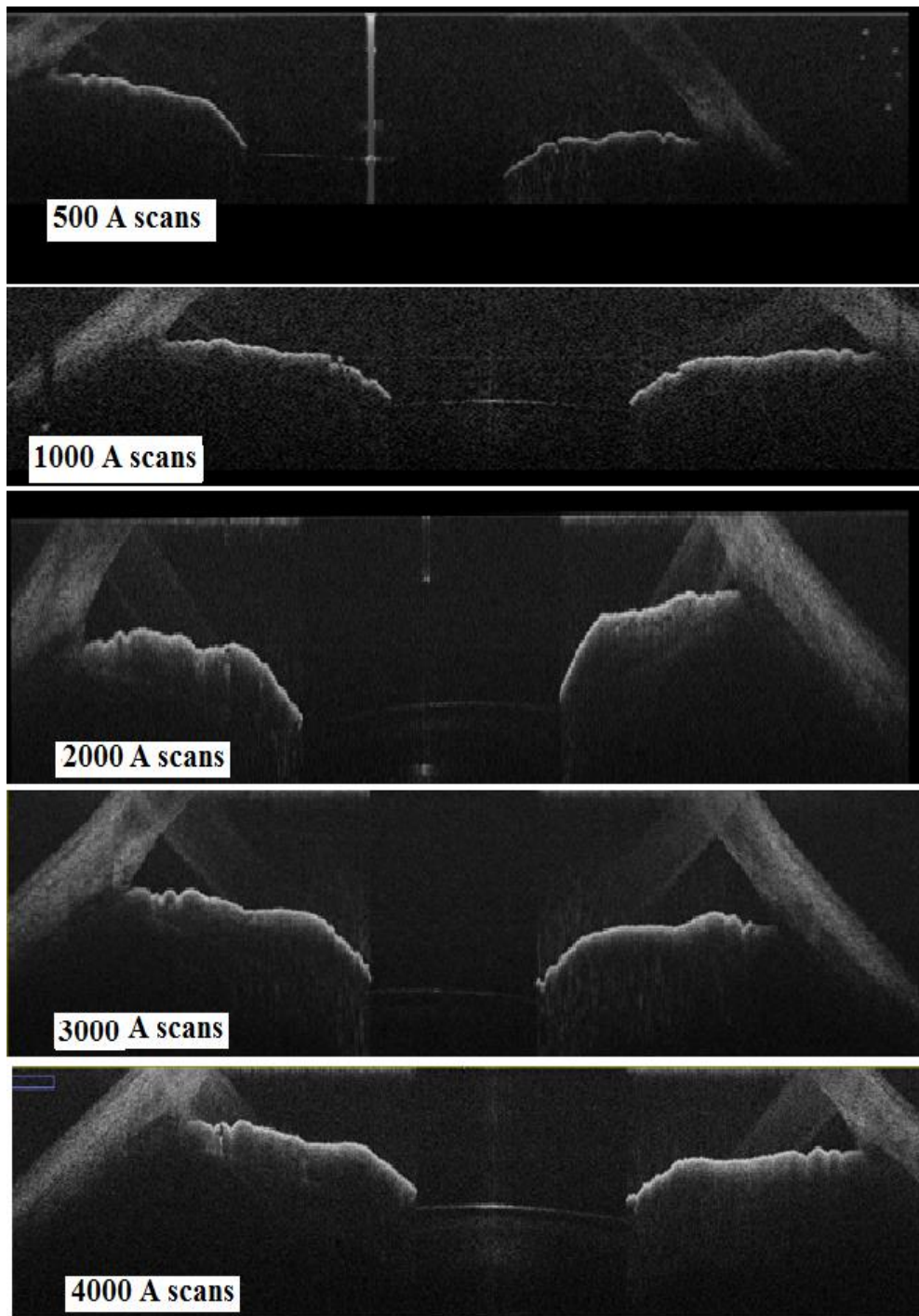


Figure 2-13: Individual B-scans at the centre of pupil consisting of different numbers of A-scans.

The B scan consisting of 500 A-scans has poor quality compared to the B- scan which is formed of 4000 A-scans. Increasing the number of A scans allowed improvement in the quality of image and better identification of angle structures and landmarks.

2.5.2.3 Outcomes of the protocol optimising

The optimal protocol for the purpose of anterior segment imaging was a horizontal raster scan of 18 mm width and 6 mm height, containing 11 B-scan with 3000 A-scans per B-scan (Figure 2-11C). The scanning duration is 0.96 seconds (Table 2-4). Therefore, anterior chamber image was easily captured and was not affected by the rapid eye movement. This protocol in general, has optimal scanning speed and provides good quality image compared to other investigated protocols.

The B-scan of 18 mm width has larger dimension than the normal adult horizontal corneal width (> 12 mm). It provided better visualisation of both angles (Figure 2-14). It gave extra 3mm space outside the average adult corneal diameter (12 mm + 3 mm in both sides). This worked better in cases of megalocornea and congenital glaucoma (corneal diameter >13 mm). The 6 mm height enabled faster scanning speed without affecting the capture of entire pupil. The final analysis was performed in this study using the individual B scan at the centre of the pupil (Figure 2-11 yellow lines). The 11 B-scans and 3000 A-scans per B-scan enabled faster capturing of image with high quality compared to other protocols of different numbers of A-scans (Figure 2-13).

The optimal speed of chosen protocol enabled easier capture of both angles in case of uncooperative child (5 months old) and in case of nystagmus.

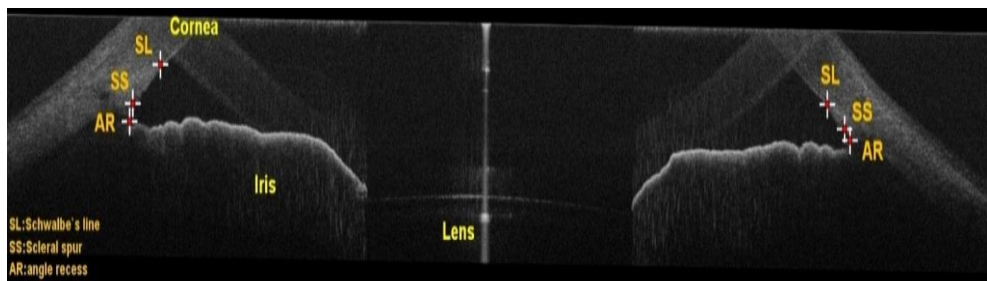


Figure 2-14: HH-OCT individual B-scan at the centre of pupil showing the anterior chamber.

Individual B-scan obtained using the protocol of 18 mm width \times 6 mm height @0.00 (horizontal) \times 11 B-scans \times 3000 A-scans \times 1 frame. The B-scan shows nasal and temporal angles. This image was saved as tiff file. The following landmarks were manually identified, SS = scleral spur, SL = Schwalbe's line and AR = angle recess.

Our selected protocol was programmed in OCT machine as 18× 6 mm @0.00 ×3000× 11× 1. The (@0.00) indicates horizontal meridian of nasal and temporal angles. This protocol was used as the final imaging protocol in this study. Four scans were obtained for each eye, 2 repeated scans for cornea and 2 repeated horizontal scans for anterior chamber angle, 8 scans in total for both eyes per participant were captured. The cornea was captured with same protocol to avoid any problem with the calibration of measurements.

2.5.3 Optimisation of scanning environment

All scans were performed under the same lighting conditions. In situations where the OCT machine was taken to different locations, the illumination was matched as closely as possible to the usual scanning room. The examination room was approximately 200lux (Figure 2-15). The intensity of illumination was measured using Testo Lux meter illumination device (Testo Ltd, UK). During the examination, cooperative children and adults were asked to look straight ahead. In such a case, usually image acquisition of 8 scan of both eyes would last between 3 to 10 minutes. However, it usually takes longer with uncooperative children. To minimise the time, the children attention was attracted by the game of naming the characters of the cartoon on the wall or by watching their favourite cartoon. Children younger than 1 year were distracted by a sound producing toy held in front of them. Children younger than 6 months were scanned in supine position while older children were scanned in sitting position (Figure 2-8).

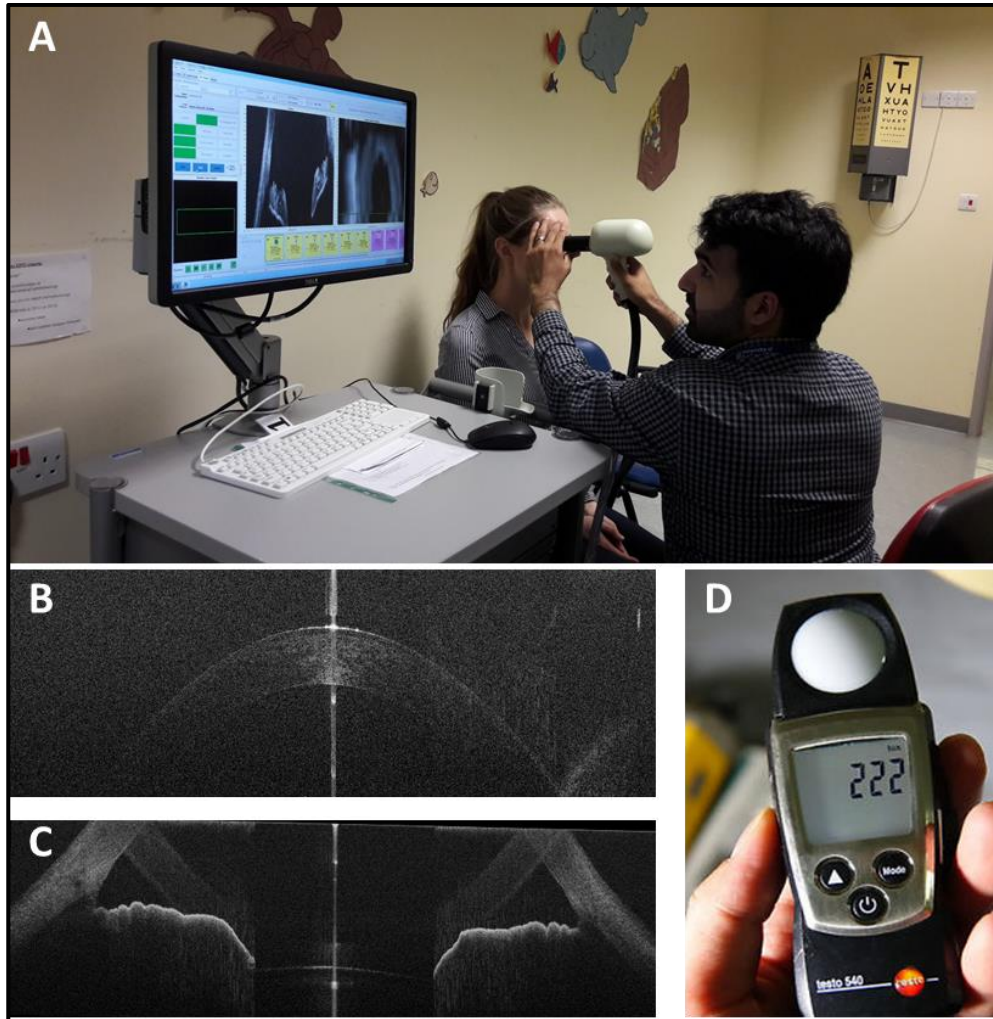


Figure 2-15: Optimisation of scanning environment

A) The examination room illumination intensity was optimised of about 200 lux. B) Example the OCT image of central cornea that the examiner is trying to capture. C) Example of the OCT image of anterior chamber image that the examiner is trying to capture. D) The illumination intensity was tested by lux metre (Testo Ltd, UK).

2.6 HH-OCT images analysis

Images were imported as OCT files into ImageJ 1.49 software (available at: <http://rsbweb.nih.gov/ij/>). The OCT reader enabled the assessment of all the obtained B scans per image. However, only the individual B-scan at the centre of pupil was selected for the final analysis to assess the nasal and temporal angle. In order to directly calculate the measurements, the image output was corrected by changing pixels in to micrometres. This correction is based on HH-OCT system information and was determined by the scanning depth of 3.4mm (2.5 mm in tissue), the number of pixels per line and the 1.38 refraction index of eye. The calibration factor of one pixel is equal to 2.45 μm . The image width is 7347 and height is 1010 pixels. The corrected image was saved as tiff (Figure 2-14).

The success rate of obtaining good quality images of the anterior chamber of healthy children was addressed in the feasibility section in chapter 3.

2.6.1 Programming of anterior chamber image analysis

As a part of this study I developed the analysis package of the anterior chamber and cornea using ImageJ. The steps of anterior chamber angle and cornea analysis were written and programmed in imageJ macro and was simplified as possible. The macro was tested with the assistance of my supervisor (Dr Proudlock). Two customised ImageJ macros were designed in this study, one for the analysis of cornea, where central corneal thickness (CCT) was calculated by manually drawing perpendicular line between the inner and outer margin of cornea (Figure 2-16). Then the CCT measurement was automatically saved as a text file.

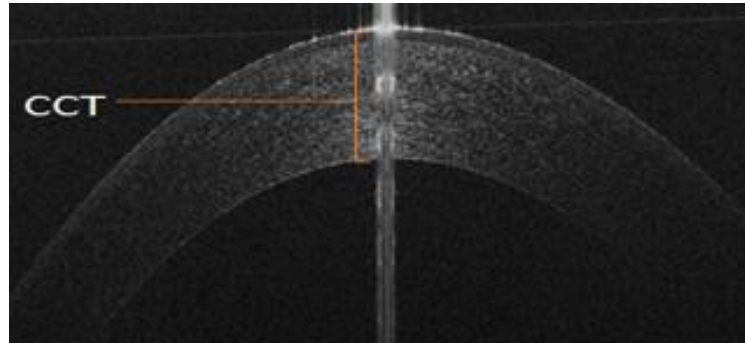


Figure 2-16: The measurement of central corneal thickness by HH-OCT. The distance between the outer and the inner surfaces of cornea represents the central corneal thickness (CCT) µm. The reflection indicates the image at the centre of pupil.

The second customised macro was used for the analysis of anterior chamber angle image.

The analysis steps designed in this macro are detailed as following:

- a) Firstly, manual identification of the position of scleral spur, Schwalbe's line and angle recess in each angle in the tiff image shown above (Figure 2-14) was saved in the ROI manager of ImageJ. The criteria of identifying the landmarks were as following:
 1. Scleral spur is identified as the point of the change of the curvature of the inner corneoscleral junction (inward protrusion) (Cumba et al., 2012).
 2. Schwalbe's line is identified at the end point of the inner corneal layer (endothelium) at the anterior end of the trabecular meshwork.
 3. Angle recess was identified as the point of junction between iris and inner corneoscleral junction;
- b) The x and y coordinates of each landmark were saved. Using the ROI manager of ImageJ, automatic calculation of the following parameters between nasal and temporal angle landmarks was established. Each measurement was calculated automatically as a distance between the landmarks values in ROI manger (Figure 2-17). The formula of calculating the distance between two points is:

$$\text{Distance} = \sqrt{(x_2 - x_1)^2 + (y_2 - y_1)^2}$$

These measurements (Figure 2-18) are:

1. Nasal scleral spur to temporal scleral spur distance (SS-SS-D)
2. Nasal Schwalbe's line to temporal Schwalbe's line distance (SL-SL-D)

3. Pupil diameter was measured manually as a distance between the margins of pupillary iris.
- c) The image was then magnified for the analysis of each angle individually. To ensure the measurements are perpendicular to the inner margin of cornea, the image was flipped in a position that showed the cornea horizontally at the bottom with iris above cornea. This alignment ensured that all measurements were calculated perpendicular to the cornea. The following anterior chamber angle parameters were individually calculated in each angle in turn, starting by nasal angle then temporal angle. These measurements (Figure 2-19, 2-20 and 2-21) are:
1. Measurements derived from identification of scleral spur only.
 - a. Scleral spur angle opening distance (SS-AOD), which is perpendicular distance between scleral spur and iris. It was measured automatically in the ROI manger (Figure 2-19) after adding the coordinates of the point where a line perpendicular to the cornea, at scleral spur, cross the iris.
 - b. Scleral spur limbal distance (SS-LD), which is perpendicular distance between scleral spur and outer margin of limbus.
 2. Measurements derived from identification of Schwalbe's line only (2-20).
 - a. Schwalbe's line angle opening distance (SL-AOD). Which is a perpendicular distance between Schwalbe's line and iris. It was measured automatically in The ROI Manger after adding the coordinate of the point where a line perpendicular to the cornea, at Schwalbe's line, cross the iris.
 - b. Schwalbe's line angle opening distance 500 (SL-AOD500). Which is perpendicular distance between a point 500 µm posterior to Schwalbe's line and iris. It was measured automatically in The ROI Manger after adding the coordinate of the point where a line perpendicular to the cornea, at 500 µm posterior to Schwalbe's line, cross the iris.
 - c. Schwalbe's line trabecular iris surface area (SL-TISA), which is a trapezoid area between SL-AOD, SL-AOD500, trabecular meshwork and iris.
 - d. Schwalbe's line limbal distance (SL-LD), which is perpendicular distance between Schwalbe's line and outer margin of limbus (2-21).
 3. Measurements derived from identification of scleral spur and Schwalbe's line.

- a. Trabecular meshwork length (TML). Is automatically calculated as a distance between the coordinates of Schwalbe's line and scleral spur (2-20).
 - b. Trabecular iris surface area (TISA). Which is a trapezoid area between SS-AOD, SL-AOD, TML and iris.
- d) All the x and y coordinates and measurements were automatically saved in text file. The text files were then imported in to Microsoft TM Excel sheet template. Each angle measurements were arranged in separate row (Figure 2.22).

The reproducibility of landmarks identification and anterior chamber angle measurements was investigated in both healthy children and patients in chapter 3.

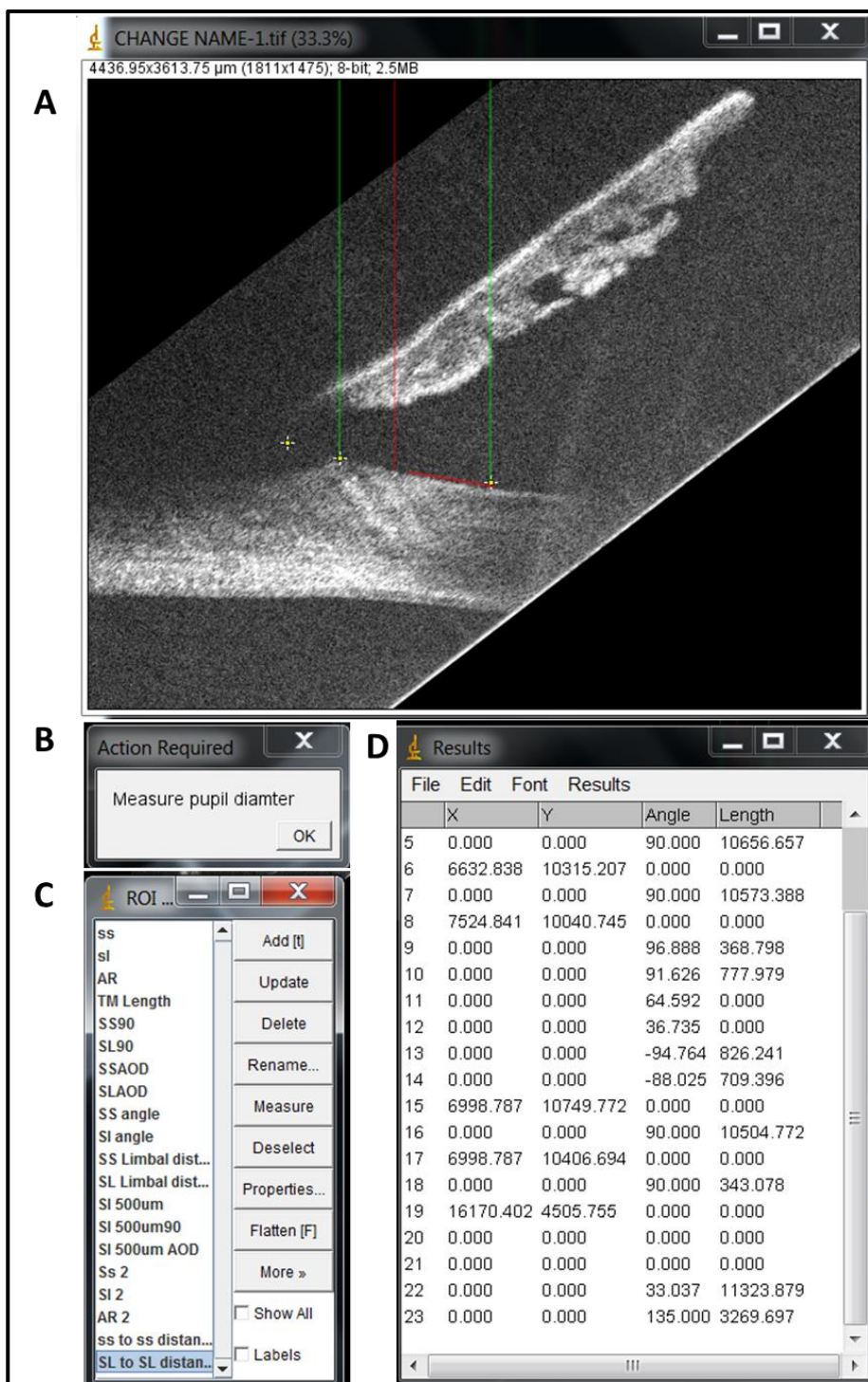


Figure 2-17: Example of the anterior chamber angle analysis using ImageJ macro.

A) The angle image is flipped with the iris above the cornea. This allowed calculating the parameters perpendicular to the cornea. B) The instruction of analysis that requires manual placement is programmed to appear in the window of action required. C) Once the action is performed, the x and y coordinates of landmarks points are recorded in ROI manager and (D) the programmed measurements are calculated automatically and saved in the results window.

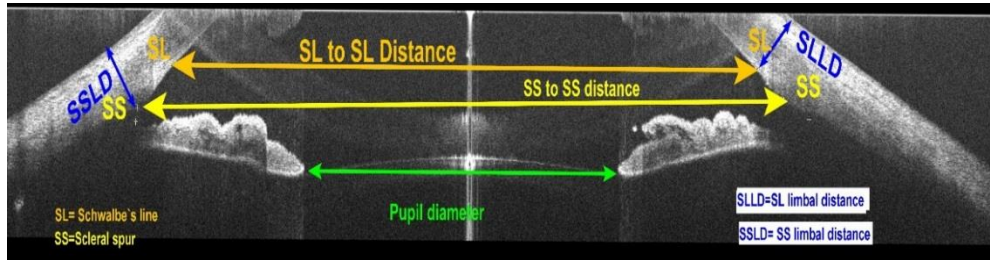


Figure 2-18: HH-OCT B-scan showing anterior chambers measurement
The shown measurements were calculated automatically by ImageJ after manual identification of landmarks, SS = scleral spur, SL= Schwalbe's line . Distance between nasal angle to temporal angle Schwalbe's lines = (SI- SL-D), Distance between nasal angle to temporal angle scleral spurs (SS-SS-D), Pupil diameter.

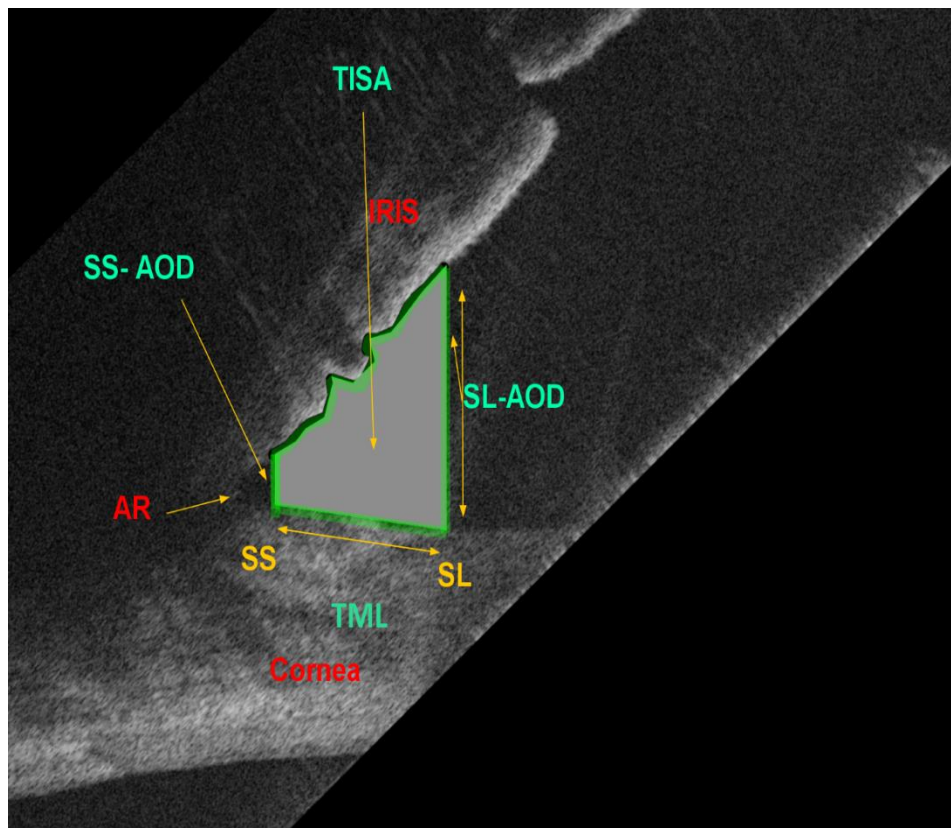


Figure 2-19: HH-OCT B-scan showing anterior chambers angle measurements
These measurements are calculated automatically by ImageJ after manual identification of landmarks. Distance between Schwalbe's line and scleral spurs represents trabecular meshwork length (TML) μm . Distance between scleral spur (SS)and iris represents scleral spur angle opening distance (SS-AOD) μm . Distance between Schwalbe's line and iris represents Schwalbe's line angle opening distance (SL-AOD) μm . The area between SL-AOD, SS-AOD, TML and iris represents trabecular iris surface area (TISA) mm^2 .

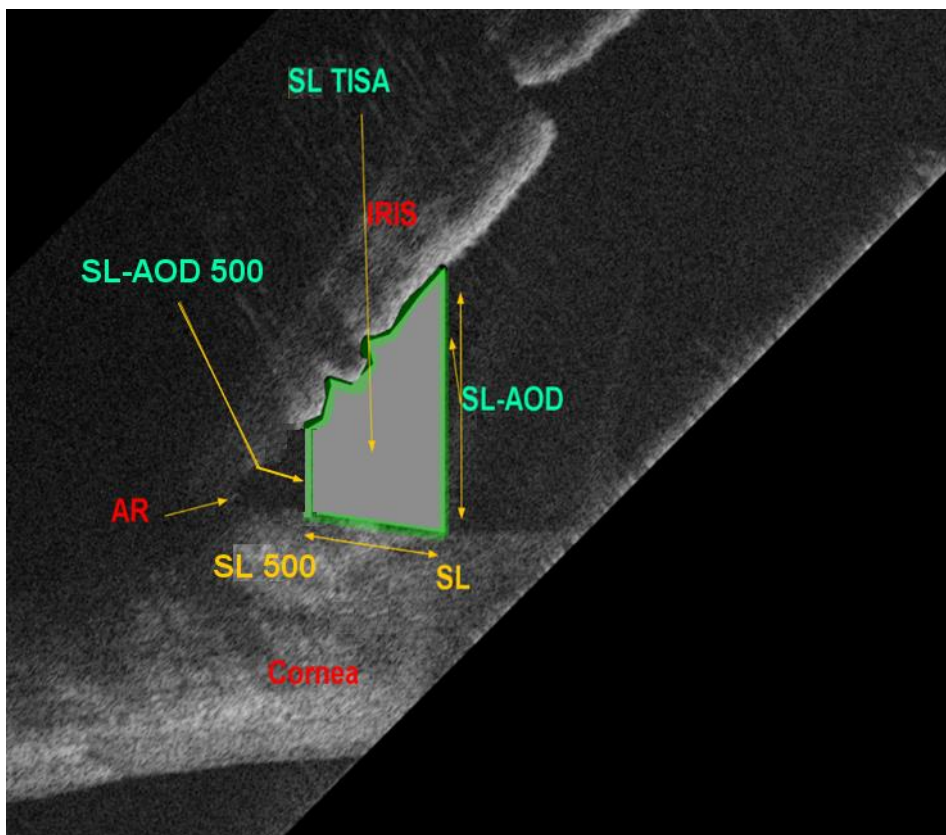


Figure 2-20: HH-OCT image showing anterior chambers angle measurements based on identification of Schwalbe's line.

After manual identification of Schwalbe's line (SL). The point at fixed 500 μm posterior to Schwalbe's line is manually placed (SL500). Distance between SL500 and the iris represents Schwalbe's line angle opening distance (SL-AOD500). The area between SL-AOD, SL-AOD500, trabecular meshwork and iris represents Schwalbe's line trabecular iris surface area (SL-TISA). These two parameters are dependent on identification of Schwalbe's line only.

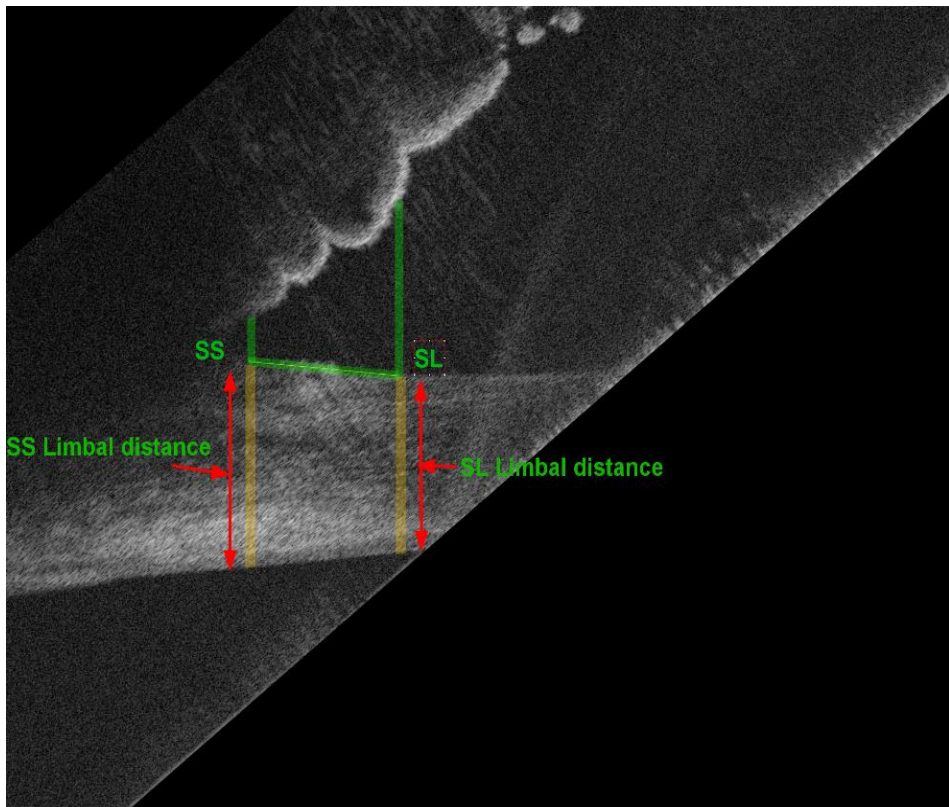


Figure 2-21: HH-OCT image showing limbal distance measurements.
Distance between Schwalbe's line (SL) and outer surface of cornea represents Schwalbe's line limbal distance (SL-LD) μm . Distance between scleral spur (SS) and outer surface of cornea represents limbal distance (SSLD) μm .

	B	C	D	E	H	I	J	K	L	M	N	O	Q	R	S	T
1	ID	TML	SSADD	SLADD	SSLD	SLLD	SL-500ADD	TISA	SL-TISA	SS-55D	SL-SL D	PD	X(ss)	Y(ss)	X(SL)	Y(SL)
2	ISABELMIN	767.926	470.4	962.878	904.05	786.45	545.572	575889.5849	387289.8211	13435.446	12243.626	5102.573	3983.7	12570.35	4748.1	12644.45
3	4ISABELMIN	866.38	286.65	904.08	896.7	749.7	514.71	565708.5295	368798.2729	13222.251	12040.292	5163.177	1764	12820.85	2623.95	12345.8
4	4ISABELMIN	805.219	308.7	1014.3	962.878	801.15	374.922	562348.7197	358038.4217	13525.739	12376.173	5108.097	2726.85	13004.6	3528	13085.45
5	4ISABELMIN	727.613	250.008	889.35	931	828.1	382.326	447398.9508	332223.619	13234.557	11935.868	5220.053	4846.1	12005	5566.4	12107.9
6	6BELLAPECU	728.437	259.7	852.6	818.3	666.4	426.3	428194.9208	330023.8519	12462.637	11453.654	4747.093	5653.5	11451.3	6384.7	11519.3
7	6BELLAPECU	647.676	227.85	646.8	948.15	801.15	279.397	312547.931	248215.9772	12591.248	11573.896	4770.98	1793.4	13252.05	2432.85	13354.95
8	6BELLAPECU	633.314	284.2	578.2	764.4	739.9	328.446	260171.0295	218503.8867	13276.261	12061.951	5430.65	4106.2	12646.9	4738.3	12607.7
9	1018BETHFINN	759.5	396.9	945.751	828.1	735	588	509871.7173	383437.75	13132.423	11955.108	6734.279	5033.55	12250	5853.05	12250
10	1018BETHFINN	936.528	308.7	1068.2	980	891.813	597.82	660371.4859	420800.7505	13067.633	11677.532	6837.412	2672.35	13940.5	3608.85	13374.8
11	1018BETHFINN	816.317	196.061	935.913	994.7	867.3	426.328	503161.4396	354391.7478	13077.433	12018.113	6313.817	4326.7	12441.1	5135.2	12553.8
12	0019JAYSAH	663.632	289.1	733.815	744.8	637	411.717	376000.5528	310505.0494	12863.143	11800.805	5210.129	4035.15	12166.7	4696.65	12220.6
13	0019JAYSAH	743.444	352.8	901.653	872.2	700.7	499.8	498181.0959	362000.4944	12737.608	11616.726	5228.615	3319.75	12896.8	4064.55	12380.1
14	10019JAYSAH	752.513	313.638	994.712	759.5	627.2	450.906	534781.0099	377755.1797	13560.694	12370.946	6124.271	4853.45	12152	5533.35	12289.2
15	20THOMASS	852.727	389.619	1242.172	815.85	712.95	801.184	689364.5522	508607.9984	13293.422	11981.007	6370.246	4917.15	12245.1	5769.75	12230.4
16	20THOMASS	842.529	367.794	1102.525	918.75	816.38	632.1	652941.2461	444287.196	13371.981	11986.731	7026.429	2227.05	13445.6	3064.35	13533.8
17	20THOMASS	933.64	298.94	980.012	1014.3	813.4	553.7	659048.1961	398384.9268	13544.82	11986.302	6951.15	2102.1	13024.2	3023.3	13176.1
18	1021TILLYFIR	781.008	284.369	651.718	916.3	896.7	509.6	402192.1445	304124.2707	14160.447	12803.611	7126.884	2486.75	12605.25	3260.95	12708.15
19	1021TILLYFIR	853.981	286.744	911.4	14322.7	896.7	573.3	518333.9752	372230.3885	13668.04	12327.832	7056.218	3841.6	13406.4	4701.55	13413.75
20	22TESSBUNT	843.453	235.315	867.331	932.277	793.8	396.9	518947.4923	332672.7104	12079.46	10895.027	6141.403	2329.95	13364.75	3160.5	13511.75
21	22TESSBUNT	793.8	338.195	1014.312	872.2	784	509.624	536786.2143	380984	12259.437	11007.422	6741.533	3453.4	13617.1	4253.2	13617.1
22	22TESSBUNT	770.719	176.4	646.819	1029.012	847.7	352.936	369762.8605	269610.9759	12039.145	10953.916	6760.865	4802	11867.8	5556.6	12024.6
23	1023JENNALA	565.596	300.551	784.007	751.333	692.533	320.2	313335.6473	281194.9966	12420.604	11488.692	5631.309	5371.216	11473.863	5936.35	11502.75
24	1023JENNALA	519.657	215.625	542.354	833	754.6	205.904	200683.6992	190524.226	12383.438	11455.363	5553.844	2101.283	13134.45	2620.683	13150.783
25	1023JENNALA	852.344	294.018	793.86	588	578.2	444.267	428621.0123	296753.7339	13790.382	12514.496	5772.011	4733.4	12232.85	5582.733	12154.45
26	1023JENNALA	856.091	388.747	777.474	826.467	728.467	486.745	490663.9822	313108.2465	13022.509	11594.099	6121.01	2583.117	12678.75	3438.963	12653.15
27	124GRACEDH	568.532	199.294	630.476	882	790.533	267.947	256225.0646	232854.9566	12253.626	1103.342	6800.522	4541.483	12593	5123.483	12635.467
28	124GRACEDH	621.199	152.216	877.114	877.1	735	347.935	338930.2354	318108.2861	12312.737	11233.726	6338.282	4044.95	13031.55	4662.35	13100.15
29	124GRACEDH	836.3	147	757.086	933.45	764.4	272.347	418178.11	270658.7434	12355.596	11103.662	6382.238	4135.6	12438.65	4966.15	12541.55
30	1025DEVDEH	519.724	176.4	681.118	769.3	637	215.823	239504.4617	239481.4145	12665.401	11510.721	5720.189	3236.45	13227.55	3750.95	13301.05
31	1025DEVDEH	673.87	117.702	617.419	896.7	823.2	158.02	266480.0627	203986.1867	12686.743	11632.036	5687.446	4498.2	12137.3	5163.5	12196.1
32	27EDIIMAC	555.864	127.494	519.423	808.5	744.8	186.264	192664.0627	186710.4832	12887.317	11853.558	5037.314	2557.8	12913.95	3111.5	12962.35
33	9DEVAMMAH	774.34	205.858	803.6	886.9	754.6	343.035	422212.7514	298937.7989	12267.77	11087.102	5572.642	3505.35	12357.8	4275.25	12446
34	9DEVAMMAH	710.217	235.2	773.239	955.5	830.55	382.271	386419.3108	302627.7055	12188.912	10363.301	5600.046	4101.3	11937.65	4806.9	12078.5
35	80SHRY KRIS	918.956	242.55	815.883	815.85	735	485.1	535916.0991	338435.9036	13271.715	11905.368	4023.747	3586.8	12318.6	4498.2	12436.2

Figure 2-22: Example of data in Excel sheet template.
The measurement from each image is saved automatically in the same row.

2.7 Normal distribution of data

Visual inspection of data histograms, normal Q-Q plots and P-P plots showed that all the anterior chamber measurements were approximately normally distributed. Examples of normal distribution of one of the measured parameters are shown in (Figure 2-23 and 2-24). We found that the Shapiro–Wilk test and Kolmogorov–Smirnov tests are statistically significant. However, this has been reported to result in case of a large sample size (> 30 subjects), where even a small deviation from normality produce a significant p value (Ghasemi and Zahediasl, 2012). Lumley et al reported that in a large sample size, the t-test and linear regression are valid for any distribution and do not require the assumption of normal distribution (Lumley et al., 2002). We attempted a transformation of our data. However, the normality tests produced similar significant tests.

For comparing between normal and abnormal development of the anterior chamber in chapter 5 and 6, the equality of variances of the two compared groups is tested using the Levene's test, which showed a p value > 0.05 , indicating equal variances.

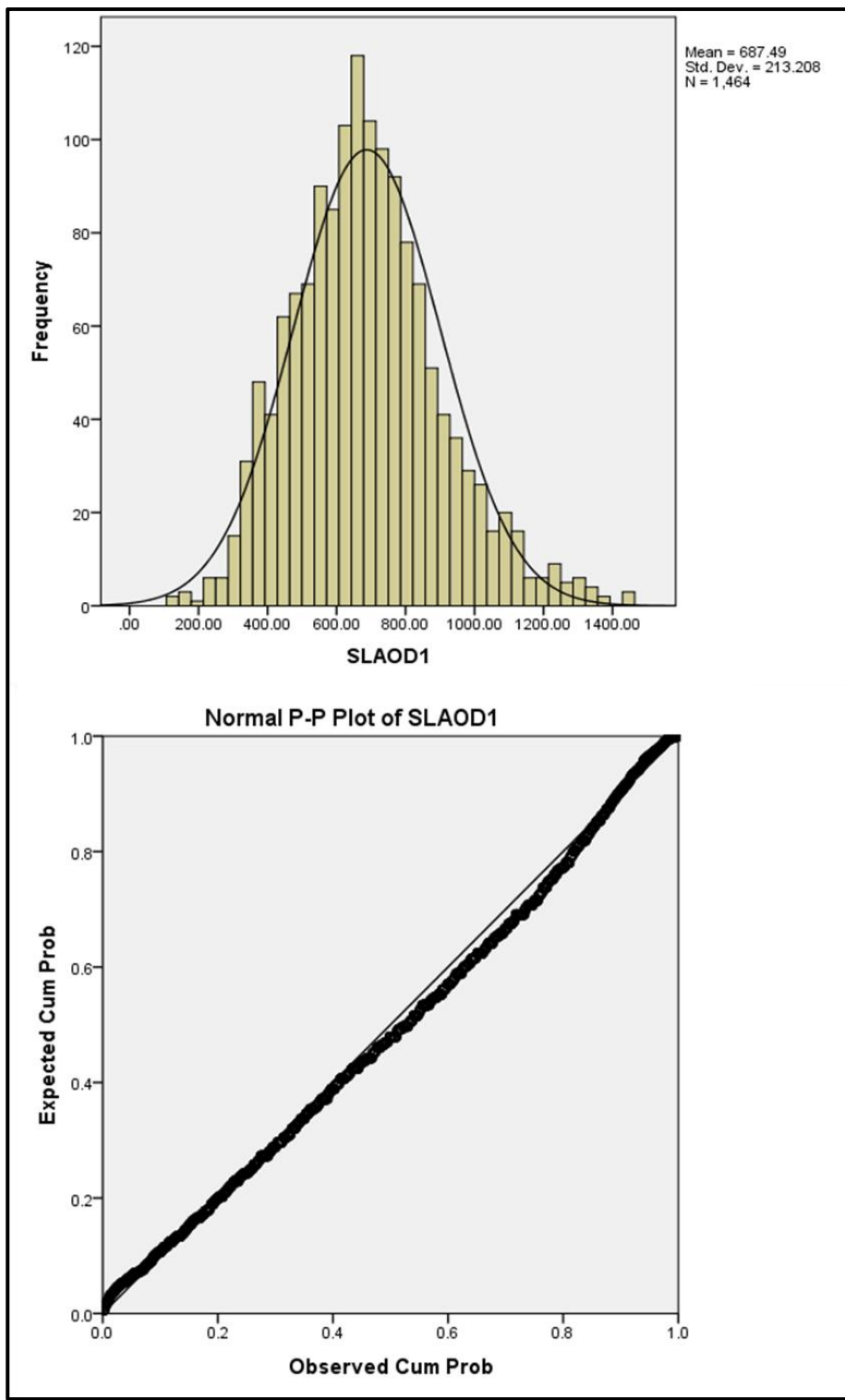


Figure 2-23: Example of the histogram and P-P plot of anterior chamber data. The histogram and p-p plot of Schwalbe's line angle opening distance (S-LAOD) indicate a normal (parametric) distribution. Histogram has one peak approximately at the centre. The P-P plot shows slight deviation at the data at the periphery from normal distribution which is the reason of positive normality tests.

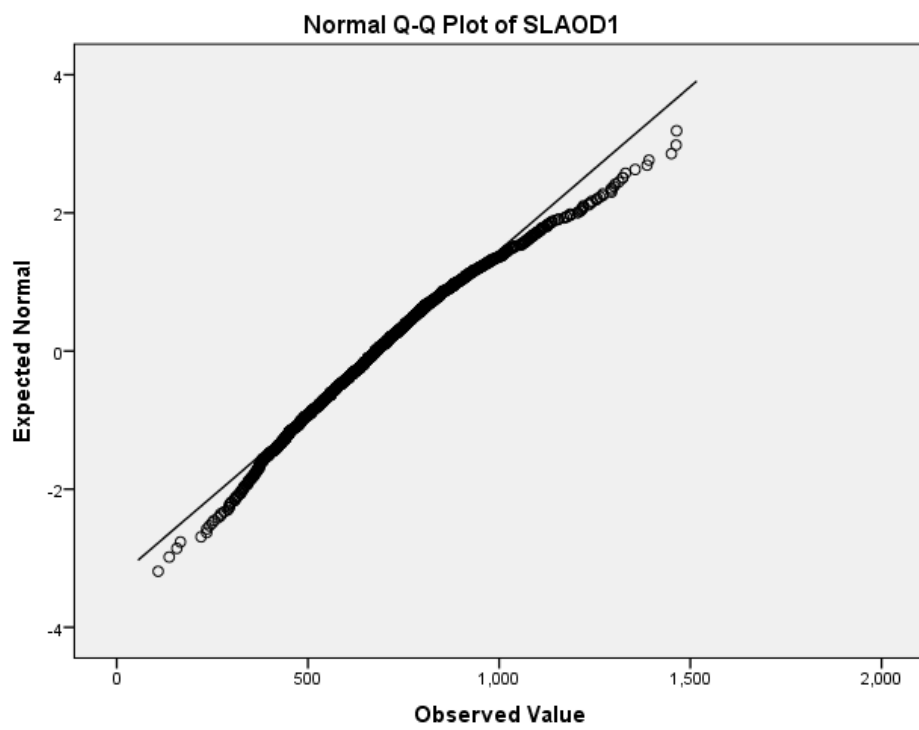


Figure 2-24: Example of Q-Q plot of normal distribution

The Q-Q plot shows some deviation of data at the the tail from normal distribution which is the reason of postive normality tests.

2.8 Statistical analysis.

2.8.1 Reproducibility of HH-OCT

The statistical analysis of reproducibility of HH-OCT (Chapter 3) was performed with SPSS™ software version 24.0 (SPSS™, Inc., Chicago, IL). The repeatability and reproducibility of HH-OCT measurements were assessed using:

1. Interclass correlation coefficients (ICC),

The ICC, with 95% confident intervals, was computed from the average of two measurements. The consistency of a two-way mixed effect model was used to assess the reproducibility of intraobserver, interobserver and test retest reproducibility. An ICC of greater than 0.9 indicates excellent reproducibility, between 0.75 and 0.9 good, between 0.5 and 0.75 moderate and less than 0.5 poor (Koo and Li, 2016)

2. Coefficient of variation (COV)

COV assesses the error of repeated measurements. We calculated the within-subject standard deviation of the two measurements per parameter then divided it by the mean of the repeated measures as a percentage. The small measurement's error (COV) indicates the more reliable parameter. COV of less than 10% is considered low enough for clinical reliability.

3. Bland-Altman plots

The absolute mean difference (bias), 95% level of agreement between the two repeated measures were described by Bland Altman plot. The significance level of the bias difference from zero was assessed by one sample t-test. A probability value of < 0.05 indicates a significant difference between the two measurements.

Two types of reproducibility of the HH-OCT in measurement of anterior chamber in children were tested

1. Intraobserver and interobserver reproducibility where the same image was analysed twice by same observer and a third time by another independent observer.
2. Test-retest reproducibility of two repeated images of the same eye obtained in the same examination.

2.8.2 Development of anterior chamber

The statistical analysis of normal and abnormal development of anterior chamber (studied in chapter 4, 5, and 6) was performed using STATA™ software (Copyright 1996-2018, Stata Corp). Multivariable fractional polynomial models were used to predict the best fit curve of the change of anterior chamber measurements with postmenstrual age. This type of regression modelling allowed automatic transformation of age to fit the changes of each measured variable. The age was transformed to the most suitable set of power (-2,-1, -0.5, 2 or 3 or log) in order to achieve the normal distribution of the skewed data. Further details of statistical modelling are described in each chapter. GraphPad Prism 7 was used to produce the graphs of the results.

2.8.3 Power calculation and sample size

Initially, the size of each age group was selected based on the rule of thumb (10 cases per predictor). Later on, G*Power (version 3.1.9.2) software (accessed on 21 June 2017) was used to calculate the achieved power of the obtained sample size (Figure 2-25). This is a free access flexible statistical program that provides power analysis for biomedical, psychological and social sciences (Faul et al., 2007). The power calculation is based on the r^2 value of mixed linear regression of Schwalbe's line angle opening distance (SL-AOD) parameter (due to unavailability of polynomial regression in G power), a sample size of 282 healthy participants, ($\alpha = 0.05$), F test, and 5 predictors (including age, gender, eye, angle and refraction). The effect size was automatically calculated based on r^2 where the effect size $f^2 = (1/1 - r^2)$. For $r^2 = 0.19$, the effect size of ($f^2 = 0.23$) had a median to strong range. The achieved power ($1-\beta$) was (0.99) which indicated a very good power and therefore an adequate sample size.

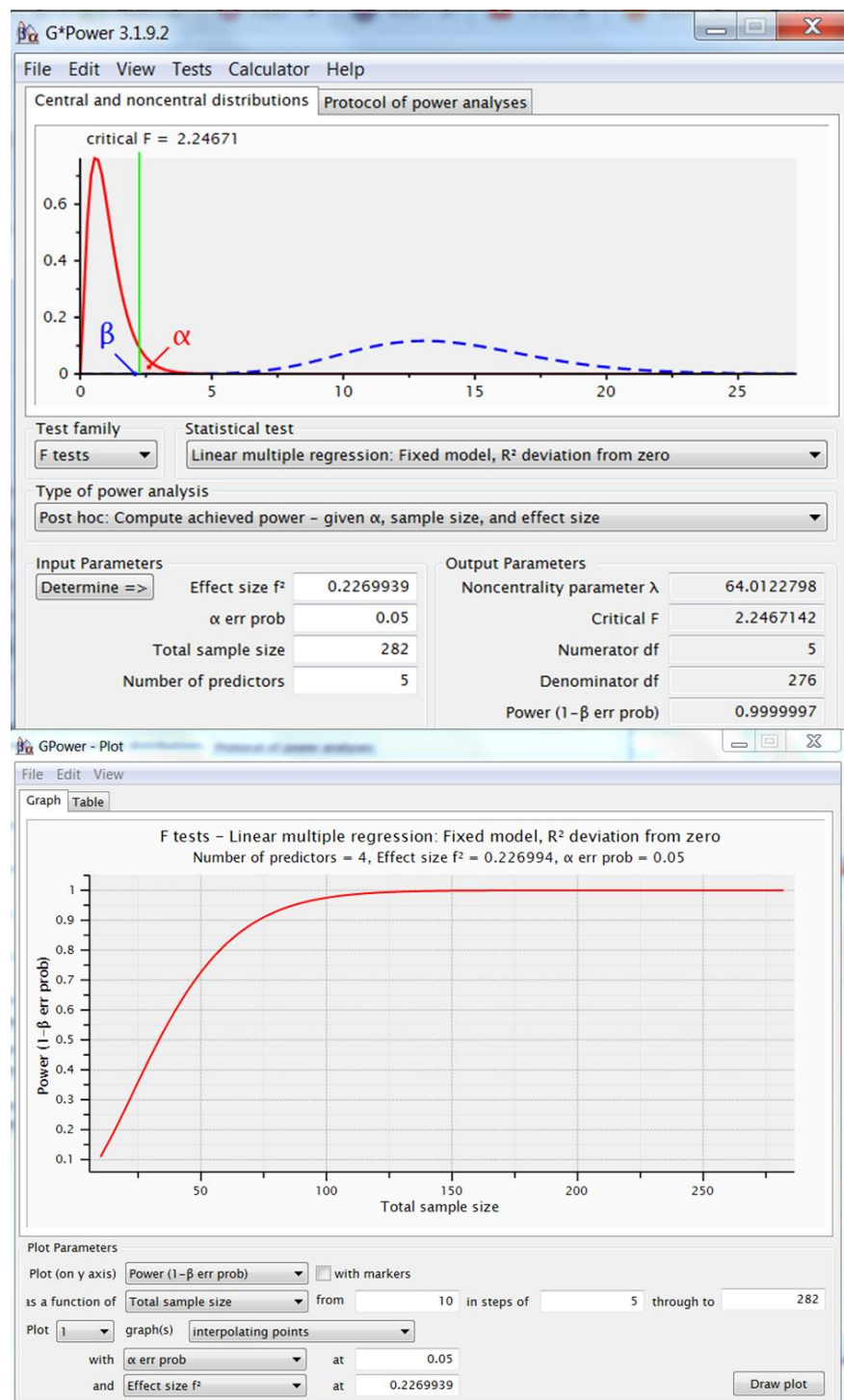


Figure 2-25: Example of calculation of achieved power of used sample size using G Power software.

The achieved power is calculated based on r^2 of multiple linear regression of Schwalbe's line angle opening distance(SI-AOD). The squared correlation coefficient ($r^2 = 0.19$) produce effect size of 0.23 and power (1- β) of 0.99 with $\alpha = 0.05$. This plot graph indicates that a sample of 150 participants can give our study a power of 99%. Therefore, Our sample size is very powerful to produce accurate results.

2.9 Discussion of the problems that were encountered in this study:

During data collection, enrolment of children between 6 months to 2 years old was quite difficult, partly because these age groups are uncooperative. So, it was hard to obtain scans easily. It was also not easy to recruit these age groups from the Children General Clinic. However, this improved when we started recruiting from nurseries.

Furthermore, although recruitment was easy from the Maternity Department in Leicester Royal Infirmary, the scanning of new-borns and prematures proved to be a challenge. The scan attempts could be long up to 1 hour as the baby is often asleep most of the time. The successful images were captured when the baby is awake. The parents sometimes withdraw the consent if there were a possibility to ask them to do the scan in a second visit, or if the session lasts for a long time.

The anterior chamber image of HH-OCT showed a reflection of cornea as an artefact. This reflection can interfere with the identification of anterior chamber angle landmarks. We attempted using MatLab program to correct the images. However, this was not possible due to limitations of time and the cost required to perform such corrections. In congenital glaucoma patients, it was not easy to get an image showing both angles together. Therefore, nasal angle and temporal angle parameters was not measured in all images.

The preliminary results showed a challenge in how to find the best fit growth curve for interpretation of the changes of parameters with age. The obtained measurements did not show linear changes. To overcome this, we used multivariable fractional polynomial modelling of Stata. It is a new modelling technique that enabled automatic estimation of the best fit curve of measurements with increasing age.

3. Chapter three: Feasibility and Reproducibility of Anterior Chamber Angle Measurements in Children Using Hand-held Spectral Domain Optical Coherence Tomography

This chapter aims are:

1. To assess the feasibility of imaging the anterior chamber in healthy children and obtaining good quality images.
2. To assess the variability of intraobserver and interobserver identification of anterior chamber angle landmarks in healthy children and children with congenital glaucoma and nystagmus
3. To assess the reproducibility of anterior chamber measurements in healthy children and children with congenital glaucoma and nystagmus.

3.1 Introduction

Anterior segment optical coherence tomography (AS-OCT) has been widely used to visualise the anterior segment of adults. Its capability of generating high-quality reproducible images has revolutionized our understanding of anterior chamber metrics (Goldsmith et al., 2005a). AS-OCT has been used to determine how anterior chamber depth, lens vault and angle width vary amongst adults of different ages (18 to 60 years) (Xu et al., 2008) and ethnicity (Nongpiur et al., 2010b) in both open-angle (Kim et al., 2011, Leung et al., 2010) and angle-closure glaucoma compared to healthy adults glaucoma (Nongpiur et al., 2013, Guzman et al., 2013). It has also provided easier angle evaluation and measurement of closure angle in adults with glaucoma than ultrasound biomicroscopy (Radhakrishnan et al., 2005a). AS-OCT has greater sensitivity in detecting narrow angles in glaucoma than gonioscopy (Sakata et al., 2008a).

Nevertheless, little is known about the anterior chamber biometry in either healthy children or those with ocular diseases. Congenital glaucoma is known to be associated with deep anterior chamber depth and large corneal diameter (deLuise and Anderson, 1983, Abu-Amero and Edward, 1993) (CD > 11mm in infants). Children with anterior segment dysgenesis might develop nystagmus, as a result of poor fixation of vision. Children with these diseases are frequently examined under general anaesthesia because they are often uncooperative. Also due to the unavailability of non-invasive techniques for paediatric eye examination, invasive techniques such as gonioscopy, are performed in order to derive a definitive diagnosis.

AS-OCT is a non-invasive technique that permits comfortable and safe examination of the eye (Ramos et al., 2009), whereas table-mounted OCT machines requires stabilisation of the head and steady gaze fixation, which is difficult to achieve in children without sedation. A hand-held spectral domain OCT (HH-OCT), designed for imaging eyes of children, has been developed to overcome these obstacles. HH-OCT has been successfully used for visualization of the fovea and optic nerve (Maldonado et al., 2010, Lee et al., 2013a) and achieves rapid scanning in a few seconds (Patel et al., 2016). However, HH-OCT application in measuring the anterior chamber angle has not been systematically investigated.

The majority of studies of anterior chamber measurement in adults are based on the identification of the scleral spur (SS) using ultrasound and Time Domain OCT (TD-OCT). (Sakata et al., 2008a, Pavlin et al., 1992). Good reproducibility of parameters derived from the SS has been shown using TD-OCT, including angle opening distance (AOD), trabecular iris surface area (TISA), and trabecular iris angle (TIA) (Cumba et al., 2012, Narayanaswamy et al., 2010b). However, localisation of SS is sometimes difficult and often unidentifiable using Spectral domain OCT (SD-OCT) (Sakata et al., 2008c, Liu et al., 2010). SD-OCT provides better visibility of SL than SS (Wong et al., 2009). The angle measurements based on the identification of Schwalbe's line (SL), have become more frequently used in SD-OCT (Wong et al., 2009). These measurement include SL-AOD, and SL-TISA.

In this study, we investigated healthy children and children with pathology, including children with glaucoma, where AS-OCT is likely to have clinical relevance. We also assess whether AS-OCT imaging is feasible in children with nystagmus, **i.e.** whether the HH-OCT

images can be acquired in the presence of continuous eye movements. We evaluate (1) the success rate of obtaining good quality AS-OCT scans, (2) the intra-observer and inter-observer assessment of identification of scleral spur and Schwalbe's line and (3) the repeatability and reproducibility of anterior chamber measurements of parameters derived from either SS or SL or both of them. These research questions are assessed in healthy children, children with congenital glaucoma and nystagmus younger than 6 years of age.

3.2 Methods

3.2.1 Participants

Children were only included if parents gave consent and older co-operative children gave assent. The total number of participants enrolled in this study were 190 healthy children, 17 children with congenital glaucoma and 18 children with nystagmus, with ages ranging from 2 days up to 6 years old. In addition, the feasibility in this age group was compared to the feasibility of older healthy children. The quality of older children images were assessed to be included in the next chapter of the normal development of anterior chamber.

All children were recruited from outpatient paediatric clinics and the neonatal unit. Healthy participants were only included if they had no known ocular or neurological pathology, no family history of ocular abnormalities, no history of previous eye disease, surgery, trauma or medication that can affect eye geometry. Children with congenital glaucoma were receiving medication and either had previous surgery or were waiting for surgical intervention. Nine of nystagmus children were diagnosed with albinism which was distinguished from idiopathic infantile nystagmus (IIN) by presence of iris trans-illumination, abnormal chiasma crossing with asymmetry of visual evoked potentials and foveal hypoplasia observed using HH-OCT retinal images (Further details of the steps of the diagnosis of albinism and IIN is described in figure 2.1).

3.2.2 OCT imaging and analysis

The anterior chamber of the children eyes were scanned with HH-OCT system without sedation in sitting position. The 25mm lens was used to obtain At least 2 repeated horizontal volumetric scans per eye on the same examination day. (The steps of image acquisition have been described in section 2.5.1.) The examination room light was controlled at ~200 lux. Scans were exported into ImageJ software v1.49 (available at <http://rsbweb.nih.gov/ij/> accessed on 12/07/2015). Each volumetric scan was evaluated and a clear B scan of anterior chamber, at the centre of pupil was selected and saved as tiff for analysis using a customised ImageJ macro (details of image analysis and measurements were described in section 2.6)

3.2.3 Feasibility analysis

The scan's success rate was assessed per age group (Table 3.1). We assessed the success rate of scanning healthy children, recruited for this study, without sedation. We also assessed the percentage of the good quality images among those obtained scans, to be sufficient to conduct quantitative measurements of the anterior chamber. The image was identified to be of a good quality if both temporal and nasal angles were clearly seen together and a clear peripheral cornea, iris and corneoscleral junction were visualized. In addition, a reflection of cornea appeared inverted inward. If scans were tilted, unclear, the aforementioned structures were partially cut or the reflection of cornea interferes with the clarity of angle structure, then the image was considered unsuccessful (Figure 3.1). The feasibility of patients was not assessed due to the small sample size of each age group of the patients.

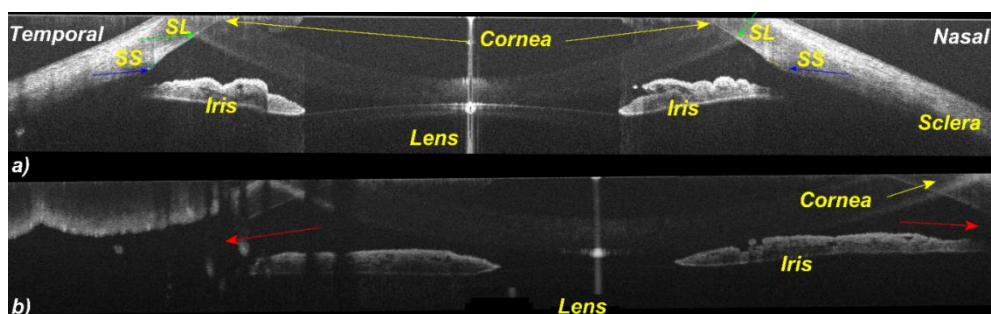
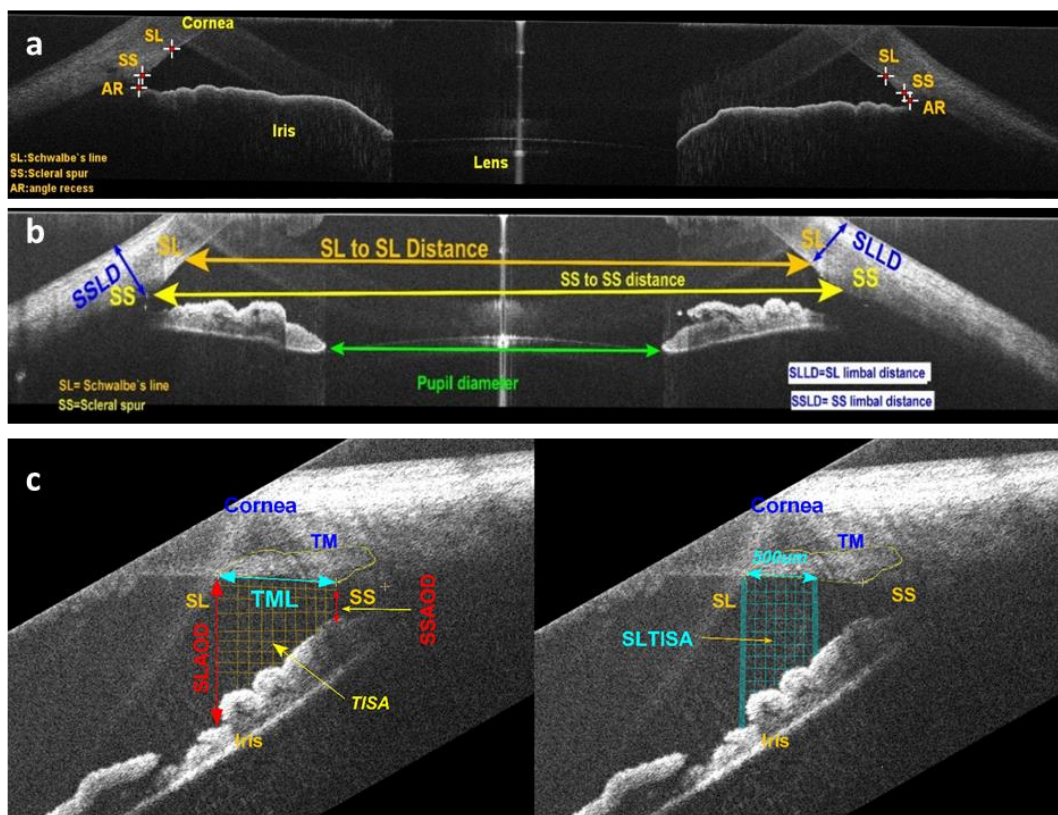


*Figure 3-1:Criteria of good quality anterior chamber image.
a) example of good HH-OCT image shows both temporal and nasal angles together, clear peripheral cornea, iris and corneoscleral junction. b) Unsuccessful image because the structures are partially cut and the angles are not clearly visible (red arrow). SL= Schwalbe's line, SS=scleral spur, AR= angle recess.*

3.2.4 Quantitative measurements of anterior chamber

The image analysis was based on manual identification of the iridocorneal angle landmarks, scleral spur (SS) and Schwalbe's line (SL) in nasal and temporal anterior chamber angle. Calculation of measurements was done semi-automatically. Criteria of identification and definition of the measurements has been described in details in section 2.6.1 and is summarized in (Figure 3.2). We measured the nasal and temporal angle parameters individually.



The criteria of identifying the landmarks or calculating the parameters

Angle landmark

Scleral spur (SS)	The point of change of the curvature of the inner corneoscleral junction (inward protrusion) (22);
Schwalbe's line (SL)	The point of termination of basement membrane of the cornea appearing at the end point of the inner cornea represents anterior end of the trabecular meshwork

Angle measurements based on SS

SSAOD	The distance calculated between scleral spur and iris perpendicular to the inner cornea.
--------------	--

Angle measurements based on SL

SLAOD	The distance calculated between Schwalbe's line and iris perpendicular to the inner cornea.
SLAOD500	The distance between trabecular meshwork 500 µm posterior to Schwalbe's line and iris perpendicular to the inner cornea
SLTISA	The trapezoidal area between SLAOD, SLAOD500, fixed 500 µm of trabecular meshwork posterior to Schwalbe's line and iris.

Angle measurements based on both SS and SL

TML	The distance between scleral spur and Schwalbe's line.
TISA	The trapezoidal area between SSAOD, SLAOD, TML and iris.

Limbal distance

SSLD	Perpendicular distance between scleral spur and outer corneoscleral junction.
SLLD	Perpendicular distance between Schwalbe's line and outer corneoscleral junction.

Anterior chamber width (ACW)

SSSSD	Anterior chamber width between nasal and temporal SSs
SLSLD	Anterior chamber width (ACW) between nasal and temporal SLs

Figure 3-2: Summary of anterior chamber measurements using HH-OCT image.

a) HH-OCT image of anterior chamber, an individual B scan consists of 3000 A scans, 18mm width and 6 mm height, captured within 0.96 sec, shows both nasal and temporal angles. The analysis based on manual identification of the iridocorneal angle landmarks, scleral spur (SS) and Schwalbe's line (SL) in nasal and temporal angle, followed by semiautomatic calculation of b) anterior chamber width (SS-SS-D and SL-SL-D and limbal distance c) angle measurements based on SS, SL or both SS and SL, anterior chamber width.

3.2.5 Reproducibility of HH-OCT measurements

The reproducibility of identification of anterior chamber landmarks and obtaining quantitative measurements using HH-OCT images was only evaluated in children younger than 6 years old, the age group in which the table-mounted OCT machine could not be used. Three groups were involved in this part of study including healthy children, children with congenital glaucoma and children with nystagmus. Due to time consuming of repeated analysis of same images, only 40 healthy children were randomly included for the reproducibility study.

3.2.5.1 Intraobserver and interobserver variability of landmark identification

The intra-observer assessment was performed by analysing the same anterior chamber image twice by the same observer (BE) at different time points. In which the angle landmarks were identified and used to calculate the quantitative anterior chamber measurements. The same images were then analysed independently by observer 2 (SSH) to assess the inter-observer agreement. SSH has also identified the landmarks and calculated the anterior chamber measurements from 50 images of each group.

3.2.5.2 Repeatability and reproducibility of anterior chamber measurements

In addition to the intra-observer (BE), and inter-observer (BE and SSH) assessment of repeatability and reproducibility of the same image. The same observer (BE) assessed the measurements of two repeated images of the same eye, obtained consecutively on the same examination day. This test-retest reproducibility was evaluated in 100, 20 and 34 repeated images, obtained consecutively in the same session, of healthy children, congenital glaucoma and nystagmus, respectively. To test the effect of accommodation on

angle measurements, the repeated images with larger pupil diameter (PD) were compared to images with smaller PD.

3.2.6 Statistical analysis

The intra-observer and inter-observer variability of localising the anterior chamber landmarks in the same image was assessed by calculating the bias and the precision (2 standard deviation of the bias) of the repeated positions of X and Y coordinates of each landmark, measured in μm (1 pixel = $2.45 \mu\text{m}$). The bias of X and Y coordinates placement represents the variability between the observers in locating the landmarks. The precision shows how close the observers have located the landmark at the same point. A one sample t-test was used to detect a significant difference in bias from zero. This could not be done in the repeated images because the landmarks coordinates have different values depending on the relative position of angle structures in each image to the frame.

Reproducibility of anterior chamber measurements were assessed by interclass correlation coefficients (ICC), the coefficient of variation (COV) and Bland Altman plots. The proportional bias of first to second measure difference as a function of average of repeated measures was assessed by regression models. All statistical analysis was performed using SPSS version24 (SPSS™, Inc., Chicago, IL).

3.3 Results

3.3.1 Feasibility

In healthy children, the rate of success in obtaining anterior segment scan among the total recruited children younger than 6 years old was 89% (169/190) compared to 100% of the healthy children older than 6 years (Table 3.1). Children aged between 1 to 6 months had the lowest success rate of 76% (16/21).

In those 89 % of anterior segment images, the percentage of good quality images showing both nasal and temporal angles was 86% (ranging from 69% to 100%). Children aged between 6 to 12 months had the lowest percentage of good anterior chamber images 69% (11/16). Cornea was easier to capture than angles with success rate ranged from 91% to 100%.

Table 3-1: Percentage of successful HH-OCT anterior chamber images among different age groups of healthy participants.

Age	Healthy participants number	Success rate of obtaining scans number (%)	Good quality scans of cornea/obtained images (%)	Good quality scans of angles/obtained images (%)
< 1 month	25	22 (88)	20 (91)	18 (82)
1-6 months	21	16 (76)	15 (94)	13 (81)
6-12 months	17	16 (100)	16 (100)	11 (69)
1-2 yrs	22	18 (77)	18 (100)	15 (83)
2-3 yrs	27	24 (89)	24 (100)	21 (88)
3-4 yrs	35	32 (91)	32 (100)	30 (94)
4-5 yrs	21	20 (95)	20(100)	17 (85)
5-6 yrs	22	21 (95)	21 (100)	21 (100)
Total	190	169 (89)	166/169 (98)	146/169 (86)
6-7 yrs	19	19 (100)	19 (100)	19 (100)
7-9 yrs	21	21 (100)	21 (100)	21 (100)
9-12 yrs	26	26 (100)	26 (100)	26 (100)
Total	265			

3.3.2 Reproducibility of HH-OCT

The reproducibility study included 40 healthy children (mean age \pm S.D: 2.8 ± 1.9 years), 18 children with congenital glaucoma (mean age 2.04 ± 2.04 years) and 18 with nystagmus (mean age 4.5 ± 1.8 years).

3.3.3 Intraobserver and interobserver variability of landmark identification

Both intra-observer and inter-observer assessments of congenital glaucoma, nystagmus and healthy children showed no significant difference in the x and y coordinates of SL (all $p > 0.05$, Table 3.2). In contrast, the inter-observer identification of SS in congenital glaucoma showed a negative bias ($p < 0.001$) because the first observer (BE) located the SS more close to angle recess (Figure 3.3), while the second observer (SSH) placed the SS away from angle recess and more close to SL.

In both assessments, the precision in identifying SL was narrower compared to SS. The precision of the repeated localization of the x coordinates of SL, by the same observer, was within a distance of 58.7 μm , 75.9 μm and 105.6 μm in healthy controls, nystagmus and glaucoma, respectively. To simplify this, the same observer could locate the SL in the repeated analysis within 58.7 away from the location of SL in the first analysis of the same image in healthy child. The intraobserver assessment was wider than the intraobserver assessment, because the second observer could locate the x coordinates of SL within a distance of 115.7 μm , 121.9 μm and 171.9 μm from the first observer in healthy controls, nystagmus and glaucoma, respectively.

Glaucoma had wider precision compared to nystagmus and healthy children, indicating more difficult identification of the landmark at the same position.

Table 3-2: The intraobserver and interobserver agreement of identification of landmarks of healthy children, nystagmus and congenital glaucoma groups.

Intraobserver			Interobserver			
Healthy controls n = 50						
Placement of landmark	Bias (precision) µm	p value	COV %	Bias (precision) µm	p value	COV %
SS x difference	-2.9 (95.8)	0.68	0.70%	-18 (158.2)	0.12	1.05%
SS y difference	0.2 (28.5)	0.94	0.07%	-4.1 (40.7)	0.17	0.09%
SL x difference	1.0 (57.7)	0.81	0.38%	-2.4 (115.7)	0.77	0.68%
SL y difference	0.6 (16.2)	0.63	0.04%	0.5 (21.5)	0.74	0.04%
Nystagmus n = 50						
SS x difference	3.9 (115.4)	0.56	0.72%	-9.5 (155.3)	0.43	1.25%
SS y difference	-1.0 (51.3)	0.82	0.08%	-3.9 (53.7)	0.25	0.11%
SL x difference	1.9 (75.9)	0.67	0.34%	2.0 (121.7)	0.64	0.72%
SL y difference	-0.3 (11.8)	0.87	0.02%	0.6 (13.6)	0.81	0.04%
Congenital glaucoma n = 50						
SS x difference	-4.9 (155.2)	0.66	0.75%	-109.5 (207.5)	<0.0001	2.05%
SS y difference	-1.6 (71.1)	0.76	0.11%	-2.1 (63.7)	0.85	0.15%
SL x difference	1.9 (105.6)	0.74	0.45%	-2.8 (172.1)	0.78	0.99%
SL y difference	0.4 (13.7)	0.89	0.02%	-0.6 (33.6)	0.81	0.07%

SS= scleral spur, SL=Schwalbe's line. The table illustrates the difference between the repeated x and y coordinates placement of each landmark (Bias) measured in µm, precision ($SD \times 1.96$) and significance level. p value indicates the significance of difference of the bias from zero assessed by one sample t test, COV = coefficient of variation ($SD/\text{average}$). The highlighted cell shows the significant difference of bias from zero.

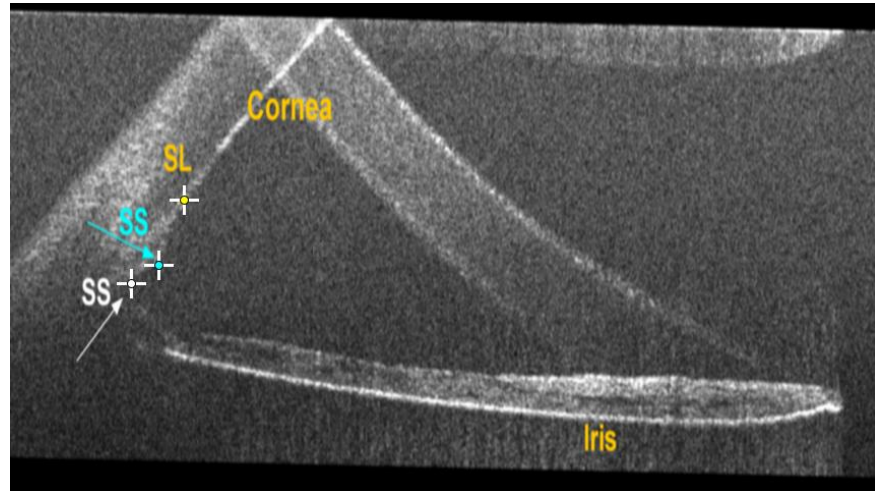


Figure 3-3: HH-OCT B-scan of the anterior chamber of 4 year old female with congenital glaucoma.

There was Inter-observer disagreement in identification of scleral spur (SS). The first observer (BE) located the scleral spur (white star) more close to angle recess (white arrow), while the second observer (SSH) placed the scleral spur (cyan star) away from angle recess and more close to Schwalbe's line (SL) (yellow star).

3.3.4 Intraobserver and interobserver (same image) reproducibility of anterior chamber measurements.

The results of the mean difference (bias), the precision and the p values, in addition to COV and ICC of all the anterior chamber measurements are shown in table 3-3. Further illustration of the intraobserver and interobserver COV and ICC of all measurements are shown in figure 3-4. Examples of good agreement and bad agreement of Bland Altman blots are shown in figures 3-5 and 3-6 respectively.

The intraobserver and interobserver assessment demonstrated that Schwalbe's line based measurements had the lowest measurement error with COVs of $\leq 5\%$ and the highest reproducibility with ICCs of > 0.95 (Figure 3.4). The SL-TISA had similar 95% level of agreement among different groups (Figure 3.5). Both SS and SL derived measurements had fair to excellent reproducibility. ICCs of TML, TISA ranged from 0.65 to 0.95. Their measurement error was less than 10% in intra-observer assessment but more than 10% in inter-observer assessment. This error was higher in congenital glaucoma compared to healthy children. Bland Altman plots showed no significant difference of the bias from zero in both assessments (all $p > 0.5$). The only exception was the inter-observer assessment of

SS-OAD in congenital glaucoma which had a high COV of 25% and significantly negative bias ($p < 0.5$) (Figure 3.6), owing to the disagreement on scleral spur localization between the two observers as described above. Surprisingly, the SS-AOD reproducibility was very good (ICC = 0.86). Further details of the bias, lower and upper level of agreement, significance from zero, ICC and COV of all the anterior chamber measurements are shown in table 3-3).

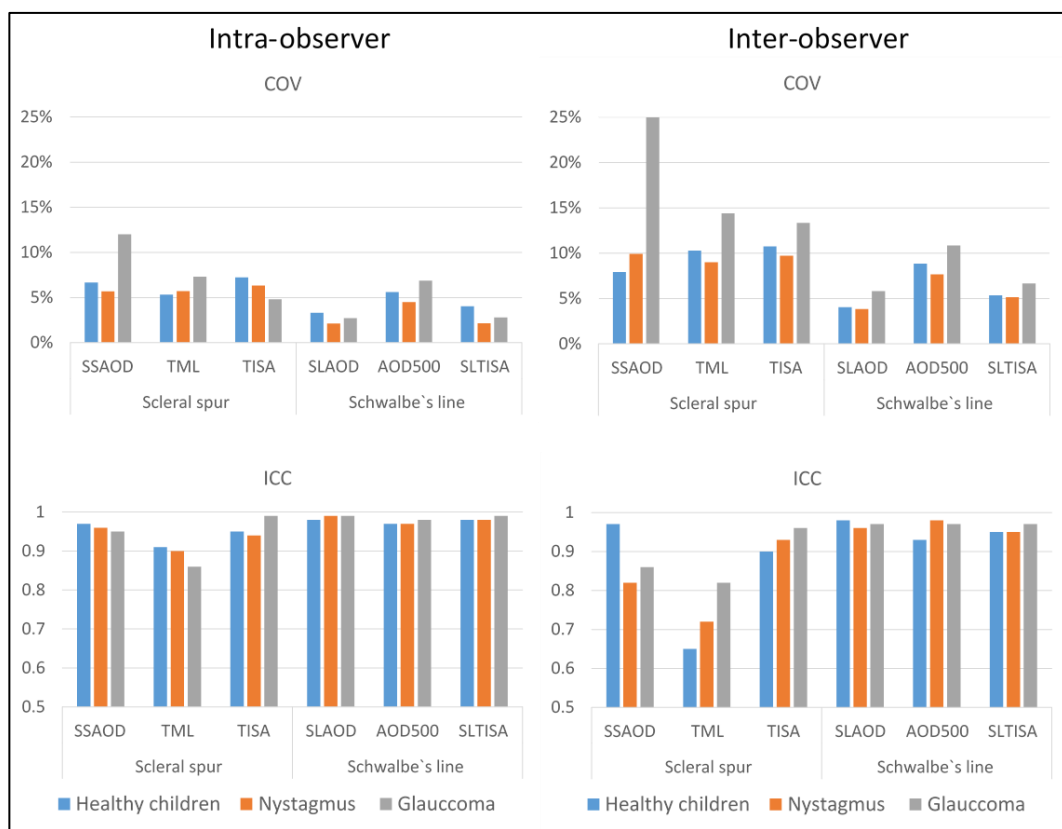


Figure 3-4: The intraobserver and interobserver coefficient of variation (COV) and interclass correlation coefficient (ICC) of anterior chamber angle measurements.

The figure shows the valued of COV and ICC for each parameter. The anterior chamber angle parameter is either based on sclera spur (SS-AOD) or Schwalbe's line (SL-AOD, SL-AOD500, SL-TISA) or both (TML, TISA) in healthy children, children with congenital glaucoma and nystagmus.

The angle measurements are: Scleral spur angle opening distance (SS-AOD), trabecular meshwork length (TML), trabecular iris surface area (TISA), Schwalbe's line angle opening distance (SL-AOD), Schwalbe's line angle opening distance 500 micrometres from Schwalbe's line (SL-AOD500) and Schwalbe's line trabecular iris surface area (SL-TISA).

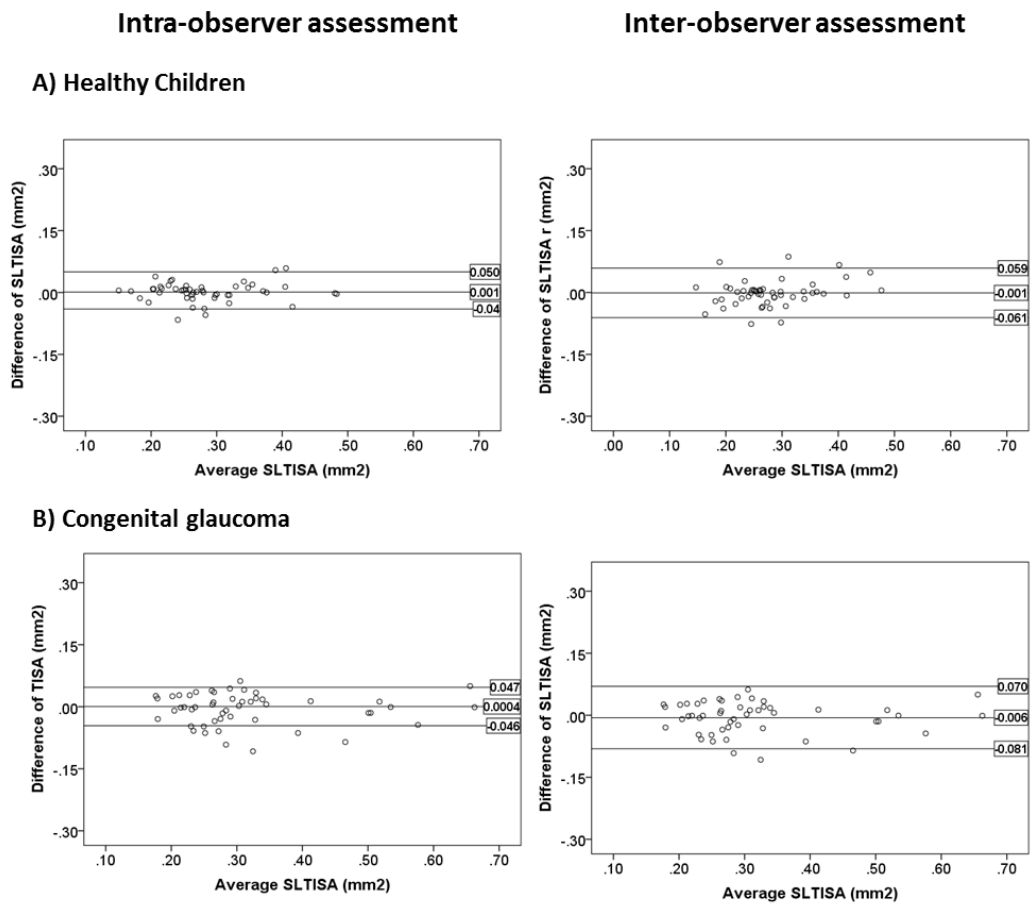


Figure 3-5: Comparison between the Bland Altman plot of intraobserver and interobserver assessment of Schwalbe's line trabecular iris surface area (SL-TISA) in healthy children and congenital glaucoma.

There was no significant difference between first and second measurements ($p > 0.05$). The level of agreement of intraobserver SL-TISA was narrower than those of interobserver in both groups

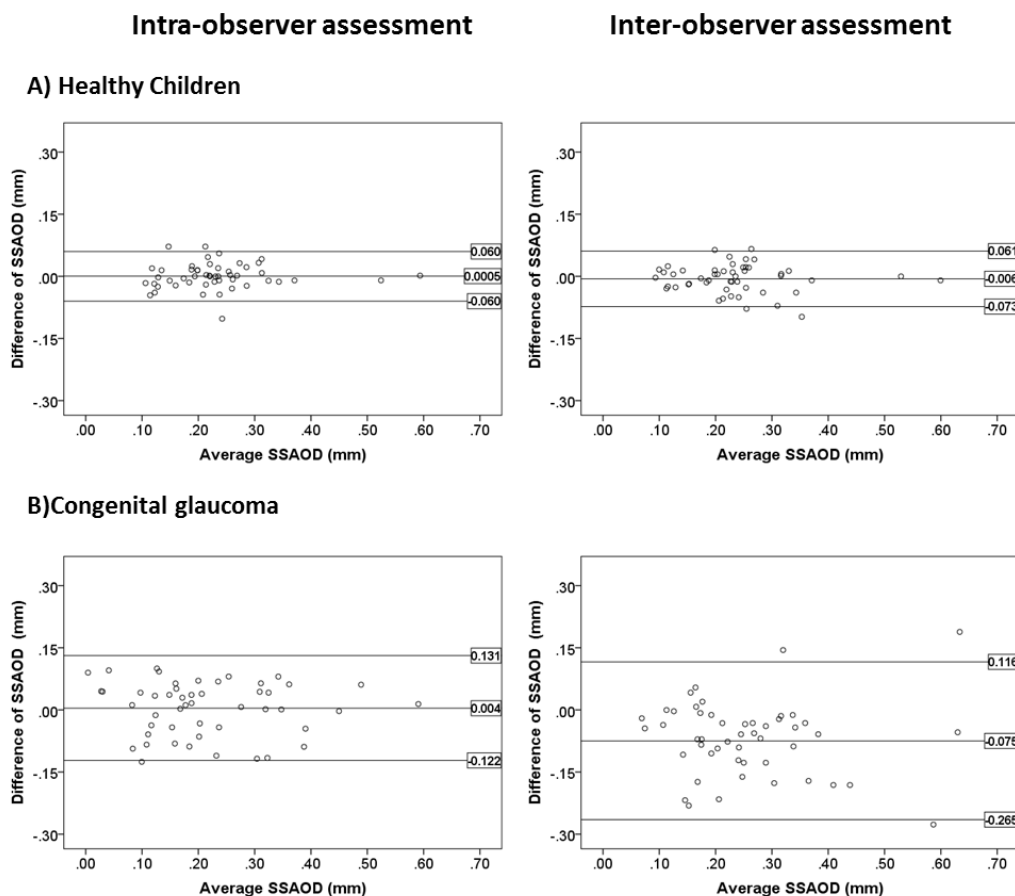


Figure 3-6: Comparison between the Bland Altman plot of intraobserver and interobserver assessment of scleral spur angle opening distance (SS-AOD), in healthy children and congenital glaucoma.

There was significant negative bias between the inter-observer measurements in congenital glaucoma (p values <0.001). The second observer measurement were larger than the first observer. The level of agreement was wider in glaucoma compared to healthy controls.

Table 3-3: Intraobserver and interobserver assessment of anterior chamber angle measurements of the same image.

	Measurements based on scleral spur (SS)		Measurements based on SS and SL		Measurements based on Schwalbe's line (SL)		
	SS-AOD (mm)	TML (mm)	TISA (mm ²)	SL-AOD (mm)	SL-AOD500 (mm)	SL-TISA (mm ²)	
Healthy children n = 50							
Intraobserver	Bias (95% LOA)	0.0005 (-0.06, 0.06)	0.002 (-0.13, 0.14)	0.004 (-0.11, 0.11)	0.0003 (-0.10, 0.10)	-0.0003 (-0.08, 0.08)	0.001 (-0.04, 0.05)
	Precision	0.06	0.14	0.11	0.10	0.08	0.05
	p value	0.92	0.83	0.63	0.96	0.96	0.71
	COV	6.7%	5.3%	7.2%	3.3%	5.6%	4.0%
	ICC	0.97	0.91	0.95	0.98	0.97	0.98
Interobserver	Bias (95% LOA)	-0.006 (-0.07, 0.06)	-0.008 (-0.28, 0.26)	0.0001 (-0.15, 0.15)	-0.001 (-0.11, 0.11)	-0.003 (-0.13, -0.13)	-0.002 (-0.06, 0.06)
	Precision	0.07	0.27	0.15	0.11	0.13	0.06
	p value	0.22	0.7	0.98	0.86	0.78	0.67
	COV	7.9%	10.3%	10.7%	4.0%	8.9%	5.4%
	ICC	0.97	0.65	0.9	0.98	0.93	0.95
Nystagmus n = 50							
Intraobserver	Bias (95%LOA)	0.002 (-0.07, 0.07)	0.003 (-0.15, 0.15)	0.001 (-0.11, 0.11)	0.003 (-0.09, 0.10)	-0.0003 (-0.08, 0.08)	0.002 (-0.04, 0.04)
	Precision	0.07	0.15	0.11	0.92	0.08	0.04
	p value	0.52	0.43	0.83	0.86	0.66	0.41
	COV	5.7%	5.7%	6.3%	2.1%	4.5%	2.1%
	ICC	0.96	0.9	0.94	0.99	0.97	0.98
Interobserver	Bias (95% LOA)	-0.006 (-0.08, 0.08)	-0.005 (-0.26, 0.25)	0.0001 (-0.13, 0.13)	0.001 (-0.10, 0.10)	-0.003 (-0.12, 0.12)	-0.002 (-0.05, 0.05)
	Precision	0.09	0.26	0.13	0.10	0.12	0.05
	p value	0.32	0.65	0.48	0.87	0.38	0.87
	COV	9.9%	9.0%	9.7%	3.8%	7.7%	5.2%
	ICC	0.82	0.72	0.93	0.96	0.98	0.95
Congenital glaucoma n = 50							
Intraobserver	Bias (95% LOA)	0.004 (-0.12, 0.13)	-0.008 (-0.27, 0.25)	0.001 (-0.10, 0.10)	0.002 (-0.11, 0.11)	0.004 (-0.13, 0.14)	0.0001 (-0.05, 0.05)
	Precision	0.13	0.26	0.10	0.11	0.13	0.05
	p value	0.67	0.67	0.93	0.82	0.67	0.91
	COV	12.0%	7.3%	4.8%	2.7%	6.9%	2.8%
	ICC	0.95	0.86	0.99	0.99	0.98	0.99
Interobserver	Bias (95% LOA)	-0.075 (-0.27, 0.12)	0.112 (-0.12, 0.34)	0.037 (-0.12, 0.19)	0.004 (-0.16, 0.17)	-0.023 (-0.19, 0.14)	-0.006 (-0.08, 0.07)
	Precision	0.19	0.23	0.16	0.16	0.16	0.08
	p value	<0.001	<0.001	0.003	0.71	0.06	0.28
	COV	25.2%	14.4%	13.4%	5.8%	10.9%	6.7%
	ICC	0.86	0.82	0.96	0.97	0.97	0.97

*Bias is the mean difference between the two measurements, precision is the SD of bias *1.96 , LOA is the level of agreement (bias ± SE*1.96), significance level p value indicates the significance of the difference of the bias from zero assessed by one sample t test, COV = coefficient of variation (SD of repeated measurements/average). ICC is interclass corelation coefficient. Highlighted cells indicate significant deviation from zero.*

3.3.5 Test retest (repeated images) reproducibility of the anterior chamber measurements

Measurements derived from Schwalbe's line, SL-AOD, SL-TISA, SL-LD showed the highest reproducibility (ICC > 0.92) and the lowest coefficient of variation (COV < 9%) (Table 3.4). In contrast, measurements derived from scleral spur (SS-AOD) had high measurement errors (COV > 16%), although their ICCs were good (> 0.80).

Measurements based on the identification of both Schwalbe's line and scleral spur, (TML and TISA) had lower reproducibility (ICC ranged from 0.60 to 0.84) and higher 'measurement' error (COV >10%).

There was no significant difference between the first and second measurements of the two repeated images (all $p > 0.5$) although the pupil diameter (PD) showing a positive bias ($p = 0.0001$) since the first image had larger PD compared to the second image. This indicates that the accommodation of pupil had no effect on angle measurement. Furthermore, the ICCs and COVs of PD were > 0.95 and < 8%, respectively, in all groups.

The 95% level of agreement of all angle measurements among the different groups was of similar range. However, the level of agreement in the repeated measurements of congenital glaucoma was wider compared to other groups.

Limbal distance measurements (SL-LD and SS-LD) showed good to high reproducibility and measurements error of lower than 8% (Table 4.5). Similarly, anterior chamber widths (SS-SS-D and SL-SL-D) were highly reproducible. Their ICC was > 0.95 and COV < 3%.

Finally, there was no proportional bias between the first and second measurements as a function of average of first to second measures showed in the mixed regression models (all $p > 0.05$).

Table 3-4: The results of test retest repeatability and reproducibility of HH-OCT anterior chamber angle measurement of images obtained in the same examination day and analysed by the same observer.

Measurements based on scleral spur (SS)		Measurements based on Schwalbe's line (SL)			Measurements based on SS and SL	
	SS-AOD (mm)	SL-AOD (mm)	SL-AOD500 (mm)	SL-TISA (mm ²)	TML (mm)	TISA (mm ²)
Control n = 100						
1st measure (SD)	0.215 (0.092)	0.649 (0.193)	0.335 (0.140)	0.257 (0.078)	0.742 (0.150)	0.354 (0.152)
2nd measure (SD)	0.213 (0.083)	0.648 (0.181)	0.329 (0.122)	0.255 (0.071)	0.729 (0.141)	0.343 (0.127)
Bias (95% LOA)	0.002 (-0.136, 0.140)	0.001 (-0.207, 0.210)	0.006 (-0.181, 0.193)	0.001 (-0.082, 0.085)	0.012 (-0.295, 0.320)	0.011 (-0.190, 0.211)
p value	0.78	0.91	0.52	0.74	0.44	0.29
ICC (95% CI)	0.81 (0.71, 0.87)	0.91 (0.87, 0.94)	0.85 (0.77, 0.90)	0.91 (0.87, 0.94)	0.59 (0.39, 0.73)	0.85 (0.77, 0.90)
COV (%)	17.9%	9.4%	16.9%	9.4%	11.6%	16.1%
Nystagmus n = 34						
1st measure (SD)	0.204 (0.076)	0.702 (0.230)	0.366 (0.133)	0.154 (0.161)	0.795 (0.131)	0.208 (0.218)
2nd measure (SD)	0.204 (0.078)	0.701 (0.216)	0.361 (0.125)	0.153 (0.160)	0.787 (0.100)	0.199 (0.210)
Bias (95% LOA)	0.0001 (-0.127, 0.128)	0.0003 (-0.167, 0.167)	0.005 (-0.128, 0.138)	0.002 (-0.045, 0.048)	0.008 (-0.233, 0.248)	0.009 (-0.106, 0.124)
p value	0.99	0.97	0.67	0.71	0.37	0.37
ICC (95% CI)	0.79 (0.57, 0.89)	0.96 (0.94, 0.98)	0.93 (0.85, 0.96)	0.99 (0.98, 1.00)	0.62 (0.24, 0.81)	0.98 (0.96, 0.99)
COV (%)	18.3%	6.7%	10.4%	6.3%	7.3%	12.0%
Congenital glaucoma n = 20						
1st measure (SD)	0.191 (0.138)	0.784 (0.247)	0.364 (0.214)	0.297 (0.113)	0.701 (0.157)	0.382 (0.189)
2nd measure (SD)	0.167 (0.091)	0.778 (0.246)	0.365 (0.189)	0.296 (0.108)	0.705 (0.157)	0.373 (0.150)
Bias (95% LOA)	0.024 (-0.149, 0.197)	0.007 (-0.183, 0.196)	0.000 (-0.142, 0.141)	0.001 (-0.068, 0.070)	-0.004 (-0.229, 0.222)	0.008 (-0.187, 0.203)
p value	0.24	0.76	0.98	0.92	0.89	0.71
ICC (95% CI)	0.84 (0.59, 0.94)	0.96 (0.90, 0.98)	0.97 (0.92, 0.99)	0.97 (0.93, 0.99)	0.85 (0.61, 0.94)	0.91 (0.77, 0.96)
COV (%)	24.9%	7.3%	12.0%	7.0%	9.3%	14.1%

The table presents the mean of 1st and 2nd measurements, standard deviation (SD) of the repeated measurements, mean difference of repeated measurements (bias) with upper and lower 95% level of agreement (LOA), p value of the significance of deviation of bias from zero, Interclass correlation coefficient (ICC) with 95% confidence interval and coefficient of variation (COV).

Table 3-5: The results of test retest repeatability and reproducibility of HH-OCT anterior chamber width, limbal distances and pupil diameter measurement of images obtained in the same examination day and analysed by the same observer.

	Limbal distance parameters (mm)		Anterior chamber width (mm)		Pupil diameter (mm)
	SS-LD	SL-LD	SS-SS-D	SL-SL-D	PD
Control n = 100					
1st measure (SD)	0.865 (0.095)	0.750 (0.083)	12.521 (0.796)	11.375 (0.693)	4.984 (1.096)
2nd measure (SD)	0.875 (0.099)	0.762 (0.078)	12.497 (0.739)	11.364 (0.670)	4.579 (1.095)
Bias (95% LOA)	-0.010 (-0.135, 0.115)	-0.012 (-0.126, 0.102)	0.023 (-0.546, 0.593)	0.011 (-0.546, 0.567)	0.405 (-0.333, 1.143)
p value	0.13	0.14	0.42	0.71	< 0.001
ICC (95% CI)	0.88 (0.82, 0.92)	0.85 (0.7, 0.90)	0.96 (0.95, 0.98)	0.96 (0.93, 0.97)	0.97 (0.96, 0.98)
COV (%)	4.0%	4.1%	1.3%	1.3%	6.0%
Nystagmus n = 34					
1st measure (SD)	0.847 (0.099)	0.728 (0.081)	12.584 (0.655)	11.477 (0.629)	4.945 (1.145)
2nd measure (SD)	0.851 (0.101)	0.733 (0.088)	12.577 (0.570)	11.490 (0.561)	4.677 (1.165)
Bias (95% LOA)	-0.004 (-0.142, 0.133)	-0.005 (-0.159, 0.150)	0.007 (-0.423, 0.438)	-0.013 (-0.520, 0.495)	0.268 (-0.138, 0.674)
p value	0.73	0.72	0.85	0.78	< 0.001
ICC (95% CI)	0.86 (0.72, 0.93)	0.72 (0.44, 0.86)	0.97 (0.93, 0.98)	0.95 (0.90, 0.98)	0.99 (0.98, 0.99)
COV (%)	4.2%	5.5%	1.0%	1.3%	3.9%
Congenital glaucoma n = 20					
1st measure (SD)	0.839 (0.158)	0.727 (0.117)	13.352 (1.027)	12.507 (0.970)	4.432 (1.088)
2nd measure (SD)	0.814 (0.153)	0.708 (0.107)	13.364 (0.865)	12.458 (0.859)	4.062 (1.069)
Bias (95% LOA)	0.025 (-0.197, 0.246)	0.019 (-0.205, 0.244)	-0.012 (-0.636, 0.631)	0.049 (-0.728, 0.826)	0.370 (-0.098, 0.837)
p value	0.34	0.46	0.87	0.59	< 0.001
ICC (95% CI)	0.85 (0.62, 0.94)	0.65 (0.11, 0.86)	0.97 (0.93, 0.99)	0.95 (0.88, 0.98)	0.98 (0.97, 0.99)
COV (%)	7.4%	8.8%	1.3%	1.9%	6.2%

The table presents the mean of 1st and 2nd measurements, standard deviation (SD) of the repeated measurements, mean difference of repeated measurements (bias) with upper and lower 95% level of agreement (LOA), p value of the significance of deviation of bias from zero, Interclass correlation coefficient (ICC) with 95% confidence interval and coefficient of variation (COV). SS-LD = Scleral spur limbal distance, SL-LD = Schwalbe's line limbal distance, SS-SS-D = nasal scleral spur to temporal scleral spur distance. SL-SL-D = nasal Schwalbe's line to temporal Schwalbe's line distance.

3.4 Discussion

To the best of our knowledge, this is the first study evaluating the feasibility, repeatability and reproducibility of anterior chamber angle measurements in children, younger than 6 years old. We demonstrated that HH-OCT is a feasible technique in visualising the anterior chamber of children without sedation, allowing identification of landmarks for quantitative measurements of the anterior chamber. Anterior chamber angle measurements derived from identification of Schwalbe's line are more reliable than those from the scleral spur. The intra-image and inter-image repeated angle measurements had high repeatability and reproducibility, not only in the healthy children but also in children with congenital glaucoma and nystagmus.

3.4.1 Feasibility

The percentage of successfully obtained images of anterior segment was high (89 %), indicating easier application of HH-OCT in imaging anterior segment compared to fovea and optic nerve (70 %)(Patel et al., 2016) . During examination, we encountered difficulty with children between 1 to 6 months old (76%). They often fell asleep or completely refuse to let the examiner get close to their eye, unless they were distracted using an animation video. The images were often considered not of good quality due to the bad acquisition of scans because the children were not easily distracted and usually keep moving especially children of 6 to 12 months of age. The anterior chamber image of HH-OCT showed a reflection of cornea as an artefact. This reflection can interfere with the identification of anterior chamber angle landmarks. Therefore, such images were considered not of good quality.

3.4.2 Landmark identification: intra-observer and inter-observer variability of the same image

Our narrower precision in Schwalbe's line identification compared to scleral spur agrees with similar studies that used spectral domain AS-OCT and report better visualisation of Schwalbe's line compared to scleral spur (Wong et al., 2009, Tun et al., 2013a, Quek et al., 2012a)

The inter-observer disagreement and high variability in identifying the SS in congenital glaucoma is likely due to the surgical distortion of the scleral spur structure in the operated children. This suggests that Schwalbe's line identification is more useful than scleral spur in calculating angle measurements in congenital glaucoma. Nevertheless, our intraobserver and interobserver precision in identifying scleral spur x and y coordinates, in both nasal and temporal angles, are consistent with what was reported in adults. Console et al found that the inter-observer 95 % agreement limits for placement of scleral spur of nasal to temporal angle ranged from 261 to 292 µm using the Visante OCT in adults (Console et al., 2008). Cumba et al reported nasal to temporal scleral spur placement in the range of 160 to 282 µm using Casia swept source OCT amongst adults (Cumba et al., 2012). Our results were similar in children. This reflects the ability of HH-OCT in producing a high quality anterior chamber images, sufficient for conducting quantitative measurements in children similar to other AS-OCT in adults.

3.4.3 Reproducibility of anterior chamber measurements

In this study, we successfully produced quantitative measurements of angle without sedation. Based on our finding in intra-observer, interobserver and test retest reproducibility, measurements based on Schwalbe's line (SL-AOD and SL-TISA) are the most accurate angle width measurements in describing the angle geometry.

The fact that, we detected lower reproducibility and higher measurement's error in scleral spur's based measurements, compared to Schwalbe's line, did not mean that SS measurements are not useful. Previous literature reported a similar measurement error of 10 % of scleral spur based measurements in healthy adult participants. (Tan et al., 2011, Li

et al., 2007) These studies considered the 10% level of variation is acceptable clinically to distinguish between open and closed angle in adults. However, considering the subjective inaccuracy in detecting scleral spur in the operated congenital glaucoma, we think that scleral spur's measurements are clinically unacceptable in congenital glaucoma. Further investigation with application of more accurate method of analysis such as the possibility of automatic landmark detection may improve accuracy.

SD-OCT allowed the identification and measurements of trabecular meshwork among adults. The Cirrus HD SD-OCT, mounted with a 60 D lens has enabled the first detection of the trabecular meshwork (TM) using OCT. (Wong et al., 2009). The mean TML reported by Cheung et al was about 0.67 ± 0.13 (Cheung et al., 2011b), by Chen et al 0.84 ± 0.13 (Chen et al., 2015), by Tun et al 0.78 ± 0.09 (Tun et al., 2013b) and by Fernandez-Vigo et al 0.49 ± 0.93 (Fernandez-Vigo et al., 2015b). Our study presents TML in children for the first time with similar average values. Our used protocol also enabled imaging of both nasal and temporal angles together. This allowed the measuring the horizontal anterior chamber width (ACW) between nasal and temporal angle landmarks. Congenital glaucoma manifests with enlargement of the eyeball (buphthalmos), which is commonly confirmed by a large corneal diameter. Progressive buphthalmos is also an indicator of unfavourable prognosis. AS-OCT enabled measuring of the ACW, which can represent anterior segment geometry more accurately than corneal diameter measured with Orbscan and IOL Master. (Kohnen et al., 2006) We detected large ACW in congenital glaucoma (Table 3). The ability of measuring the ACW can be a valuable addition to the diagnosis and follow up of congenital glaucoma. We present for the first time measurements of ACW between nasal SS and temporal SS and between nasal SL to temporal SL. Huang et al reported the ACW between that two angle recesses using the Visante AS-OCT in healthy adults (Huang et al., 2015b) as 11.58 ± 0.37 mm, which was smaller than our measurements. Probably because our age groups were younger than 6 years and the ACW has been reported to reduce with increasing age.(Nongpiur et al., 2010b) Huang and colleagues study also involved Chinese ethnicity which is well documented to associate with smaller anterior chamber measurements. (Wang et al., 2012)

The current study also reported wider anterior chamber angle measurements in congenital glaucoma compared to the values reported in adult's glaucoma. Cheung et al

(Cheung et al., 2011b) reported measurements of the SL-AOD and SL-TISA as 0.32mm and 0.11 mm² in open angle glaucoma, and 0.13mm and 0.05 mm², in angle closure glaucoma, respectively. This variability in angle measurements suggests the presence of different pathology in paediatric and adult glaucoma. In chapter 5, we explored the development of the anterior chamber angle measurements in congenital glaucoma compared to healthy children. HH-OCT could revolutionize the management of congenital glaucoma, by providing more information prior to surgery and replace the need of frequent examination under anaesthesia for follow up.

3.4.4 Illumination

Many publications have studied the effect of illumination and reported that due to decreased pupil diameter, the angle measured in light is significantly wider than that measured in the dark (Dacosta et al., 2008, Masoodi et al., 2014). Although we tried to control the illumination at 200 lux and asked the children to look straight at cartoon pictures, they were often interested in the reflection of their eye in the HH-OCT lens. So, accommodation and pupil constriction is unavoidable. Nevertheless, the slight change in accommodation that we detected did not affect the angle measurements. This finding is in accordance with other studies, (Monsalvez-Romin et al., 2017, Dominguez-Vicent et al., 2014) that reported no significant impact of the accommodative state of -1, -3 and -4 dioptre on angle measurements.

Despite that our analysis being based on manual identification of landmarks which is prone to subjective error, it yielded high reproducibility compared to other studies in adults where analysis was done by either the OCT machine built in software, which required only localization of SS (Maram et al., 2015a, Kim et al., 2011), a programmed automatic detection of scleral spur (Console et al., 2008), a programmed automatic detection of Schwalbe's line (Akil et al., 2017a, Pan et al., 2015), or those who used swept source OCT. (Mak et al., 2013, McKee et al., 2013)

3.4.5 Limitations of HH-OCT

It is well documented, using AS-OCT in adults, that a narrow anterior chamber angle is associated with a shallow anterior chamber depth (Nongpiur et al., 2011b). Unfortunately, HH-OCT cannot measure the anterior chamber depth since the scan depth is only 2.5 mm.

The test-retest and the intra-image inter-observer assessments had similar reproducibility. This suggests that the variability in results is related to the subjective error of different observers. Such uncertainty could be eliminated by automatic image analysis, which probably can produce more reliable and accurate measurements.

Passing of light through different media including cornea and aqueous humor can cause geometric distortion of measurements. *Cheung et al* has corrected the refraction distortion of Cirrus SD-OCT images by a customised MatLab program (Cheung et al., 2011b). This was suggested to produce excellent reproducibility of SL measurements. We think similar approach could improve our results. However, this would be at the expense of the time taken to analyse the measurements. This study has a limitation of not assessing the reproducibility of the nasal and temporal angles, separately. We also did not test other meridians as this was difficult to achieve without retracting the eyelid. In adults, the visibility of angle landmarks is significantly better at nasal and temporal meridians compared to superior and inferior angles (Liu et al., 2011). This difference is yet to be investigated in children.

The HH-OCT has provided quantitative measurements of anterior chamber in children. We hope that our findings can be used as a preliminary basis for future investigations. A study, comparing two SD-OCT measurements in adults based on SL, has found excellent agreement (Akil et al., 2017b, Marion et al., 2015). In contrast, a comparison between two TD-OCT measurements based on SS showed poor agreement (Leung et al., 2008). Therefore, a comparison of HH-OCT with other SD-OCT machines is possible and can add more credit to the advantage of HH-OCT in children.

3.4.6 Summary

This study has investigated the intra-image and inter-image reliability of HH-OCT. The results indicate that HH-OCT can provide objective and quantitative anterior chamber angle measurements in children. Schwalbe's line based measurements showed higher reproducibility than those of scleral spur. SL-AOD and SL-TISA were the most reliable measurements to define the anterior chamber angle metrics. HH-OCT can enhance our understanding of angle morphometry and development and can provide further insights to our understanding and assessment of congenital glaucoma.

4. Chapter four: Postnatal Anterior Chamber Development: An In Vivo Quantitative Study Using High Resolution Hand-held Optical Coherence Tomography

The aims of this section of thesis are:

- 1) To establish normative anterior chamber measurements for children using HH-OCT.
- 2) To understand the time course of anterior chamber development and identify when the maturity of anterior chamber is reached.
- 3) To investigate the impact of factors such as gender, eye and refraction variation on the anterior chamber development.

4.1 Introduction

4.1.1 Anterior chamber biometry in adults

The morphometric changes of anterior chamber in adults have been well documented (Narayanaswamy et al., 2010a, Goldsmith et al., 2005b) for demographic factors such as age, gender, ethnicity as well as refractive error. For example, senescence is associated with shallow anterior chamber depth, increased lens thickness and narrow irido-corneal angle (Qin et al., 2012). Closed angle glaucoma is more common in elderly women because they have a narrower anterior chamber compared to men (Friedman et al., 2008, He et al., 2008). Closed angle glaucoma prevalence is also higher among Chinese ethnicity (Nongpiur et al., 2010a), especially in females (Lavanya et al., 2008), because Chinese have shallower anterior chamber compared to Caucasians (Leung et al., 2010, Qin et al., 2012).

Hypermetropia is associated with shallow anterior chamber while myopic people had deep anterior chamber (Vossmerbaeumer et al., 2013).

4.1.2 Importance of anterior chamber biometry

Measurements of axial length (AL), anterior chamber depth (ACD), corneal curvature and lenticular thickness biometry are a clinical necessity in order to accurately calculate the intraocular lens power (IOL) after cataract extraction (Chen et al., 2016). The success of corrective refractive surgery is also depending on a precise preoperative evaluation of refraction and ocular biometry. Anterior chamber angle geometry is valuable for the management of anterior segment diseases, such as glaucoma (Sharma et al., 2014).

The aforementioned clinical applications are limited to date to adult subjects. There is only scarce information about anterior chamber measurements in children.

4.1.3 Ocular biometry in children

Munro et al (2015) have studied the development of the eye in full term and preterm children using MRI from birth up to the age of 20 years and have revealed that axial length and anterior chamber depth increase with age, the cornea becomes flat, and lens thickness does not change (Figure 4.1) (Munro et al., 2015). Studies investigating children older than 6 years of age have reported that the lens thickness decreases in early childhood (Hashemi et al., 2015), and then slightly increases in late childhood (Shimizu et al., 2017). The central corneal thickness becomes thinner with increasing age in children (Wang et al., 2018). Full term neonates are highly likely to be hypermetropic while premature children are myopic (Varughese et al., 2005).

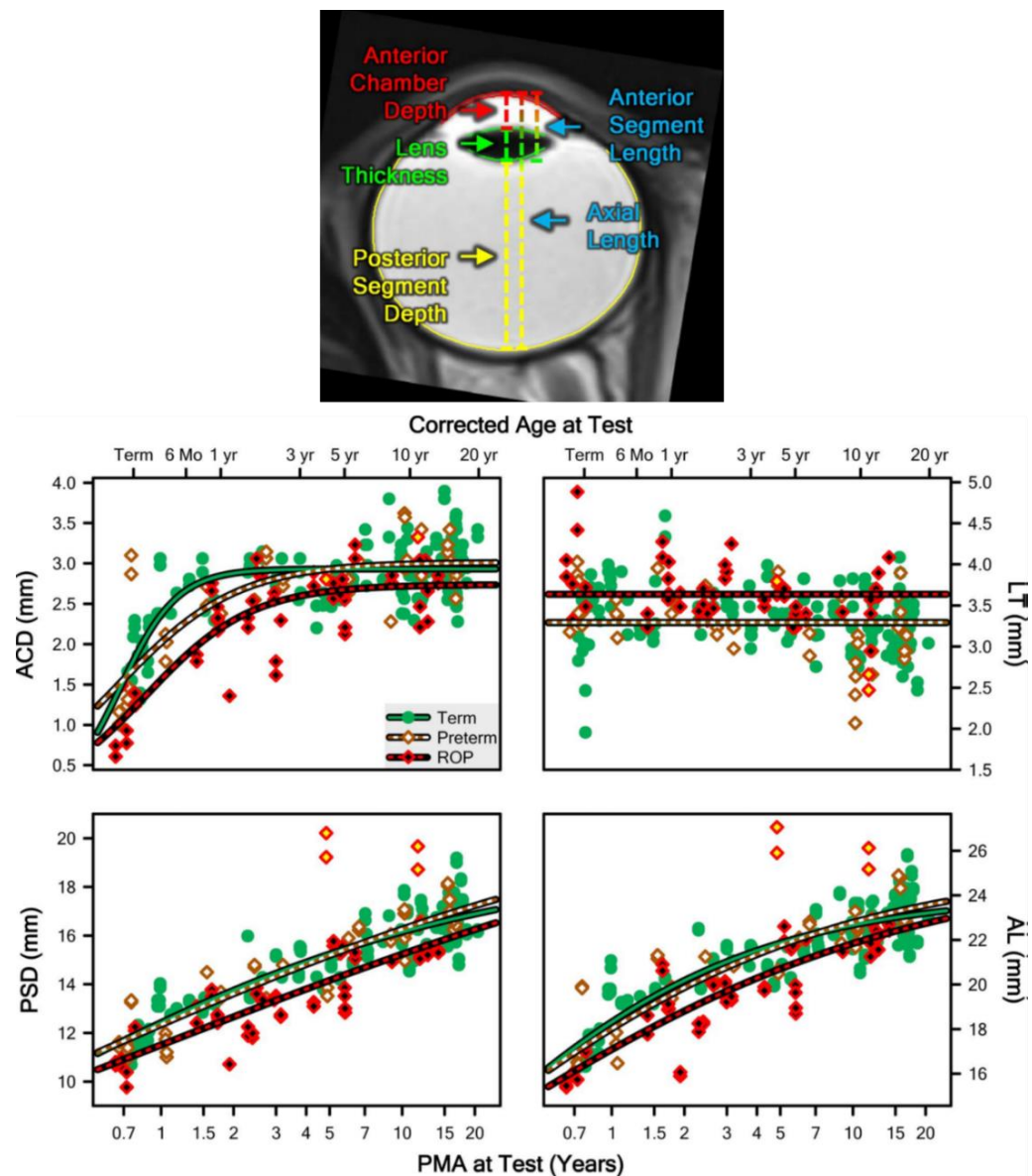


Figure 4-1: Development of the eye from birth up to age of 20 years using magnetic resonance imaging.

The development of the eye measured using MRI in full-term, preterm with and without ROP showed that the axial length (AL), anterior chamber depth (ACD) and posterior segment depth (PSD) increase with age while lens thickness (LT) development showed a plateau (Munro et al., 2015). The growth of ACD is matured by age of 2 years.

4.1.4 Gaps in the research literature

The *in vitro* normal development of anterior chamber angle from birth throughout childhood has been studied histologically (described in section 1.1.2). The *in vivo* postnatal development of anterior chamber has been poorly investigated. The questions of how and when the anterior chamber develops postnatally and reaches maturity are still not completely answered. In a previous study, ultrasound bio-microscopy (UBM) was used to establish normative quantitative anterior chamber measurements in children aged from 1 to 60 months. A positive linear correlation between the anterior chamber biometry and the logarithm of age is due to a rapid phase of anterior chamber growth during the first 18 months of age (Kobayashi et al., 1999). However, UBM is very invasive, requiring direct manipulation of the infant's eye, instilling local anaesthesia and forceful opening of the eyelid with a retractor. In addition, the direct pressure of the UBM probe on the cornea may affect the accuracy of the anterior chamber angle measurements. The invasive application of UBM is not clinically desirable in paediatric examination. In contrast, AS-OCT has the advantage of non-invasive high-resolution imaging. In the previous chapter, we proved the feasibility and the reproducibility of quantitative measurements of the anterior chamber in children using the HH-OCT without sedation. In this chapter, we use this child-friendly machine to elucidate the postnatal normal development of anterior chamber.

4.2 Methods

4.2.1 Participants

The cohort of this study included 223 full-term infants and children (104 females and 119 males). The age of children ranged between 2 days and 15.4 years (mean: 5.7 ± 4.1 years). We also studied the data from 59 adults (41 females and 18 males), aged between 16.1 to 47.1 years (mean: 33.5 ± 8.7 years). New-borns were recruited from the Maternity Unit, at Leicester Royal Infirmary. Older children were recruited from different Leicester City nurseries, schools and general clinics for children at the Leicester Royal Infirmary. Adult participants were friends, students and staff of the University of Leicester. The details of the ethical approval and the recruitment of participants and acquiring consents are described in the methodology chapter (section 2.3.1).

4.2.2 Clinical examination

The visual acuity of participants was examined using different methods, suitable for each age (these methods have been previously mentioned in section 2.4.2.1). All participants were free of any ocular pathology and had a visual acuity of at least 6/9. Refraction was tested using a portable Plusoptix Auto-refractometer when possible or recorded from the medical notes of the participants. Details of measurements of refraction by Plusoptix was discussed in section 2.4.2.2). In case the children were wearing glasses, the refractive power was recorded based on the glasses' power to fit the inclusion criteria. The spherical equivalent of participants ranged from -3 to +3 D for inclusion in this study.

For comparison between refraction and HH-OCT measurements, only children where the refraction was measured using Plusoptix were included. Children, who had a refraction, reported using cycloplegic retinoscopy and was not measured with Plusoptix auto-refractometer, were excluded.

4.2.3 HH-OCT imaging

The anterior segments of participants were imaged by HH-OCT without sedation. (Details of steps of acquisition of images are described in section 2.5.1). At least one scan of the anterior chamber and one of the cornea was obtained per eye. The images from both eyes per participant were included. Only good quality images were included (criteria of good quality image is described in chapter 3, section 3.2.3). If the participant had bad quality image of either left or right eye, only the eye with good quality image was included.

Where possible, the same eye that was imaged in different examination time (longitudinal samples) in children younger than two years, were included to strengthen the sample size of this age group (Lee, 2014). The longitudinal data of 4 children who were scanned at 2 months, 3 months, 4 months and 9 months of age followed by a second scan after 3 months interval were included.

4.2.4 HH-OCT image analysis

The OCT images were imported into ImageJ software for analysis. The best individual B scan showing both nasal and temporal angle was selected. The analysis of the anterior chamber image is based initially on manual identification of angle landmarks; scleral spur (SS) and Schwalbe's line (SL). These landmarks were then used to calculate the anterior chamber measurements (steps of image analysis have been described in section 2.6).

In this chapter, only the angle parameters which showed high reproducibility according the results of chapter 3 were included, to study the normal development of the anterior chamber. These are:

- 1) Measurements that represent the anterior chamber width (ACW):
 - a. Nasal scleral spur to temporal scleral spur distance (SS-SS-D).
 - b. Nasal Schwalbe's line to temporal Schwalbe's line distance (SL-SL-D).
- 2) Angle measurements derived from identification of Schwalbe's line including:
 - a. Schwalbe's line angle opening distance (SL-AOD) and
 - b. Schwalbe's line trabecular iris surface area (SL-TISA).
- 3) Trabecular meshwork length (TML). The TML was included due to its importance, although it had only fair reproducibility.

- 4) Central corneal thickness (CCT). This was measured manually from the corneal image.

4.2.5 Statistical analysis.

Multivariable fractional polynomial regression models were used to estimate the best fit curve of the relation of the anterior segment measurements with age. It involved transformation of age to the best power, suitable to predict the change of each parameter and to describe the anterior chamber development (Details of different power were described in section 2.8.2). We established normative anterior chamber measurements by calculating the mean measure, 95% confidence intervals of the mean and 95% upper and lower prediction intervals for each age group. The nasal and temporal angle measurements were calculated separately. As we were interested in the development of the anterior chamber, we calculated the rate of change of each measurement per year and identified when it reached the maximum value or a plateau that represents the adult mean.

Mixed multiple models adjusted for transformed age, eye and gender were used to compare between nasal and temporal angle measurements. We also compared the anterior chamber measurements in female and males after adjusting the transformed age, eye and angle variation.

The correlation between spherical refractive errors and the anterior chamber measurements was investigated using mixed multiple models after adjusting the effect of age, gender, eye and angle variations. As the mixed model did not give the correlation coefficient (r), we calculated (r) using first order partial correlation. The angle predictor was omitted in case of ACW and CCT. All statistics analysis was carried out using Stata15 (2017). College Station, TX: Stata Corp LLC.

4.3 Results

4.3.1 Subjects

The demography of children and adult categorised per each age group is summarised in table 4-1. A total of 1464 anterior chamber measurements and 574 central corneal thickness measurements from a total of 282 participants at different ages were included in this study. Table 4-2 shows the demography of the analysed images.

Table 4-1: Demography of healthy participants categorized by age group.

Age group	Number	Mean ± SD	Minimum	Maximum
< 1 week	11*	2.3 ± 1.5 days	1 day	4 days
1 week-1 month	7*	17.8 ± 3.1 days	15.0 days	23 days
1-6 mes	12*	3.0 ± 1.5 month	0.8 month	5.8 months
6-12 mes	11	9.10 ± 1.90	6.20	11.90
1-2 yrs	17	1.40 ± 0.30	1.03	1.96
2-3 yrs	20	2.33 ± 0.23	2.00	2.73
3-4 yrs	29	3.44 ± 0.29	3.04	3.92
4-5 yrs	18	4.34 ± 0.26	4.01	4.96
5- 6 yrs	17 ^	5.40 ± 0.26	5.02	5.77
6-7 yrs	18 ^	6.47 ± 0.28	6.01	6.96
7-9 yrs	20 ^	8.01 ± 0.46	7.18	8.72
9-12 yrs	24^	10.57 ± 0.90	9.03	11.91
12-16 yrs	19 ^	13.84 ± 1.13	12.06	15.43
16-20 yrs	15	17.55 ± 0.67	16.09	18.67
20-45 yrs	44	33.19 ± 7.41	21.11	47.06
Total	282			
Ethnicity	Number (%)			
White European	180 (64)			
White North African	41 (15)			
Indian	47 (17)			
Others ^	14 (5)			
Gender	Number (%)			
Female	145 (51)			
Male	137 (49)			

(*) refraction could not be recorded by Plusoptix in all children younger than 6 months.

Visual acuity was assessed by flowing objects or preferential looking test.

(^) total 39 children were either wearing glasses or the refraction was collected from medical notes, based on the cycloplegic refraction.

(^) Others include mixed ethnicity, Afro-Caribbean.

Table 4-2: Demography of the HH-OCT measurements per eye and angle.

Anterior chamber angle images n=1464			
Left eye		Right eye	
702 (48%)		762 (52%)	
Temporal	Nasal	Temporal	Nasal
350 (24%)	352 (24%)	369 (25%)	393 (27%)
Total temporal		Total nasal	
719 (49%)		745 (51%)	
Corneal images n=574			
Left eye		Right eye	
287 (50%)		287 (50%)	

4.3.2 Refraction data

Sixty nine participants from the 223 children were excluded. Those included 30 children younger than 6 months, where we either could not acquire the refractive power in supine position or children were uncooperative. Although we were able to examine the refraction in one (2.4 months) child who has been held in upright position. Further 39 participants were excluded because their refraction were based on measuring the refractive power of the used glasses, measured by cycloplegic refraction. The data from 154 children (age ranged from 6 months to 15.4 years, 44% males and 56% females) were included in this part of study. The average spherical equivalent power was 0.5 ± 1.1 Dioptries. Refraction was compared to the anterior chamber measurements from 800 anterior chamber angle images, (414 right eye (52%) and 386 (48%) left eye) and 289 corneal images, (143 (49%) right eye and 146 (51%) left eye).

4.3.3 Non-quantitative inspection of anterior chamber development

The changes of anterior chamber structures with age can be seen clearly on OCT images, particularly throughout the first year of life (Figure 4-2), indicating typical anterior

chamber development. It is clearly visible that the 2 day old new-borns had different anterior chamber dimensions compared to older children and adults. Firstly, the iris was thin, flat, its anterior and posterior layers appeared similar and no visible crypts were detected compared to children of an older age. The iris was attached horizontally to the corneo-scleral junction with its uveal thinner end. The trabecular meshwork appeared as a small dense hyper-reflected structure, within the corneo-scleral junction, and slightly exposed to the anterior chamber angle at the interior corneal side. It extended anteriorly to Schwalbe's line. The latter was identified as the termination of the visible inner layer of cornea. Posteriorly the trabecular meshwork attached to scleral spur, the inner most protruded part of the corneo-scleral junction. With increased age, the iris became thicker at the pupillary side and iris crypts started to form at the anterior layers. The uveal part of the iris was moved backwards, exposing the trabecular meshwork and widening the anterior chamber angle. By the age of 12 months, the anterior chamber structures relatively resembled those of older children and adults. By the age of 4 years, the posterior layer of iris became less visible especially in a dark coloured iris. The iridocorneal angle was wider with backward bowing of the pupillary iris part. The latter changes are similar to 16 years old children and adults. The ciliary process and ciliary body could not be seen because their pigmentation absorbs the light and preventing visibility.

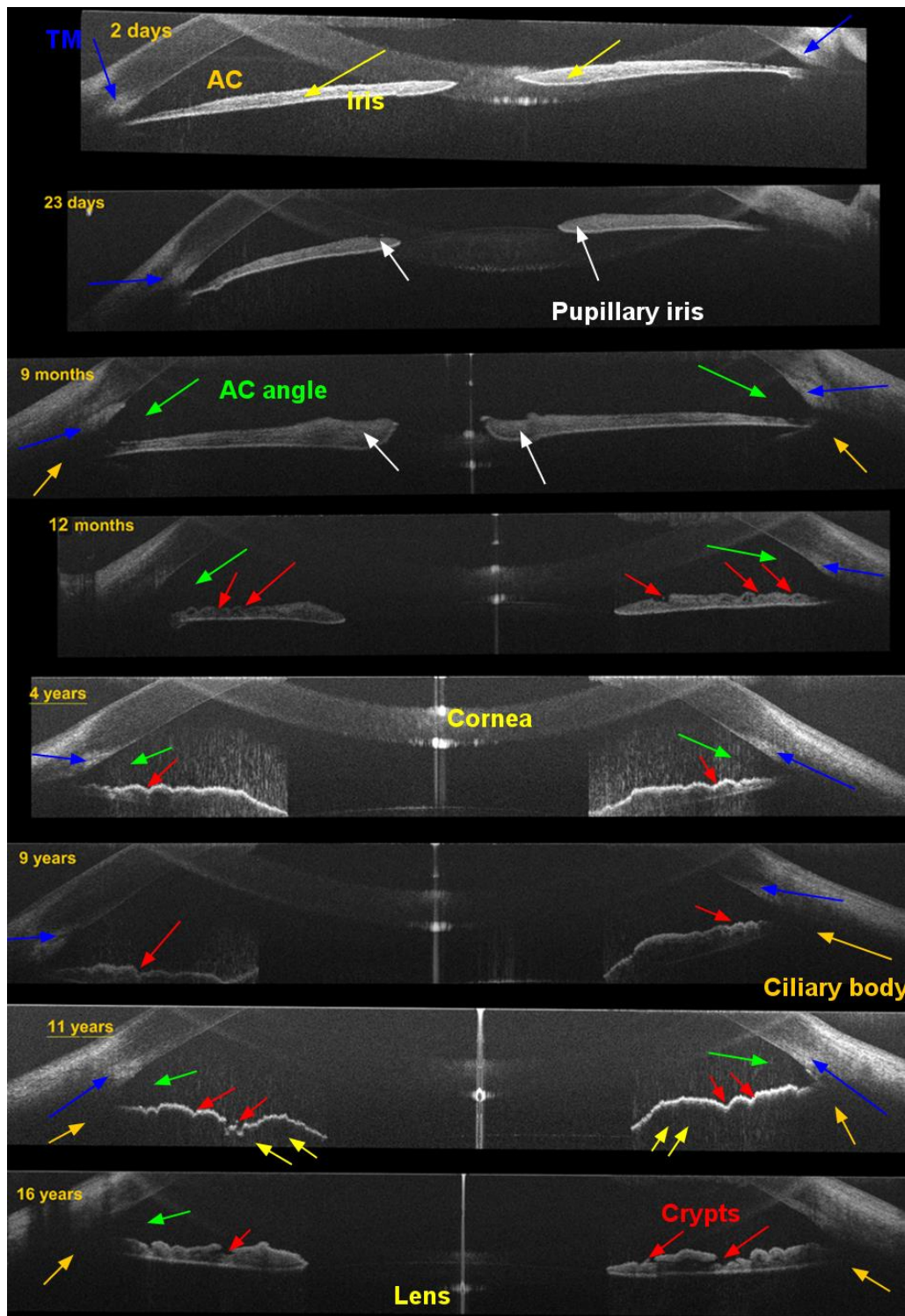


Figure 4-2: Anterior segment OCT images at different ages ranging between 2 days and 16 years of age.

At 2 days, the iris was thin, flat, with no visible crypts (yellow arrow). The trabecular meshwork (TM) appeared as a small dense hyper-reflected structure (blue arrow), within the

corneoscleral junction, partially exposed to the anterior chamber (AC) angle at the interior corneal side (green arrow). At 23 days the iris configuration changed by thickening of the pupillary part (white arrow) and posterior movement of the uveal part exposing the TM. The TM elongated and at 9 months appeared as a trapezoid structure (blue arrow). At 12 months, the iris crypts were visible (red arrows) but the uveal part of the ciliary process and ciliary body could not be seen because their pigmentation is absorbing light and preventing its reflection (orange arrows). At 4 years, the configuration of anterior chamber was similar to 9, 11 and 16 years old children. The posterior layer of iris became less visible especially in dark coloured irises (yellow arrows), the anterior chamber angle widened (green arrow) with the backward bowing of pupillary iris and well-formed iris crypts.

4.3.4 Quantitative measurements of anterior chamber development

The mean values and 95% prediction intervals of ACW (SS-SS-D and SL-SL-D), CCT and nasal and temporal angle measurements (TML, SL-AOD and SL-TISA) per age group are presented in (Tables 4-3 and 4-4). The changes of these measurements with age are shown in (Figures 4-3 and 4-4). The best fit curve of all measured parameters predicted a non-linear relation with age, demonstrating that the most prominent development of the anterior chamber happened during the first year of life. The ACW and anterior chamber angle measurements increased significantly with increasing age (all $p < 0.001$). In contrast, there was reduction of the central corneal thickness with increasing age ($p < 0.001$). The rate of the anterior chamber growth per year and the level of reaching maturity are shown in figure 4-5. Further details about the percentage of growth categorised in each age group are presented in table 4-5.

Table 4-3: Established normative measurements of the anterior chamber width and central corneal thickness categorised by different age group.

Age	Anterior chamber width		Central corneal thickness
	SL-SL-D (mm)	SS-SS-D (mm)	CCT (μm)
<1m	9.44 (8.42, 10.46)	10.13 (9.05, 11.22)	593.7 (503.7, 663.3)
1-6 mos	10.31 (9.29, 11.32)	11.21 (10.13, 12.30)	566.5 (482.2, 654.3)
6-12 mos	10.99 (9.98, 12.01)	12.07 (10.98, 13.15)	553.2 (474.2, 634.5)
1-1.5 yrs	11.25 (10.23, 12.26)	12.38 (11.30, 13.46)	549.4 (471.2, 627.1)
1-2 yrs	11.38 (10.36, 12.39)	12.54 (11.46, 13.62)	546.4 (469.5, 623.7)
2-3 yrs	11.46 (10.45, 12.48)	12.65 (11.57, 13.73)	545.1 (467.9, 622.5)
3-4 yrs	11.51 (10.50, 12.53)	12.71 (11.63, 13.80)	544.1 (467.3, 621.0)
4-5 yrs	11.53 (10.52, 12.55)	12.74 (11.66, 13.83)	543.7 (466.9, 620.4)
5-6 yrs	11.55 (10.53, 12.56)	12.76 (11.68, 13.85)	543.4 (466.7, 620.0)
6-8 yrs	11.56 (10.54, 12.57)	12.78 (11.69, 13.86)	543.2 (466.5, 619.8)
8-10 yrs	11.56 (10.54, 12.57)	12.79 (11.70, 13.87)	543.0 (466.4, 619.6)
10-14 yrs	11.55 (10.54, 12.56)	12.79 (11.71, 13.87)	542.9 (466.3, 619.5)
14-18 yrs	11.53 (10.51, 12.54)	12.79 (11.70, 13.87)	542.8 (466.2, 619.4)
18-25 yrs	11.49 (10.47, 12.50)	12.77 (11.69, 13.85)	542.8 (466.2, 619.4)
25-35 yrs	11.40 (10.39, 12.42)	12.72 (11.64, 13.80)	542.7 (466.2, 619.3)
35-45 yrs	11.27 (10.26, 12.29)	12.62 (11.54, 13.71)	542.7 (466.2, 619.3)
> 45 yrs	11.09 (10.07, 12.11)	12.44 (11.34, 13.53)	542.7 (466.2, 619.3)

SS-SS-D = nasal scleral spur to temporal scleral spur distance, SL-SL-D = nasal Schwalbe's line to temporal Schwalbe's line distance and CCT= central cornea thickness. Mean value of each measurement per age with 95% upper and lower prediction intervals are shown.

Table 4-4: Established normative measurements of nasal and temporal anterior chamber angle measurements categorised by different age group.

Anterior chamber angle measurements						
	Temporal			Nasal		
Age	TML (μm)	SL-AOD (μm)	SL-TISA (mm ²)	TML (μm)	SL-AOD (μm)	SL-TISA (mm ²)
Mean (lower and upper 95% prediction intervals)						
<1m	547.23 (295.77, 798.69)	311.05 (-81.18, 703.28)	0.12 (-0.03, 0.28)	543.61 (275.64, 811.59)	369.34 (-5.8, 743.93)	0.14 (-0.02, 0.29)
1-6 mes	623.40 (373.95, 872.86)	485.62 (96.34, 874.90)	0.19 (0.04, 0.35)	590.99 (323.89, 858.09)	498.03 (125.8, 870.18)	0.19 (0.04, 0.34)
6-12 mes	683.14 (434.28, 932.00)	617.05 (228.90, 1005.20)	0.24 (0.09, 0.40)	647.12 (380.73, 913.52)	614.27 (243.8, 985.21)	0.24 (0.09, 0.39)
1-1.5 yrs	708.65 (459.83, 957.47)	668.66 (280.69, 1056.63)	0.26 (0.11, 0.42)	675.16 (408.98, 941.35)	656.95 (286.8, 1027.71)	0.26 (0.01, 0.41)
1-2 yrs	722.43 (473.61, 971.26)	693.21 (305.26, 1081.16)	0.27 (0.12, 0.43)	693.44 (427.33, 959.54)	678.59 (307.8, 1049.33)	0.27 (0.02, 0.42)
2-3 yrs	735.63 (486.82, 984.44)	711.97 (324.01, 1099.93)	0.28 (0.13, 0.43)	713.17 (447.10, 979.24)	696.60 (325.8, 1067.34)	0.28 (0.02, 0.43)
3-4 yrs	745.09 (496.31, 993.87)	722.17 (334.20, 1110.15)	0.29 (0.13, 0.44)	726.76 (460.69, 992.83)	706.17 (335.8, 1076.93)	0.28 (0.03, 0.43)
4-5 yrs	751.66 (502.92, 1000.40)	727.00 (339.02, 1114.98)	0.29 (0.13, 0.44)	733.84 (467.77, 999.92)	710.13 (339.8, 1080.89)	0.28 (0.03, 0.43)
5-6 yrs	758.17 (509.47, 1006.88)	730.28 (342.29, 1118.26)	0.29 (0.13, 0.44)	739.63 (473.54, 1005.72)	712.80 (342.8, 1083.56)	0.28 (0.03, 0.43)
6-8 yrs	764.44 (515.77, 1013.11)	732.31 (344.32, 1120.30)	0.29 (0.14, 0.44)	745.85 (479.74, 1011.95)	715.20 (344.8, 1085.97)	0.28 (0.03, 0.44)
8-10 yrs	772.12 (523.49, 1020.76)	733.95 (345.96, 1121.95)	0.29 (0.14, 0.44)	751.36 (485.24, 1017.49)	716.86 (346.8, 1087.64)	0.28 (0.03, 0.44)
10-14 yrs	781.92 (533.31, 1030.54)	735.11 (347.11, 1123.11)	0.29 (0.14, 0.44)	756.96 (490.83, 1023.10)	718.06 (347.8, 1088.84)	0.28 (0.03, 0.44)
14-18 yrs	795.78 (547.13, 1044.43)	735.94 (347.94, 1123.94)	0.29 (0.14, 0.44)	762.83 (496.69, 1028.97)	718.83 (348.8, 1089.61)	0.28 (0.03, 0.44)
18-25 yrs	808.29 (559.54, 1057.04)	736.28 (348.28, 1124.28)	0.29 (0.14, 0.44)	768.61 (502.49, 1034.74)	719.18 (348.8, 1089.97)	0.29 (0.03, 0.44)
25-35 yrs	826.04 (577.06, 1075.03)	736.53 (348.53, 1124.54)	0.29 (0.14, 0.44)	781.58 (515.43, 1047.73)	719.45 (348.8, 1090.23)	0.29 (0.03, 0.44)
35-45 yrs	842.84 (593.52, 1092.17)	736.65 (348.64, 1124.65)	0.29 (0.14, 0.44)	800.98 (534.48, 1067.49)	719.55 (348.8, 1090.34)	0.29 (0.03, 0.44)
>45 yrs	858.78 (609.03, 1108.54)	736.70 (348.70, 1124.71)	0.29 (0.14, 0.44)	819.09 (551.88, 1086.29)	719.59 (348.8, 1090.38)	0.29 (0.03, 0.44)

TML= Trabecular meshwork length, SL-AOD = Schwalbe's line angle opening distance, SL-TISA = Schwalbe's line trabecular iris surface. Mean value per age and 95% upper and lower prediction intervals are shown.

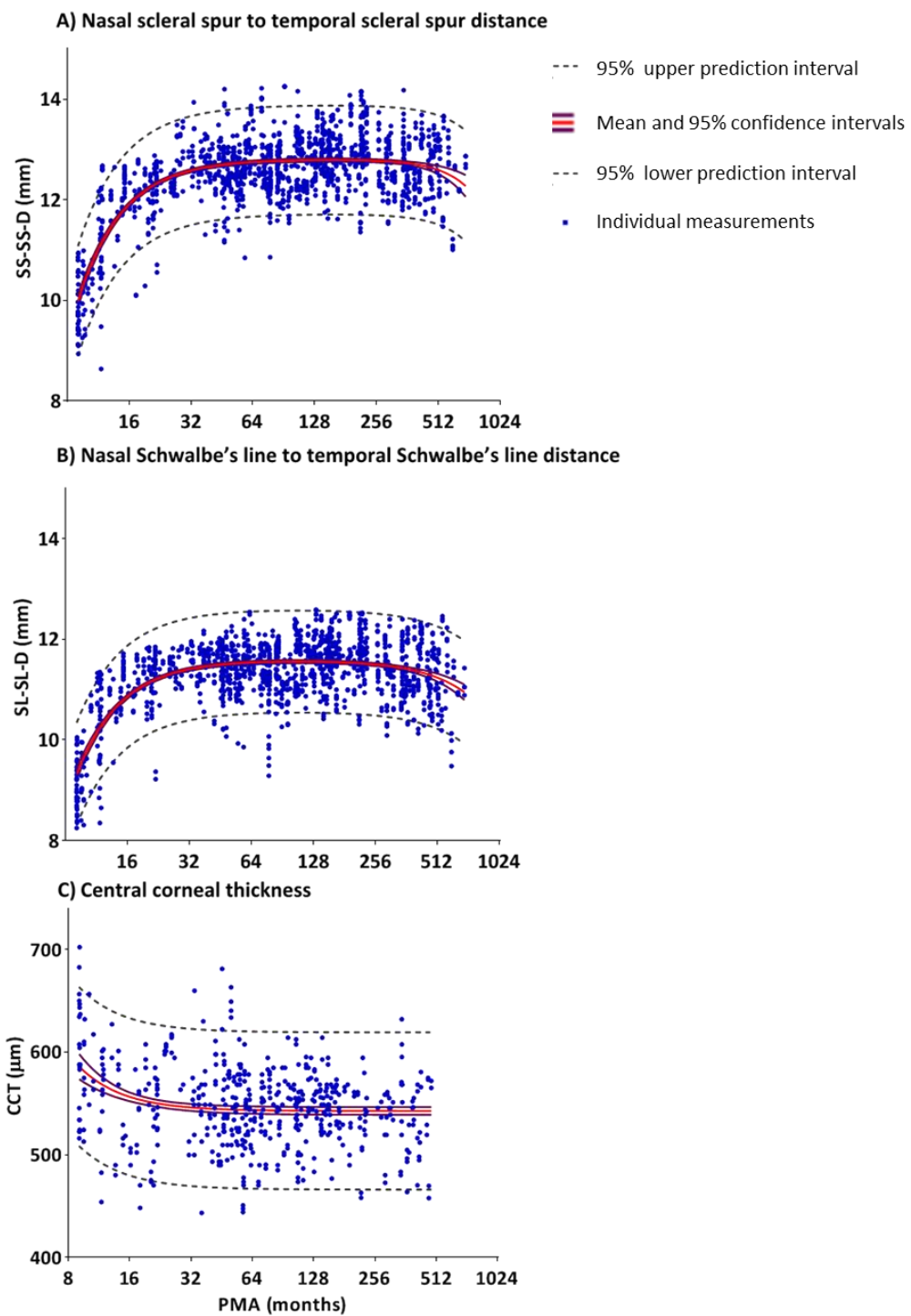


Figure 4-3: Scatter plots showing the development of anterior chamber width and central corneal thickness.

(A) nasal scleral spur to temporal scleral spur distance (SS-SS-D) and (B) Nasal Schwalbe's line to temporal Schwalbe's line distance (SL-SL-SD), in mm. (C) central cornea thickness (CCT) in μm , with postmenstrual age in months are shown. Mean value (red lines), 95% confidence intervals of mean (blue lines), 95% prediction intervals (dashed lines) and individual measurements (blue dots) are shown.

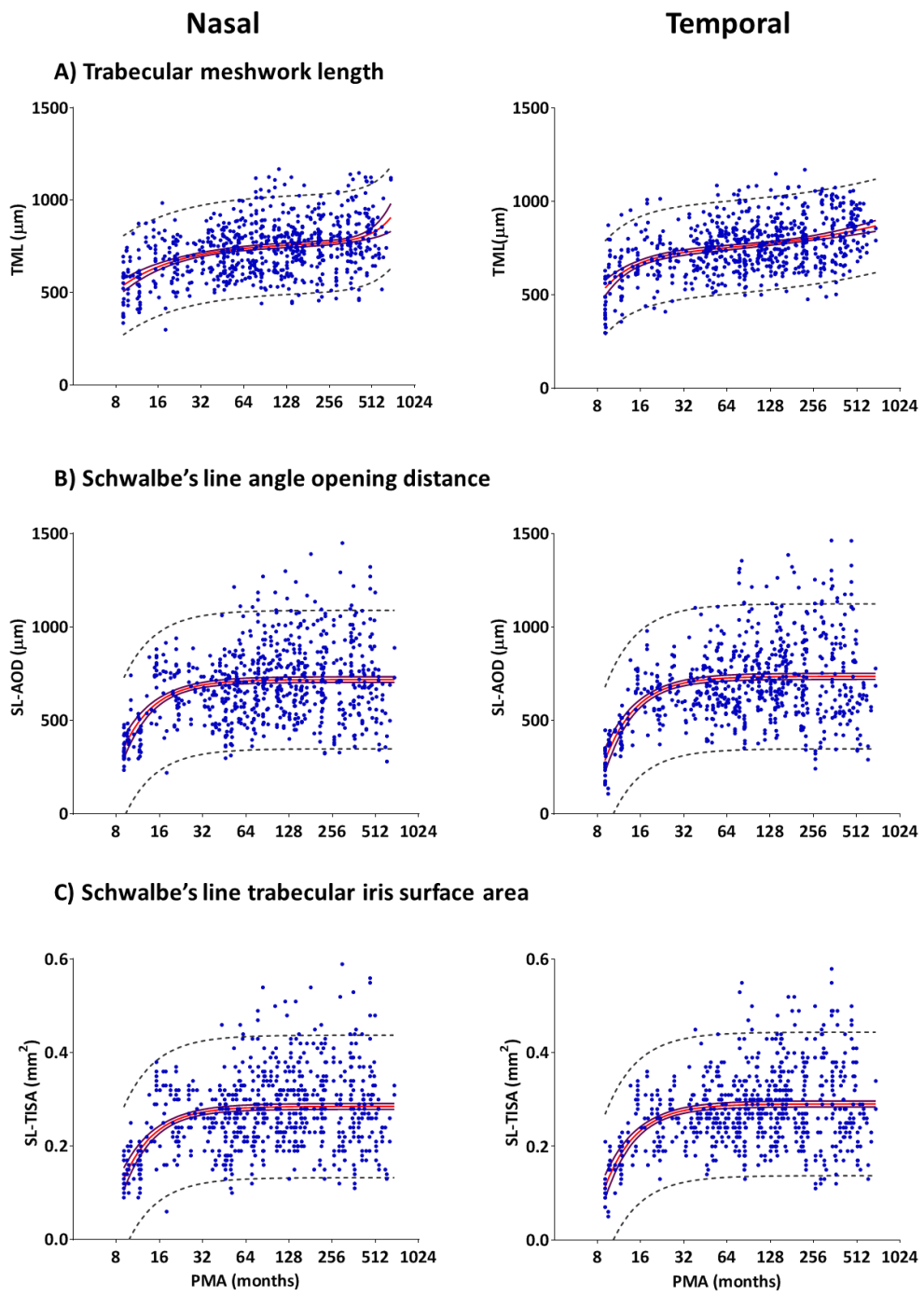


Figure 4-4: Scatter plots showing the development of nasal and temporal anterior chamber angle measurements.

(A) trabecular meshwork length (TML) in microns (B) Schwalbe's line angle opening distance (SL-AOD) in microns. (C) Schwalbe's line trabecular iris surface area (SL-TISA) in micromes, with postmenstrual age in months. Mean value (red lines), 95% confidence intervals of mean (blue lines), 95% prediction intervals (dashed lines) and individual measurements (blue dots) are shown for nasal and temporal angles separately.

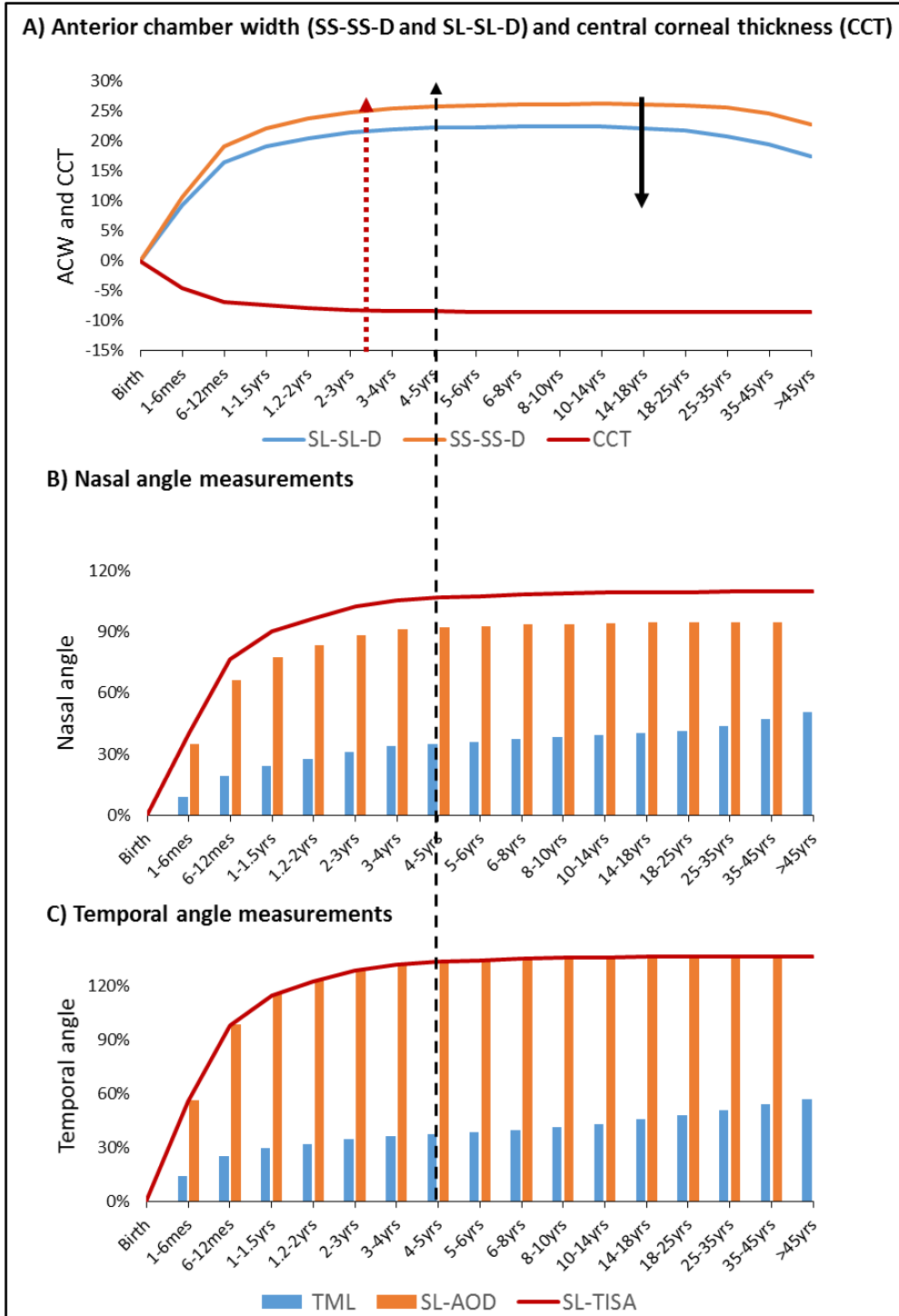


Figure 4-5: The rate of changes of the anterior chamber measurement per age.

A phase of rapid development happened during the first 1.5 years. Anterior chamber widening (including SS-SS-D and SL-SL-D) and central corneal thickness (CCT) thinning reached a plateau by age of 3 years (dashed red arrow). ACW started to decrease by age of 18 years (black arrow). The nasal and temporal angle width (SL-AOD and SL-TISA) doubled during the first year then stabilized by about age of 5 years (dashed black arrow).

Table 4-5: Rate of growth of the anterior chamber measurements per year

Age intervals	Anterior chamber width		CCT	Anterior chamber angle measurements						
	SL-SL-D	SS-SS-D		TML		SL-AOD		SL-TISA		
				Temporal	Nasal	Temporal	Nasal	Temporal	Nasal	
0-6 mes	9%	11%	-5%	14%	9%	56%	35%	56%	40%	
0-12 mes	16%	19%	-7%	25%	19%	98%	66%	98%	77%	
1-2 yrs	3%	4%	-1%	6%	3%	12%	17%	12%	11%	
2-3 yrs	1%	1%	0%	2%	3%	3%	3%	3%	3%	
3-4 yrs	0%	0%	0%	1%	2%	1%	1%	1%	1%	
4-5 yrs	0%	0%	0%	1%	1%	1%	1%	1%	1%	
5-6 yrs	0%	0%	0%	1%	1%	0%	0%	0%	0%	
6-8 yrs	0%	0%	0%	1%	1%	0%	0%	0%	0%	
8-10 yrs	0%	0%	0%	1%	1%	0%	0%	0%	0%	
10-14 yrs	0%	0%	0%	1%	1%	0%	0%	0%	0%	
14-18 yrs	0%	0%	0%	2%	1%	0%	0%	0%	0%	
18-25 yrs	0%	0%	0%	2%	1%	0%	0%	0%	0%	
25-35 yrs	-1%	0%	0%	2%	2%	0%	0%	0%	0%	
35-45 yrs	-1%	-1%	0%	2%	2%	0%	0%	0%	0%	
>45 yrs	-1%	-1%	0%	2%	2%	0%	0%	0%	0%	

SS-SS-D = nasal scleral spur to temporal scleral spur distance, SL-SL-D = nasal Schwalbe's line to temporal Schwalbe's line distance and CCT= central cornea thickness TML= Trabecular meshwork length, SL-AOD = Schwalbe's line angle opening distance, SL-TISA = Schwalbe's line trabecular iris surface. The highlighted cells indicate the level of maturity with no further growth.

4.3.5 Anterior chamber development

The developmental trajectories of each anterior chamber measurement are described below:

4.3.5.1 Development of anterior chamber width

The nasal angle to temporal angle distances between scleral spurs (SS-SS-D) and between Schwalbe's lines (SL-SL-D) significantly increased with age (both $p < 0.0001$), representing the growth of anterior chamber width (ACW) (Figures 4-3A and 4-3B). SS-SS-D increased by 19% from a mean of 10.13 mm at birth to 12.07 mm at one year of age (Figure 4-5 and Table 4-3). Similarly, the SL-SL-D increased by 16% from 9.44 mm at birth to 10.99 mm at one year of age. SS-SS-D and SL-SL-D reached maximum levels of 12.77 and 11.55 mm by the age of 4 years, respectively. Interestingly, they started to decrease slightly in size after the ages of 18 and 14 years, respectively.

4.3.5.2 Development of central cornea

The CCT became thinner with age ($p = 0.0003$) (Figure 4-3C). CCT decreased by 40 μm (7%) from 593.7 to 553.2 during the first year of age and reached a plateau by approximately age of 3 years (Table 4-3 and Figure 4-5).

4.3.5.3 Development of anterior chamber angle

4.3.5.3.1 Anterior chamber angle width

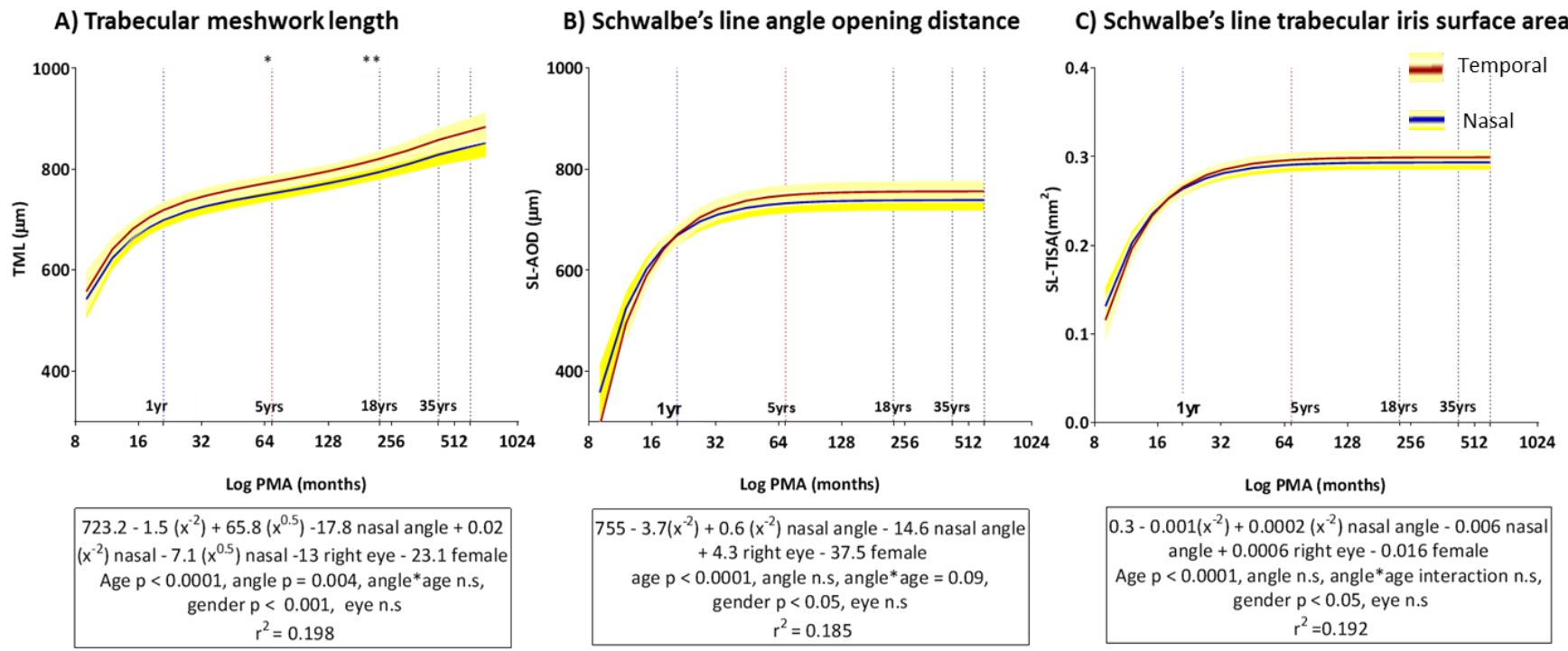
The SL-AOD and SL-TISA of both nasal and temporal angles increased significantly with age (all $p < 0.0001$), indicating widening of anterior chamber angle (Figure 4-4). This widening was greater for the temporal angle compared to the nasal angle, although, it was not statistically significant (Figure 4-6). The rate of increase in the nasal SL-AOD and SL-TISA was 66% and 77% during the first year of age, respectively. In contrast, there was an increase of 98 % in the temporal SL-AOD and SL-TISA angle. (Table 4-5 and Figure 4-5). This rate of growth of both angles slowed down to about 1% throughout childhood and reached a plateau by the age of 5 years.

4.3.5.3.2 Trabecular meshwork length (TML)

The major TM development occurred during the first year of age, where the temporal and nasal trabecular meshwork elongated by 25% and 19%, from 547.23 µm and 543.61 µm to 683.14 µm and 647.12 µm, respectively (Table 4-4 and Figure 4-4 A). The developmental trajectories of TML showed continuous slight elongation of trabecular meshwork up to adulthood (Figure 4-5).

4.3.5.4 Variation of nasal and temporal trabecular meshwork development.

The mixed model showed that the TML elongation was significantly greater in temporal angle compared to nasal angle ($p < 0.05$). When we analysed the significance of this difference at different points of age, including birth, 1, 5, 18 and 35 years (Figure 4-6A). The analysis showed that the nasal and temporal TML were not different at birth (p value = 0.59). However, at age of 5 years, the rate of elongation in temporal TML became statistically higher compared to the nasal TML increase ($p < 0.05$). The rate of temporal and nasal TML elongation was 45% and 40% respectively, for the first 18 years of age ($p < 0.01$). At age of 35, the temporal and nasal TML became similar ($p > 0.05$).



Nasal to temporal difference									
	TML (μm)			SL-AOD (μm)			SL-TISA (mm²)		
	β	p value	95% CI	β	p value	95% CI	β	p value	95% CI
Birth	-16.76	0.56	-73.51 39.99	66.47	0.11	-14.64 147.59	0.016	0.35	-0.017 0.048
1 yr	-19.70	0.05	-39.66 0.27	-1.92	0.86	-22.80 18.96	-0.002	0.67	-0.010 0.007
5 yrs	-21.52	0.03	-40.96 -2.08	-13.95	0.18	-34.26 6.35	-0.005	0.24	-0.013 0.003
18 yrs	-23.20	0.004	-39.83 -6.57	-16.27	0.13	-37.35 4.81	-0.005	0.21	-0.014 0.003
35 yrs	-34.30	0.07	-71.78 3.17	-17.29	0.12	-38.78 4.21	-0.006	0.19	-0.014 0.003

Figure 4-6: Polynomial plots comparing the development of nasal and temporal anterior chamber angle measurements.

(A) trabecular meshwork length (in μm). (B) Schwalbe's line angle opening distance (in μm) and (C) Schwalbe's line trabecular iris surface area (in mm^2). Nasal mean curvefit (blue lines), temporal mean curvefit (red lines) and 95% confidence intervals of each curve fit (yellow highlighted areas) are shown. The equation of each model and significance value of each predictor variable is given in the box under each curve. Table shows the coefficient and significance of difference and 95% confidence interval of differences between nasal and temporal parameter at different ages. The increase of temporal trabecular meshwork length (TML) was statistically significant compared to the nasal TML increase. We did not detect a significant statistical difference between the widening of temporal angle (SL-AOD and SL-TISA) and nasal angle.

4.3.6 The impact of predictor factors on anterior chamber development

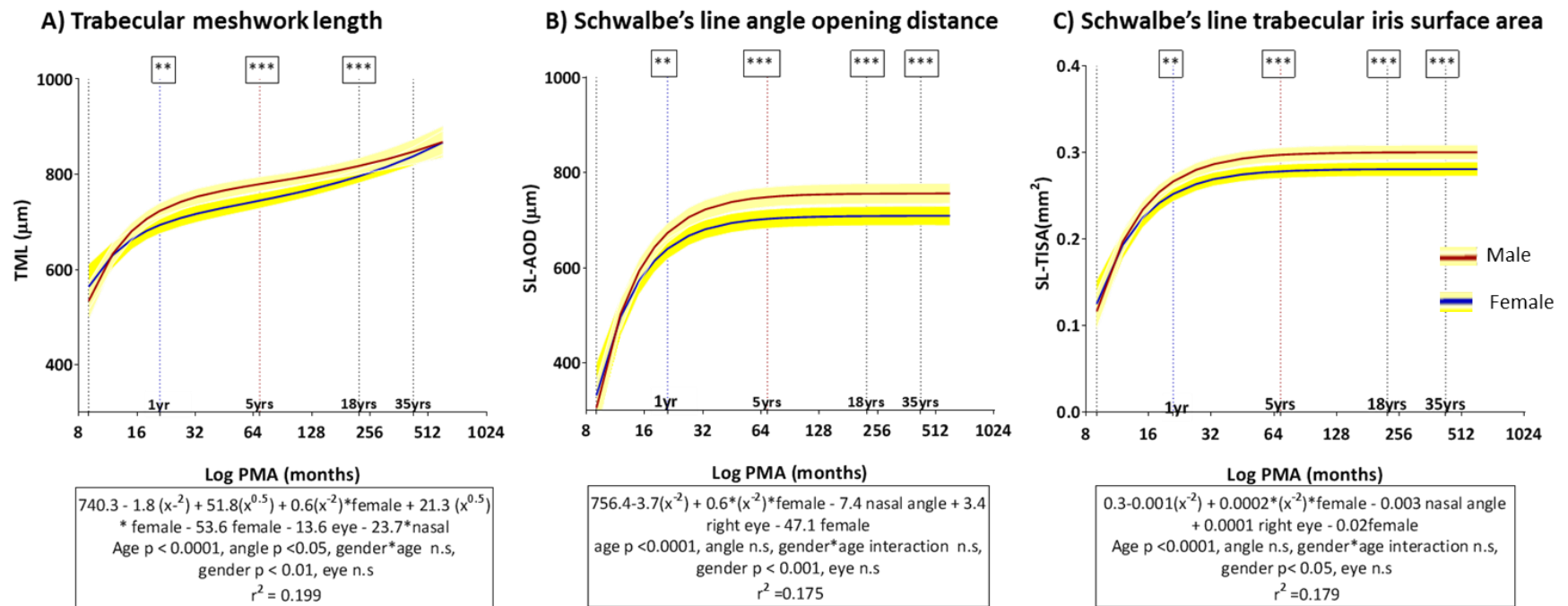
4.3.6.1 Gender and eye variation of anterior chamber parameters.

Our mixed multiple models showed that females had narrower anterior chamber angle measurements (Table 4-6) (Figure 4-7), narrower ACW (SS-SS-D and SL-SL-D) compared to males, p values < 0.05 (Figure 4-8). However, by analysing the gender difference of ACW at different ages we detected an age gender interaction ($p < 0.001$). This interaction indicates that, when ACW began to reduce at adulthood, the difference gender measurements became reversed, with narrower ACW in males compared to females. In contrast, no significant gender difference of CCT was detected ($p > 0.05$). There was not any significant difference between the right and left eye in all the measurements at any age ($p > 0.05$).

Table 4-6: The correlation of the development of each anterior chamber measurement with gender, eye and angle variation after controlling the effect of age.

		Anterior chamber angle measurements			Anterior chamber width		Central corneal thickness
		TML (μm)	SL-AOD (μm)	SL-TISA (mm^2)	SS-SS-D (mm)	SL-SL-D (mm)	CCT (μm)
		n=1464			n=1419		n=575
Gender	r^2	0.197	0.186	0.091	0.549	0.465	0.091
	β	-23.280	-37.110	-0.015	-0.100	-0.090	-3.320
Eye	p value	0.001	0.0003	0.0002	0.001	0.001	NS
	β	-12.490	4.460	0.001	0.020	0.020	2.730
Angle	p value	Ns	Ns	Ns	Ns	Ns	NS
	β	-23.290	-8.830	-0.004	-	-	-
	p value	0.001	Ns	Ns	-	-	-

Predictor variables are gender, angle and eye variations. The baseline was male, left eye and temporal angle. Ns= non-significant (p value > 0.05), n= number of images. r^2 = coefficient of determination. β =coefficient of difference. The highlighted cells indicate significant differences (p values). TML = trabecular meshwork length. SL-AOD = Schwalbe's line angle opening distance. SL-TISA = Schwalbe's line trabecular iris surface area. ACW = anterior chamber width. SS-SS-D = nasal scleral spur to temporal scleral spur distance. SL-SL-D = nasal Schwalbe's line to temporal Schwalbe's line distance. CCT = central corneal thickness. The highlighted cells in red indicate significantly smaller measurements of females compared to males and smaller nasal TML compared to temporal TML.

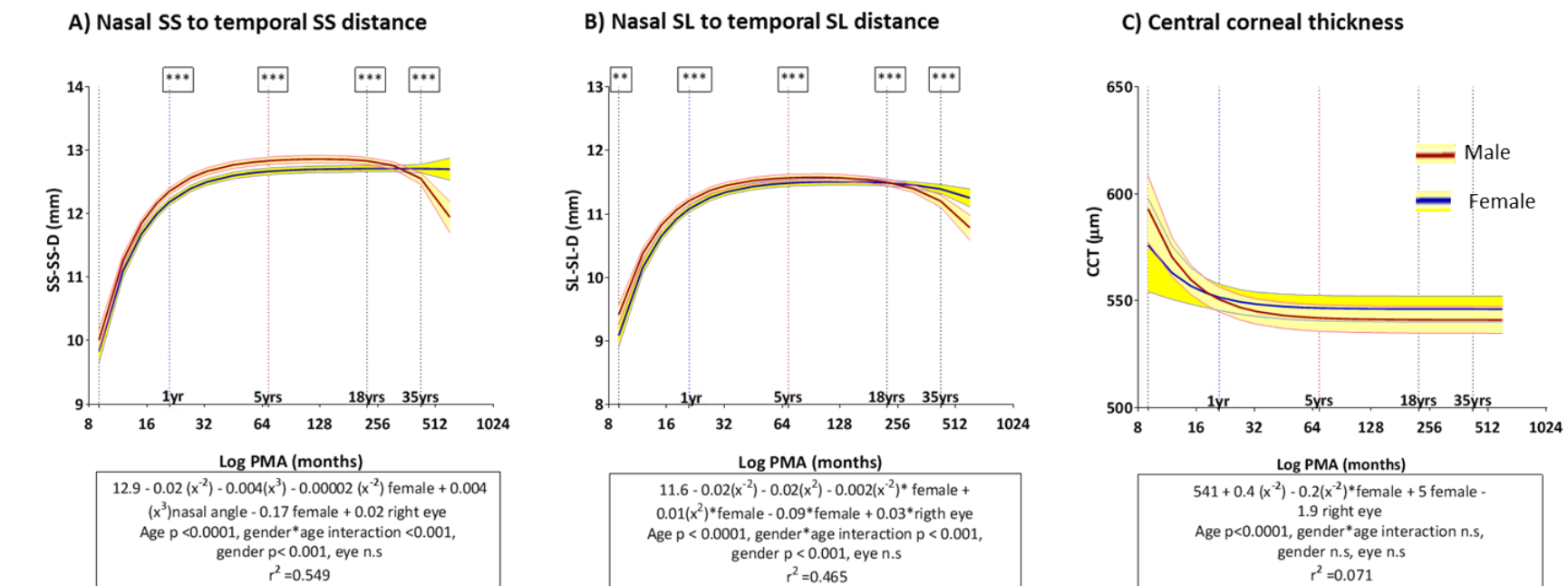


Female to male difference

TML (μm)				SL-AOD (μm)				SL-TISA (mm^2)				
	β	p value	95% CI		β	p value	95% CI		β	p value	95% CI	
Birth	30.01	0.333	-30.73	90.75	26.40	0.554	-61.03	113.83	0.01	0.633	-0.03	0.04
1 yr	-29.70	0.005	-50.47	-8.93	-33.63	0.003	-55.54	-11.71	-0.01	0.001	-0.02	-0.01
5 yrs	-36.28	0.000	-56.23	-16.33	-44.19	0.000	-64.98	-23.40	-0.02	0.000	-0.03	-0.01
18 yrs	-33.54	0.000	-50.60	-16.49	-46.22	0.000	-67.78	-24.66	-0.02	0.000	-0.03	-0.01
35 yrs	-1.14	0.955	-41.13	38.85	-47.12	0.000	-69.10	-25.13	-0.02	0.000	-0.03	-0.01

Figure 4-7: Polynomial plots comparing the development of anterior chamber angle of males and females.

(A) trabecular meshwork length in μm (B) Schwalbe's line angle opening distance in μm and (C) Schwalbe's line trabecular iris surface area in mm^2 . Female mean curvefit (blue lines), male mean curvefit (red lines) and 95% confidence intervals of each curve fit (yellow highlighted areas). The difference in anterior chamber angle measurements between males and females at different ages (vertical dashed line) are indicated using asterisks where ** represents $p < 0.01$ and *** represents $p < 0.001$. The equation of each model and significance value of each predictor variable are shown in the box under each curve. The table shows the coefficient and significance of difference and 95% confidence interval of differences between female and male parameters at different ages. The increase of the male trabecular meshwork length (TML) was statistically greater than the female TML. We detected a statistically significant wider angle (SL-AOD AND SL-TISA) in males compared to females.



Female to male difference											
SS-SS-D (mm)				SL-SL-D (mm)				CCT(μm)			
	β	p value	95% CI		β	p value	95% CI		β	p value	95% CI
Birth	-0.17	0.174	-0.42 0.08		-0.33	0.006	-0.56 -0.09		-16.95	0.207	-43.27 9.36
1 yr	-0.17	0.000	-0.23 -0.10		-0.13	0.000	-0.19 -0.07		1.01	0.779	-6.02 8.03
5 yrs	-0.17	0.000	-0.23 -0.10		-0.09	0.005	-0.16 -0.03		4.17	0.240	-2.78 11.11
18 yrs	-0.17	0.000	-0.23 -0.10		-0.08	0.019	-0.14 -0.01		4.77	0.194	-2.43 11.98
35 yrs	0.76	0.000	0.46 1.06		0.47	0.000	0.23 0.71		5.04	0.178	-2.30 12.38

Figure 4-8: Polynomial plots comparing the development of the anterior chamber width and central corneal thickness of males and females.
(A) Nasal scleral spur to temporal scleral spur distance (SS-SS-D) (in mm) (B) Nasal Schwalbe's line to temporal Schwalbe's line distance (SL-SL-D) (in mm) and (C) Central corneal thickness (CCT) (in μm). Female mean curvefit (blue lines), male mean curvefit (red lines) and 95% confidence intervals

*of each curve fit (yellow highlighted areas). The difference in measurements between males and females at different ages (vertical dashed line) are indicated using asterisks where ** represents $p < 0.01$ and *** represents $p < 0.001$. The equation of each model and significance value of each predictor variable is attached. Table shows the coefficient and significance of difference and 95% confidence interval of differences between female and male mean at different ages. The increase of male anterior chamber width (SS-SS-D AND SL-SL-D) was statistically greater than female ACW. No significant gender difference in CCT was detected.*

4.3.6.2 Correlation between anterior chamber measurements and refractive error

A shift from hypermetropia to myopia with increasing age was noted (Table 4-7 and Figure 4-9). By adjusting the effect of age, there was a significant negative correlation between spherical refractive power and angle width measurements (all $p < 0.001$) and CCT ($p < 0.01$) In contrast, the ACW was associated with positive shift of spherical power (all $p < 0.05$).

Table 4-7: First order partial correlation between anterior chamber measurements and spherical power.

		Anterior chamber angle measurements			Anterior chamber width		Central corneal thickness
		TML	SL-AOD	SL-TISA	SS-SS-D	SL-SL-D	CCT
		n=800					
Spherical power	r	0.02	-0.26	-0.24	0.10	0.08	-0.13
	β	2.38	-43.25	-0.02	0.05	0.03	-4.63
	p value	Ns	<0.0001	<0.0001	0.004	0.03	0.002

TML = trabecular meshwork length SL-AOD = Schwalbe's line angle opening distance. SL-TISA = Schwalbe's line trabecular iris surface area. ACW = anterior chamber width; SS-SS-D = nasal scleral spur to temporal scleral spur distance. SL-SL-D = nasal Schwalbe's line to temporal Schwalbe's line distance. CCT = central corneal thickness. Pearson correlation coefficient (r), coefficient of difference (β). The effect of age was adjusted. Highlighted red cells indicate significant correlation.

The above findings indicate that:

- 1) Myopic eyes (negative refractive error) had wider angles while hypermetropic eyes (positive error) had shallower angles after controlling for the effect of age (Figure 4-9).
- 2) CCT was negatively correlated with the refractive power. Thick cornea was associated with myopia while thin cornea is associated with hypermetropia.
- 3) The increase of ACW with age was associated with a weak hypermetropic shift (from negative to positive refraction error).

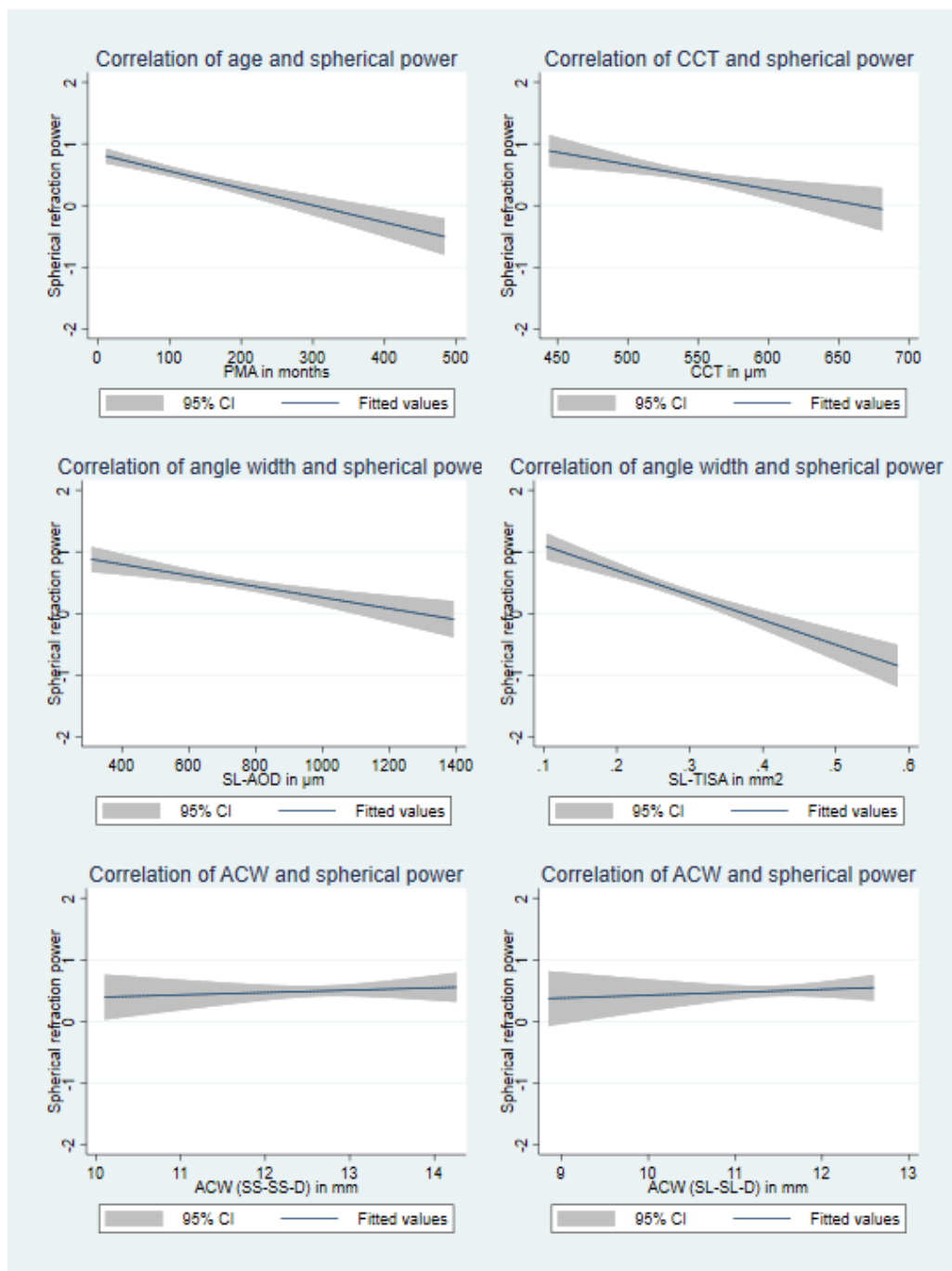


Figure 4-9: Correlation between anterior chamber measurements, postmenstrual age and spherical equivalent.

The increase of anterior chamber width (ACW) was associated with a hypermetropic shift (change to more positive spherical refraction), while the widening of the anterior chamber angle and increased age were associated with a myopic shift (change to more negative spherical refraction). Increased central cornea thickness (CCT) was associated with negative refractive error. CCT became thinner with age.

4.4 Discussion

To the best of our knowledge, this is the first study of the normal development of the anterior chamber in children since birth using anterior segment OCT. We have presented normative measurements and 95% prediction limits for anterior chamber width, central corneal thickness and anterior chamber angle measurements in children. These measurements have enabled us to clarify how and when the anterior segment of the eye grew and reached maturity. We found that postnatal anterior chamber development rapidly occur during the first 1.5 years of age, similar to the previously mentioned study using ultrasound biomicroscopy (Kobayashi et al., 1999). We also found that the growth slowed down afterwards and reached maturity approximately by the age of 5 years. This is consistent with histological studies which have previously revealed that the development of the anterior chamber continues postnatally in both human (Anderson, 1981, Reme and Depinay, 1981, Worst, 1968) and mice (Choudhary et al., 2007, Cvekl and Tamm, 2004) . The trajectory of anterior chamber growth is also in agreement with the development of axial length (Hussain et al., 2014), optic nerve (Patel et al., 2016) and fovea (Lee et al., 2015, Hendrickson and Yuodelis, 1984). This study also detected significant gender variation of anterior chamber biometry and presented possible role of anterior chamber width (ACW) development on emmetropisation.

4.4.1 Anterior chamber development

4.4.1.1 Comparison of Histology and OCT imaging

A histological study by Reme et al (1981) found that the anterior chamber angle reaches the configuration of the adult eye by 1 to 4 years after birth and the final cellular and extracellular maturation of trabecular meshwork is achieved by 1 to 8 years of age (Reme and Depinay, 1981). In the same year, Anderson et al described the normal development of the anterior chamber angle (Anderson, 1981) through histological examination of 40 eyes of children (age range from 20 weeks gestational age to 5 years of postnatal age) under light and electron microscope (details is described in section 1.2.2). Our study presented similar findings to these histological studies (Figure 4-10) with the advantage of in vivo quantitative measurements that is based on a large sample size of healthy children

and an establishment of normative trajectories of anterior chamber with 95% prediction intervals.

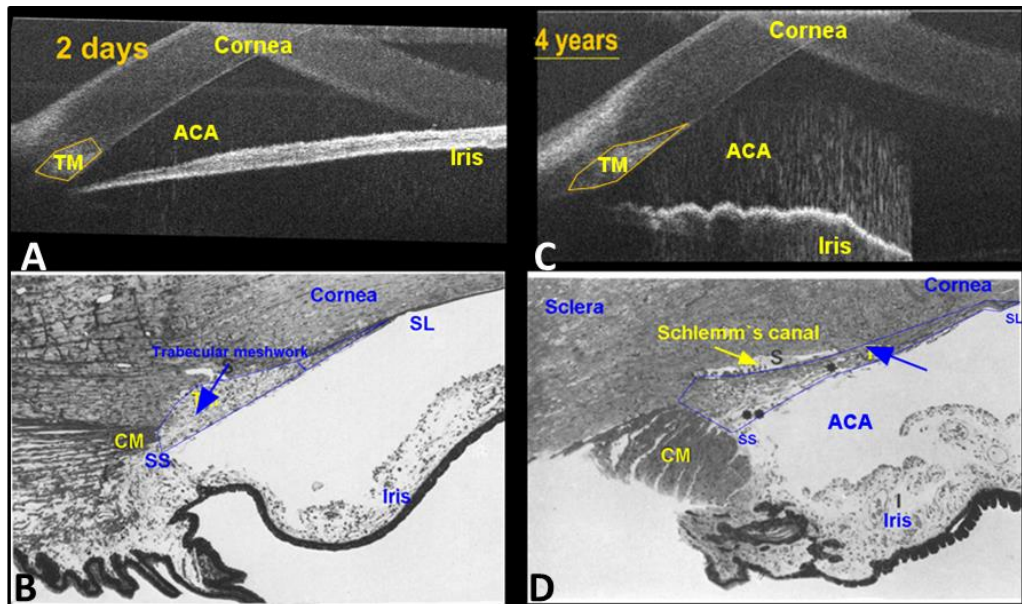


Figure 4-10: Comparison of HH-OCT image and histology of anterior chamber angle.
 A) Anterior chamber angle (ACA) image of 2 days old child. B) Histology of anterior chamber angle of new-born child (modified from Reme et al (1981)(Reme and Depinay, 1981). C) Anterior chamber angle image of 4 years old child. D) Histology of anterior chamber angle of 4 years old child. CM = ciliary muscle, TM= trabecular meshwork, SL =Schwalbe's line, SS = scleral spur. At birth the posterior part of the trabecular meshwork (TM) is embedded in the corneoscleral junction and overlapped by the ciliary process and the iris. The iris is curved forward. Shortly after birth, the ciliary muscles and process slide posteriorly, in relation to the cornea and sclera. The iris recesses behind the scleral spur, exposing the TM in the anterior chamber. The ciliary processes eventually extend into the peripheral iris, lie side by side to the ciliary muscle (CM). As a consequence, the anterior chamber angle is widening.

4.4.1.2 Quantitative development of anterior chamber

In our study, the anterior chamber biometry increased rapidly during the first 18 months followed by steady slow phase throughout the early childhood. During this period, the TM exposed and started to elongate with continuous widening of nasal and temporal angle (Figure 4-11). The nasal and temporal angle width doubled during the first year.

Consistently, the anterior chamber widened and then stabilized by the age of 3 years. The findings of this study also showed that TM continued to elongate posteriorly up to adulthood in a slow rate. The anterior chamber angle achieved the width of adulthood and became well developed by the age of about 5 years.

The continuous steady TM elongation and the stability of angle width demonstrate the likelihood that the change of axial length (AL), iris and lens playing an important role in angle widening. Using A scan ultrasonography, the AL was reported to increase rapidly during the first 18 months, from about 16.8 mm at birth to 20 mm at one year (about 19% increase similar to our rate of ACW development) and to 21 mm at age 4 years (Hussain et al., 2014). Using magnetic resonance imaging (MRI), Munro et al (2015), detected that ACD increased and reached a plateau by age of 2 years while the AL continue to increase at slower rate up to 20 years old (Munro et al., 2015). Similarly, a study (2015) using LenStar Biography (based on optical low coherence reflectometry), among 6 to 18 years old students in Iran, detected continuous increase in AL by 0.09 mm per year till age of 18 years (Hashemi et al., 2015). The antero-posterior elongation of TML may be result from the continuous increase of AL until adulthood, in the presence of stable ACW.

In addition, iris bowing, independent to ACD change, was reported to play a crucial role in the size of the angle width (Cheung et al., 2010, Mak et al., 2013). Sng et al have reported that the (forward) iris curvature and the iris area increase with age .This AS-OCT study has showed that forward iris curvature is associated with narrowing of the anterior chamber angle (Sng et al., 2013). This would mean that the size of the angle is not changing, since the increase of the AL would be balanced by the iris bowing. To simplify this assumption, we have drawn a schematic model from our measurements showing a possible role of AL and iris change (Figure 4-11). However, this is only one possible theory of why the size of anterior chamber angle did not change during late childhood and early adulthood.

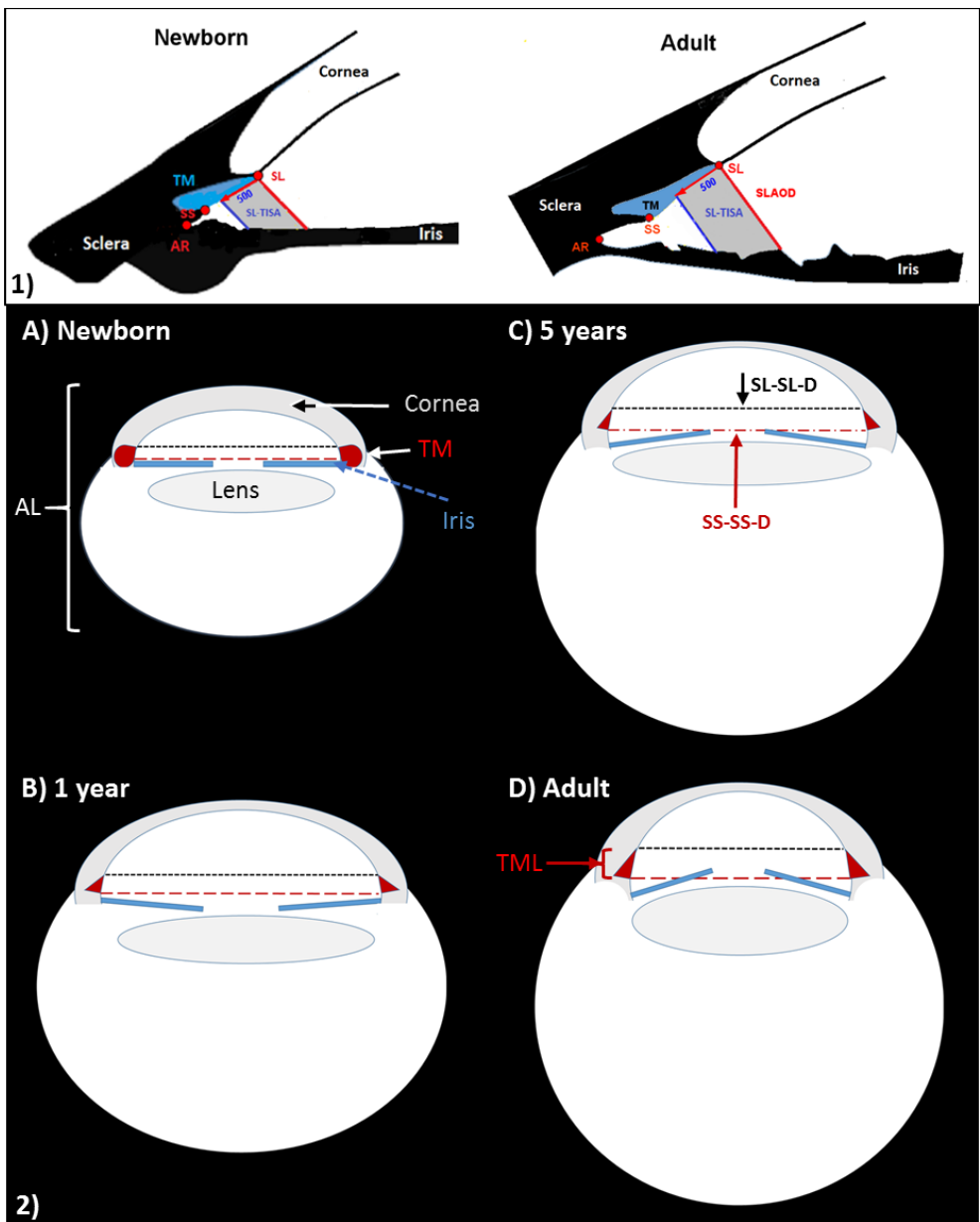


Figure 4-11: Schematic illustration of the postnatal development of anterior chamber.

1) The anterior chamber angle becomes wider in adulthood compared to newborn angle. There is increase in the Schwalbe's line angle opening distance and trabecular iris surface area with elongation of trabecular meshwork length. **2)** Schematic representation of the eye globe showing the developmental progress of the anterior chamber width and trabecular meshwork with regards to the changes of axial length, the lens and iris. The eye globe changes from oblate to spherical and eventually becomes prolate. The anterior chamber width increases rapidly during the first year, stabilises by the age of 3 years, and then starts to diminish by the age of 18 years. The anterior chamber angle stabilises by the age of 5 years due to the forward bowing of iris, the increased lens thickness and the continuous elongation of the trabecular meshwork. The angle width does not change afterwards as the iris bowing is balanced with the increase of axial length, anterior chamber depth throughout adulthood. The ACW begins to reduce in size by age of 18 giving the globe a more prolate configuration.

4.4.2 Comparison between ocular biometry in children and adults

Ocular measurements in adult had different trends as in children. A significant reduction of AL, ACD, angle measurements and ACW, by the age of 40 years, has been reported using AS-OCT (Amerasinghe et al., 2009b). However, exact timing of this reduction was not investigated. *Shimizu et al* compared anterior chamber measurements in children (mean 7.1 +/- 3.3 years; range, 3-16) to those of adults (mean: 73.7 +/- 7.8 years; range: 50-85) using swept source OCT (Shimizu et al., 2017). They found that adults had a shallower anterior chamber, a shorter ACW (inter-scleral distance), a narrower AOD, a thinner CCT and a thicker lens vault. Similarly, Yan et al reported a non-significant shorter anterior chamber width (nasal and to temporal inter-angle recess distance), of subjects older than 40 years compared to children (> 6 years) among Chinese ethnicity (Yan et al., 2010). Our finding showed a reduction of ACW and more specifically a decrease in nasal Schwalbe's line to temporal Schwalbe's line distance (SL-SL-D) by age of the 14 years and a decrease in nasal scleral spur to temporal scleral spur distance (SS-SS-D) by the age of 18 years. The earlier reduction of SL-SL-D compared to the SS-SS-D decrease contributes to the continuous trabecular meshwork elongation. This further configuration of ACW contribute to the final shape of the anterior chamber and whole eye globe during adulthood. In addition, we did not detect any narrowing of either nasal or temporal angle during adulthood. This is in agreement with a recent study of Chinese children (aged from 6- 18 years) using Pentacam Scheimpflug camera, which found that the anterior chamber angle degree is stable in this age group (Wang et al., 2018). In addition, the association between wider angle and longer TM is well documented among adults (Lee et al., 2016). Our study presented similar novel findings among very young children and described the development of trabecular meshwork and anterior chamber angle width for the first time.

4.4.3 Gender variation of anterior chamber development

Previous work of adults revealed that women had smaller anterior chamber compared to men (Amerasinghe et al., 2009b). They had narrower anterior chamber angle, shallower ACD, shorter ACW (Nongpiur et al., 2010a) and thicker lens. Similar studies of school age children between 6 to 18 years have reported significantly greater ACD, corneal diameter and AL in boys compared to girls (Twelker et al., 2009). In contrast, girls had a thicker lens

compared to boys (Hashemi et al., 2015). Furthermore, AL development was found to be slower in girls than that in boys (Pennie et al., 2001). This findings could explain why women tend to have shallower anterior chamber with increasing age. In concordance with these studies, we detected narrower ACW and anterior chamber angle in females compared to male throughout childhood and adulthood. In addition, previous studies have failed to detect gender variation of TM measurements in adults (Fernandez-Vigo et al., 2015b, Tun et al., 2013b) and children (age 3-18) (Fernandez-Vigo et al., 2017). However, they detected an association of glaucoma with a shorter TM (Tun et al., 2013b, Chen et al., 2015, Stegman et al., 1996). Interestingly, for the first time, we found that the trabecular meshwork became longer in males compared to females. This might explain why closed angle glaucoma is more common among elderly women as the female's shorter TM is easier to get blocked by the iris.

4.4.4 Association of refraction variation and eye biometry

The relation between the shape of eye and spherical refractive error has been well established (Logan et al., 2004). The hypermetropic eye is oblate, the emmetropic eye is nearly spherical while the myopic eye is prolate (figure?). This classification is based on the ratio between the axial length (anteroposterior globe diameter) and transfer diameter of the eye globe. This ratio was found to be <1 , ~ 1 and >1 for hypermetropic, emmetropic and myopic eyes, respectively (Wang et al., 1994), indicating an association of myopia with longer axial length. In contrast, hypermetropic eyes had shorter axial length. Hypermetropia is also associated with shallower anterior chamber depth compared to myopic and emmetropic eyes.(Bhardwaj and Rajeshbhai, 2013).

Given these facts, the negative correlation between the angle measurements and spherical refraction was predictable. The myopic eye has a wider anterior chamber angle while the hypermetropic eye had a shallower angle (Vossmerbaeumer et al., 2013). On the other hand, we identified a myopic shift with aging, which is in good agreement with emmetropisation, a physiological process that matches axial length and optical power of the cornea and lens (Brown et al., 1999), forcing the eye to change from the oblate to the prolate shape (Ishii et al., 2011, Munro et al., 2015). This phenomenon is well known to

happen rapidly during first 12 months of life and is associated with an increase in AL and ACD (Pennie et al., 2001). Emmetropisation results also from thinning and flattening of the lens and cornea reducing the refractive power of both the cornea and the lens (Mutti et al., 2005). The later causes a shift from myopic to hypermetropic refraction and balances the myopic shift of growing AL. Our results of reduced CCT and increased ACW are in agreement with this phenomenon. The ACW development is likely to reduce the corneal power by minimising the corneal curvature.

The eye shape also becomes more prolate by accommodation (Walker and Mutti, 2002) owing to significant elongation of axial length (Read et al., 2010b). Other changes in accommodation include reduced ACD (Du et al., 2012), increased lens thickness (Bolz et al., 2007), constriction of pupil and decreased IOP (Read et al., 2010a). Although we found that accommodation did not affect the repeatability of anterior chamber measurements (chapter 3), we could not completely rule out its influence on our findings. This is an important issue for future research to be undertaken to evaluate the influence of the accommodative state on both anterior chamber, axial length development and emmetropisation

4.4.5 Clinical impact of understanding the normal development of anterior chamber

The scope of this research of understanding the growth of eye, has important clinical applications. The availability of ocular biometry since birth is essential to improve the outcome of the surgical management of paediatric ocular diseases such as congenital cataract and glaucoma.

The success of cataract and refractive surgery depends on in vivo accurate ocular measurements. It is essential to calculate the AL, ACD and corneal curvature in order to calculate the intraocular lens (IOL) power for cataract and refractive correction surgery (Chen et al., 2016). We showed that changes of the anterior chamber width had impact on the refractive shift both during early childhood and adulthood. The American Association for Paediatric Ophthalmology and Strabismus (AAPOS) survey showed increased preference for IOL implantation from 4% in 1997 to 21% in 2001 following cataract

extraction in congenital cataract below 2 years of age (Lambert et al., 2003). However, the little tendency to implant IOL after congenital cataract extraction is due to the limited information about children biometry and normal eye growth. The majority of surgeons preferred to use correcting contact lenses with aphakia. This is suggested to become the more accepted approach (Lim et al., 2017b), because of the high rates of intraoperative and postoperative complication of IOL implantation (Solebo et al., 2015), which requires secondary intraocular surgery (Infant Aphakia Treatment Study et al., 2014). In addition, the unpredictable postoperative myopic shift requires the exchange of IOL power frequently. Therefore, a recent review (2017) has recommended to perform cataract extraction by the age of 6 weeks for unilateral cataract and between 6 and 8 weeks for bilateral cases, respectively (Lim et al., 2017b). It also suggests management of the aphakia with spectacles or contact lenses and to implant IOLs by the age of 4-5 years. Our findings of anterior chamber development supports this recommendation as by the age the 5 years, ocular biometry has reached the mature adult level, making accurate calculation of the IOL possible.

Anterior segment OCT in childhood could assist to improve corrective refractive surgery. Knowledge of the eye maturation and stabilisation of refraction, is likely to help deciding the best time for surgery. Moreover, knowing how the ageing affects the biometry of the eye can help to predict later development of refractive error.

Having knowledge of the normal development of the anterior chamber has a prospective role in enabling the detection and evaluation of anterior chamber pathology. Several studies addressed the mechanism of congenital glaucoma through investigating the abnormal development of the anterior chamber in vitro or using mice models. HH-OCT has the advantages of providing non-invasive visualisation of the anterior chamber structure in children starting at birth. HH-OCT has a potential to aid the diagnosis of infantile glaucoma and other anterior segment dysgenesis. Comparing the anterior chamber measurements of infantile glaucoma with our predicted normative limits can improve our understanding of the progression of disease and the prognosis of its management. Evaluations of the abnormal development of anterior chamber are addressed in the next chapters.

4.4.6 Limitations of study

Tun et al measured TML in adult using SS-OCT and found a significant longer TML in inferior and superior angle compared to nasal and temporal angle (Tun et al., 2013a). The average TML of different quadrants varied from 710 to 890 µm. We found identical value of similar adult age group, however, we only studied the nasal and temporal angle. Nevertheless, we detected significantly shorter nasal TM compared to temporal TM. This could be in line with the nasal-temporal asymmetries which have been previously reported in 3D modelling of the eye using MRI. (Singh et al., 2006, Logan et al., 2004)

The refraction was examined grossly using portable auto-refractometer, it might not reflect the accurate refractive power similar to cycloplegic auto-refraction where the accommodation is controlled. The youngest age we were able to measure refraction was 2.4 months, we could not record the refractive power of younger children. Therefore, comparison with refractive data was limited by missing data of very young children. A further study with focusing on this topic and using cycloplegic retinoscopy would be interesting.

As we were limited by the 2.5 mm (in tissue) scanning depth of HH-OCT, the used protocol restricted the scanning of the whole thickness of the iris. The inability of AS-OCT to visualise structures behind the iris and ciliary structures prevented measuring AL or ACD in our study. However, by adjusting the scanning protocol in the future, there would be a possibility for determining the role of iris in anterior chamber development.

The anterior chamber development is not easy to interpret without taking into account all other ocular measurements. Future studies are recommended to investigate the correlation between angle measurements and AL, ACD, lens thickness, iris curvature and area, foveal measurement and refraction. By conducting such studies, it would be possible to produce a model eye that best explain the development of anterior chamber in relation to the whole eye globe. It might also be possible to use ACW, angle measurements and refraction as well as possible iris measurements to create a model eye that might possibly predict IOL power change with age.

4.4.7 Summary

This section of thesis provides information about the normative postnatal development of anterior chamber and elucidates the trajectories of anterior chamber development from birth to adulthood. Using HH-OCT, we have presented *in vivo* normative data of the anterior chamber width, trabecular meshwork length, anterior chamber angle width and central corneal thickness for children for the first time. Anterior chamber has a rapid phase of development during the first 18 months of age and reaches the maturity by age 5 years. Girls have smaller anterior chamber compared to boys. There is nasal temporal asymmetry in the development of trabecular meshwork length during childhood and early adulthood.

5. Chapter five: Novel In Vivo Morphometric Measurements of Anterior Chamber in Children with Congenital Glaucoma Using Hand Held Spectral Domain Optical Coherence Tomography

The aim of this chapter is to compare the development of anterior chamber measurements of operated congenital glaucoma with age-matched healthy children.

5.1 Introduction

5.1.1 Primary congenital glaucoma (PCG)

Congenital glaucoma usually manifests by enlarged eye globe (buphtalmos), cloudy cornea, photosensitivity, blephерospasm and hyper-lacrimation that either occur at birth or during the first years of life. There are three types of congenital glaucoma according to the age of onset:

1. **Primary new-born type congenital glaucoma.** This is the most severe type. It is clinically apparent between birth and one month of age, caused by *CYP1B1* (Zhao et al., 2015) or *LTBP2* mutations and is inherited in an autosomal recessive manner.
2. **Primary infantile congenital glaucoma.** It is clinically recognized between one month and two years of age (Walton and Katsavounidou, 2005).
3. **Juvenile (late-recognized) primary infantile glaucoma.** This is clinically apparent after two years of age.

On examination, presence of a large corneal diameter (of more than 11 mm), high IOP and optic disc cupping are a typical triad for diagnosis. In advanced stages, it can present with corneal oedema and opacification, iris atrophy, scleral thinning and rupture of Descemet's membrane of cornea (Haab's striae). The progressive optic nerve cupping and atrophy causes impaired vision and can eventually lead to blindness. Congenital glaucoma

diagnosis often requires examination under anaesthesia (EUA). The IOP often drops under the effect of anaesthesia and is mistaken as low or normal. However, presence of progressive optic neuropathy and other aforementioned manifestations of congenital glaucoma is sufficient to initiate treatment (Mandal and Chakrabarti, 2011).

Urgent intervention, mostly surgical, to minimize the dramatic destructive effect of high IOP on optic nerve is recommended as early as possible (Barkan, 1947). The surgical opening of trabecular meshwork (trabeculotomy), used to facilitate aqueous humour drainage outflow, has shown up to 80 % success rate in improving the raised IOP (Neustein and Beck, 2017, Chang and Cavuoto, 2013, Shi et al., 2017). The steps of diagnosis of congenital glaucoma and management are illustrated in flow chart (Figure 5.1). Features of anterior segment dysgenesis and other syndrome associated with glaucoma in children were described in chapter 1 section.

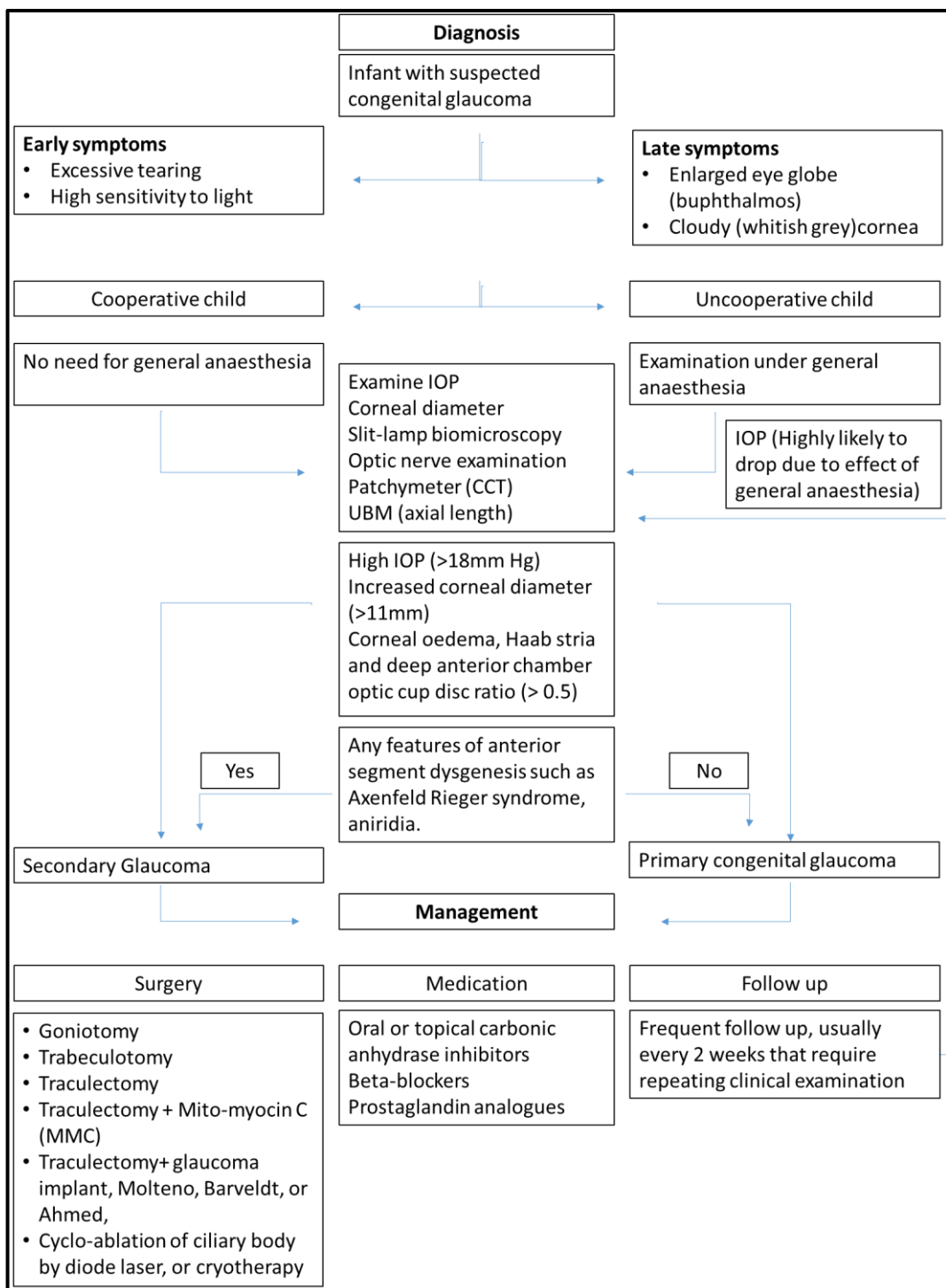


Figure 5-1: Steps of the diagnosis and management of congenital glaucoma.
The B scan of ultrasound biomicroscopy (UBM) is used to measure the axial length.

5.1.2 The pathology of primary congenital glaucoma

The exact etiology of congenital glaucoma is still unknown. Many theories have attributed the impaired drainage of the aqueous humour to developmental abnormalities in the trabecular meshwork (TM) and anterior chamber angle (Tamm, 2009).

Barkan (1955) described presence of shiny membrane covering the anterior chamber angle using gonioscopy (Barkan's membrane) (Barkan, 1955). This hypothesis was initially accepted, owing to the fact that, surgical incision of TM lowered the high IOP. However, this hypothesis has since been invalidated and a new hypothesis is proposed by Anderson (Anderson, 1981) and Maumenee (Maumenee, 1958, Maumenee, 1959, Maumenee, 1963). Both Anderson, and Maumenee could not find evidence of the abnormal membrane either histopathologically or during gonioscopy examination. Instead, a thickened layer of normally perforated uveal meshwork was observed using light and electron microscopy. This layer becomes shiny and looks hyper reflecting after goniotomy. Maumenee also suggested that "failure of TM uveal fibres to lengthen" and "the incomplete differentiation of the angle" are more likely to be the reasons for infantile glaucoma (Maumenee, 1959). A histological study of fragments of anterior chamber angle, removed by surgical trabeculectomy from congenital glaucoma patients, has revealed diminished inter-trabecular spaces, presence of normally functioning Schlemm's canal and the high insertion of the iris (Rojas et al., 2006).

5.1.3 Genetic and molecular mechanism of congenital glaucoma

Genetic studies have so far detected more than 20 genes associated with glaucoma development (Souzeau, 2018). These genes were briefly described in chapter 1 (section 1.1.3.3). Recently, the association between *CYP1B1* mutation and congenital glaucoma has been widely reported and revealed potential mechanisms of primary congenital glaucoma (Firasat et al., 2017, Garcia-Anton et al., 2017, Chouiter and Nadifi, 2017, Reis et al., 2016, Zhao et al., 2015, Micheal et al., 2015, Li et al., 2011). According to the findings of these studies, it is clear that the pathogenesis of congenital glaucoma is multifactorial (Shohdy et al., 2017). Nevertheless, the exact mechanism that causes congenital glaucoma is still unclear (Reis et al., 2016). In normal postnatal development, the exposure of eye to

oxygen rich environment, shortly after birth, enhances the normal process of TM remodelling (reconstruction of cellular and extracellular structure). During this process, endogenous substrates are produced to stimulate the modulation the TM's extracellular matrix (ECM) protein (Zhao et al., 2013). Normally, the *CYP1B1* enzyme regulates the migration of these important endogenous substrates to TM through aqueous humour. Therefore, *CYP1B1* plays an important role in TM remodelling and development. The *CYP1B1* mutation, associated with congenital glaucoma, has been reported to disrupt the regulation of these regulating protein (endogenous substrates), resulting in impairment of TM development (Shohdy et al., 2017). However, the clear pathway and characterisation of regulating protein is not well understood yet and still under investigation. Molecular studies have reported that the expressed protein of mutant *CYP1B1* enzyme is detected in the ciliary body but it is absent in the TM at birth in human and mice (Doshi et al., 2006, Choudhary et al., 2007, Bejjani et al., 2002). *CYP1B1* mutation affects the normal function of the regulating protein. Therefore, the TM remodelling is not stimulated and incomplete (Doshi et al., 2006). This findings supports the hypothesis of failure of TM differentiation after birth (Maumenee, 1959) and clarifies the postnatal mechanisms of glaucoma.

In a recent study, Reis et al connected pathological mutations of *CYP1B1* with decreased levels of periostin; a secreted extracellular matrix protein in trabecular meshwork (Reis et al., 2016). The pathological mutation of *CYP1B1* is also associated with increased levels of oxidative stress (Zhao et al., 2013). These two findings were suggested to play a role in TM remodelling and permeability. The increased levels of reactive oxygen also impairs the TM function and apoptosis through MYOC up-regulation (Reis et al., 2016). However, this is suggested to contribute more in developing adult open angle glaucoma rather than early onset glaucoma in children owing to the association of high level of reactive oxygen with low steroid metabolism (Mookherjee et al., 2012, Banerjee et al., 2016). Furthermore, *CYP1B1* mutation has a critical effect by disturbing the retinol metabolism, which plays an important role in ocular development (Chambers et al., 2007). This is why *CYP1B1* and Tyrosinase deficit mice were found to have severe form of angle dysgenesis that responded well to L- DOPA treatment (Libby et al., 2003). Identification of the TM modulating substrate could revolutionise the management of congenital glaucoma. Zhao et al (2013) has succeeded in restoring the structural abnormality of TM in *CYP1B1* deficit mice through administration of antioxidant and resuming the *CYP1B1* expression (Zhao et

al., 2013). This could focus the attention to a new approach of maintaining the TM remodelling to preserve its normal function (Shohdy et al., 2017). Such approaches may provide an alternative method of glaucoma management and could minimise or, potentially replace the need for surgical intervention.

5.1.4 Anterior chamber morphometry of congenital glaucoma and research gaps

The aforementioned studies show that most of the work in this field is currently devoted to assessing the molecular pathology of congenital glaucoma. Other studies have concentrated on the surgical outcome of congenital glaucoma (Scuderi et al., 2015, Sood et al., 2018, Yassin, 2017). Literature has shown that measurement of in vivo ocular biometry in congenital glaucoma is restricted to either corneal diameter (Cronemberger et al., 2014), central corneal thickness (Henriques et al., 2004, Wygnanski-Jaffe and Barequet, 2006, Paletta Guedes et al., 2016) and/or axial length (Kohlhaas et al., 2006). Although the enlarged corneal diameter is used in the diagnosis of congenital glaucoma, the mechanism accounting to the enlargement of the corneal diameter is not clearly explained.

The morphometric changes of the anterior chamber in congenital glaucoma is poorly investigated compared to adult glaucoma. The poor availability of a practical technique to examine the children ocular biometry and the limited information about the pathogenesis of congenital glaucoma could be the reason. The anterior chamber in congenital glaucoma has been studied by ultrasound biomicroscopy (UBM) (Gupta et al., 2007, Engels et al., 1999, Hussein et al., 2014). Gupta et al have reported abnormal morphology of the anterior chamber in congenital glaucoma. An abnormal thin stretched ciliary body, abnormal tissue at the anterior chamber angle and abnormal insertion of iris have been observed (Gupta et al., 2007). UBM has detected that congenital glaucoma is associated with a wider anterior chamber angle, deeper anterior chamber depth and thicker central corneal thickness compared to controls (Hussein et al., 2014). However, UBM is not widely used in the clinical routine evaluation of congenital glaucoma for many reasons. The UBM is invasive technique that requires examination under anaesthesia. The resolution of UBM images is low and the UBM probe, which needs to be directly placed on the cornea, can affect the accuracy of measurement.

AS-OCT is a non-contact technique that provides better resolution of anterior chamber. Using Spectralis AS-OCT to scan operated patients with primary congenital glaucoma, Gupta et al have recently described a presence of an abnormal hyperreflective membrane covering the trabecular meshwork (Gupta et al., 2017). This supports the hypothesis of Barkan membrane. However, they included already operated patients with mean age of 14.2 ± 3.0 years. Gupta et al attributed the abnormal morphology, at this advanced age, to the developmental abnormalities, irrespective of the scarring effect of repeated surgeries that the children have undergone. This weakens the proposed findings by Gupta. In addition, the presence of an abnormal membrane contradicts the findings by Anderson, Munamee and others, who did not detect evidence of any developmental membrane using electron microscopy.

5.1.5 Research aims and questions

Studying the quantitative measurements of the anterior chamber angle, which is believed to be the affected structure in congenital glaucoma, has the potential to provide better understanding of the mechanism of morphometric changes in congenital glaucoma. In vivo studies of postnatal anterior chamber development in congenital glaucoma have not been performed due to the unavailability of non-invasive techniques that can be used with newborns and infants. In section 3.3.1.2, we presented reproducible anterior chamber angle measurements of operated children with congenital glaucoma younger than 6 years of age using HH-OCT. Studying the anterior chamber angle measurements could highlight to what extent the angle development has been altered either due to the disease itself or as a result of surgical intervention. It might also provide a clue regarding the prognosis of congenital glaucoma management.

The research questions of this part of study are:

1. To what extent are the anterior chamber angle measurements in congenital glaucoma different from healthy children?
2. Is there a difference between the nasal and temporal development of the anterior chamber angle in congenital glaucoma?
3. Is there an association between the IOP and the anterior chamber measurements in congenital glaucoma?

5.2 Methods

5.2.1 Patients and controls

Patients diagnosed with congenital glaucoma were recruited from Birmingham Children Hospital during their routine follow up clinic. Thirty seven patients with congenital glaucoma were recruited, in which 31 were definitively diagnosed with primary congenital glaucoma, 4 children were diagnosed with unilateral glaucoma secondary to Sturge Weber (port wine stain) syndrome, and 2 children had congenital glaucoma associated with congenital cataract extraction. Secondary glaucoma to Sturge Weber syndrome has similar clinical and histopathological features to primary congenital glaucoma (Akhter and Salim, 2014). The two patients of secondary glaucoma associated with cataract extraction, were excluded, because the angle morphometry is affected by the presence of the artificial intraocular lens (pseudophakia) or the absence of lens (aphakia). Further two children, who were scanned under general anaesthesia, were also excluded, because we found that the IOP had dropped to about 11 mmHg and this could affect the real angle morphometry.

We compared 33 children with congenital glaucoma (mean age 4.3 ± 3.6 years; range from 2.4 months to 9.7 years) to 180 age-matched full-term healthy children (mean age 3.8 ± 2.9 years; range from 2 days to 10.3 years). The control group was selected from our database of healthy children. Details of demographic data of patients and controls are described in table 5.1. Clinical information including surgical operations of patients are described in an appendix table 9-1.

Table 5-1: Demography of congenital glaucoma and control groups.

Race	Diagnosis	
	Congenital glaucoma	Controls
	Number (%)	
European	16 (43)	122 (68)
Asian	18(49)	51 (28)
African	2 (5)	7 (4%)
Gender	Number (%)	
	Male	102 (57)
	Female	78 (43)
Total	37 (100)	180 (100)
<hr/>		
Congenital glaucoma participants n= 37		
Primary n=31*		
Secondary to Sturge Weber syndrome n = 4**		
Glucoma associated with congenital cataract with:		
Pseudophakia*** n = 1		
Aphakia*** n = 1		

(*) 2 participants were scanned under general anaesthesia were excluded
(**) only the affected unilateral eye was included
(***) participants with pseudophakia and aphakia were excluded

5.2.2 History and clinical examination

Medical history was extracted from the patient's medical notes. Most patients were receiving medication and had one or repeated operation to relieve the increased IOP (summary about operations was described in appendix). The congenital glaucoma patients had a full orthoptic and ophthalmologic examinations. The visual acuity, refraction, ocular motility, slit-lamp examination, funduscopy, IOP, were examined. Details of the methods and instruments used on examination were described in the general methods chapter (section 2.4.2). IOP measurements were undertaken using ICare rebound tonometry. Measurements of central corneal thickness, corneal diameter and axial length were usually undertaken during operations.

5.2.3 OCT imaging and analysis

All participants' eyes were imaged using HH-OCT without sedation. An ImageJ macro was used to measure the anterior chamber after manual identification of angle landmarks; Schwalbe's line (SL) and scleral spur (SS). Central corneal thickness (CCT), anterior chamber width (ACW) as a distance between nasal and temporal angle landmarks, scleral spur and Schwalbe's line (SS-SS-D and SL-SL-D), nasal and temporal Schwalbe's line angle opening distance (SL-AOD) and trabecular iris surface area (SL-TISA) were measured. We did not include trabecular meshwork length (TML), because the coefficient of variation of TML was >10% in congenital glaucoma (chapter 3 and section 3.3.4).

We included the longitudinal data obtained from 5 children with congenital glaucoma. Summary of the mixed cross sectional and longitudinal anterior chamber scans obtained for this part of study is shown in table 5.2. We obtained 146 mixed cross sectional and longitudinal anterior chamber scans which included 70 from the right eye (48%) and 76 from the left eye (52%); and 78 corneal scans which includes 38 from the right eye (49%) and 40 from the left eye (51%) in glaucoma group. These were compared to 427 (49%) and 473 (51%) anterior chamber images from the right and left eyes, respectively, and 394 (52% right and 48% left) corneal scans, obtained from age, gender and ethnicity matched controls. In cases of unilateral glaucoma, only affected eyes were included. We obtained preoperative images of 3 patients with primary congenital glaucoma, at the initial first examination under general anaesthesia (this was done to confirm the diagnosis). However, these scans were excluded and only the longitudinal data of postoperative images, obtained without anaesthesia, of those 3 patients were included. The preoperative images can be used in a future study to compare between patients preoperatively and postoperatively.

Table 5-2: Demography of HH-OCT images analysed per eye and per angle in congenital glaucoma and control groups.

	Congenital glaucoma	Controls
	Anterior chamber images number (%)	
Right eye	70 (48)	427 (47)
Nasal	35 (24)	218 (24)
Temporal	35 (24)	209 (23)
Left eye	76 (52)	473 (53)
Nasal	38 (26)	247 (27)
Temporal	38 (26)	226 (26)
Total	146 (100)	900 (100)
	Corneal images number (%)	
Right eye	38 (49)	204 (52)
Left eye	40 (51)	190 (48)
Total	78 (100)	349 (100)

5.2.4 Statistical analysis

Multivariable fractional polynomial models were used to predict the relationship between age and measured parameters in both groups. It is based on automatic transformation of age to a power that best fits the changes of each parameter (detailed in chapter 2). Mixed models adjusted for transformed age, gender, eye variations and interaction between transformed age and groups were used to compare between anterior chamber measurements in congenital glaucoma and controls.

The lincom command of Stata was used to calculate the mean and 95% confidence interval of each measurement per year based on the equation of regression model, for congenital glaucoma and controls separately. This command also enabled calculating the mean difference, z score, significant level and 95% confidence intervals of the mean difference between preterm and age-matched full term born children with regard to each measurement, at different ages. The significance level between controls and congenital glaucoma were calculated for different ages including at 3 months, 1, 3, 5 and 10 years.

Partial correlations adjusted for age were used to evaluate the relationship between the CCT, ACW and angle measurements with IOP in congenital glaucoma. Measurements taken from 146 mixed cross sectional and longitudinal anterior chamber images and 78 corneal images were compared to IOP, measured on the same day of image acquisition.

The statistical analysis was done busing STATA IC 15 software (Copyright 1996 - 2018) and GraphPad Prism 7. Example of the commands of Stata and the outputs of results is shown in appendix, section 9.3.

5.3 Results

5.3.1 Morphology of anterior chamber in congenital glaucoma

Example of HH-OCT images of the anterior chamber in congenital glaucoma compared to healthy age-matched control is shown in Figure 5.2. The anterior chamber of congenital glaucoma appeared wider and deeper than the healthy anterior chamber. The iris in congenital glaucoma appeared flat, atrophied with no visible crypts and the iris root appeared displaced anteriorly and highly attached to TM compared to healthy iris. The scleral spur (SS) was distorted and not easily identified, while Schwalbe's line was clear. The trabecular meshwork (TM) structure was also distorted and thickened.

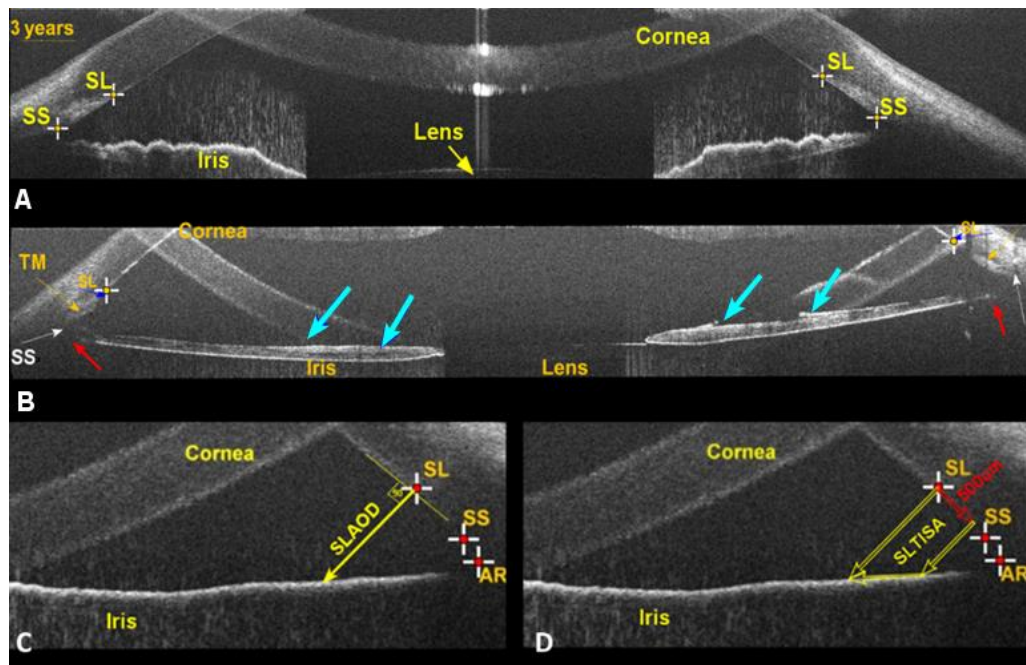


Figure 5-2: HH-OCT images of the anterior chamber of a 3 year old, female with congenital glaucoma compared to age-matched healthy female child.
A) Both nasal and temporal angles of a 3 year old healthy child. B) Both nasal and temporal angles of a 3 year old child with congenital glaucoma. The iris in congenital glaucoma appeared flat, atrophied with no visible crypts (cyan arrows) and displaced anteriorly and highly attached to TM (red arrows), compared to healthy control. The scleral spur (SS) in the congenital glaucoma was distorted and not easily identified (white arrow). TM was thickened (yellow arrow). C) The measurements of anterior chamber angle width Schwalbe's line angle opening distance (SL-AOD). D) The measurements of trabecular iris surface area (SL-TISA).

5.3.2 Measurements of anterior chamber in congenital glaucoma

The mean and 95% prediction intervals of anterior chamber angle measurements in congenital glaucoma and controls for each age group are presented in tables 5-3 and 5-4. The measurements of anterior chamber width and central corneal thickness are presented in table 5-5. The rate of development of anterior chamber per year in congenital glaucoma and controls is shown in tables 5-6 and 5-7.

Table 5-3: The mean and 95% prediction interval of nasal and temporal Schwalbe's line angle opening distance in children with congenital glaucoma and age-matched healthy controls.

		Temporal	Nasal	
		Schwalbe's line angle opening distance (SL-AOD) in μm		
		Controls	Congenital glaucoma	Controls
Age		Mean SL-AOD (lower and upper 95% prediction intervals)		
1-6 mos	485.62 (96.34, 874.90)	679.67 (189.46, 1152.21)	498.03 (125.8, 870.18)	844.27 (494.84, 1192.92)
6-12 mos	617.05 (228.90, 1005.20)	839.10 (366.04, 1285.38)	614.27 (243.8, 985.21)	850.76 (501.90, 1199.30)
1-2 yrs	693.21 (305.26, 1081.16)	943.28 (517.83, 1342.70)	678.59 (307.8, 1049.33)	858.40 (508.02, 1209.09)
2-3 yrs	711.97 (324.01, 1099.93)	1001.66 (608.87, 1399.42)	696.60 (325.8, 1067.34)	872.21 (524.96, 1218.72)
3-4 yrs	722.17 (334.20, 1110.15)	1023.67 (634.09, 1412.83)	706.17 (335.8, 1076.93)	891.87 (542.83, 1240.78)
4-5 yrs	727.00 (339.02, 1114.98)	1028.55 (638.23, 1418.96)	710.13 (339.8, 1080.89)	903.45 (554.80, 1254.47)
5-6 yrs	730.28 (342.29, 1118.26)	1032.28 (641.75, 1423.01)	712.80 (342.8, 1083.56)	917.69 (567.74, 1270.16)
6-8 yrs	732.31 (344.32, 1120.30)	1035.77 (646.54, 1425.00)	715.20 (344.8, 1085.97)	938.46 (589.47, 1286.87)
8-10 yrs	733.95 (345.96, 1121.95)	1038.58 (648.79, 1428.07)	716.86 (346.8, 1087.64)	968.87 (607.74, 1329.26)

Table 5-4: The mean and 95% prediction interval of nasal and temporal Schwalbe's line trabecular iris surface area (SL-TISA) in children with congenital glaucoma and age-matched healthy controls.

		Temporal	Nasal	
		Schwalbe's line trabecular iris surface area (SL-TISA) in mm ²		
		Controls	Congenital glaucoma	Controls
Age		Mean SL-TISA (lower and upper 95% prediction intervals)		
1-6 mos		0.19 (0.04, 0.35)	0.25 (0.06, 0.43)	0.19 (0.04, 0.34)
6-12 mos		0.24 (0.09, 0.40)	0.30 (0.12, 0.47)	0.24 (0.09, 0.39)
1-2 yrs		0.27 (0.12, 0.43)	0.34 (0.18, 0.49)	0.27 (0.02, 0.42)
2-3 yrs		0.28 (0.13, 0.43)	0.36 (0.21, 0.51)	0.28 (0.02, 0.43)
3-4 yrs		0.29 (0.13, 0.44)	0.36 (0.21, 0.51)	0.28 (0.03, 0.43)
4-5 yrs		0.29 (0.13, 0.44)	0.37 (0.22, 0.52)	0.28 (0.03, 0.43)
5-6 yrs		0.29 (0.13, 0.44)	0.37 (0.22, 0.52)	0.28 (0.03, 0.43)
6-8 yrs		0.29 (0.14, 0.44)	0.37 (0.22, 0.52)	0.28 (0.03, 0.44)
8-10 yrs		0.29 (0.14, 0.44)	0.37 (0.22, 0.52)	0.28 (0.03, 0.44)

Table 5-5: The mean and 95% prediction interval of anterior chamber width (ACW) and central corneal thickness (CCT) measurements in children with congenital glaucoma and age-matched healthy controls.

		Anterior chamber width (ACW)		Central corneal thickness	
		SS-SS-D (mm)	SL-SL-D (mm)	CCT (μm)	
		Controls	Congenital glaucoma	Controls	Congenital glaucoma
Age		Mean (lower and upper 95% prediction intervals)			
1-6 mos		10.31 (9.29, 11.32)	12.39 (9.26, 15.38)	11.21 (10.13, 12.30)	11.58 (8.58, 14.45)
6-12 mos		10.99 (9.98, 12.01)	13.34 (10.29, 16.18)	12.07 (10.98, 13.15)	12.47 (9.56, 15.19)
1-2 yrs		11.38 (10.36, 12.39)	13.94 (11.17, 16.69)	12.54 (11.46, 13.62)	13.01 (10.37, 15.63)
2-3 yrs		11.46 (10.45, 12.48)	14.29 (11.71, 16.87)	12.65 (11.57, 13.73)	13.29 (10.82, 15.74)
3-4 yrs		11.51 (10.50, 12.53)	14.27 (11.71, 16.86)	12.71 (11.63, 13.80)	13.19 (10.73, 15.70)
4-5 yrs		11.53 (10.52, 12.55)	14.19 (11.59, 16.78)	12.74 (11.66, 13.83)	13.08 (10.58, 15.59)
5-6 yrs		11.55 (10.53, 12.56)	14.05 (11.43, 16.65)	12.76 (11.68, 13.85)	12.91 (10.38, 15.43)
6-8 yrs		11.56 (10.54, 12.57)	13.84 (11.29, 16.39)	12.78 (11.69, 13.86)	12.67 (10.23, 15.12)
8-10 yrs		11.56 (10.54, 12.57)	13.52 (10.93, 16.15)	12.79 (11.70, 13.87)	12.31 (9.82, 14.85)

SS-SS-D = nasal scleral spur to temporal scleral spur distance, SL-SL-D = nasal Schwalbe's line to temporal Schwalbe's line distance

Table 5-6: The rate of development of anterior chamber width (SS-SS-D and SL-SL-D) and central corneal thickness (CCT) measurements in children with congenital glaucoma and age-matched healthy controls per year.

Controls				Congenital glaucoma		
	Anterior chamber width		Central corneal thickness	Anterior chamber width		Central corneal thickness
Age interval	SS-SS-D mm (%)	SL-SL-D mm (%)	CCT µm (%)	SS-SS-D mm (%)	SL-SL-D mm (%)	CCT µm (%)
0 - 1yr	2.623 (19.3%)	2.290 (16.2%)	-22.24 (-7.2%)	4.29 (45.6%)	4.437 (53.1%)	-77.69 (-11.6%)
1 -2yrs	0.186 (4.0%)	0.109 (3.1%)	-6.07 (-1.1%)	0.219 (1.6%)	0.078 (0.6%)	-21.19 (-3.6%)
2 -3yrs	0.030 (1.1%)	0.001 (1.0%)	-2.83 (-0.3%)	0.011 (0.1%)	-0.031 (-0.2%)	-5.70 (-1.0%)
3 -4yrs	0.004 (0.0%)	-0.010 (-0.1%)	-1.64 (-0.3%)	-0.003 (0.0%)	-0.033 (-0.3%)	-4.18 (-0.7%)
4 -5yrs	-0.001 (0.0%)	-0.010 (-0.1%)	-1.07 (-0.2%)	-0.007 (-0.1%)	-0.030 (-0.2%)	-3.20 (-0.6%)
5 -6yrs	-0.002 (0.0%)	-0.008 (-0.1%)	-0.75 (-0.1%)	-0.008 (-0.1%)	-0.026 (-0.2%)	-2.53 (-0.5%)
6 -7yrs	-0.003 (0.0%)	-0.006 (-0.1%)	-0.56 (-0.1%)	-0.008 (-0.1%)	-0.022 (-0.2%)	-2.04 (-0.4%)
7 -8yrs	-0.002 (0.0%)	-0.005 (0.0%)	-0.43 (-0.1%)	-0.008 (-0.1%)	-0.018 (-0.1%)	-1.69 (-0.3%)
8 -9yrs	-0.002 (0.0%)	-0.004 (0.0%)	-0.34 (-0.1%)	-0.013 (-0.1%)	-0.029 (-0.2%)	-2.63 (-0.5%)
9-10yrs	-0.002 (0.0%)	-0.003 (0.0%)	-0.28 (-0.1%)	-0.010 (-0.1%)	-0.021 (-0.2%)	-1.95 (-0.4%)

SS-SS-D = nasal scleral spur to temporal scleral spur distance, SL-SL-D = nasal Schwalbe's line to temporal Schwalbe's line distance. The highlighted cells indicate when the ACW started to reduce.

Table 5-7: The rate of development of temporal and nasal anterior chamber angle measurements in children with congenital glaucoma and age-matched healthy controls.

Temporal angle				
	Controls		Congenital glaucoma	
Age interval	SL-AOD μm (%)	SL-TISA mm^2 (%)	SL-AOD μm (%)	SL-TISA mm^2 (%)
0 -1yr	341.56 (98.4%)	0.138 (98.8%)	487.97 (155.8%)	0.205 (357.8%)
1 -2yrs	45.95 (12.0%)	0.019 (12.0%)	66.33 (8.3%)	0.027 (10.6%)
2 -3yrs	14.86 (3.1%)	0.006 (2.8%)	13.54 (1.6%)	0.005 (2.0%)
3 -4yrs	7.11 (1.0%)	0.003 (0.9%)	9.17 (1.0%)	0.003 (1.3%)
4 -5yrs	4.55 (0.6%)	0.001 (0.5%)	6.92 (0.8%)	0.002 (1.0%)
5 -6yrs	3.70 (0.5%)	0.001 (0.3%)	5.77 (0.6%)	0.002 (0.8%)
6 -7yrs	3.60 (0.5%)	0.001 (0.3%)	5.25 (0.6%)	0.001 (0.7%)
7 -8yrs	3.89 (0.5%)	0.000 (0.2%)	5.11 (0.5%)	0.001 (0.7%)
8 -9yrs	3.42 (0.6%)	0.000 (0.2%)	10.75 (1.1%)	0.001 (1.4%)
9-10yrs	3.13 (0.7%)	0.000 (0.1%)	12.49 (1.3%)	0.001 (1.6%)

Nasal angle				
	Controls		Congenital glaucoma	
Age interval	SL-AOD μm (%)	SL-TISA mm^2 (%)	SL-AOD μm (%)	SL-TISA mm^2 (%)
0 -1yr	291.01 (66.3%)	0.123 (77.1%)	136.64 (19.0%)	0.052 (19%)
1 -2yrs	38.96 (16.9%)	0.016 (11.3%)	18.29 (2.1%)	0.007 (2.2%)
2 -3yrs	12.26 (2.8%)	0.005 (2.9%)	3.54 (0.4%)	0.001 (0.4%)
3 -4yrs	5.37 (0.8%)	0.002 (0.8%)	2.22 (0.3%)	0.001 (0.3%)
4 -5yrs	2.82 (0.7%)	0.001 (0.6%)	1.48 (0.2%)	0.001 (0.2%)
5 -6yrs	1.66 (0.2%)	0.001 (0.2%)	1.04 (0.1%)	0.000 (0.1%)
6 -7yrs	1.06 (0.1%)	0.000 (0.2%)	0.76 (0.1%)	0.000 (0.1%)
7 -8yrs	0.72 (0.1%)	0.000 (0.1%)	0.57 (0.1%)	0.000 (0.1%)
8 -9yrs	0.51 (0.1%)	0.000 (0.1%)	0.78 (0.1%)	0.000 (0.1%)
9-10yrs	0.37 (0.1%)	0.000 (0.1%)	0.50 (0.1%)	0.000 (0.1%)

SL-AOD = Schwalbe's line angle opening distance, SL-TISA = Schwalbe's line trabecular iris surface area. The highlighted cells show the maximum rate of increase of measurements occurred during the first year of age. The rate of increase of nasal angle width in glaucoma is small during the first years of age compared to temporal angle width increase of controls and glaucoma (highlighted in red).

5.3.3 Development of anterior chamber in congenital glaucoma

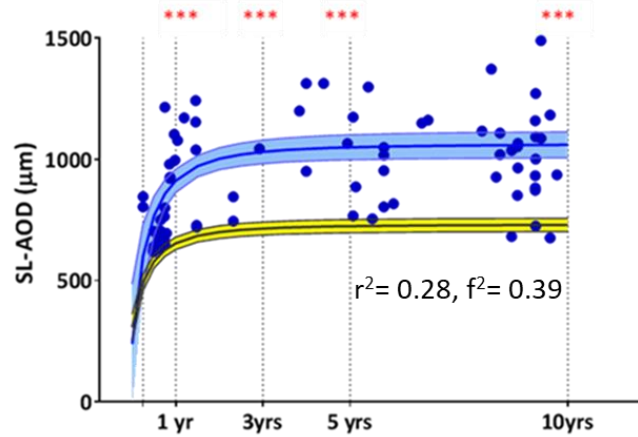
Our findings in congenital glaucoma compared to control for each measurement show that:

5.3.3.1 Anterior chamber angle

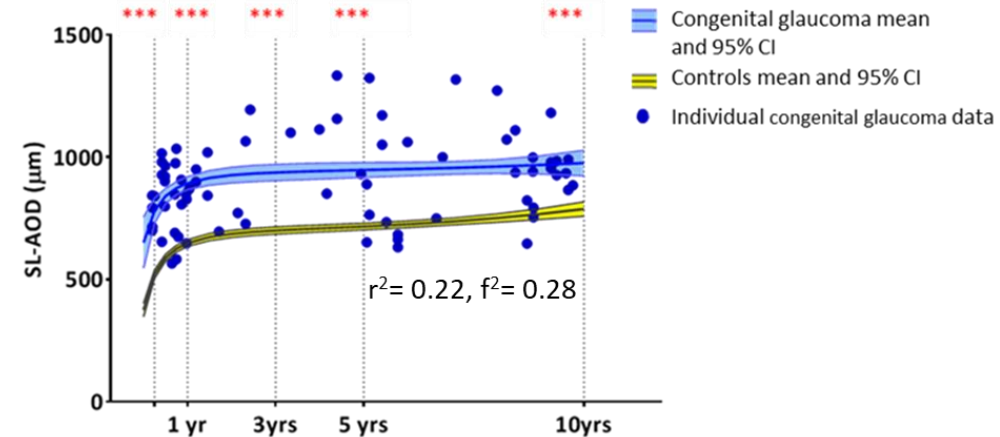
Children with congenital glaucoma had significantly wider nasal SL-AOD and SL-TISA throughout childhood compared to controls (both $p < 0.05$) (Figure 5-3 and Table 5-8). The temporal SL-AOD and SL-TISA became significantly wider in congenital glaucoma compared to controls by the age of 12 months ($p < 0.001$). Nasal angle widening developed earlier than the temporal angle in both groups (Figure 5.3). The nasal angle was significantly wider in congenital glaucoma compared to controls by the age of three months ($p < 0.01$). In contrast, the temporal angle was not significantly different in both groups at age of 3 months ($p > 0.05$). During the first year, the nasal angle was already wide compared to controls and did not show great change, the nasal SL-AOD and SL-TISA both increased by only 19% in congenital glaucoma compared to 66% and 77% increase in age-matched controls, respectively (Table 5.7). The temporal SL-AOD and SL-TISA increased by 156% and 358% in congenital glaucoma and by 98% in controls, respectively.

Temporal

A) Schwalbe's line angle opening distance



Nasal



B) Schwalbe's line trabecular iris surface area

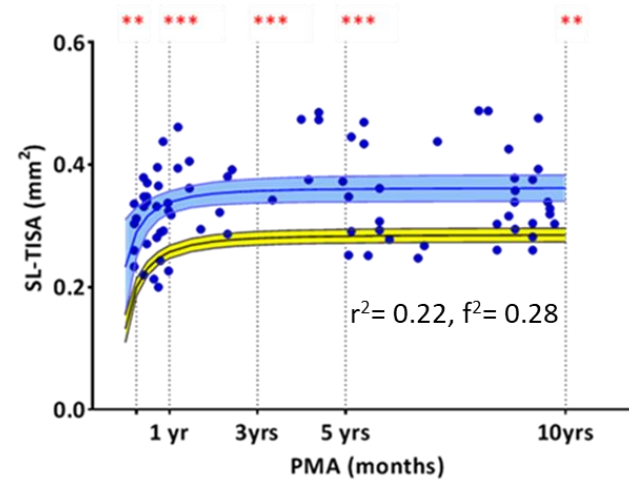
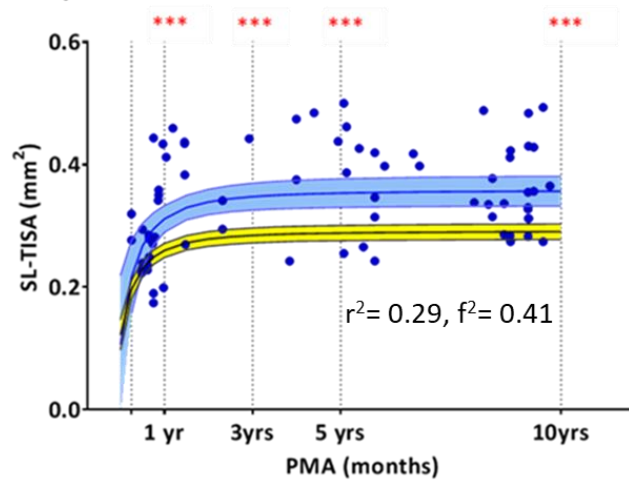


Figure 5-3: Fractional polynomial curve fit comparing the angle measurements of children with congenital glaucoma and age-matched controls from the age of 3 months up to 10 years old.

*Individual measurements from children with congenital glaucoma are indicated with blue dots with mean angle measurement (blue curve fit) and with 95% CI (blue area) shown. Mean angle measurements (black curve fit) and 95 % CI (yellow area) for controls are also shown. The difference in anterior chamber angle measurements between children with congenital glaucoma and age-matched controls at different ages (vertical dashed line) are indicated using asterisks where ** represents $p < 0.01$ and *** represents $p < 0.001$. Temporal SL-AOD r^2*

Table 5-8: The difference of the anterior chamber angle measurements between children with congenital glaucoma and age-matched controls at different ages.

		Temporal angle		Nasal angle				
	SL-AOD (μm)		SL-TISA (mm^2)		SL-AOD (μm)		SL-TISA (mm^2)	
Age	β (95% CI) <i>p</i> value		β (95% CI) <i>p</i> value		β (95% CI) <i>p</i> value		β (95% CI) <i>p</i> value	
3 months	-1.38 (-328.64, 325.89)	0.993	-0.06 (-0.19, 0.08)	0.41	351.17 (156.13, 546.21)	< 0.0001	0.13 (0.04, 0.22)	0.005
1 year	145.04 (88.96, 201.12)	< 0.0001	0.04 (0.02, 0.07)	< 0.0001	196.81 (152.92, 240.70)	< 0.0001	0.06 (0.04, 0.08)	< 0.0001
3 years	169.92 (104.07, 235.78)	< 0.0001	0.06 (0.03, 0.09)	< 0.0001	172.15 (122.81, 221.49)	< 0.0001	0.05 (0.02, 0.07)	0.001
5 years	178.85 (110.17, 247.54)	< 0.0001	0.07 (0.04, 0.10)	< 0.0001	166.79 (114.13, 219.46)	< 0.0001	0.04 (0.02, 0.07)	0.002
10 years	242.54 (160.81, 324.26)	< 0.0001	0.11 (0.07, 0.14)	< 0.0001	163.01 (107.66, 218.34)	0.002	0.04 (0.02, 0.08)	0.001

The table illustrates the coefficient of difference (β), significance level (*p* value) and 95 % confidence interval of the difference between the two groups. SL-AOD = Schwalbe's line angle opening distance, SL-TISA = Schwalbe's line trabecular iris surface area. The significant differences are highlighted in red.

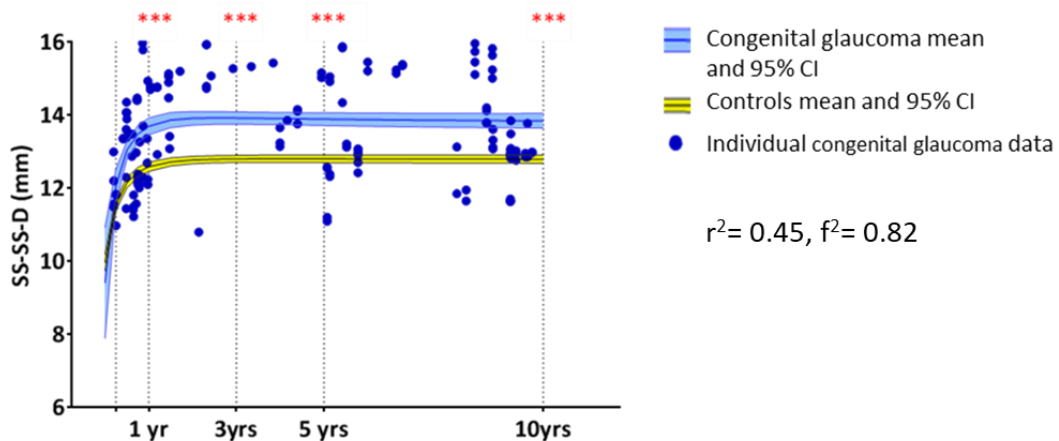
5.3.3.2 Anterior chamber width

The anterior chamber width (ACW) increased significantly in congenital glaucoma compared to controls during the first year of life (Figure 5-4 and table 5-9). The SS-SS-D and SL-SL-D increased by 46% and 53% in congenital glaucoma compared to 19% and 16% in controls, respectively (Table 5-6). The ACW became wider in congenital glaucoma by 1.11mm and 1.26 mm for SS-SS-D and SL-SL-D, respectively at the age of one year (both $p < 0.001$), although they were not significantly different at the age of three months (both $p > 0.05$) (Table 5-9). Interestingly, ACW began to reduce in both congenital glaucoma and controls by the age of 4 years (Table 5-6), but the ACW remained significantly higher in congenital glaucoma compared to controls by about 1 mm at age of 10 years.

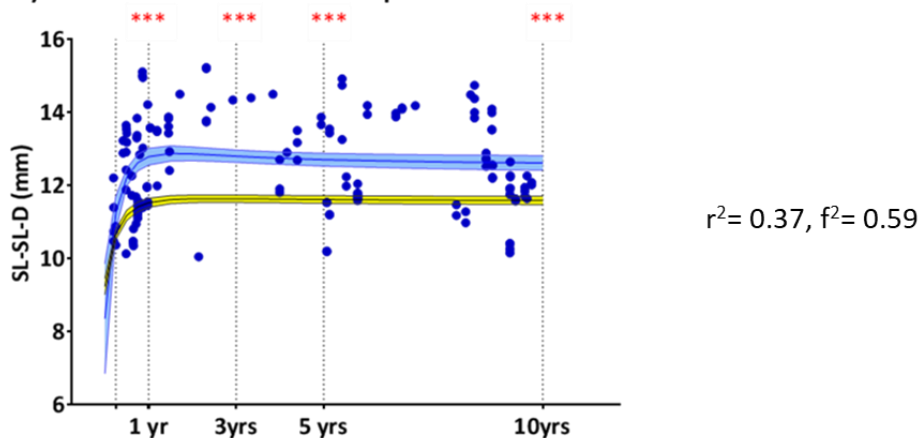
5.3.3.3 Central corneal thickness

Central corneal thickness (CCT) was significantly thicker in congenital glaucoma compared to controls by about 91 μm ($p < 0.001$) at age of three months (Figure 5-4 and Table 5-9). This difference diminished to only 9 μm and became not significant ($p > 0.05$) by the age of 5 years. This difference occurred because the rate of CCT reduction was higher in congenital glaucoma compared to controls during the first 3 years of age (Table 5-6).

A) Nasal scleral spur to temporal scleral spur distance



B) Nasal Schwalbe's line to temporal Schwalbe's line distance



C) Central corneal thickness

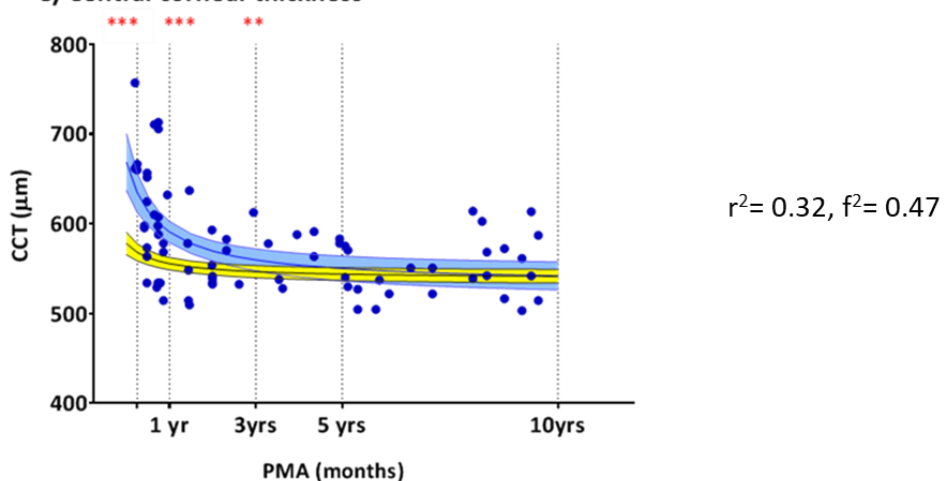


Figure 5-4: Fractional polynomial curve fit comparing the anterior chamber width (SS-SS-D & SI-SL-D) and central corneal thickness (CCT) in children with congenital glaucoma and age-matched controls from 3 months up to 10 years old.

*Individual measurements from children with congenital glaucoma are indicated with blue dots with mean measurement (blue curve fit) and with 95% CI (blue area) shown. Mean measurements (black curve fit) and 95 % CI (yellow area) for controls are also shown. The difference in anterior chamber width and CCT measurements between children with congenital glaucoma and age-matched controls at different ages (vertical dashed line) are indicated using asterisks where * represents $p < 0.05$, ** $p < 0.01$ and *** represents $p < 0.001$.*

SL-SL-D = Nasal Schwalbe's line to temporal Schwalbe's line distance, SS-SS-D = Nasal scleral spur to temporal scleral spur distance.

Table 5-9: The difference of the anterior chamber width and central corneal thickness measurements between children with congenital glaucoma and age-matched controls at different ages.

Age	Anterior chamber width		Central corneal thickness
	SS-SS-D (mm)	SL-SL-D (mm)	CCT (μm)
	β (95% CI) p value	β (95% CI) p value	β (95% CI) p value
3 months	-0.56 (-2.08, 0.97)	-0.88 (-2.40, 0.63)	90.61 (57.24, 123.98)
	0.47	0.25	< 0.0001
1 year	1.11 (0.87, 1.35)	1.26 (1.03, 1.50)	35.16 (23.54, 46.77)
	< 0.0001	< 0.0001	< 0.0001
3 years	1.13 (0.97, 1.30)	1.20 (1.03, 1.36)	15.96 (5.03, 26.90)
	< 0.0001	< 0.0001	0.004
5 years	1.10 (0.94, 1.26)	1.12 (0.97, 1.28)	8.89 (-3.59, 21.37)
	< 0.0001	< 0.0001	0.16
10 years	1.05 (0.86, 1.25)	1.03 (0.84, 1.22)	0.34 (-14.82, 15.50)
	< 0.0001	< 0.0001	0.97

The table illustrates the coefficient of difference (β), significance level (p value) and 95 % confidence interval of the difference between the two groups. SS-SS-D = nasal scleral spur to temporal scleral spur distance, SL-SL-D = nasal Schwalbe's line to temporal Schwalbe's line distance and CCT= central cornea thickness. The significant differences are highlighted.

5.3.4 Correlation between IOP and central corneal thickness in congenital glaucoma

The central corneal thickness in congenital glaucoma was positively correlated with IOP after adjusting for age ($r = 0.397, p = 0.0004$) while CCT was negatively correlated with age ($r = -0.33, p = 0.003$).

There was no correlation detected between ACW and CCT or IOP ($p > 0.05$) and no correlation was detected between IOP and angle measurements (SL-AOD and SL-TISA) (all $p > 0.05$).

5.4 Discussion

This study presented for the first time anterior chamber measurements in congenital glaucoma using OCT. We detected wider nasal and temporal anterior chamber angles and anterior chamber width measurements in congenital glaucoma compared to age-matched controls. This agreed with the findings detected using UBM (Hussein et al., 2014). Interestingly, we detected that nasal angle widening in congenital glaucoma happened prior to temporal angle widening. In addition, we found that the temporal angle and ACW became wider in congenital glaucoma compared to control after the age of 3 months. While the nasal angle was already wider in congenital glaucoma compared to controls before the age of 3 months. We also confirm the findings from previously published work by Cronemberger et al and Paletta Guedes et al, which demonstrated a positive correlation between CCT and IOP in congenital glaucoma (Cronemberger et al., 2014, Paletta Guedes et al., 2016).

5.4.1 Development of anterior chamber angle in congenital glaucoma

To simplify the interpretation of the aforementioned findings, we tried to answer the following question “Why is the anterior chamber angle wider in congenital glaucoma compared to controls?”

Anderson (1981) attributes the raised IOP in congenital glaucoma to the increased outflow resistance rather than complete obstruction of aqueous humour drainage (Anderson, 1981). This resistance results from presence of compressed trabecular sheets and thickened trabecular beams. Relieving this compression by either goniotomy or trabeculotomy, often, produces successful reduction of IOP. In this theory, which is based on histopathological findings of post-mortem children, Anderson suggests that the TM filtration is not completely impaired at birth but deteriorates by the outflow of aqueous humour. Similarly, in histological findings of *CYP1B1* deficit mice, TM appeared relatively normal in the first 2 weeks postnatally and the TM started to be disrupted by the third week of life (Teixeira et al., 2015), where the TM beams, become compressed and flattened and eventually atrophied, which leads to decreased permeability of aqueous humour (Avtar and Srivastava, 2007). Therefore, the impaired function of the TM

combined with increased IOP forces the anterior chamber angle to dilate and entire anterior chamber to stretch against outflow resistance.

We presented in chapter 4 section 4.3.2.2 that the rapid phase of normal postnatal development of TM occurs in the first year of age and is associated with an increase in angle width. It is likely that the increased IOP against outflow resistance together with the normal age effect contribute to the occurrence of greater nasal and temporal angle widening in congenital glaucoma compared to, the only age induced, angle widening in healthy controls. After the age of one year, the age has minimal effect on the width of the anterior chamber angle as shown in our control group. Continuous presence of outflow resistance to the high IOP in congenital glaucoma produces a pathological dilating effect on the angle width even after 1 year of age. This clarifies why the anterior chamber angle in congenital glaucoma is widening more than that in controls after one year of age under the effect of high IOP.

Surprisingly, we found that the nasal angle in congenital glaucoma became wider at an earlier age (before the age of 3 months) compared to the temporal angle, which widens by the age of 12 months. According to our findings in normative development of TM (chapter 4 section 4.3.5.3.2), the nasal TML is shorter than the temporal TML. Hence, it is likely that the higher resistance to aqueous humour outflow occurs at the shorter nasal TM compared to the outflow resistance through the longer temporal TM. This higher resistance against the impaired function of TM would force the nasal angle to dilate earlier than the temporal angle.

The fact that we did not detect significant difference in temporal angle width between children with congenital glaucoma and controls at the age of 3 months could be due to two reasons. Firstly, the early surgical intervention has slowed down the temporal angle widening by reducing the dilating effect of high IOP. Stability or reduction in anterior chamber angle widening could reflect the successful control of IOP. Secondly, it is possible that the TM structure at birth is similar in healthy and affected children. While the progressive impairment of TM function, affects the shorter nasal TM early, the longer temporal TM has a maintained function until the age of about 12 months. The increased

outflow resistance would gradually force the entire meridians of the anterior chamber angle to dilate.

The temporal angle in congenital glaucoma showed progressive widening that continued until the age of 10 years. This could indicate complete impairment of temporal TM function. In contrast, the nasal angle width showed stability. One could speculate whether the position of surgical intervention has a role herein. Goniotomy and trabeculectomy are commonly performed at the nasal angle.

5.4.2 The role of ocular biometry in the management of congenital glaucoma.

Congenital glaucoma requires frequent follow up appointments (Scuderi et al., 2015) because complications are common and could affect stable cases (de Silva et al., 2011). Periodic examination of the IOP, optic disc, CCT and corneal diameter (CD) are routinely performed. CD is positively correlated to the size of the anterior chamber which is enlarged in congenital glaucoma.

High IOP during the first 3 years of age is associated with significant increase in axial length (AL) and horizontal CD (Sampaolesi and Caruso, 1982). The enlarged AL and CD are suggested to result from both initial abnormal growth due to high IOP and age induced normal growth. Enlarged CD was used both to diagnose (Kiskis et al., 1985) and follow up the treatment of congenital glaucoma (Cronemberger et al., 2014). The larger preoperative AL and CD in congenital glaucoma tend to increase postoperatively regardless of IOP control (Kiefer et al., 2001, Cronemberger et al., 2014). Failure of surgical intervention is likely to occur in those patients with initial high preoperative measurements. Therefore, early intervention is important to preserve smaller ocular biometry for better prognosis (Chang and Cavuoto, 2013).

Measurement of anterior chamber width using AS-OCT has provided accurate biometry of the anterior chamber compared to measurement of CD with Orbscan and IOL Master (Kohnen et al., 2006). Using HH-OCT, we found that ACW became significantly wider in congenital glaucoma compared to controls but it became stable and even resumed the

normal decline similar to controls by age of 4 years. Unlike CD, which increases postoperatively (Cronemberger et al., 2014), we did not detect continuous ACW increase in the operated children. The ACW stability could be a sign of controlled IOP and an effective treatment.

5.4.3 Central corneal thickness (CCT) in congenital glaucoma

In this study, the CCT was thicker in congenital glaucoma compared to controls. Corneal oedema could be the reason. This is in agreement with the finding by Paletta Guedes et al, who reported preoperative CCT of 663 µm (mean age 5.5 months) and postoperative CCT of 557 µm (mean age 9.2 months) in congenital glaucoma compared to 551 µm in age-matched healthy controls (Paletta Guedes et al., 2016). These findings were measured using ultrasound pachymetry under general anaesthesia. Oberacher-Velten et al measured the CCT using ultrasound pachymetry in 9 children with congenital glaucoma, aged from 2 weeks to 6 months, before and after operation. Their mean CCT was 651 ± 138 µm before trabeculotomy, which decreased to 592 ± 119 µm after trabeculotomy, and showed further postoperative reduction to 569.4 ± 16 µm after 3 months (Oberacher-Velten et al., 2008). These postoperative figures are consistent with our CCT measurements of similar age group (Appendix Table 5).

In contrast, Henriques et al reported a significantly thinner central cornea in children with operated congenital glaucoma (mean age was 16.6 ± 10.6 months) compared to controls (Henriques et al., 2004). Wygnanski-Jaffe et al compared glaucomatous eyes to the healthy fellow eyes, or to the less affected eye in case of bilateral glaucoma (mean age 4.7 ± 4 years). The operated glaucomatous eyes had thinner CCT. Hence, Wygnanski-Jaffe et al have linked the severity of disease to the thinning of the cornea (Wygnanski-Jaffe and Barequet, 2006). Both aforementioned studies had many limitations. Firstly, all cases with corneal oedema were excluded although the corneal oedema is a possible reason of thickening of the cornea. Secondly, the enrolled children with congenital glaucoma were examined under general anaesthesia, which could have an influence on the CCT measurement. Finally, unlike our study, the normal thinning of CCT with increasing age was not considered.

Our result shows higher rate of thinning of CCT with age in congenital glaucoma compared to controls. This difference in CCT between both congenital glaucoma and controls became non-significant at the age of 5 years. In addition, the positive correlation between the reduced CCT and IOP may indicate effective treatment with stable disease. However, we should be careful in interpreting this because thicker corneas are associated with overestimated IOP (Mansoori and Balakrishna, 2018, Kohlhaas et al., 2006, Feltgen et al., 2001). We suggest that the IOP should be interpreted carefully in congenital glaucoma not only taking CCT measurements into account but also the age of child.

5.4.4 Limitations of study

As the congenital glaucoma patients were recruited from outpatients clinic, they were already operated. Therefore, we could not compare preoperative and postoperative measurements. Most patients involved in this study are currently scanned at their follow up examinations at the children glaucoma clinic. Therefore, a future longitudinal study about consecutive measurements with promising information about the prognosis of treatment is forthcoming.

All data analysis was performed by the same observer (BE) to ensure accurate recording of data and to avoid bias. Analysis was conducted manually and hopefully in the future this could be done through automated means. The manual identifications of angle landmarks were time consuming and automatic analysis probably could be more beneficial.

We included both primary congenital glaucoma and secondary congenital glaucoma associated with Sturge Weber syndrome. They might have different underlying aetiology but they share the pathological influence of increased IOP and were treated with similar procedures.

5.4.5 Possible applications of HH-OCT and future studies of congenital glaucoma

Based on the promising findings of this study, we think that the HH-OCT can be used to monitor the management of congenital glaucoma. Early surgical intervention aims to

control IOP and minimise the enlargement of the globe. Repeated measurements of IOP during routine follow up is not always possible and often imprecise. Ocular measurement obtained by HH-OCT could be more informative indicating whether the IOP has stretched the ocular structures. A steady increase or even a decline in angle measurement in routine follow up may reflect whether the IOP was controlled throughout the period of treatment. A future longitudinal study comparing pre-operative and postoperative anterior chamber measurements could confirm whether angle changes can reflect the control of IOP and stabilisation of disease.

The stability of ACW and anterior chamber angle widening may indicate the effectiveness of glaucoma control. However, further longitudinal investigations with larger sample and precise measurement of IOP are required to evaluate if angle widening and ACW could be used prognostically for congenital glaucoma management.

We did not detect continuous ACW increase in the operated children. However, it is not known whether ACW change is different compared to the CD, which tends to increase postoperatively or ACW is more sensitive than CD. This requires further investigation to evaluate the correlation between ACW, CD and IOP.

Moreover, we anticipate that early widening of nasal angle could be used to aid detection of congenital glaucoma. However, including younger non-operated congenital glaucoma patients would be necessary to test this hypothesis.

In normative development, we found an association between angle measurements and refractive power of the eye. The visual acuity of children with congenital glaucoma is usually severely impaired and can lead to blindness (Haddad et al., 2009). This is due to both the damaged optic nerve as well as the enlarged anterior segment. It would be interesting to conduct a future study to address this topic in order to understand the relation between enlarged anterior chamber measurements, visual impairment and early surgical intervention.

A correction formula of IOP based in CCT (Ehlers et al., 1975) was introduced to adjust the measurement of IOP in relation to CCT. This formula became routinely used (Lleo et al., 2003). However, recent studies have criticised the accuracy of the Ehlers formula (Gunvant

et al., 2010, Jethani et al., 2016). Taking this into consideration, the new technique of using ocular response analyser (ORA) (Kaushik and Pandav, 2012) to measure the corneal compensated IOP (IOPcc) and corneal hysteresis, may provide better IOP monitoring in congenital glaucoma. The ORA device can provide corneal compensated IOP (IOPcc) measurement regardless of the impact of corneal thickness (Dascalescu et al., 2016). In addition, IOP based on Goldmann applanation technology can be recorded simultaneously by this device. Corneal hysteresis is a sensitive indicator of presence and progression of glaucoma even in the presence of normal IOP (Deol et al., 2015). The low corneal hysteresis is associated with progressive loss of visual field. Congenital glaucoma is associated with low corneal hysteresis compared to healthy controls (Gatzioufas et al., 2013). ORA is also based on noncontact tonometer technology. So, it is probably suitable to be used in children without sedation. However, this has not been investigated yet. It would be interesting to design a study of congenital glaucoma using HH-OCT and ORA. The ability to measure IOP corrected to corneal changes and corneal hysteresis by ORA in congenital glaucoma has a potential role in improving management and prognosis. This would produce more accurate IOP measurements which could be used to investigate the correlation between IOP (independent of corneal changes) and anterior chamber measurements with HH-OCT.

5.4.6 Summary

HH-OCT is a promising non-invasive tool to investigate the developmental changes in congenital glaucoma. In this study, we found that the anterior chamber angle and anterior chamber width are wider in congenital glaucoma compared to age-matched healthy children regardless of whether treatment was with medication or surgical intervention.

6. Chapter six: Development of Anterior Chamber of Premature Born Children

The aim of this chapter is to determine whether the premature born children have abnormal anterior chamber development compared to age-matched full term born children

6.1 Introduction

6.1.1 Ocular abnormalities of prematurity

Premature children, born before 37 weeks of pregnancy, are at high risk for developing ocular abnormalities. (This was described in chapter 1 section 1.1.6). Retinopathy of prematurity (ROP), amblyopia and particularly myopia are common problems associated with prematurity (Fledelius, 1996, Bhatti et al., 2016, Varghese et al., 2009). The growth of premature eye and the refractive state have been the focus of many studies. At birth, full term babies usually have hypermetropia (Holmstrom et al., 1998). In contrast, preterm born babies usually have myopia, correlating negatively with increasing gestational age (Varughese et al., 2005). The refraction of premature infants becomes hypermetropic after 52 weeks of postmenstrual age (Cook et al., 2003). It was suggested that ocular biometry plays an important role in the determination of the refractive state and susceptibility to ocular diseases in premature children. The association between prematurity and postmenstrual age, birth weight, axial length, anterior chamber depth, corneal curvature and lens thickness were well documented. Unlike full term children, where long axial length is associated with myopia, premature children have shorter axial length and myopia (Modrzejewska et al., 2010). It was suggested that abnormal anterior chamber morphology and not abnormal axial length development was associated with myopia in prematurity (Zha et al., 2017a). Prematurity is associated with increased corneal curvature and increased lens thickness (Snir et al., 2004, Ecsedy et al., 2014). The increase of refractive power of the cornea and lens rather than the change of axial length is

postulated the mechanism of myopia in premature babies (Baker and Tasman, 2008, Bhatti et al., 2016).

6.1.2 Anterior chamber of premature children

Premature children have shallow anterior chamber depth (Tian et al., 2015). Recent study has connected prematurity to possible risk of angle closure glaucoma and increased intraocular pressure (IOP) later on in adult life (Robinson et al., 2018). There is very little information about the development of anterior chamber angle in premature children. Using gonioscopy, Chang et al recently detected narrow anterior chamber angle in children with ROP (Chang et al., 2017). However, it is not clear whether the angle narrowing resulted from disturbed anterior chamber development due to prematurity or due to the alteration of anterior chamber morphology secondary to ROP.

This chapter focused on the anterior chamber development of premature born children up to age of 6 years, without history of ROP. We compared the development of anterior chamber of premature born children to age-matched full-term born children using HH-OCT.

6.2 Methods

6.2.1 Subjects

The cohort of this study included 17 premature born children (10 males and 7 females). They were compared to 137 age and race matched healthy full-term born controls (74 males and 63 females). All controls were born full term between 37 to 40 weeks gestational age. The premature children were born between 24 and 36 weeks gestational age. The age of premature born children, at the time of examination, was corrected to 40 weeks, the mean postmenstrual age was 28.3 ± 20.4 months (range: 8.8 to 70.7). The mean postmenstrual age of controls, at time of examination, was 35.3 ± 19.3 months (range; 9.0 to 71.4). Demographic data in details is summarized in table 6.1. Criteria of inclusion and exclusion of full-term born children were described in chapter 4.

Premature born children were recruited from Neonatal Unit and Ophthalmology/Orthoptic clinics in Leicester Royal Infirmary during their follow up appointment. This study focused on the preterm born children without retinopathy of prematurity (ROP) or other ocular diseases. All participant's medical history was carefully evaluated to record the exact gestational age and to exclude any neurological or ocular abnormalities. All children were examined for visual acuity, refraction and ocular motility. Fundus and slit lamp examination were carried out if possible (Further details of these tests was discussed in chapter 2, section 2.4.2). All controls had equal vision in both eyes and refraction error ranging from -0.5 to +2 D in any axis. The difference between both eyes was not greater than 1.5D in any axis. All premature born children were hyperopic with refractive error ranging from +0.75 to +3.5 except one female who was myopic with spherical equivalent of -3 in right eye and -2.25 in left eye.

Table 6-1: Clinical information of premature born children.

ID	Refraction (spherical, cylindrical and axis)		Gender	Gestational age in weeks +days	Birth weight kg	Age in months without correction	Age in months corrected to 40 weeks gestational age
	Right eye	Left eye					
1	2, -0.75@180	2,-0.75@180	F	30+3	1.09	3.33	1.10
2	1, -0.5 @90	1.5,-0.5@90	M	30+1	0.95	1.40	-0.90
3	3.5	4.25	M	28+1	0.99	1.90	-0.87
4	3, -1.5@180	3.5,-2.5@180	F	24+5	0.74	3.30	-0.27
5	2	2	M	29	1.12	7.03	4.47
6	2.5	2.75	M	29	1.38	7.03	4.47
7	2.5	2.25	M	29	1.14	7.03	4.47
8	3.5	3.5	F	28+4	0.77	12.70	10.03
9	2.75,-1@170	2, -1@170	M	29+5	1.63	19.50	17.10
10	1.25,-0.5@180	1.75	F	24+1	0.69	31.73	28.03
11	2.5	1.75	M	26+3	0.83	33.57	30.40
12	-2.5, 0.5@90	-3, 0.75, 90	F	27+2	0.62	40.50	37.53
13	0.75, 2.75@90	0.75, 2.75@90	F	27+3	1.07	49.23	46.30
14	2	2	M	27+2	0.66	53.17	50.20
15	Plano	Plano	F	36	2.04	61.97	61.03
16	1.5	2	M	30+1	0.95	1.87	-0.43
17	2	2.5	M	26+3	0.83	27.63	24.47

6.2.2 Image analysis

The anterior chamber of the included children was scanned by HH-OCT without sedation. At least 2 anterior segment scans per eye were included from each participant. One scan showing both nasal and temporal angles together. The second scan showed the central cornea (Figure 6.1). Images were exported to imageJ for analysis as previously described). An individual B scan was selected to calculate the measurements. All measurements were calculated from the B scan that showed the reflection of light through the centre of the pupil (the criteria of choosing the B scan is discussed in chapter 3). The anatomical landmarks, scleral spur and Schwalbe's line were identified manually in the temporal and nasal angle and then used for automatic calculation of anterior chamber parameters. In this study we measured the following anterior chamber parameters (Figure 6-1):

- 1) Anterior chamber width (ACW) including nasal scleral spur and temporal scleral spur (SS-SS-D) and between nasal Schwalbe's lines and temporal Schwalbe's line distance (SL-SL-D).
- 2) Anterior chamber angle measurements of TML, SL-AOD and SL-TISA.
- 3) Central corneal thickness (CCT).

Measurements were included from both left and right eyes if possible. The SS-SS-D, SL-SL-D and CCT were measured in 72 images of premature born children, 45 (63%) and 27 (38%) images from the right and left eyes, respectively. They were compared to 606 cross sectional anterior chamber images which include 319 (53%) and 287 (47%) images from the right and left eyes, respectively in controls. Based on our findings in chapter 3, we only included the angle measurements based on identification of Schwalbe's line. However, TML was included due to its significance. The SL-AOD, SL-TISA and TML were measured in 312 (51%) and 35 (49%) nasal angle images and 295 (49%) and 37 (51%) temporal angle images in controls and premature children, respectively.

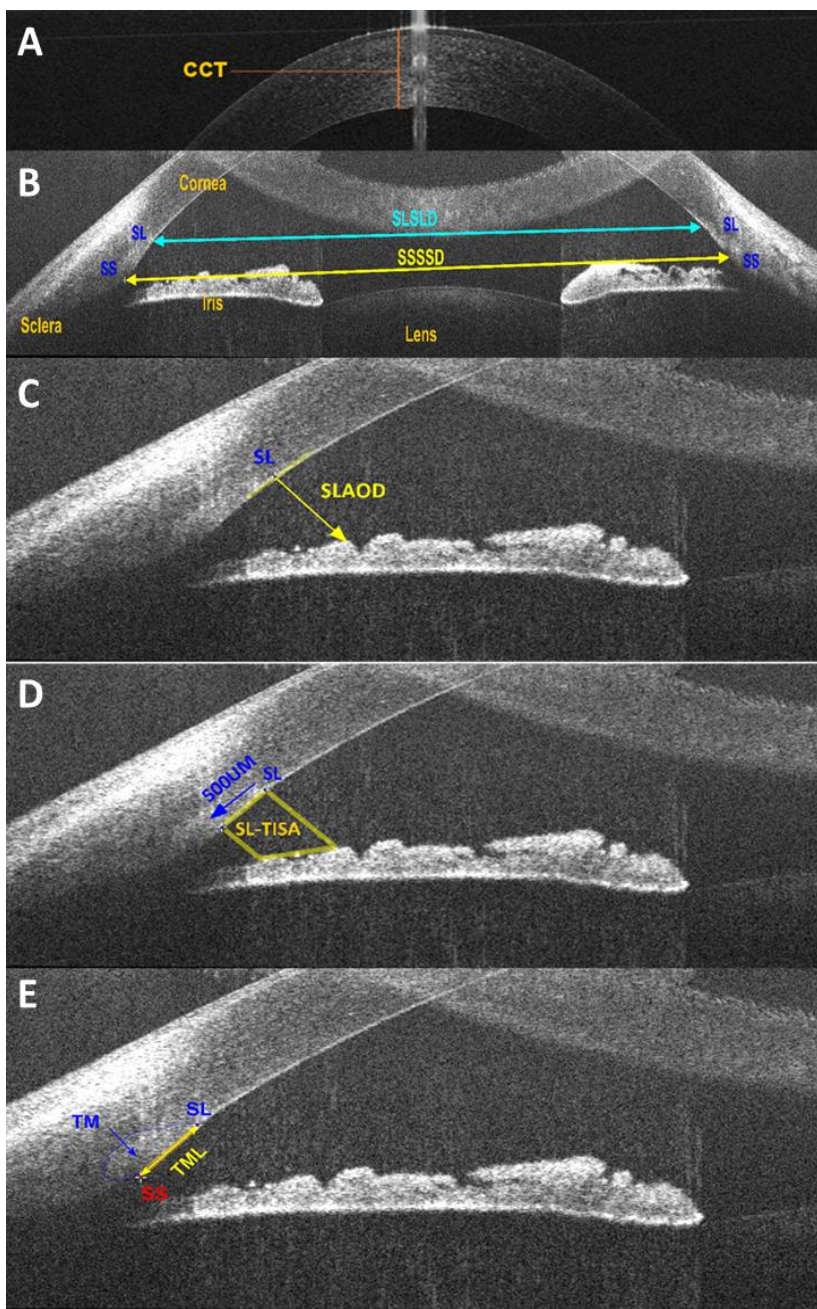


Figure 6-1: HH-OCT images of the anterior chamber of a premature child.

A) An individual B scan at the centre of pupil showing the central corneal thickness (CCT).

B) An individual B scan at centre of pupil showing the nasal and temporal angle, the anatomical landmarks, scleral spur (SS) and Schwalbe's line (SL), were localised manually followed by automatic calculation of the anterior chamber width (ACW), as a linear distance between nasal and temporal scleral spur (SS-SS-D) and a linear distance between nasal and temporal Schwalbe's line (SL-SL-D). Anterior chamber angle measurements were, calculated separately for nasal and temporal angle, including;

C) Schwalbe's line angle opening distance (SLAOD) in microns,

D) Schwalbe's line trabecular iris surface area (SL-TISA) and

E) trabecular meshwork length (TML).

6.2.3 Statistical analysis.

The anterior chamber measurements of premature born children were plotted on the established normative data graphs, (that was described in chapter 4), showing the mean and 95 % predictive intervals.

In order to statistically detect the difference between the premature and full-term children's anterior chamber development. Multivariable fractional polynomial was used first to predict the best fit curve for the changes of measurement of both investigated groups with postmenstrual age. It based on transforming the age to the best fitted power including -2,-1,-0.5, 2, 3 or log age. Mixed models adjusted for the effect of the variation of groups (preterm and full-term born children), transformed age, the interaction between age and groups were used to compare between the preterm and full-term children with regards to measurements of ACW (SS-SS-D and SL-SL-D), CCT, TML, SL-AOD and SL-ATISA.

The lincom command of Stata was used to calculate the mean and 95% confidence interval of each measurement per year, for preterm and full-term children separately. This command also enabled calculating the mean difference, z score, significant level and 95% confidence intervals of the mean difference between preterm and age-matched full-term born children with regard to each measurement, at different ages. These ages were at birth, 1, 3, 5 and 6 years of age.

We compared the time course of the anterior chamber development between the preterm and age-matched full-term born children by calculating the rate of change of the mean of each measurement per year. Angle measurements TML, SL-AOD and SL-TISA for nasal and temporal angle were compared individually between the two investigated groups.

6.3 Results

6.3.1 Development of anterior chamber in premature born children

This study presents the mean value and 95% prediction interval of anterior chamber width, central corneal thickness and anterior chamber angle measurements of TML, SL-AOD and SL-TISA, in premature and full-term born children during the first 6 years of age (Table 6-2 and 6-3). The anterior chamber of premature children showed significant development throughout early childhood, between birth and 6 years of age, similar to the age-matched, full-term born children. This can be seen in the scatter plots (Figures 6-2 and 6-3). However, most of the individual premature children measurements were found to lie below the mean curve fit of normative data. Therefore, when we compared the two groups, we demonstrated that the anterior chamber in premature born children, had significantly shorter anterior chamber width (Figure 6-4 A and B) and narrower temporal anterior chamber angle (Figure 6-5) compared to age-matched full-term children. In contrast, no statistically significant difference was detected between the preterm and full-term children with regards to central corneal thickness (Figure 6-4C) and nasal angle measurements. Details of results are described below.

Table 6-2: The mean and 95% prediction intervals of anterior chamber width and central corneal thickness measurements in premature and full-term born children.

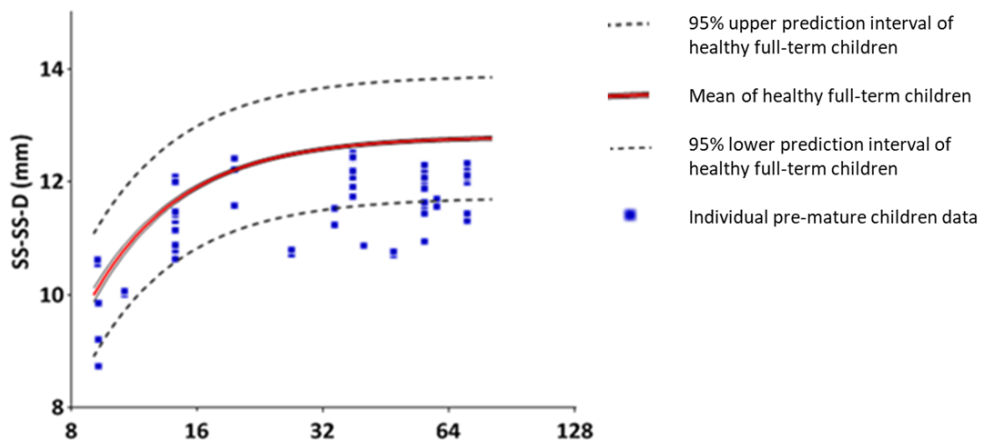
Age	Anterior chamber width				Central corneal thickness	
	SL-SL-D (mm)		SS-SS-D (mm)		CCT (μm)	
	Mean (lower and upper 95% prediction intervals)					
Full-term children	Premature children	Full-term children	Premature children	Full-term children	Premature children	
<1m	9.44 (8.42, 10.46)	9.24 (8.16, 10.32)	10.13 (9.05, 11.22)	9.89 (8.75, 11.03)	593.7 (503.7, 663.3)	596.6 (521.7, 671.4)
1-6 mos	10.31 (9.29, 11.32)	10.09 (8.60, 11.19)	11.21 (10.13, 12.30)	10.96 (9.30, 12.14)	566.5 (482.2, 654.3)	541.4 (453.6, 632.8)
6-12 mos	10.99 (9.98, 12.01)	10.49 (9.47, 11.51)	12.07 (10.98, 13.15)	11.47 (10.39, 12.55)	553.2 (474.2, 634.5)	530.0 (455.5, 604.6)
1-2 yrs	11.38 (10.36, 12.39)	10.66 (9.64, 11.68)	12.54 (11.46, 13.62)	11.68 (10.60, 12.76)	546.4 (469.5, 623.7)	540.1 (467.2, 613.1)
2-3 yrs	11.46 (10.45, 12.48)	10.75 (9.71, 11.79)	12.65 (11.57, 13.73)	11.80 (10.69, 12.89)	545.1 (467.9, 622.5)	551.5 (475.6, 626.0)
3-4 yrs	11.51 (10.50, 12.53)	10.80 (9.76, 11.83)	12.71 (11.63, 13.80)	11.86 (10.76, 12.95)	544.1 (467.3, 621.0)	560.4 (484.4, 634.9)
4-5 yrs	11.53 (10.52, 12.55)	10.81 (9.79, 11.83)	12.74 (11.66, 13.83)	11.87 (10.79, 12.95)	543.7 (466.9, 620.4)	564.4 (453.6, 691.4)
5-6 yrs	11.55 (10.53, 12.56)	10.82 (9.80, 11.85)	12.76 (11.68, 13.85)	11.89 (10.81, 12.97)	543.4 (466.7, 620.0)	565.5 (491.3, 639.6)

SS-SS-D = nasal scleral spur to temporal scleral spur distance and SL-SL-D = nasal Schwalbe's line to temporal Schwalbe's line distance.

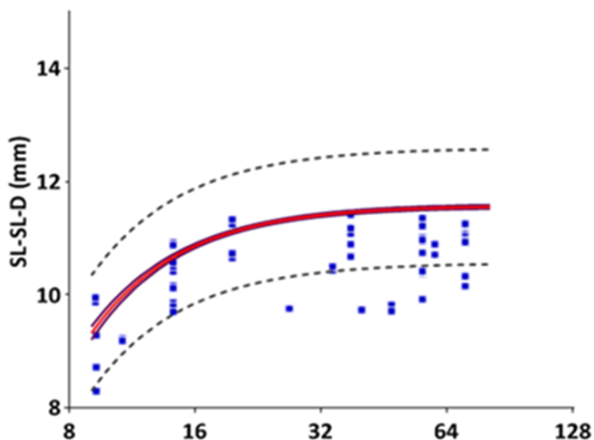
Table 6-3: The mean and 95% prediction interval of temporal and nasal anterior chamber angle measurements per age in premature and full-term born children.

		Temporal		Nasal
		Trabecular meshwork length (TML) mean (95% PI) in µm		
Age	Full-term children	Premature children	Full-term children	Premature children
<1m	547.23 (295.77, 798.69)	426.69 (268.67, 583.86)	543.61 (275.64, 811.59)	484.58 (332.44, 635.83)
1-6 mos	623.40 (373.95, 872.86)	574.16 (344.64, 731.30)	590.99 (323.89, 858.09)	594.19 (389.84, 748.23)
6-12 mos	683.14 (434.28, 932.00)	639.90 (493.02, 786.78)	647.12 (380.73, 913.52)	646.17 (501.79, 790.56)
1-2 yrs	722.43 (473.61, 971.26)	668.52 (521.28, 815.77)	693.44 (427.33, 959.54)	667.88 (523.10, 812.67)
2-3 yrs	735.63 (486.82, 984.44)	684.54 (533.31, 834.07)	713.17 (447.10, 979.24)	679.48 (532.17, 825.18)
3-4 yrs	745.09 (496.31, 993.87)	693.13 (542.72, 841.46)	726.76 (460.69, 992.83)	686.55 (539.27, 832.26)
4-5 yrs	751.66 (502.92, 1000.40)	694.52 (546.60, 842.44)	733.84 (467.77, 999.92)	687.61 (542.19, 833.02)
5-6 yrs	758.17 (509.47, 1006.88)	696.39 (548.40, 844.37)	739.63 (473.54, 1005.72)	689.02 (543.56, 834.49)
Schwalbe's line angle opening distance (SL-AOD) mean (95% PI) in µm				
Age	Full-term children	Premature children	Full-term children	Premature children
<1m	311.05 (-81.18, 703.28)	285.86 (-0.99, 571.67)	369.34 (-5.8, 743.93)	275.59 (77.75, 472.00)
1-6 mos	485.62 (96.34, 874.90)	444.62 (84.94, 723.54)	498.03 (125.8, 870.18)	459.38 (172.48, 662.88)
6-12 mos	617.05 (228.90, 1005.20)	515.38 (247.83, 782.93)	614.27 (243.8, 985.21)	546.53 (359.19, 733.88)
1-2 yrs	693.21 (305.26, 1081.16)	546.19 (277.98, 814.40)	678.59 (307.8, 1049.33)	582.94 (395.07, 770.80)
2-3 yrs	711.97 (324.01, 1099.93)	563.44 (290.73, 834.43)	696.60 (325.8, 1067.34)	602.37 (410.38, 791.65)
3-4 yrs	722.17 (334.20, 1110.15)	572.68 (300.66, 842.54)	706.17 (335.8, 1076.93)	614.23 (422.38, 803.43)
4-5 yrs	727.00 (339.02, 1114.98)	574.18 (304.74, 843.62)	710.13 (339.8, 1080.89)	616.00 (427.32, 804.68)
5-6 yrs	730.28 (342.29, 1118.26)	576.19 (306.64, 845.74)	712.80 (342.8, 1083.56)	618.38 (429.62, 807.13)
Schwalbe's line trabecular iris surface area (SL-TISA) mean (95% PI) in mm ²				
Age	Full-term children	Premature children	Full-term children	Premature children
<1m	0.12 (-0.03, 0.28)	0.10 (0.01, 0.19)	0.14 (-0.02, 0.29)	0.11 (0.03, 0.19)
1-6 mos	0.19 (0.04, 0.35)	0.17 (0.05, 0.26)	0.19 (0.04, 0.34)	0.19 (0.07, 0.27)
6-12 mos	0.24 (0.09, 0.40)	0.20 (0.12, 0.28)	0.24 (0.09, 0.39)	0.22 (0.14, 0.30)
1-2 yrs	0.27 (0.12, 0.43)	0.21 (0.13, 0.30)	0.27 (0.02, 0.42)	0.24 (0.16, 0.32)
2-3 yrs	0.28 (0.13, 0.43)	0.22 (0.13, 0.31)	0.28 (0.02, 0.43)	0.25 (0.16, 0.32)
3-4 yrs	0.29 (0.13, 0.44)	0.22 (0.14, 0.31)	0.28 (0.03, 0.43)	0.25 (0.17, 0.33)
4-5 yrs	0.29 (0.13, 0.44)	0.23 (0.14, 0.31)	0.28 (0.03, 0.43)	0.25 (0.17, 0.33)
5-6 yrs	0.29 (0.13, 0.44)	0.23 (0.14, 0.31)	0.28 (0.03, 0.43)	0.25 (0.17, 0.33)

A) Nasal scleral spur to temporal scleral spur distance



B) Nasal Schwalbe's line to temporal Schwalbe's line distance



C) Central corneal thickness

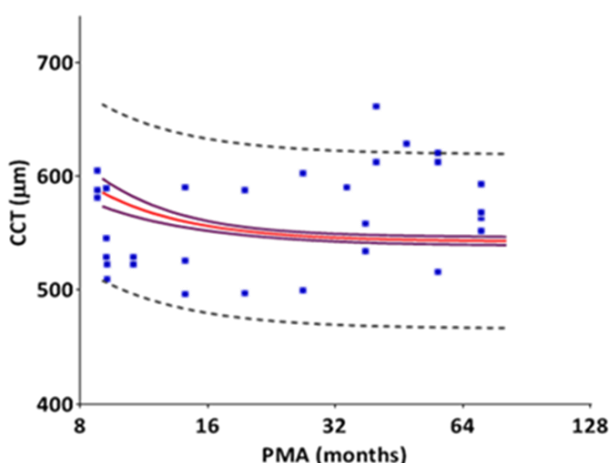


Figure 6-2: Individual anterior chamber width and central corneal thickness measurements of premature children with regards to mean and 95% prediction intervals of the development of anterior chamber of healthy full-term born children.

(A) nasal scleral spur to temporal scleral spur distance (SS-SS-D) and (B) nasal Schwalbe's line to temporal Schwalbe's line distance (SL-SL-D), in mm. (C) central cornea thickness (CCT) in μm , with log postmenstrual age in months. The age ranges from birth to 6 years. Mean value (red line), 95% confidence intervals of mean (blue lines), 95% prediction intervals (PI) (dashed lines) and individual measurements (blue dots) are shown. The individual premature born children measurements (blue dots) of the ACW (both SS-SS-D and SL-SL-D) lie below the mean normative curve fit and below the lower 95% PI. While the premature CCT are distributed within the 95% PI.

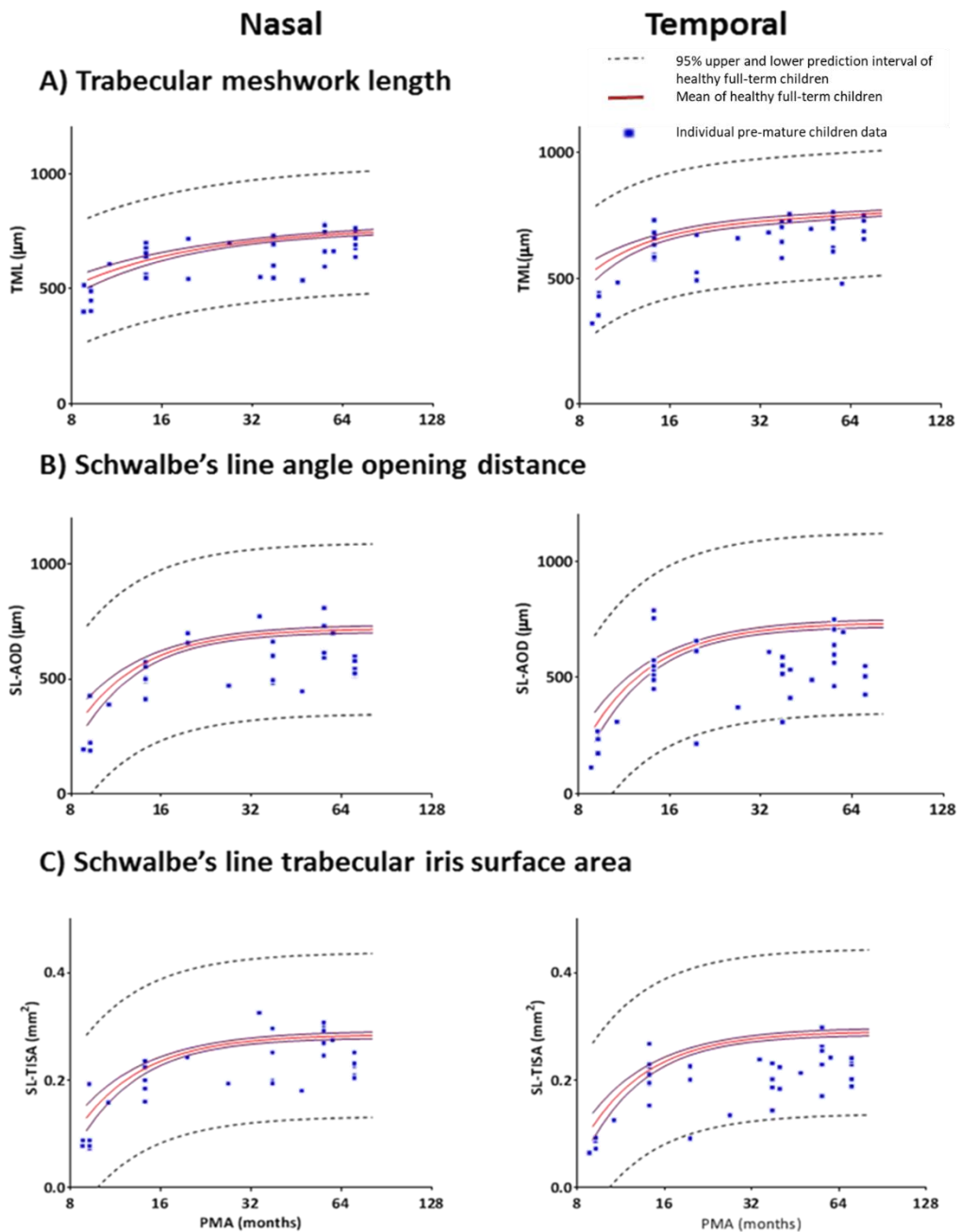
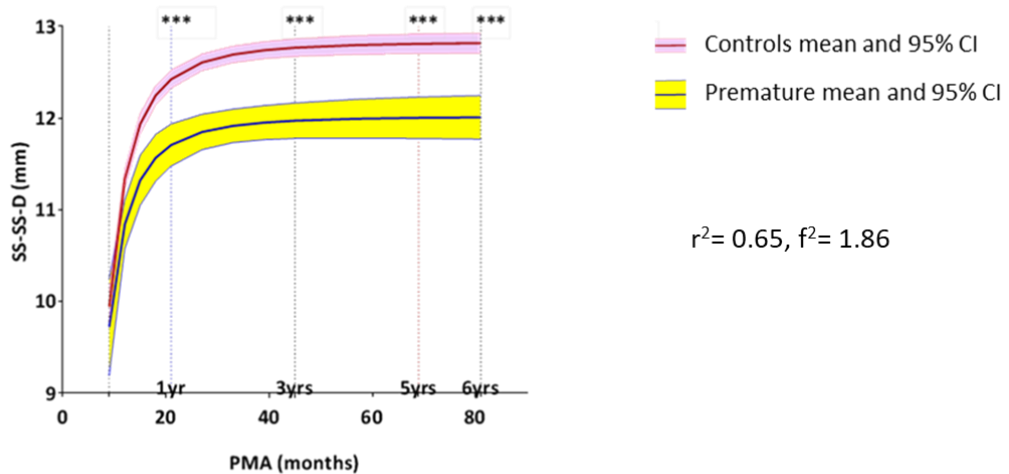


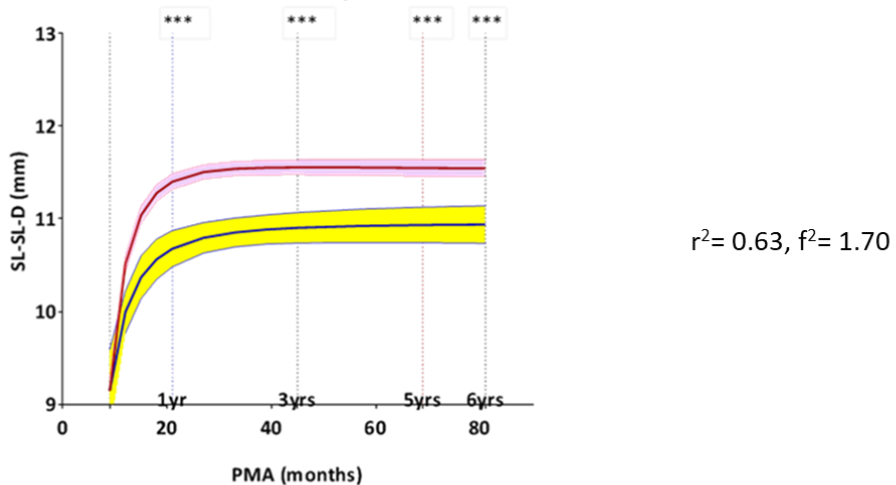
Figure 6-3: Individual anterior chamber angle measurements of premature children with regards to mean and 95% prediction intervals of the development of nasal and temporal anterior chamber angle of healthy full-term born children.

(A) trabecular meshwork length (TML) in μm (B) Schwalbe's line angle opening distance (SL-AOD) in μm . (C) Schwalbe's line trabecular iris surface area (SL-TISA) in mm^2 , with log postmenstrual age in months. Mean value (red line), 95% confidence intervals of mean (blue lines), 95% prediction intervals (dashed lines). The individual premature born children measurements (blue dots) are shown. The temporal premature measurements lie below the mean normative curve fit and within the lower 95% PI. While the premature nasal angle measurements distributed around the mean curve.

A) Nasal scleral spur to temporal scleral spur distance



B) Nasal Schwalbe's line to temporal Schwalbe's line distance



C) Central corneal thickness

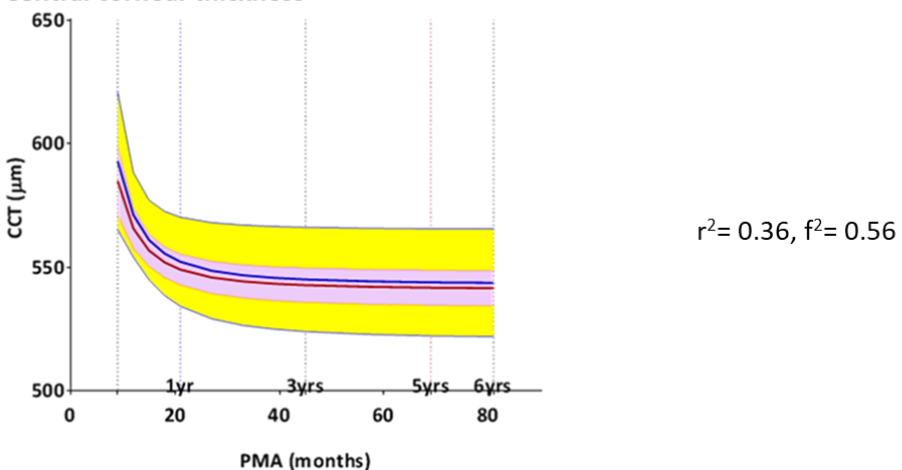


Figure 6-4: Polynomial curve fit comparing the development of anterior chamber width and central cornea thickness of premature and full-term born children.

(A) Nasal scleral spur to temporal scleral spur distance (SS-SS-D). (B) Nasal Schwalbe's line to temporal Schwalbe's line distance (SL-SL-D), in mm. (C) central cornea thickness (CCT) The

postmenstrual age is shown in log months. Premature children mean value (Blue line) and 95% confidence intervals (yellow area) of premature children are shown. The mean value (purple line) and 95% confidence intervals (pink area) of full-term children are shown. The significance of difference between premature and full-term children was tested at different ages (dashed vertical line). () indicates $p < 0.05$, (**) indicates $p < 0.01$, (***) indicates $p < 0.001$. (Details of coefficient of difference, 95% confidence intervals and p values is shown in table 6.2).*

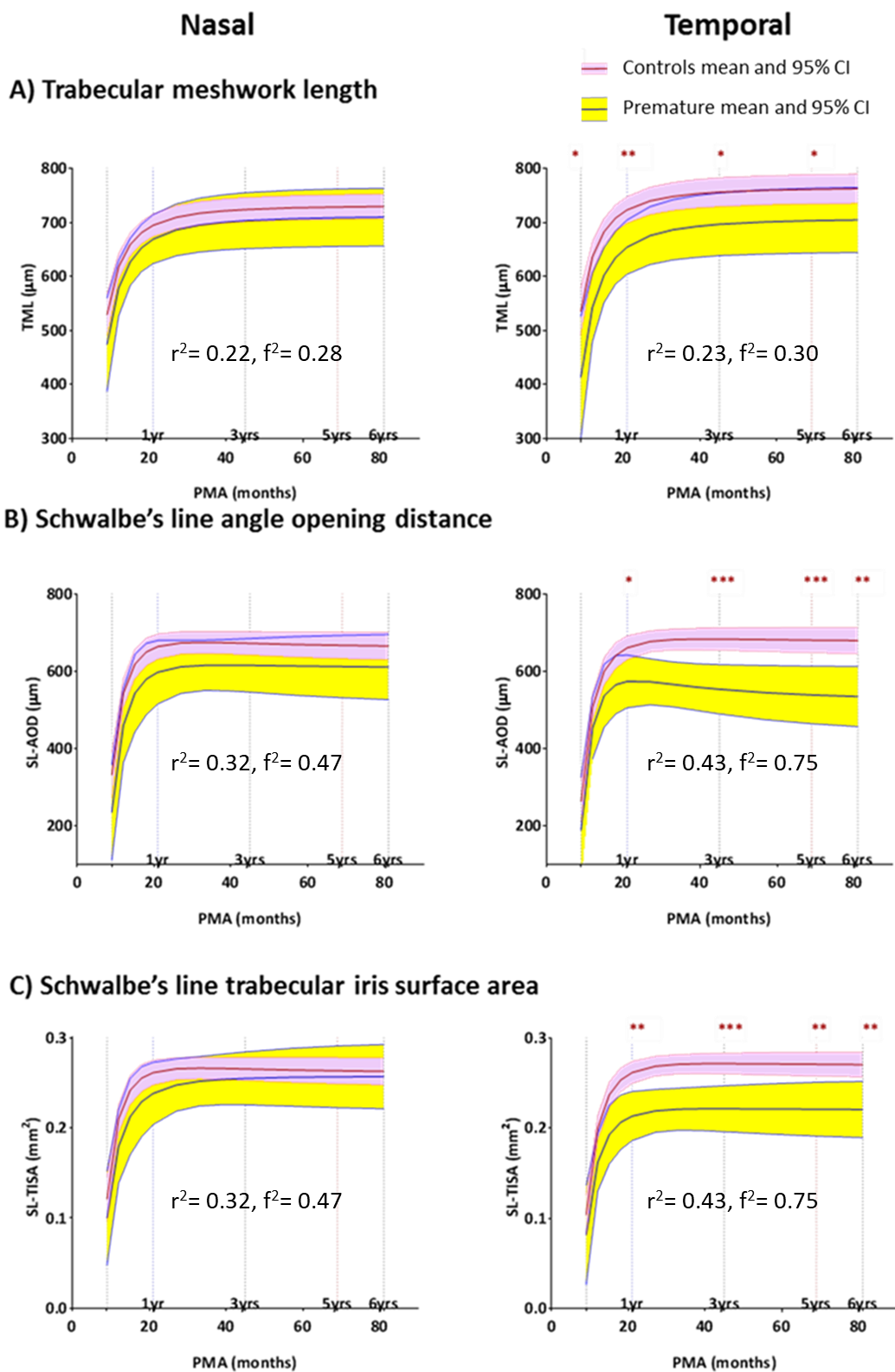


Figure 6.5: Polynomial curve fit comparing the development of nasal and temporal angles of premature and full-term born children.

(A) Trabecular meshwork length (TML) in μm (B) Schwalbe's line angle opening distance (SL-AOD) in μm . (C) Schwalbe's line trabecular iris surface area (SL-TISA) in mm^2 , with log postmenstrual age in months. Premature children mean value (blue line) and 95% confidence intervals (yellow area) of premature children are shown. The mean value (purple line) and 95% confidence intervals (pink area) of full-term children are shown. The significance of difference between premature and full-term children was tested at different ages (dashed vertical line). (*) indicates $p < 0.05$, (**) indicates $p < 0.01$, (***) indicates $p < 0.001$. (more details of difference coefficient, 95% confidence intervals and p values is shown in table 6-6)

6.3.1.1 Anterior chamber width (ACW)

The anterior chamber horizontal width in premature children (SS-SS-D and SL-SL-D) became significantly shorter in early childhood, throughout the 6 years period (Figure 6.4), compared to age-matched full-term children ($p < 0.0001$), although no difference was found at birth ($p > 0.05$). The details of the coefficients and significance of difference are presented in table 6.4. The difference between the ACW of premature and full-term children is caused by the different rate of growth in full-term compared to premature children. Details of the rate of development of SS-SS-D and SL-SL-D per year is shown in table 6.5.

6.3.1.2 Central cornea thickness (CCT)

There was no significant difference in the CCT between premature children and full-term children ($p > 0.05$) (Table 6.4). The CCT in both groups decreased significantly with age ($p < 0.0001$). During the first year, CCT decreased by 7.20% (from 585 to 549 μm) and 6.88% (from 593 to 552 μm) in controls and premature children, respectively (Table 6.5).

Table 6-4 : Difference between premature and full-term born children in anterior chamber width and central corneal thickness at different ages.

Age	Anterior chamber width				Central corneal thickness				
	SL-SL-D		SS-SS-D		CCT				
	β	95% Confidence interval	p value	β	95% Confidence interval	p value	β	95% Confidence interval	p value
Birth	0.001	-0.46, 0.46	0.995	-0.22	-0.76, 0.32	0.422	8.1	-22.75, 38.96	0.61
1 year	-0.72	-0.92, -0.53	0.0001	-0.72	-0.95, -0.49	0.0001	3.18	-14.67, 21.03	0.73
3 years	-0.67	-0.81, -0.52	0.0001	-0.79	-0.96, -0.62	0.0001	2.39	-18.25, 23.04	0.82
5 years	-0.62	-0.80, -0.43	0.0001	-0.81	-1.02, -0.59	0.0001	2.17	-19.42, 23.77	0.84
6 years	-0.58	-0.80, -0.35	0.0001	-0.81	-1.08, -0.55	0.0001	2.08	-19.92, 24.09	0.85

Nasal Schwalbe's line to temporal Schwalbe's line distance (SL-SL-D), nasal scleral spur to temporal scleral spur distance (SS-SS-D)in mm and central cornea thickness (CCT) in μm are shown. Coefficient of difference (β), 95 % confidence intervals of difference and significance level are shown. The highlighted cells in red indicate significantly smaller anterior chamber width in premature born children compared to full-term born children.

Table 6-5: The rate of change of anterior chamber width and central corneal thickness measurements in premature and full-term born children.

Age interval	Anterior chamber width				Central corneal thickness	
	SS-SS-D difference mm (%)		SL-SL-D difference mm (%)		CCT difference μm (%)	
	Term children	Premature children	Term children	Premature children	Term children	Premature children
Birth to 1 year	2.623 (19.3%)	1.99 (20.44)	2.290 (16.2%)	1.53 (16.77)	-22.24 (-7.2%)	-40.79 (-6.88)
1 to 2 years	0.186 (4.0%)	0.21 (1.79)	0.109 (3.1%)	0.18 (1.64)	-6.07 (-1.1%)	-5.46 (-0.99)
2 to 3 years	0.030 (1.1%)	0.06 (0.47)	0.001 (1.0%)	0.05 (0.46)	-2.83 (-0.3%)	-1.72 (-0.31)
3 to 4 years	0.004 (0.0%)	0.02 (0.18)	-0.010 (-0.1%)	0.02 (0.19)	-1.64 (-0.3%)	-0.75 (-0.14)
4 to 5 years	-0.001 (0.0%)	0.01 (0.08)	-0.010 (-0.1%)	0.01 (0.09)	-1.07 (-0.2%)	-0.40 (-0.07)
5 to 6 years	-0.002 (0.0%)	0.01 (0.04)	-0.008 (-0.1%)	0.01 (0.05)	-0.75 (-0.1%)	-0.23 (-0.04)

Nasal Schwalbe's line to temporal Schwalbe's line distance (SL-SL-D), nasal scleral spur to temporal scleral spur distance (SS-SS-D) and central cornea thickness (CCT) are shown.

6.3.1.3 Nasal and temporal angle measurements

Similar to the full-term born children, the anterior chamber angle, in premature born children, rapidly increased during the first year of age, followed by a slow growth phase (Figure 6.5). *P* values of both SL-AOD and SL-TISA were < 0.001 . Interestingly, premature children had a significantly narrower temporal angle compared to age-matched full-term born children throughout the period of 6 years of age ($p < 0.05$), although no significant difference was detected at birth ($p > 0.05$). Details of differences between premature and full-term born children at different ages are shown in table 6.6. During the first year, both the temporal SL-AOD and SL-TISA in full-term children increased by 98% compared to 205% increase in SL-AOD and 162% increase in SL-TISA in premature children. The details of the rate of development are presented in table 6.7.

In contrast, there was no significant difference of the nasal angle width between the two investigated groups (the *p* values of difference at different ages were > 0.05). The nasal SL-AOD and SL-TISA increased by 66% and 77% in full-term children, respectively, compared to 155% increase in SL-AOD and 138 % increase in SL-TISA in premature children.

Similarly, the temporal trabecular meshwork length (TML) of premature children was significantly shorter than that of full-term children ($p < 0.05$). However, unlike the angle width, temporal TML was significantly different between the two groups at birth and up to the age of 5 years. At age of 6, the difference in temporal TML reduced and became insignificant (the *p* value was 0.055). In contrast, the difference between premature and full-term nasal TML was not statistically significant at any age ($p = 0.29$). During the first year of age, the temporal and nasal TML of premature children increased by 58% and 41% respectively. While, there was 25% temporal and 19% nasal increase in TML, respectively in full-term children. The growth slowed down with increased age in both groups.

Interestingly, it was noted that the difference in temporal angle width (β coefficients) between the preterm and full-term children increased with age. While, the difference in nasal angle width and both nasal and temporal TML (β coefficients) was reduced with increased age regardless whether this difference was significant or not. This shows an asymmetry in the development of nasal and temporal anterior chamber angle in premature children.

Table 6-6: Difference between premature and full-term born children at different ages in temporal and nasal anterior chamber angle measurements.

Temporal				Nasal			
Trabecular meshwork length (TML)							
Age	β	95% Confidence interval	p value	β	95% Confidence interval	p value	
birth	-122.09	-240.80, -3.37	0.044	-55.27	-146.75, 36.21	0.24	
1 year	-68.88	-115.10, -22.66	0.004	-25.83	-67.94, 16.28	0.23	
3 years	-60.38	-114.14, -6.62	0.028	-21.13	-69.67, 27.41	0.39	
5 years	-58.01	-114.85, -1.18	0.045	-19.82	-70.79, 31.15	0.45	
6 years	-57.02	-115.24, 1.21	0.055	-19.27	-71.33, 32.79	0.47	
Schwalbe's line angle opening distance (SL-AOD)							
Age	β	95% Confidence interval	p value	β	95% Confidence interval	p value	
Birth	-74.76	-220.14, 70.62	0.314	-97.19	-229.48, 35.09	0.15	
1 year	-87.07	-155.56, -18.58	0.013	-66.43	-149.21, 16.34	0.12	
3 years	-124.23	-180.79, -67.67	<0.0001	-57.97	-121.25, 5.30	0.07	
5 years	-142.08	-214.41, -69.75	<0.0001	-54.87	-134.20, 24.47	0.18	
6 years	-153.31	-241.24, -65.38	0.001	-53.18	-149.68, 43.31	0.28	
Schwalbe's line trabecular iris surface (SL-TISA)							
Age	β	95% Confidence interval	p value	β	95% Confidence interval	p value	
Birth	-0.02	-0.08, 0.04	0.456	-0.021	-0.08, 0.03	0.46	
1 year	-0.05	-0.08, -0.02	0.001	-0.023	-0.06, 0.01	0.20	
3 years	-0.05	-0.07, -0.03	<0.0001	-0.012	-0.04, 0.01	0.37	
5 years	-0.05	-0.08, -0.02	0.001	-0.007	-0.04, 0.03	0.69	
6 years	-0.05	-0.08, -0.01	0.006	-0.003	-0.04, 0.04	0.87	

Coefficient of difference (β), 95 % confidence intervals of difference and significance levels are shown. Significant differences between the premature and full-term measurements are shown in red.

Table 6-7: The rate of growth of temporal and nasal anterior chamber angle measurements in premature and full-term born children per year.

		Temporal		Nasal	
		Trabecular meshwork length (TML) differences μm (%)			
Age interval		Full-term children	Premature children	Full-term children	Premature children
Birth to 1 year		187.33 (24.97)	240.54 (58.15)	165.57 (19.29)	195.01 (41.15)
1 to 2 years		45.08 (6.47)	32.20 (4.92)	22.17 (3.19)	26.11 (3.90)
2 to 3 years		7.89 (1.85)	10.13 (1.48)	6.97 (2.97)	8.21 (1.18)
3 to 4 years		3.46 (1.06)	4.44 (0.64)	3.06 (0.62)	3.60 (0.51)
4 to 5 years		1.82 (0.84)	2.33 (0.33)	1.61 (0.22)	1.89 (0.27)
5 to 6 years		1.07 (0.54)	1.38 (0.20)	0.95 (0.13)	1.12 (0.16)
Schwalbe's line angle opening distance (SL-AOD) difference μm (%)					
Age interval		Full-term children	Premature children	Full-term children	Premature children
Birth to 1 year		341.56 (98.4%)	385.79 (205.46)	291.01 (66.3%)	363.43 (155.33)
1 to 2 years		45.95 (12.0%)	-7.83 (-1.36)	38.96 (16.9%)	17.46 (2.92)
2 to 3 years		14.86 (3.1%)	-12.68 (-2.24)	12.26 (2.8%)	0.13 (0.02)
3 to 4 years		7.11 (1.0%)	-8.70 (-1.57)	5.37 (0.8%)	-1.59 (-0.26)
4 to 5 years		4.55 (0.6%)	-5.85 (-1.07)	2.82 (0.7%)	-1.51 (-0.25)
5 to 6 years		3.70 (0.5%)	-4.07 (-0.76)	1.66 (0.2%)	-1.21 (-0.20)
Schwalbe's line trabecular iris surface (SL-TISA) difference mm^2 (%)					
Age interval		Full-term children	Premature children	Full-term children	Premature children
Birth to 1 year		0.138 (98.8%)	0.132 (161.51)	0.123 (77.1%)	0.138 (138.37)
1 to 2 years		0.019 (12.0%)	0.008 (3.52)	0.016 (11.3%)	0.013 (5.60)
2 to 3 years		0.006 (2.8%)	0.001 (0.28)	0.005 (2.9%)	0.003 (1.31)
3 to 4 years		0.003 (0.9%)	0.000 (-0.12)	0.002 (0.8%)	0.001 (0.46)
4 to 5 years		0.001 (0.5%)	0.000 (-0.16)	0.001 (0.6%)	0.001 (0.20)
5 to 6 years		0.001 (0.3%)	0.000 (-0.14)	0.001 (0.2%)	0.000 (0.10)

6.4 Discussion

Our results revealed that the development of the anterior chamber in premature born children is delayed compared to age-matched full-term born children. The growing eyes of premature children had shorter anterior chamber widths and narrower iridocorneal angles. However, we only detected a difference in the temporal angle while the nasal angle was similar in premature and full-term children.

6.4.1 Ocular development of premature children

Munro et al (2015) reported a phase of rapid development, but at different rates, of both healthy eyes and eyes with ROP, during the early years after birth. Using MRI to create a model eye, they detected that eyes of full-term infants grew more in length than in width compared to the eyes of children with ROP. By the age of 3 years, the eyes became similar in size and shape between children with ROP and children born at full-term (Munro et al., 2015).

Using UBM, Zha et al (2017) detected shorter AL, shorter vitreous diameters (VD), shallower ACD, thicker lenses and steeper corneae in premature Chinese children, without ROP, compared to full-term children (Zha et al., 2017b). Feiss et al had similar findings using a Pentacam Scheimpflug camera, in addition, they found that premature born children have shorter corneal diameters, compared to term children up to the age of 7 years (Fiess et al., 2017).

For the best of our knowledge, this is the first study measuring ACW in infants. We found that at birth, the ACW was not different in premature and full-term children. ACW became shorter in the growing premature children, compared to age-matched full-term children throughout the period of 6 years.

These aforementioned studies indicate that the higher resolution imaging instruments are better than the MRI (which has low resolution), in detecting that the delayed development of the anterior chamber in premature children continued beyond the age of 3 years.

6.4.2 Central corneal thickness in premature and full-term children

The central corneal thickness has been widely investigated. Using patchymeter. Karahan et al. reported CCT of 576.5 µm (95 %CI: 545 - 616) in premature and 562.7 µm (533-611) in full-term newborns (Karahan et al., 2015). This was lower than our recorded mean CCT of similar age group (Table 6.2). Our findings in full-term new-born children for CCT was consistent with the findings of Roman et al, who reported CCT of 585 µm (ranging from 446-706 µm), using an ultrasonic patchymeter (Remon et al., 1992).

As expected, the central cornea became thinner with increasing age. This was well documented in the literatures (Autzen and Bjornstrom, 1991, Portellinha and Belfort, 1991, Autzen and Bjornstrom, 1989, Ferreira and Tavares, 2017). Remon et al., 1992 suggested that corneal thinning begins to happen during the first days after birth due to hydration control of the eyes. Premature newborns had greater central corneal thickness compared to full-term new-born children (Portellinha and Belfort, 1991, Remon et al., 1992). We failed to detect this difference in our study. We did not scan the majority of premature born children shortly after birth. Therefore, the process of corneal thinning, according to Roman et al, could already have happened. This could explain why we could not detect thicker CCT in premature children. However, our youngest full-term new-born infants whom were scanned one day after birth, showed thicker central corneas (Table 6.2) in accordance with previous studies. Similar to our data, Fiess et al did not detect any significant difference in CCT between older premature and full-term born children aged between 4 to 10 years (Fiess et al., 2017).

Thicker central corneas in premature new-born children were found to be associated with higher intraocular pressure compared to age-matched full-term babies (Uva et al., 2011). Both CCT and IOP were positively correlated with each other and negatively correlated with increasing age in premature infants (Sekeroglu et al., 2015). Racci (1999) has attributed the decrease of IOP in premature new-born children, during the first month of age, to the maturation of aqueous drainage system (Ricci, 1999). We detected narrower angle in premature children compared with full-term children. This size of the angle was positively correlated with age. Widening of angle with increasing age probably improves aqueous drainage and results in reduction of the IOP. Therefore, we postulate that the

higher IOP in premature children is associated with narrow anterior chamber angle. Future studies focusing on the relation between the anterior chamber angle development and IOP, in both full-term and preterm children, could provide better answers to this hypothesis.

6.4.3 Anterior chamber angle in premature and full-term children

During our search of publications addressing the anterior chamber angle of preterm children in PubMed, Scopus and Web of Science, we only found one article about the anterior chamber angle in preterm born children without ROP (Kobayashi et al., 1997) and two articles investigated premature children with ROP (Cernichiaro-Espinosa et al., 2014) (Chang et al., 2017).

Using ultrasound biomicroscopy, Kobayashi et al studied the development of the anterior chamber angle of premature infants and found that the angle widens with increasing age. This is in agreement with our findings. However, they studied only a short period of development between 25 to 40 weeks gestational ages as Kobayashi et al scanned the babies only within two weeks after birth. They did not present statistical comparison between premature and full-term new-born children. They reported an average angle measurements depending on the identification of the scleral spur which are not comparable to our study because we based our measurements on Schwalbe's line.

Using SD-OCT, Cernichiaro-Espinosa et al detected wider anterior chamber measurements in premature infant with ROP compared to full-term infants. This is opposite to our findings. It is noteworthy that they used the non-parametric Mann Whitney test to compare between 14 ROP and un-matched 13 full-term control children. Therefore, age difference was not adjusted. In contrast, our study had the advantage of following the normal distribution. In addition, we studied a difference between preterm and age-matched full-term born children at different ages through the 6 years period of postnatal development of the anterior chamber.

The recent study by Chang et al 2017, revealed similar findings to our study using gonioscopy, the gold standard technique for anterior chamber angle evaluation. They detected a narrower anterior chamber angle in ROP children compared to healthy

controls. These narrowing was significant in the temporal, nasal and superior angle but not the inferior angle (the *p* values were < 0.001, < 0.001, 0.002 and 0.16; respectively) (Chang et al., 2017).

6.4.4 Nasal temporal asymmetry

This is the first study presenting measurement of trabecular meshwork in preterm and full-term born children. We found that premature children have shorter temporal trabecular meshwork compared to full-term children. However, while the difference in temporal TML reduced with increasing age between the premature and full-term children, similar to the nasal TML and angle width, the difference in the temporal angle width increased with age. This indicates nasal temporal angle width asymmetry in the growing premature children. This might suggest that the temporal meridian is more susceptible to pathological change than nasal meridian. Iris morphology is highly likely to play a role in this asymmetry. Therefore, future study of the relation of the iris and anterior chamber development is important.

Read and colleagues have recently reported nasal temporal asymmetries in scleral and conjunctival thickness measurement using AS-OCT. They found that nasal sclera is thinner and nasal conjunctiva is thicker compared to temporal meridians. This asymmetry was postulated to be associated with the location of extraocular muscles insertion on the sclera.(Read et al., 2016). Using AS-OCT, medial rectus muscle insertion at the nasal side is located more proximal compared to the insertion of the lateral rectus muscle at the temporal side. Prematurity was reported to be associated with exotropia and esotropia which are treated by surgery of extraocular muscle. It would be interesting to investigate whether there is an association between squint and anterior chamber angle biometry in future studies.

6.4.5 Importance of this study

The association between prematurity (with or without ROP) and increased risk of high intraocular pressure and glaucoma during adulthood has been documented (Ziemssen et al., 2004, Robinson et al., 2018). A case study has presented an acute attack of angle closure glaucoma in a premature child with history of ROP (Wu et al., 2015). The attack followed pupil dilatation during routine retinal examination. We agree with the study of Chang et al to suggest that the presence of narrow angle and forward bowing of the iris, in addition to our detected shorter trabecular meshwork, might be the reasons why premature born children are susceptible to closed angle glaucoma. Severe ROP is often managed by surgical intervention e.g laser photocoagulation. Hence, morphological changes of anterior chamber are a possible consequence. Our study included only premature children without ROP. Our findings showed that the delayed anterior chamber development and the possible risk for glaucoma in prematurity can occur irrespective of presence of ROP. Future investigation of the development of anterior chamber angle comparing premature children with and without ROP, could clarify whether differences in anterior chamber angle narrowing occur in ROP. In addition, it is noteworthy to mention that the refractive state of our subjects was known. Both the premature and controls children were predominantly hypermetropic. While hypermetropia is associated with narrow angle, myopia is associated with wide angle (This was detected in chapter 4 section 4.3.6.2), while ROP is usually associated with myopia. One speculate is refractive state of prematurity influence the size of angle?

6.4.6 Limitations of study

This study has a limitation of small sample size of premature children. Recruitment of healthy newborns was easier than that of newly born premature children, due to the critical health condition of the premature infants. Finding suitable subjects and obtaining consents were more difficult than obtaining the HH-OCT scans. Unfortunately, we could not scan most of the eligible children because their pupils were dilated for fundus and refractive examination. The small sample size of premature children ($n = 17$) may be the reason of insignificant results regarding the nasal angle and cornea. In case of a small sample size, caution must be applied, as the findings might not be accurate. For this

reason, we also did not address the refraction state or the influence of gender on the anterior chamber development. Unfortunately, our study has a limitation of not measuring the iris thickness. Exploring the role of iris thickness in determining the angle width in prematurity in future studies could clarify the nasal temporal asymmetry in prematurity.

It was suggested that an abnormal anterior chamber plays a role in producing different pattern of myopia compared to the full-term myopia (Modrzejewska et al., 2010, Zha et al., 2017a, Snir et al., 2004, Ecsedy et al., 2014). A more focused study comparing the refractive state and anterior chamber biometry in premature children is therefore suggested. Another limitation was that only the nasal and temporal angle was investigated. Exploration of the different meridians would be very interesting. We hope that this topic could be investigated in future studies with larger and more controlled sample size of premature group at different ages.

6.4.7 Summary

This study detected delayed development of the anterior chamber of premature born children. Premature born children had shorter anterior chamber width and narrower temporal anterior chamber angle compared to age-matched full-term born children up to 6 years of age. This may be a key factor of the increased risk of ocular disease, associated with prematurity, both in childhood and adulthood. This study highlights future studies that could add more to our understanding of the anterior chamber development of premature children.

7. Chapter seven: Clinical Exploration of Congenital Anterior Segment Abnormalities Using HH-OCT

In this chapter, we aim to explore the potential clinical use of HH-OCT in aiding the diagnosis of congenital abnormalities of the anterior segment without sedation by using examples.

7.1 Introduction

Congenital abnormalities of anterior segment, such as aniridia or anterior segment dysgenesis, manifest by abnormal structures of anterior segment. Details of the characteristic clinical features of these congenital abnormalities were described in chapter 1, section 1.1.4. Secondary congenital glaucoma is commonly associated with anterior segment abnormalities. The diagnosis depends on clinical visualisation of these features by slit lamp biomicroscopy, gonioscopy, funduscopy and UBM. These methods are not easily applicable in very young children without sedation. It was reported that UBM is a valuable tool for evaluating the anterior segment of paediatric patients. However UBM requires examination of children under anaesthesia (El Shakankiri et al., 2009). The feasibility of Visante TD-OCT for evaluating the abnormal structures of anterior segment of paediatric patients without sedation has previously been validated. However, the images acquisitions of young children were challenging and difficult (Cauduro et al., 2012). We proved that HH-OCT is a feasible and reliable device for imaging children since birth without sedation. In this chapter, we used HH-OCT to identify the abnormalities of anterior segments associated with syndromes affecting anterior segment.

7.2 Methods:

This is an observational case study. We recruited children with confirmed diagnosis of congenital anterior segment abnormalities from Leicester Royal Infirmary and Birmingham Children Hospital. Consent forms were obtained from the parents of children prior to examination. The history and clinical information were collected from the medical notes. The children were scanned by HH-OCT without sedation. Anterior chamber images were

exported to imageJ for analysis. The B scans showing the structures of anterior chamber were evaluated to identify the known typical abnormal clinical features of the anterior chamber, characteristic for each investigated disease.

7.3 Results

The study explored the HH-OCT images of the anterior chamber of seven children with confirmed diagnosis of congenital anterior segment abnormalities. One child was diagnosed with aniridia, three children with Peters anomalies, two children with Axenfeld Rieger syndrome, and one with Sturge Weber syndrome. Summary of the diagnosis and the age of children is shown in table 7.1.

HH-OCT provided images of the anterior chamber without sedation. The scans were easily obtained. The children were cooperative and comfortably sitting. Therefore, each scan was captured within seconds. However, Obtaining of successful scans of both eyes showing clear structures of anterior chamber was not possible in all children (Table 7.1). The difficulties in identifying the anterior chamber structures on the screen of the HH-OCT device resulted in bad acquisitions of images. These structures are usually not well developed for example in aniridia, the iris is not clear. We did not assess the feasibility and perform quantitative measurements of anterior chamber because of the small sample size of each diagnosis.

The findings of HH-OCT images of anterior chamber of each disease are described below.

Table 7-1: Clinical information of the patients with congenital abnormalities of anterior segment.

ID	Diagnosis	Age	Gender	Etnicity	IOP mmHg		Glaucoma operations	Other features and medical information	Gestational age weeks	Clear image
					Right eye	Left eye				
1	Aniridia	1.8 years	F	A	30	38	Baervelt 350 + scleral graft	Microcephaly, Parents are first cousins	39	Left eye
2	Peters Anomaly type 1	7 years	M	C	13	12	No	No family history of similar case or glaucoma	-	Left eye
3	Peters Anomaly type 1	1.8 years	M	A	8	10	Lensectomy and corneal graft^	Left amblyopia, Cloudy cornea, Parents related-consanguinity	40 + 4	Right eye
4	Peters Anomaly type 2	8 months	F	C	10	9	bilateral iridectomy	Family history of early onset cataract	38	Right eye
5	Axenfield Rieger	11 years	M	A	-	-	Bilateral repeated goniotomy	Left amblyopia, Latent nystagmus, No family history of glaucoma	39+3	Both eyes
6	Axenfield Rieger Syndrome	4 years	M	C	27	34	Goniotomy and trabeculotomy	Polycoria, Positive family history of similar features	37+4	Both eyes
7	Right Sturge Weber syndrome	8 months	M	C	23	12	Right goniotomy	Seizures (carbamazepine + aspirin). No family history of glaucoma	39	Both eyes

(*) All cases are receiving medication to control IOP. A=Asian, C=Caucasian, F=Female, M=Male. AC= Anterior chamber. (-) IOP is not recorded. ^ Operations were performed after obtaining the scans.

7.3.1 Aniridia

The HH-OCT image of 1.8 years Asian female with confirmed diagnosis of aniridia is shown (Figure 7.1). We observed that the iris is underdeveloped and appears as small structure attached to the corneoscleral junction. The cornea is thickened with hyper-reflected area. The corneoscleral junction looks thin without distinguished scleral spur or a hyper-reflected structure of trabecular meshwork. The anterior pole of lens is clearly shown. The absence of complete structure of iris is a typical manifestation of aniridia.

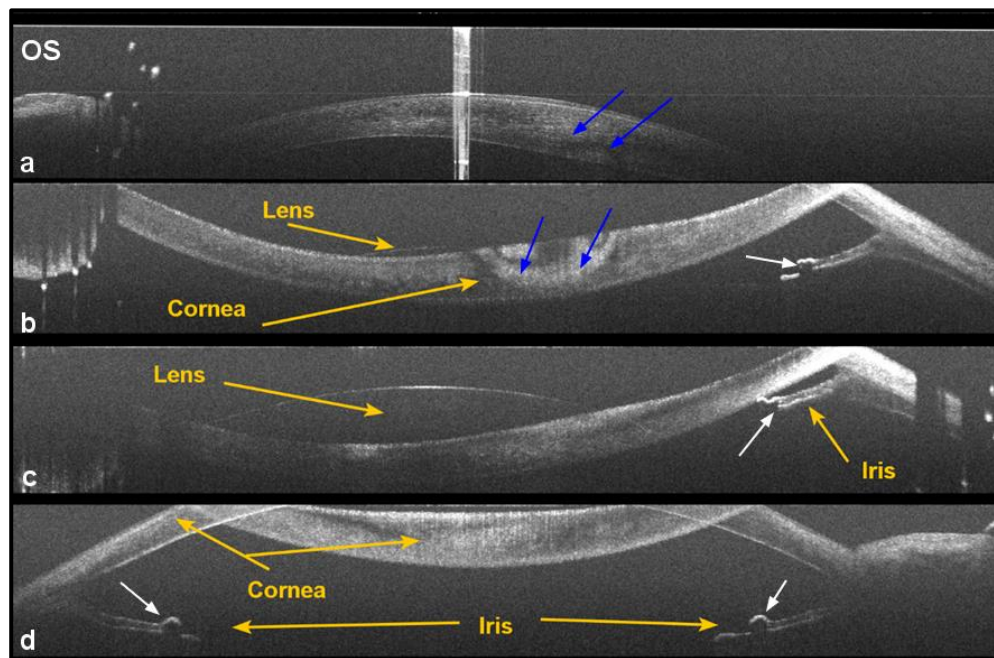


Figure 7-1: HH-OCT images of the anterior chamber of left eye of a known case of aniridia. The figure shows different B scans of the left anterior chamber: (a) and (b) The cornea has increased hyper-reflectivity and appears distorted (blue arrows). The cornea is inverted because the hand-held probe of OCT device was placed closer to the eye in order to show the anterior chamber angles. (c) a clear structure of anterior pole of lens is shown. A remnant of partial and under-developed iris are shown (white arrows) in (b, c and d).

7.3.2 Peters anomaly

Figure 7-2A shows the anterior chamber of a seven year old Caucasian male with iridocorneal adhesion of Peters anomaly type 1. The HH-OCT image of left eye shows that the iris at the nasal side is displaced forward and adhered to the cornea. The nasal anterior chamber angle is very narrow. This child had glaucoma and is under medications. Figure 7-2B represents the anterior segment of a 1.8 years old Asian male with iridocorneal adhesion of Peters anomaly type 1. The HH-OCT image of the right eye shows adhesion between the pupillary end of iris and the cornea at the temporal side. The cornea appears thickened and pulled inward. The iris at the nasal side appears underdeveloped and short. The pupil is not central and pulled toward nasal side. Figure 7-2C shows the anterior segment of an 8 months old Caucasian female with lenticular-corneal adhesion of type 2 Peters anomaly. The HH-OCT image shows an adhesion between the cornea and the anterior pole of the lens, with presence of abnormal dense and hyper-reflective tissue.

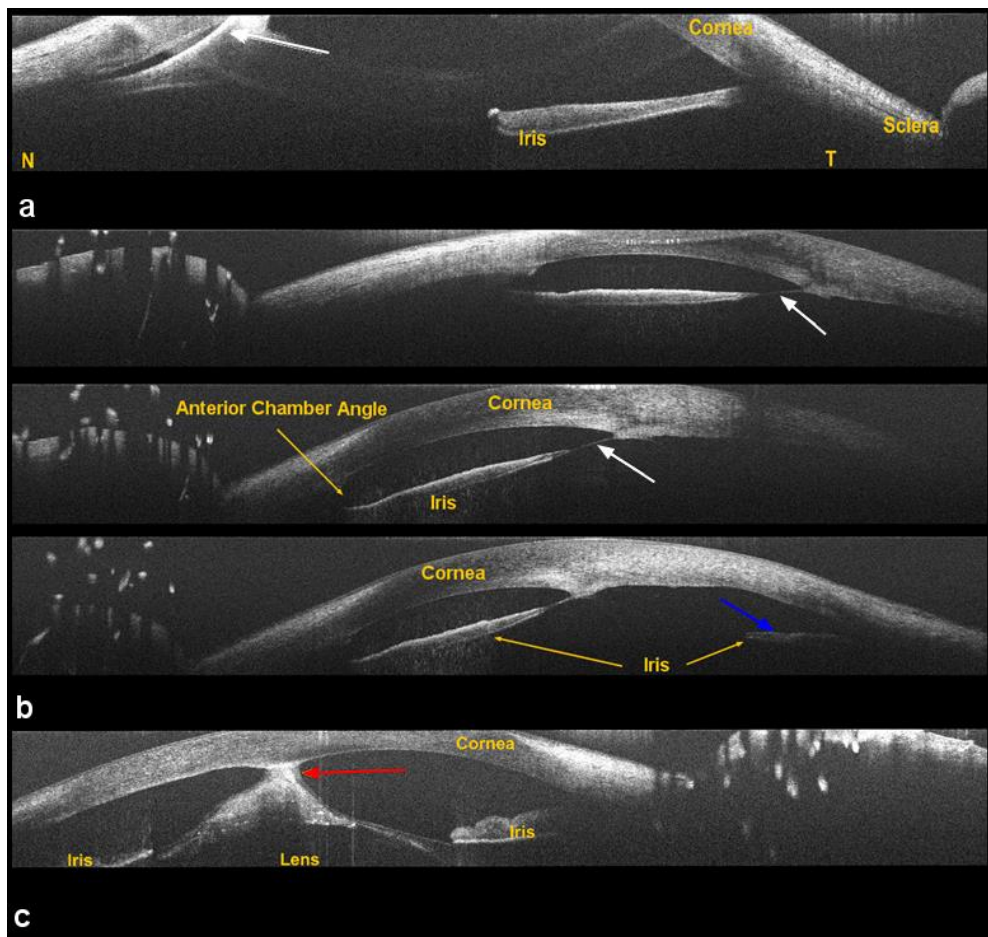


Figure 7-2: HH-OCT images of the anterior chamber, in three children with Peters' anomaly.

a) Peters anomaly type 1 of iridocorneal adhesion of a 7 year old Caucasian male, where the iris is adherent to the cornea at the nasal side of the left eye (white arrow). b) Peters anomaly type 1 of 1.8 year old Asian male, where the iris is adherent to the cornea at the temporal side of the right eye (white arrows), while the nasal iris is under developed (blue arrow). c) Peters anomaly type 2 of lenticulo-corneal adhesion of 8 month Caucasian female, where an adhesion is seen between cornea and lens (red arrow).

7.3.3 Axenfeld Rieger syndrome

The HH-OCT images showed the typical features of Axenfeld Rieger syndrome. Figure 7.3 shows the anterior chamber image of 11 year old Asian male diagnosed with Axenfeld Rieger syndrome. The image of the anterior chamber showed that the structure of iris looks thin and not well differentiated. Strands of iris are misplaced forward and attached to trabecular meshwork and Schwalbe's line, which is known as posterior embryotoxon. The pupil is not central and slightly shifted towards the temporal side. Figure 7.4 shows the anterior chamber image of a 4 year old Caucasian male diagnosed with Axenfeld Rieger syndrome. The iris of the left eye was underdeveloped with misplaced strands toward the cornea. Polycoria (multiple pupils) was seen in the B scans of the right eye (Figure 7.4D). The anterior chamber appeared narrow.

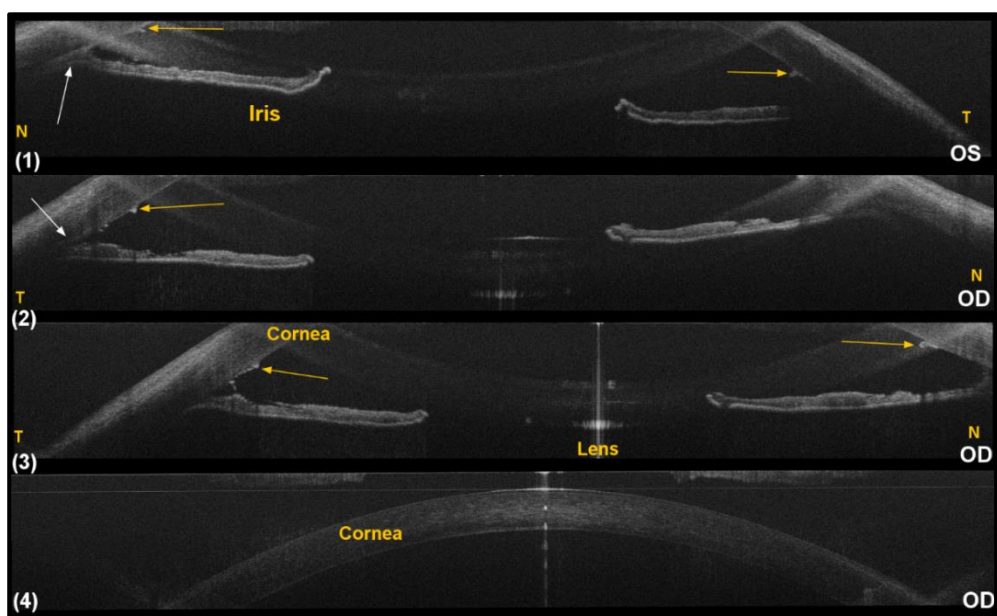


Figure 7-3: HH-OCT images of the anterior chamber of an 11 year old Asian male diagnosed with Axenfeld Rieger syndrome.

Different B scans of the anterior chamber of right (OD) and left (OS) eyes. The structure of the iris looks thin and not well differentiated. Strands of iris are misplaced forward and attached to trabecular meshwork and Schwalbe's line, corresponding to a posterior embryotoxon (yellow arrows). The pupil is not central and slightly shifted toward temporal side (T).

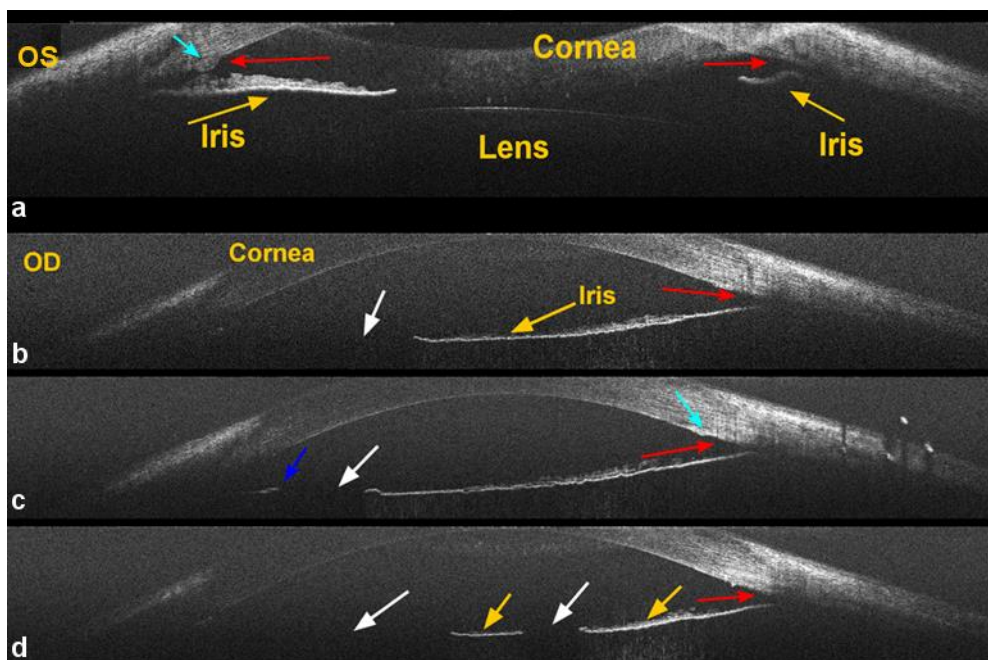


Figure 7-4: HH-OCT images of the anterior chamber of a 4 year old male with confirmed diagnosis of Axenfeld Rieger syndrome.

The anterior chamber of both eye appears shallow without clear structures of anterior chamber angle (red arrows). Posterior embryotoxin is shown (cyan arrows). a) The iris of the left eye (OS) is underdeveloped (yellow arrows). b) the iris of the right eye (OD) appears atrophied and flat (yellow arrows). c) A different B-scan of the right eye shows a cut section below the level of (b), where the temporal margin of pupil is shown (blue arrow). d) Another B-scan of the right eye at lower level to (c) where the polycoria (multiple pupils) is seen (white arrows).

7.3.4 Sturge Weber Syndrome

Figure 7-6 shows the anterior chamber image of an 8 month old Caucasian male with Sturge Weber Syndrome. This child was diagnosed with secondary glaucoma in the right eye. The child has undergone goniotomy and is treated with Latanoprost and Azargan (glaucoma eye drops). He had seizures controlled by medications (Carbamazepine) and port wine stain at the right side of face. There was no family history of any ocular or chronic diseases. HH-OCT findings of anterior chamber of the affected right eye showed similar features to the primary congenital glaucoma (described in chapter 5 Figure 5.2). The anterior chamber of the right glaucomatous eye appeared wider and deeper than the healthy left anterior chamber. The iris appeared flat, atrophied with no visible crypts and highly inserted to the corneoscleral junction compared to healthy iris. The scleral spur (SS) was distorted and not easily identified, while Schwalbe's line was clear. The trabecular meshwork (TM) structure was also distorted and thickened. In contrast, the left eye shows normal features of anterior chamber similar to figure 4.2 in chapter 4.

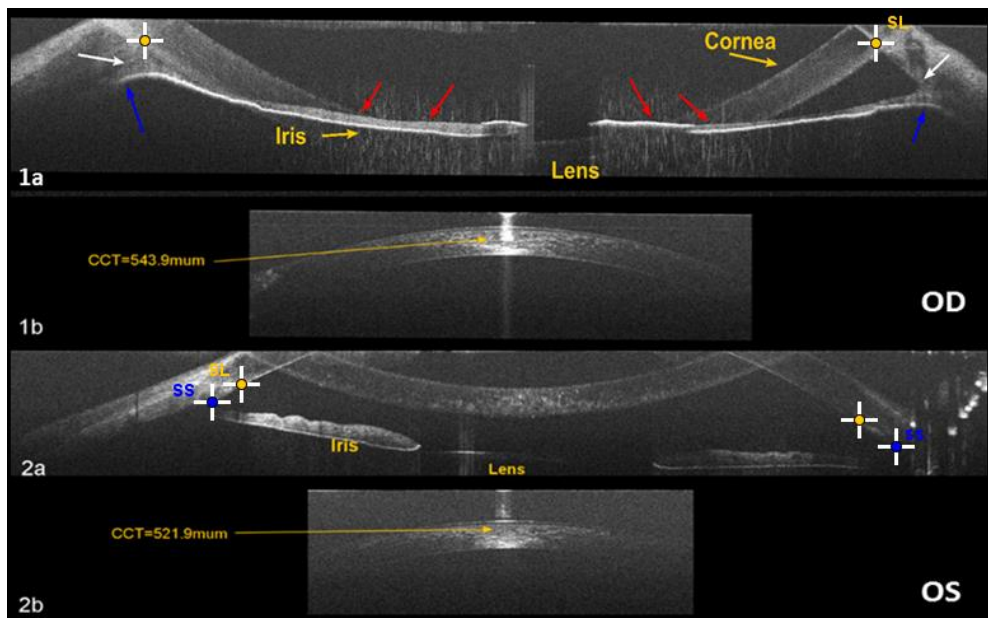


Figure 7-5: HH-OCT images of the anterior chamber of 8 month old Caucasian male diagnosed with Sturge Weber Syndrome.

(1) The image of the right (OD) anterior chamber and cornea shows similar features to the morphology of primary congenital glaucoma (Figure 5-2). (2) The image of the left eye (OS) shows normal structures of anterior chamber and cornea. (1a) The anterior chamber of the right glaucomatous eye appeared wider and deeper than the healthy left anterior chamber (2a). The iris appeared flat, highly inserted to the corneoscleral junction (blue arrows,) atrophied with no visible crypts (red arrows), compared to healthy left iris. The scleral spur (SS) was distorted and not easily identified (white arrows), while Schwalbe's line (SL) was clear (yellow dot).

7.4 Discussion

We presented examples of the potential clinical application of HH-OCT in identifying the anterior segment abnormalities without sedation.

In cases such as Aniridia, Peters anomaly, Axenfeld Rieger syndrome, HH-OCT has enabled the identification of the characteristic features of these syndromes. There was partial presence, which is the characteristic feature of aniridia (Lim et al., 2017a). Our finding of type 1 and type 2 Peters anomalies are in agreement with the previous study of Majander et al which explored the phenotypes of corneal opacity using CASIA SS-OCT (Majander et al., 2012). The posterior embryotoxon, polycoria and corectopia (non-central pupil) are characteristic features of Axenfeld Rieger syndrome (Seifi and Walter, 2018).

The observed abnormal structures of anterior chamber angle in aniridia, Axenfeld Rieger syndrome explain the high risk of associated developmental glaucoma.

We found that the features of Sturge Weber syndrome resembled the features of primary congenital glaucoma. This confirms the report showing that Sturge Weber syndrome has identical clinical findings of primary congenital glaucoma. Anterior displacement of iris root, poorly development of scleral spur, thickened uveal meshwork are ocular features of Sturge Weber syndrome (Akhter and Salim, 2014).

7.4.1 Summary

HH-OCT is a useful method in identifying congenital abnormalities of the anterior segment and may help to exactly classify anterior segment changes and study the pheno- genotype correlations.

8. Chapter eight: General Conclusions and Future Studies

8.1 General conclusions

This thesis has provided the first use of HH-OCT for in vivo quantitative investigation of the anterior chamber of children eye. The results have demonstrated the successful use of HH-OCT in providing reproducible anterior chamber measurements of healthy children and children with ocular pathology such as nystagmus and congenital glaucoma. HH-OCT was successfully applied in studying the postnatal normal development of the anterior chamber of the children and investigating the abnormal development of anterior chamber in congenital glaucoma and premature born children.

Lack of non-invasive techniques for imaging the eye of children has limited the in vivo studies of anterior chamber development. The potential of investigating the development of the eyes of children has become possible with the advances of non-invasive optical coherence tomography technique. The availability of child-friendly hand-held OCT device facilitates the evaluation of the in vivo ocular development of children and the diagnosis of developmental ocular diseases. The HH-OCT has been successfully used to study the development of the fovea (Lee et al., 2015) and optic nerve (Patel et al., 2016) in infants and children without sedation. The HH-OCT was also proposed as diagnostic aid in anterior segment dysgenesis (Pilat et al., 2017). However, HH-OCT application in imaging the anterior chamber of children has not been systematically investigated. In chapter 3, we evaluated the feasibility of HH-OCT in imaging children since birth, without sedation. We successfully scanned 89% of our recruited healthy children aged less than 6 years old. We tested the reproducibility and repeatability of anterior chamber measurements of healthy children and children with ocular pathology, including congenital glaucoma and nystagmus younger than six years. Our results revealed that HH-OCT had high reproducibility and repeatability of the measurements of anterior chamber width and nasal and temporal angle measurements derived from Schwalbe's line (SL-AOD and SL-TISA, with ICCs of > 0.9). This indicates that HH-OCT is a reliable device for imaging the anterior chamber of

children even in presence of the rapid eye movement of nystagmus and the abnormal anterior chamber angle morphology of congenital glaucoma.

In chapter 4, the changes of highly reproducible Schwalbe's line derived angle measurements with increasing age were used to investigate the postnatal normal development of anterior chamber angle. Trabecular meshwork length (TML) represents the length of the exposed part of trabecular meshwork to the anterior chamber. The aqueous humour filtrates through this exposed part of trabecular meshwork to maintain the IOP. We present for the first time measurements of trabecular meshwork length in children. The association of short TM with juvenile primary open angle glaucoma (Stegman et al., 1996) and angle closure glaucoma (Tun et al., 2013b, Chen et al., 2015) has been previously detected in adults. Therefore, the TML is an important parameter that worth to be included in studying the nasal and temporal angle development, although we found moderate reproducibility of TML with ICC~ 0.7.

The histological studies have reported that the development of trabecular meshwork and anterior chamber continues postnatally and matures by 1 to 4 years of age. The complete cellular differentiation of trabecular meshwork is taking place by age of eight year (Reme and d'Epinay, 1981). Our findings of the anterior chamber development among 223 children, imaged without sedation using HH-OCT, revealed a rapid phase of anterior chamber growth during the first 18 months of age. This concurred with a previous UBM study that reported positive linear correlation of anterior chamber measurement with log age (Kobayashi et al., 1999). However, our complex non-linear model has the advantage of presenting the mean and 95% prediction intervals of anterior chamber measurements for each year of age during the period from birth up to 35 years old. The anterior chamber width and the central corneal thickness reached the adult size by age of 3 years. The nasal and temporal angle width stabilised by age of 5 years. In contrast, we found that the TML continued to elongate at a very slow rate during adulthood. In a previous study using UBM, Stegman et al detected a positive correlation between axial length and trabecular meshwork length in adult. Several studies of axial length development have reported a continuous increase in axial length up to the age of 16 to 18 years (Munro et al., 2015, Hashemi et al., 2015). This may explain the continuous growth of TM.

In addition, our results showed that the development of the anterior chamber angle is influenced by gender, angle meridians and changes in refraction. Firstly, similar to the AS-OCT studies among adults, we found evidence that females have smaller anterior chamber measurements compared to males. Secondly, we detected nasal temporal asymmetry in the development of trabecular meshwork length. The nasal TM was shorter than temporal TM due to the greater growth of the temporal TM compared to nasal TM. This finding has explained our results of the next chapters exploring the development of the anterior chamber angle in premature born children and children with congenital glaucoma. Finally, although we measured the refractive errors grossly using portable Plusoptix auto-refractor without cycloplegia (dilatation of pupil with topical medication), we were able to detect a myopic shift with increasing age, which is consistent with the physiological process of emmetropisation. This myopic shift is associated with an increase in nasal and temporal angle width.

Congenital glaucoma is believed to result from failure of the complete development of trabecular meshwork and anterior chamber angle (Maumenee, 1959). The association of congenital glaucoma with genetic mutation of *CYP1B1* has revealed many potential mechanisms of the defect in trabecular meshwork development (Firasat et al., 2017, Garcia-Anton et al., 2017). In a histological study of TM in *CYP1B1* deficit mice, the authors have reported presence of a healthy TM at birth. The postnatal development of TM became altered by age of 3 weeks (Teixeira et al., 2015). This suggests that congenital glaucoma results from defect in postnatal TM development. In chapter 5, we compared the development of anterior chamber measurements of children with operated congenital glaucoma and age-matched healthy children up to the age of 10 years and presented the significance of differences between the two groups at different ages. We propose a potential explanation of the angle widening in congenital glaucoma that concurred with the findings of previous literature of the disturbed development of trabecular meshwork. It is likely that the anterior chamber angle dilates as a result of increased pressure outflow of aqueous humour against the progressive impaired function of trabecular meshwork. We found that the nasal angle widening occurred earlier than the temporal angle widening. Unlike the nasal angle, the temporal angle width in congenital glaucoma was similar to healthy control before the age of one year. The trabecular meshwork of the nasal angle is shorter than that of temporal angle. Hence, the resistance of outflow at the

nasal angle is greater, causing earlier nasal angle dilatation, compared to temporal angle. Our study of congenital glaucoma has also revealed that the anterior chamber width has stabilised in the operated congenital glaucoma during childhood. This may reflect effective treatment. In addition, congenital glaucoma is associated with greater central corneal thickness, which reduces with increased age. There was positive correlation between central corneal thickness and IOP.

Premature born children are at high risk of ocular diseases. Recent study has connected prematurity to possible risk of angle closure glaucoma and increased intraocular pressure (IOP) later on in adult life (Robinson et al., 2018). In chapter 6, we found that the development of premature anterior chamber is delayed compared to age-matched full-term children up to the age of 6 years and premature children have narrower temporal anterior chamber angle.

In chapter 7, we explored the clinical application of HH-OCT in detecting the characteristic features of anterior chamber defects in children with aniridia, Peters anomalies and Axenfield Rieger syndromes. We showed that HH-OCT can aid the diagnosis of anterior segment abnormalities of infants and young children.

This study provided evidence that HH-OCT is a useful device for imaging children from birth. The study of normal and abnormal development of anterior chamber development has demonstrated interesting results. We established normative data of anterior chamber since birth. Details of normal development of trabecular meshwork, anterior chamber angle, anterior chamber width and central corneal thickness have been modelled. This provides a base for identifying abnormal development of the anterior chamber. Studying condition such as congenital glaucoma has revealed the possible underlying mechanism of the destructive effect of increased intraocular pressure on angle morphology. Association of prematurity with delayed development of anterior chamber can be the key of the increased risk of ocular diseases in premature born children such as myopia and possible attach of acute glaucoma. The potential significance of our findings is summarised below. However, future studies may provide more informative details about the applications of HH-OCT in clinical practice and for research.

8.2 Summary of the significance of findings

We showed that HH-OCT could help to measure of anterior chamber parameters in presence of nystagmus and glaucoma. Therefore, clinical application to aid diagnosis of anterior segment abnormalities that is associated with nystagmus is possible.

The availability of normative anterior chamber measurements in children may have important clinical applications. They could improve the formula for calculation of IOL power in cases of congenital cataract operation. Understanding the normal postnatal development of the anterior chamber and when it reaches maturity can help the surgeons to decide the best age of implanting IOL post cataract extraction and help to predict the size of artificial lens. Understanding the development of anterior chamber and cornea in particular could have great impact on the outcome of the refractive corrective surgery. Due to the little availability of information about accurate anterior chamber geometry in children, refractive surgery, including implanting intraocular lens, is suggested less predictable in infants as the eye is still developing. The availability of normative anterior chamber measurements at different ages throughout childhood could make the surgical correction of refractive error more predictable at younger ages.

The narrower anterior chamber angle and the shorter anterior chamber width of premature born children could be the reason of the increased risks of angle closure glaucoma in prematurity.

Our findings of congenital glaucoma measurements, have significant clinical importance. The widening of nasal angle happened before the age of 3 months. This could be an earlier sign for diagnosis of congenital glaucoma. Detecting a wide nasal angle at birth can raise suspicion of the occurrence of glaucoma. We also hypothesise that the stabilisation of angle width could be an indicator of the successful surgical interventions that restore aqueous humour outflow and maintain normal IOP. Furthermore, we detected that the age plays a role in the association between the central corneal thickness and IOP.

Therefore age should be considered for the interpretation of IOP measurement.

Shohdy et al (Shohdy et al., 2017) suggests that *CYP1B1* mutation is associated with alteration or dysregulation of the proteins that modulate the process of TM remodelling and differentiation. Detection of these modulating proteins and clearly understanding the

mechanism of TM remodelling could provide a new approach of therapeutic intervention in congenital glaucoma. Such approach could preserve and maintain the function of TM, which in turn could mean that the infantile glaucoma might become curable. We found that temporal angle width of congenital was not altered before the age of one year. This finding may support the hypothesis that the postnatal changes in development of trabecular meshwork in congenital glaucoma might be prevented by early treatment.

8.3 Recommendations of future studies

Using UBM, shorter trabecular meshwork have been detected in patients with juvenile primary open angle glaucoma compared to controls (Stegman et al., 1996). The size and area of trabecular meshwork might be associated with the susceptibility for glaucoma in children. Trabecular meshwork length, area and width have been measured in adult. Kegemann et al have previously described the trabecular meshwork as a trapezoid shape, dense, hyper-reflected structure using SD-OCT (Kagemann et al., 2010). During the analysis of the anterior chamber images, we observed that the trabecular meshwork was clearly visible in some of the HH-OCT images (Figure 8.1). Unfortunately, due to the limitation of time, I could not modify the analysis program and include the measurements of the TM area and thickness. It would be interesting to evaluate the feasibility of visualising TM and study the development of trabecular meshwork length, depth and area in children. These measurements could be associated with risk of developing glaucoma. Such study could require only developing of a new ImageJ macro to analyse the already used images in this study.

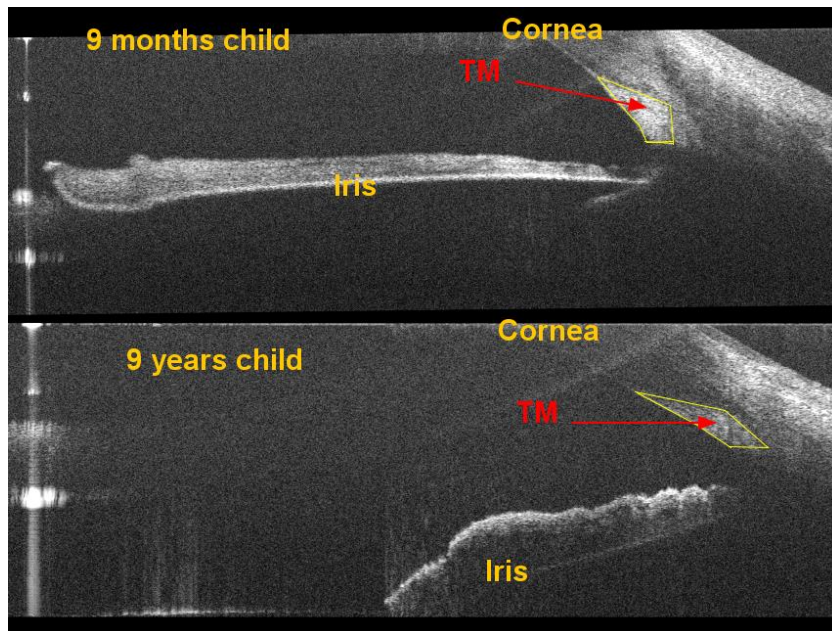


Figure 8-1: HH-OCT image of the anterior chamber angle showing the trabecular meshwork.

The trabecular meshwork (TM) appears as a hyper-reflective trapezoid shape of the eye of a 9 months and a 9 year old child. Measuring the area of the drawn shape (yellow trapezium) is likely to correlate to the size of TM.

Nasal temporal asymmetries in scleral and conjunctival thickness measurement using AS-OCT have recently been reported (Read et al., 2016). Nasal sclera was thinner and nasal conjunctiva was thicker compared to temporal meridians. In our study, we presented good reproducibility of the measurements of nasal and temporal limbal thickness (SS-LD and SL-LD). A future study investigating the development of limbal thickness could provide further information about the development of anterior chamber and the nasal temporal asymmetry. Furthermore, we hypothesise that thin limbal thickness could be associated with congenital glaucoma.

Our study did not investigate the role of the iris in the development of anterior chamber angle. Adjustment of acquisition protocol of HH-OCT for better acquisition of the entire image of the iris could help to study the normal and abnormal development of the iris. In addition, it has been observed that the iris morphology in congenital glaucoma is different from that of healthy controls. The Iris looks thinner and not well differentiated (Figure 8.2). Future studies to investigate the influence of the iris on angle development would be important.

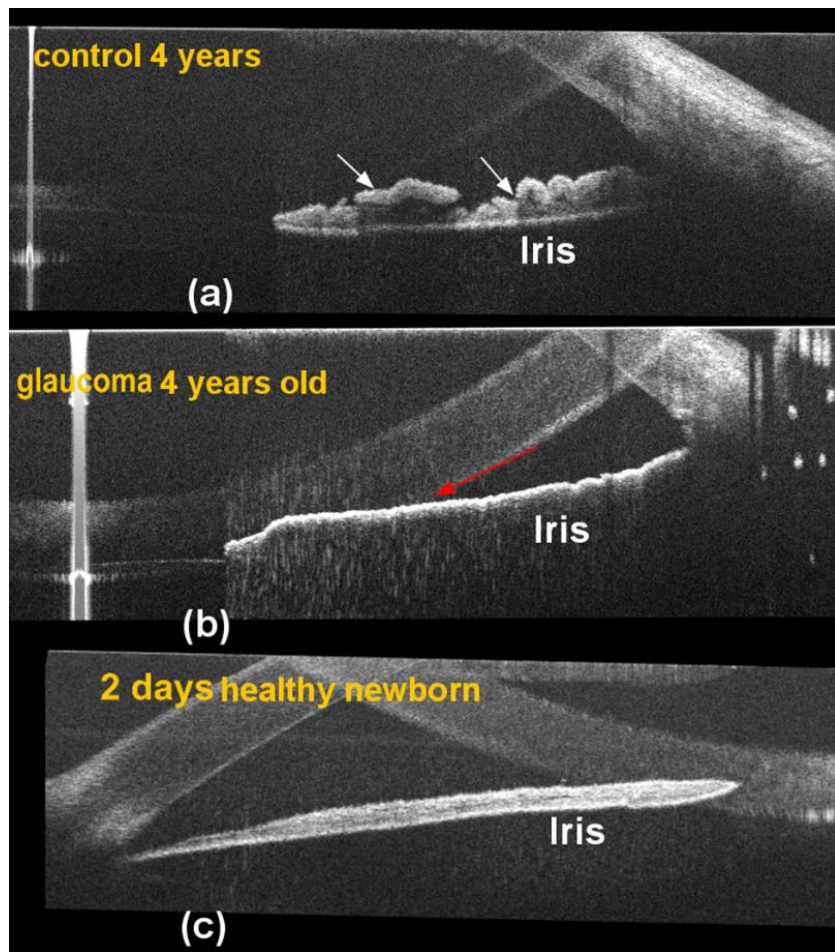


Figure 8-2: HH-OCT images comparing between the a) healthy iris of a 4 year old child, b) the iris of an age-matched child with congenital glaucoma and c) the iris of healthy newborn child.

In congenital glaucoma the iris looks thin, flat, not well developed and without visible crypts at the anterior layer (red arrow) compared to the healthy iris (white arrows). The glaucomatous iris looks similar to the iris of newborn shown in (c).

Measurements of preoperative biometry in congenital cataract is useful to estimate the contact lens power used in aphakic children (Trivedi et al., 2014). We suggest that HH-OCT could be a useful method for preoperative and postoperative assessment of congenital cataract. It can provide longitudinal data that would help to understand how the eye grows and compensates the surgical intervention and when it is suitable for IOL implantation.

We studied the anterior chamber angle in premature children without ROP. The narrow angle in premature born children could be more pronounced in children who have ROP. Future study to compare healthy children to premature born children with or without ROP

could provide valuable answers. In addition, the anterior segment is suggested a major determinant of the refractive state in premature children irrespective of axial length. Future study focusing on the changes of refractive state in relation to delayed development of anterior chamber in premature children could provide better explanation why myopia is common with prematurity.

We speculate that the stabilisation of ACW and anterior chamber angle measurements could reflect the control of IOP in treated congenital glaucoma. However, comparison between preoperative and postoperative congenital glaucoma in cases of controlled and uncontrolled IOP could confirm this theory. Furthermore, comparison between the changes of anterior chamber measurement and the changes of optic nerve in congenital glaucoma with age could highlight the association of anterior chamber angle widening and progressive optic nerve damage. Comparing the measurements of anterior chamber and optic nerve using HH-OCT to the corneal hysteresis, corneal compensated IOP (IOPcc), corneal resistance factor and Goldmann IOP measurements of ocular response analyser could add a valuable improvement in the management of children with congenital glaucoma. HH-OCT and ORA are non-invasive methods and can be easily applied in examining the children. More details about the ocular response analyser are described in appendix.

Viral et al have characterized *in vivo* abnormalities of the iris associated with albinism using AS-OCT and reported nasal temporal asymmetry of the ciliary end of iris in albinism compared to age-matched healthy adults (Sheth et al., 2013). We presented anterior chamber measurements of children with nystagmus including albinism and idiopathic infantile nystagmus (IIN). It would be interesting to compare the anterior chamber measurement of albinism and IIN to age- matched healthy controls and investigate whether iris abnormality of albinism is affecting anterior chamber morphology in children.

The manual identification of anterior chamber landmarks of HH-OCT images is time consuming and subjective to personal error. Developing an automatic image analysis would be more accurate and time and cost savings. Clinically, it is not practical to transform the scans from the HH-OCT machine to imageJ to perform the analysis. Availability of a built in software to perform the measurements in the same device is essential for a clinical applicability of HH-OCT.

9. Chapter nine: Appendix

9.1 Appendix of chapter 5

9.1.1 Congenital glaucoma surgical management

The surgical managements of congenital glaucoma included goniotomy, trabeculotomy, trabeculectomy, and Diode laser cyclo-photocoagulation. In goniotomy, a needle is used to make incisions in the TM visible through the gono-lens if the cornea was clear. When the cornea was not clear, performing incisions in the TM through the sclera is called trabeculotomy. The third surgical option is trabeculectomy that involves partial excision of TM if the above operations failed to control IOP.

Trabeculectomy is sometimes accompanied with tube insertion and Mitomycin C (MMC); an antineoplastic medication, to maintain the drainage of aqueous humour. The tube may need flushing.

Diode laser cyclo-photocoagulation is usually done if the previous mentioned surgeries are failed or not preferred as first option of surgical intervention

Table 9-1: Demography of congenital glaucoma patients

ID	Gender	Ethnicity	Diagnosis	Operation	Age/year	IOP(mm Hg)	
						OD	OS
1	M	Caucasian	Primary glaucoma	Bilateral goniotomy	0.42	28	18
2	F	Caucasian	Primary glaucoma	Bilateral goniotomy	0.49	43	38
3	M	Caucasian	Primary glaucoma	Bilateral goniotomy-	4.39	15	21
4	M	Asian	Primary glaucoma	Bilateral trabeculectomy	13.64	18.1	30.6
5	F	Caucasian	Primary glaucoma	Left trabeculectomy, right goniotomy	1.48	12	21
6*	M	Caucasian	Right secondary glaucoma to Sturge Weber syndrome	Right goniotomy	0.71	23	12
7	M	Asian	Primary glaucoma	Bilateral diode laser and goniotomy	0.61	55	33
8	M	Asian	Primary glaucoma	Bilateral goniotomy, right trabeculectomy, left diode laser, right Baerveldt tubes and right cyclo laser	9.64	16	17
9	M	Asian	Primary glaucoma	Bilateral diode laser	0.74	18	7.8
10	M	Asian	Primary glaucoma	Bilateral diode laser	0.79	18	30
11	M	African	Primary glaucoma	Bilateral cyclo-diode laser. Left nasal goniotomy, Left trabeculectomy	0.49	32	18
12*	M	Caucasian	Right secondary to Sturge Weber syndrome	Right goniotomy	1.45	11	14
13	M	Asian	Primary glaucoma	Bilateral diode laser and goniotomy None	0.65 0.2	34 30	36 28
14	M	Asian	Primary glaucoma	Bilateral goniotomy, right trabeculotomy and diode laser, right Baerveldt tubes and cyclo laser	3.99	20.9	24.3
15	F	Asian	Primary glaucoma	Bilateral trabeculectomy, repeated right trabeculectomy	9.26	35	31
16	F	Asian	Primary glaucoma	Bilateral trabeculectomy, repeated right trabeculectomy	8.85	39	36
17	F	Caucasian	Primary glaucoma	Left trabeculectomy, right goniotomy. repeated right goniotomy	0.87	33	17
19**	M	Asian	Secondary glaucoma	Right pseudophakia, goniotomy	0.75	22	25

20	M	Caucasian	Primary glaucoma	BE cyclo diode laser. LE nasal goniotomy attempted. LE trabeculectomy	5.18 5.6 5.86	38 28 24	18 29 22
21	F	Caucasian	Primary glaucoma	Repeated right goniotomy Repeated right goniotomy	2.34 2.91	21 17	18 18
22**	F	Caucasian	Secondary glaucoma	Right aphakia 2016, right contact lens	5.51	26	17
23	F	Caucasian	Primary glaucoma	Repeated bilateral goniotomy	5.77	13	17
24	M	Asian	Primary glaucoma	Repeated bilateral goniotomy	8.71	21	18
25	F	Caucasian	Primary glaucoma	Repeated bilateral goniotomy	9.25	19	14
26	M	Asian	Primary glaucoma	Bilateral Trabeculectomy+ MMC	1.43	39	36
27	F	Asian	Primary glaucoma	Bilateral Trabeculectomy+ MMC, repeated right Trabeculectomy at 4 years old	9.48	30	28
28	M	African	Primary glaucoma	Repeated bilateral goniotomy	8.44	24	22
29	F	Caucasian	Primary glaucoma	Bilateral nasal goniotomy. Repeated left goniotomy. Right Trabeculectomy+ MMC.	5.42	38	44
30	F	Asian	Primary glaucoma	Bilateral diode. Bilateral nasal goniotomy. Left temporal goniotomy. Bilateral trabeculotomy Repeated bilateral goniotomy	0.25 0.96 2	38 22 25	44 15 27
31	F	Asian	Primary glaucoma	Trabeculotomy & Trabeculectomy	2.02	9*	11*
32	F	Asian	Primary glaucoma	Right trabeculotomy	5.12	22	22
					7.42	18	26
33	M	Caucasian	Primary glaucoma	Bilateral goniotomy	8.11 8.33	18 21	28 22
34*	F	Asian	Secondary left glaucoma to Sturge Weber syndrome	Left goniotomy	7.16 7.72	13 12	18 19
35*	F	Caucasian	Secondary right glaucoma to Sturge Weber syndrome	Right goniotomy	5.56 4.99 4.75	19 21 19	11 13 17
36*	F	Caucasian	Primary glaucoma	Trabeculotomy & Trabeculectomy	3.62 4.29	25 11*	22 11*
37	M	Asian	Primary glaucoma	diode laser cyclo-photocoagulation	0.48	19	25

(*) Unilateral glaucoma secondary to Sturge weber syndrome

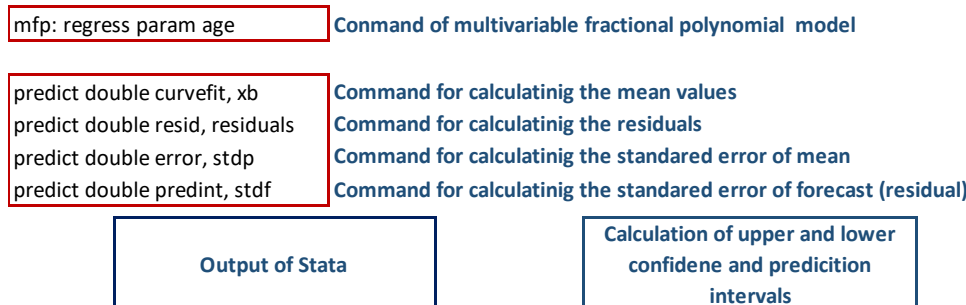
(**) Secondary glaucoma either with pseudophakia or aphakia

(***) primary glaucoma examined under general anaesthesia with low IOP.

In some cases more than one operation was done

9.2 Examples of steps of statistical analysis

9.2.1 Calculating the mean value and 95 % confidence and prediction intervals



A	B	C	D	E	B+(D*1.96)	B-(D*1.96)	B+(E*1.96)	B-(E*1.96)
aage_1	curvefit	resid	error	predint	error+	error-	pred+	pred-
-145.61	70.95	97.74	1.08	20.50	73.07	68.83	111.12	30.78
-145.61	70.95	-18.00	1.08	20.50	73.07	68.83	111.12	30.78
-145.61	70.95	-12.71	1.08	20.50	73.07	68.83	111.12	30.78
-145.61	70.95	-11.46	1.08	20.50	73.07	68.83	111.12	30.78
-145.61	70.95	-23.83	1.08	20.50	73.07	68.83	111.12	30.78
-145.61	70.95	-24.13	1.08	20.50	73.07	68.83	111.12	30.78
-145.61	70.95	-52.51	1.08	20.50	73.07	68.83	111.12	30.78
-145.61	70.95	-36.72	1.08	20.50	73.07	68.83	111.12	30.78
-145.61	70.95	-37.26	1.08	20.50	73.07	68.83	111.12	30.78
-145.58	70.95	-2.56	1.08	20.50	73.06	68.83	111.12	30.77
-145.58	70.95	-9.07	1.08	20.50	73.06	68.83	111.12	30.77
-145.58	70.95	-38.48	1.08	20.50	73.06	68.83	111.12	30.77
-145.58	70.95	28.52	1.08	20.50	73.06	68.83	111.12	30.77
-145.58	70.95	3.34	1.08	20.50	73.06	68.83	111.12	30.77
-145.51	70.94	50.02	1.08	20.50	73.06	68.83	111.12	30.77
-145.51	70.94	-16.70	1.08	20.50	73.06	68.83	111.12	30.77
-145.14	70.93	21.56	1.08	20.50	73.05	68.82	111.11	30.76
-145.14	70.93	-70.93	1.08	20.50	73.05	68.82	111.11	30.76
-145.08	70.93	15.65	1.08	20.50	73.05	68.82	111.10	30.76
-145.08	70.93	-11.63	1.08	20.50	73.05	68.82	111.10	30.76
-145.04	70.93	6.40	1.08	20.50	73.04	68.82	111.10	30.76
-144.88	70.93	13.52	1.08	20.50	73.04	68.81	111.10	30.75
-144.88	70.93	2.87	1.08	20.50	73.04	68.81	111.10	30.75
-144.88	70.93	-11.14	1.08	20.50	73.04	68.81	111.10	30.75

9.2.2 Comparing the difference of two groups

- Commands of multivariable fractional polynomial regression to transform the age automatically to the best fit power

```
mfp, center(no): reg slaod aage
```

Command

Deviance for model with all terms untransformed = 15551.885, 1161 observations

Variable	Model (vs.)	Deviance	Dev diff.	P	Powers	(vs.)
aage	lin.	FP2 15551.885	185.541	0.000+	1	-2 -2
	FP1	15368.793	2.449	0.296	-2	
	Final	1.5e+04		-2		

Transformations of covariates:

```
> gen double laage_1 = X^-2 if e(sample)
 (where: X = aage/100)
```

The age is transformed to different power

Final multivariable fractional polynomial model for slaod

Variable	-----Initial-----	-----Final-----				
	df	Select	Alpha	Status	df	Powers
aage	4	1.0000	0.0500	in	2	-2

Source | SS df MS Number of obs = 1,161
F(1, 1159) = 328.74
Model | 10817241.7 1 10817241.7 Prob > F = 0.0000
Residual | 38137475.8 1,159 32905.5011 R-squared = 0.2210
Adj R-squared = 0.2203
Total | 48954717.5 1,160 42202.3427 Root MSE = 181.4

slaod | Coef. Std. Err. t P>|t| [95% Conf. Interval]

laage_1 -3.181834 .1754905 -18.13 0.000 3.526149 -2.83752
_cons 728.621 6.083671 119.77 0.000 716.6848 740.5573

Deviance:15368.793.

The p value of the model

2. Commands of conducting mixed model adjusted for transformed age, angle, gender and eye variation and comparing the nasal and temporal angle measurements.

COPY FROM STATA INTO HERE (LEAVE EMPTY IF LINEAR)						CHECK MODEL
TRANSFORMATIONS		offset	adder	divider	laage_1	
gen double laage_1 = X^-2 if e(sample)	<i>age</i>	9	0	100	-2	ERROR
	0	9.0	9	0.09	123.457	0.000
	3	12.0	12	0.12	69.444	0.000
	6	15.0	15	0.15	44.444	0.000
	9	18.0	18	0.18	30.864	0.000
ADDER - DIVIDER	12	21.0	21	0.21	22.676	0.000
(where: X = aage/100)	18	27.0	27	0.27	13.717	0.000
	24	33.0	33	0.33	9.183	0.000
	36	45.0	45	0.45	4.938	0.000
	48	57.0	57	0.57	3.078	0.000
	60	69.0	69	0.69	2.100	0.000
	72	81.0	81	0.81	1.524	0.000
	96	105.0	105	1.05	0.907	0.000
	120	129.0	129	1.29	0.601	0.000
	168	177.0	177	1.77	0.319	0.000
	216	225.0	225	2.25	0.198	0.000
	300	309.0	309	3.09	0.105	0.000
	420	429.0	429	4.29	0.054	0.000
	600	609.0	609	6.09	0.027	0.000
COPY AND PASTE INTO STATA						
MODEL ESTIMATIONS						
mixed slaod ib0.angle##c.laage_1 i.eye i.gender id:, covariance(identity) nocons						
The output of command						
<pre>slaod Coef. Std. Err. z P> z [95% Conf. Interval] -----+ 1.angle -17.30587 10.96996 -1.58 0.115 -38.80659 4.194847 lpma_1 -3.762826 .2609255 -14.42 0.000 -4.274231 -3.251422 angle#c.lpma_1 1 .6786002 .3619209 1.87 0.061 -.0307517 1.387952 1.eye 4.432726 10.00249 0.44 0.658 -15.1718 24.03726 1.gender -37.74084 10.1004 -3.74 0.000 -57.53726 -17.94442 _cons 756.4646 10.9312 69.20 0.000 735.0398 777.8893 -----+ chi2(2) = 4.30 Prob > chi2 = 0.1167</pre>						
 Non significant difference between nasal and temporal SL-AOD						

3. Commands of lincom function for calculating the coefficient of variation, the z score and the significance levels between two groups at different ages

COPY AND PASTE INTO STATA		group	baseline		
TIME POINT DIFFERENCES	factors	interaction term 1	interaction term 2		
lincom i1.angle + 123.45679012345	i1.angle	123.456790123457 * i1.angle		0	
lincom i1.angle + 22.675736961451	i1.angle	22.6757369614512 * i1.angle		12	
lincom i1.angle + 4.9382716049382	i1.angle	4.93827160493827 * i1.angle		48	
lincom i1.angle + 1.5241579027587	i1.angle	1.52415790275873 * i1.angle		120	
lincom i1.angle + 0.0269628263513	i1.angle	0.0269628263513095 * i1.angle		420	

The output of command on Stata

```

SELECT ALL AND PASTE
1
2 .lincom i1.angle + 123.456790123457 * i1.angle#c.ipma_1
3
4 ( 1) [slaod]1.angle + 123.4568*[slaod]1.angle#c.ipma_1 = 0
5
6 -----
7   slaod | Coef. Std. Err. z P>|z| [95% Conf. Interval]
8   -----+
9   (1) | 66.47193 41.38532 1.61 0.108 -14.64181 147.5857
10
11
12 .
13 .lincom i1.angle + 22.6757369614512 * i1.angle#c.ipma_1
14
15 ( 1) [slaod]1.angle + 22.67574*[slaod]1.angle#c.ipma_1 = 0
16
17 -----
18   slaod | Coef. Std. Err. z P>|z| [95% Conf. Interval]
19   -----+
20   (1) | -1.918114 10.65272 -0.18 0.857 -22.79707 18.96084
21
22
23 .
24 .lincom i1.angle + 4.93827160493827 * i1.angle#c.ipma_1
25
26 ( 1) [slaod]1.angle + 4.938272*[slaod]1.angle#c.ipma_1 = 0
27
28 -----
29   slaod | Coef. Std. Err. z P>|z| [95% Conf. Interval]
30   -----+
31   (1) | -13.95476 10.36208 -1.35 0.178 -34.26406 6.35454
32
33
34 .
35 .lincom i1.angle + 1.52415790275873 * i1.angle#c.ipma_1
36
37 ( 1) [slaod]1.angle + 1.524158*[slaod]1.angle#c.ipma_1 = 0
38
39 -----
40   slaod | Coef. Std. Err. z P>|z| [95% Conf. Interval]
41   -----+
42   (1) | -16.27158 10.75435 -1.51 0.130 -37.34972 4.806564
43

```

Summary of statistics on excel template

TIME POINT GROUP DIFFERENCES								
offset	group 1	group 2	time	Coef.	Std. Err.	z	P>z	95% Conf Interval
Postmenstrual age	9	1	0	9	66.47	41.39	1.61	0.11 -14.64 147.59
	20	1	0	21	-1.92	10.65	-0.18	0.86 -22.80 18.96
	31	1	0	57	-13.95	10.36	-1.35	0.18 -34.26 6.35
	42	1	0	129	-16.27	10.75	-1.51	0.13 -37.35 4.81
	53	1	0	609.0	-17.29	10.97	-1.58	0.12 -38.78 4.21

4. Commands of lincom function for calculating the measurement of parameter for each group at given age according to outcome of the equation of model curve

The output of command on Stata

COPY AND PASTE INTO STATA

MEAN POINT ESTIMATIONS	group	age	factor 1	age factor	interaction 1	interaction 2	
lincom_cons + 123.456790123457*		123.456790123457			0	baseline	
lincom_cons + 69.4444444444444*		69.4444444444444			3	0	
lincom_cons + 44.4444444444444*		44.4444444444444			6		
lincom_cons + 30.8641975308642*		30.864197530864			9		
lincom_cons + 22.6757369614512*		22.675736961451			12		
lincom_cons + 13.7174211248285*		13.717421124828			18		
lincom_cons + 9.18273645546373*		9.1827364554637			24		
lincom_cons + 4.93827160493827*		4.9382716049382			36		
lincom_cons + 3.07787011388119*		3.0778701138811			48		
lincom_cons + 2.10039907582441*		2.1003990758244			60		
lincom_cons + 1.52415790275873*		1.5241579027587			72		
lincom_cons + 0.90702947845805*		0.9070294784580			96		
lincom_cons + 0.600925425154738		0.6009254251547			120		
lincom_cons + 0.319193079894028		0.3191930798940			168		
lincom_cons + 0.197530864197531		0.1975308641975			216		
lincom_cons + 0.104732878792639		0.1047328787926			300		
lincom_cons + 0.054335718671383		0.0543357186713			420		
lincom_cons + 0.026962826351305		0.0269628263513			600		
lincom_cons + i1.angle + 123.456790123457*i1.angle		123.456790123457	57 * i1.angle#i1		0	group	
lincom_cons + i1.angle + 69.4444444444444*i1.angle		69.4444444444444	44 * i1.angle#i1		3	1	
lincom_cons + i1.angle + 44.4444444444444*i1.angle		44.4444444444444	44 * i1.angle#i1		6		
lincom_cons + i1.angle + 30.864197530864*i1.angle		30.864197530864	42 * i1.angle#i1		9		
lincom_cons + i1.angle + 22.675736961451*i1.angle		22.675736961451	42 * i1.angle#i1		12		
lincom_cons + i1.angle + 13.717421124828*i1.angle		13.717421124828	35 * i1.angle#i1		18		
lincom_cons + i1.angle + 9.18273645546373*i1.angle		9.1827364554637	73 * i1.angle#i1		24		
lincom_cons + i1.angle + 4.93827160493827*i1.angle		4.9382716049382	27 * i1.angle#i1		36		
lincom_cons + i1.angle + 3.07787011388119*i1.angle		3.0778701138811	19 * i1.angle#i1		48		
lincom_cons + i1.angle + 2.10039907582441*i1.angle		2.1003990758244	41 * i1.angle#i1		60		
lincom_cons + i1.angle + 1.52415790275873*i1.angle		1.5241579027587	73 * i1.angle#i1		72		
lincom_cons + i1.angle + 0.90702947845805*i1.angle		0.9070294784580	35 * i1.angle#i1		96		
lincom_cons + i1.angle + 0.600925425154738*i1.angle		0.6009254251547	38 * i1.angle#i1		120		
lincom_cons + i1.angle + 0.319193079894028*i1.angle		0.3191930798940	128 * i1.angle#i1		168		
lincom_cons + i1.angle + 0.197530864197531*i1.angle		0.1975308641975	31 * i1.angle#i1		216		
lincom_cons + i1.angle + 0.104732878792639*i1.angle		0.1047328787926	39 * i1.angle#i1		300		
lincom_cons + i1.angle + 0.054335718671383*i1.angle		0.0543357186713	83 * i1.angle#i1		420		
lincom_cons + i1.angle + 0.026962826351305*i1.angle		0.0269628263513	395 * i1.angle#i1		600		

Summary of statistics on excel template

TIME POINT MEAN ESTIMATES

GROUP	0							
offset	group	Age	Coef.	Std. Err.	z	P>z	[95% Conf. Interval]	
9	0	9	291.9181	30.20596	9.66	0	232.7155	351.1207
20	0	12	495.1572	17.61068	28.12	0	460.6409	529.6735
31	0	15	589.2279	12.87855	45.75	0	563.9864	614.4694
42	0	18	640.328	11.09746	57.7	0	618.5774	662.0786
53	0	21	671.1397	10.46616	64.12	0	650.6264	691.653
64	0	27	704.8483	10.25209	68.75	0	684.7546	724.942
75	0	33	721.9115	10.34534	69.78	0	701.6351	742.188
86	0	45	737.8827	10.55275	69.92	0	717.1997	758.5658
97	0	57	744.8831	10.67866	69.75	0	723.9533	765.8129
108	0	69	748.5612	10.75301	69.61	0	727.4856	769.6367
119	0	81	750.7295	10.79942	69.52	0	729.563	771.8959
130	0	105	753.0516	10.85121	69.4	0	731.7836	774.3196
141	0	129	754.2034	10.8777	69.33	0	732.8835	775.5233
152	0	177	755.2635	10.90253	69.27	0	733.895	776.6321
163	0	225	755.7213	10.91339	69.25	0	734.3315	777.1112
174	0	309	756.0705	10.92173	69.23	0	734.6643	777.4767
GROUP	1							
offset	group	time	Coef.	Std. Err.	z	P>z	[95% Conf. Interval]	
207	1	9	358.3901	29.54229	12.13	0	300.4882	416.2919
218	1	12	524.9764	17.38611	30.2	0	490.9002	559.0525
229	1	15	602.082	12.83504	46.91	0	576.9258	627.2382
240	1	18	643.9666	11.11669	57.93	0	622.1782	665.7549
251	1	21	669.2216	10.49667	63.76	0	648.6485	689.7947
262	1	27	696.8511	10.26437	67.89	0	676.7333	716.9689
273	1	33	710.8371	10.33608	68.77	0	690.5787	731.0954
284	1	45	723.928	10.51684	68.84	0	703.3154	744.5406
295	1	57	729.6659	10.62936	68.65	0	708.8327	750.499
306	1	69	732.6806	10.69632	68.5	0	711.7162	753.645
317	1	81	734.4579	10.73826	68.4	0	713.4113	755.5045
328	1	105	736.3612	10.78519	68.28	0	715.2226	757.4998
339	1	129	737.3053	10.80923	68.21	0	716.1196	758.491
350	1	177	738.1743	10.8318	68.15	0	716.9443	759.4042
361	1	225	738.5495	10.84167	68.12	0	717.3002	759.7988
372	1	309	738.8357	10.84926	68.1	0	717.5715	760.0999

9.3 Examples of information leaflets and consent forms

The following pages shows examples of information leaflet and consent forms used for recruitment of children without ocular problem and children with ocular problems.

INFORMATION LEAFLET FOR PARENTS/GUARDIANS OF CHILDREN WITHOUT EYE PROBLEMS

Characterisation of normal and abnormal ocular development using ultra-high resolution optical coherence tomography (UHR-SD OCT)

Principal Investigator: Professor Irene Gottlob, Ophthalmology

We invite you and your child to consider taking part in a research project. Before you decide it is important for you to understand why the research is being done and what it will involve. Please take time to read the following information carefully and discuss it with others if you wish. Ask us if there is anything that is not clear or if you would like more information. Take time to decide whether or not you wish to take part.

What is the purpose of the study?

The retina is a structure at the back of the eye that is important for vision. It creates a picture that is sent to the brain via the optic nerve to produce the image that we see. It is made up of 'seeing cells' called rods and cones. The development of the retina is not completely understood and maybe affected by our genes and other eye conditions.

We wish to study the normal and abnormal development of the retina and optic nerve in infants and children and compare it to adults. We hope that the knowledge we gain from this research will lead to improved diagnosis, management and treatment of conditions affecting retinal development.

What will be involved if my child takes part in the study?

We will ask you some questions about your family and child's medical history including any problems they may have had with their eyes.

We will then perform eye examinations and special tests as described below. If we perform all the examinations it will take between 30 minutes and 2 hours but we can spread out the tests over a number of visits and give you and your child sufficient time to rest. All these examinations are completely harmless.

Eye examination

We will examine how clearly your child can see (similar to the tests performed at the opticians), how well the eyes move in different directions and check for a squint. We will also use a special microscope to examine the front and back of the eye in detail.

This examination will be performed at the University Hospitals of Leicester NHS Trust in an ophthalmology clinic and should take no longer than an hour.

Optical Coherence Tomography (OCT)

We will take images of the back of the eye using a scanning light (OCT). To ensure the best quality pictures we may put drops into your child's eyes to dilate the pupil. The eye drops may sting when inserted and will blur his/her vision for 4-6 hours after they have been used. All the effects of the drops are temporary.

This examination will be performed at the University Hospitals of Leicester NHS Trust in an ophthalmology clinic and should take no longer than 30 minutes depending on how easily we can take the images.

Repeat examinations

After your first visit, we may invite you and your child to attend further appointments to repeat the examinations.

The eye continues to develop throughout early childhood and our study aims to monitor these changes.

If you agree we may ask you to attend regular appointments:

- every 3 months until the age of 1 year
- every 6 months until 3 years of age
- yearly until 7 years of age.

This will be a maximum of 12 examinations over a period of 5 years however each examination is optional and you can choose which (if any) repeat reviews you would like.

Future appointments may include some or all of the examinations above depending on the age of your child. The repeat examinations may take up to 2 hours to complete and can be spread over a number of visits if required.

What is the benefit of this study to others and your child?

This study aims to improve our understanding of the development of the retina and optic nerve in people with and without eye anomalies. This may not lead to direct benefits for participants to the study, however increasing our knowledge of ocular development will hopefully lead to early diagnosis and treatment of patients in the future.

What will happen if any abnormalities are found during the study?

If any examinations or tests demonstrate an abnormality that may affect your child's health you will be informed by your General Practitioner or hospital consultant.

Will information obtained in the study be confidential?

Any personal information and individual results will be kept confidential. The tests will be recorded in your child's medical records and will be treated with the usual degree of confidentiality under the Data Protection Act. Your child will not be identified in any documents relating to the study. Any information will be accessible by research staff only and will be stored within the research department in a secure and locked location and/or on a password-protected database.

What will happen to the data obtained in this study?

The data collected during this study may include clinical information and images. As part of this process we will allocate a unique coding number to your child's data. This unique code and images may be given to collaborators. This is to ensure only those researchers that have a direct link to the project within this department will have access to personal data.

What if my child is harmed by the study?

All the tests within this study have minimal risk but if your child is harmed by taking part in this research project, there are no special compensation arrangements. If your child is harmed due to someone's negligence, then you may have grounds for a legal action but you may have to pay for it. Regardless of this, if you have any concerns about any aspect of the way you have been approached or treated during the course of this study, the normal National Health Service complaints mechanisms should be available to you. This can be done by contacting the NHS Patient Information and Liaison Service (PILS) on 0808178 8337 or by writing to:

The Chief Executive
Trust Headquarters
Gwendolen House
Gwendolen Road
Leicester, LE5 4QF

Who is organising and funding the research?

The project is being undertaken by the University of Leicester Ophthalmology Group. It is being sponsored by The University of Leicester and is being funded by the Medical Research Council.

Who has reviewed the study?

All research in the NHS is looked at by an independent group of people called a Research Ethics Committee to protect your safety, rights, wellbeing and dignity. This study has been reviewed and given favourable opinion by a Research Ethics Committee.

What happens if I do not want my child to participate in this study or if I want to withdraw from the study?

Your child is not under any obligation to participate in this study. If your child does enter the study and you subsequently wish to withdraw their participation please inform the Ophthalmology Group at the University of Leicester. You do not need to give a reason for doing so. Your child's medical care will not be affected if you decide not to participate in the study.

Will we receive out of pocket expenses for taking part in the study?

Return travel expenses from your home to the Leicester Royal Infirmary may be reimbursed if you come especially for the research.

What will happen to the results of the research study?

The clinical information and images that we take and analyse are for research purposes only, to help us investigate the development of the eye. This study may take over five years to complete and the results will be published in medical journals.

Who do I contact for further information?

Professor Irene Gottlob
Ophthalmology
The Robert Kilpatrick Clinical Sciences Building
PO Box 65, The Leicester Royal Infirmary
Leicester, LE2 7LX.

Tel: 0116 2586291
Fax: 0116 2558810

Thank you for reading this

Centre Number:
Study Number:
Patient Identification Number for this trial:

University Hospitals of Leicester **NHS**
NHS Trust

Leicester Royal Infirmary
Leicester
LE1 5WW

Tel: 0116 2541414
Fax: 0116 2585631
Minicom: 0116 2586878

CONSENT FORM FOR PARENTS/GUARDIANS OF CHILDREN WITHOUT EYE PROBLEMS

**Characterisation of normal and abnormal ocular development using ultra-high resolution
optical coherence tomography (UHR-SD OCT)**

Name of Researcher/Principal Investigator: Professor Irene Gottlob
Professor of Ophthalmology
Tel: 0116 2586291

Name of participant: _____

Address of participant: _____

DOB of participant: _____

This form shall be read in conjunction with the Information Leaflet for Parents/Guardians of Children Without Eye Problems Version 2 dated 18th February 2013.

Please initial the following box(es):

- I confirm that I have read and understand the Information Leaflet for Parents/Guardians of Children Without Eye Problems Version 2 dated 18th February 2013 for the above study and have had the opportunity to ask questions.
- I understand that I may withdraw my consent at any time without justifying my decision and without affecting my child's normal care and medical management.
- I understand that if my child's investigations produce information that has immediate clinical relevance to my child, I will be informed by my hospital consultant or GP and be given an opportunity to discuss the results.
- I understand that sections of any of my child's medical notes may be looked at by responsible individuals from the research team, [Ophthalmology, University of Leicester], Sponsor and NHS trust or from regulatory authorities where it is relevant to my child taking part in research. I give permission for these individuals to have access to his/her records.

OCT and ocular development
Consent Form for Parents/Guardians of Children Without Eye Problems Version 2 dated 18/02/13

Centre Number:
Study Number:
Patient Identification Number for this trial:

5. I understand that images of my child may be transferred to non-commercial research partners of the University Hospitals of Leicester NHS Trust and Ophthalmology, University of Leicester but that the personal information will be removed prior to transfer.

6. I agree to my child taking part in the following eye examinations (tick):

- Eye examination
- Optical coherence tomography

7. I agree for any images/videos collected to be used for teaching purposes and/or publications

8. I agree to my child taking part in the above study

I agree for my child to take part in the above study.

Signature of parent/guardian : _____

(Name in BLOCK LETTERS): _____

Date: _____

I agree to take part in the above study (to be completed by child).

Signature of child (if applicable): _____

(Name in BLOCK LETTERS): _____

Date: _____

I confirm I have explained the nature of the Study, as detailed in the Information Leaflet for Parents/Guardians of Children Without Eye Problems Version 2 dated 18th February 2013 in terms, which in my judgment are suited to the understanding of the adult.

Signature of investigator: _____

(Name in BLOCK LETTERS): _____

Date: _____

INFORMATION LEAFLET FOR PARENTS/GUARDIANS OF CHILDREN WITH EYE PROBLEMS

Characterisation of normal and abnormal ocular development using ultra-high resolution optical coherence tomography (UHR-SD OCT)

Principal Investigator: Professor Irene Gottlob, Ophthalmology

We invite you and your child to consider taking part in a research project. Before you decide it is important for you to understand why the research is being done and what it will involve. Please take time to read the following information carefully and discuss it with others if you wish. Ask us if there is anything that is not clear or if you would like more information. Take time to decide whether or not you wish to take part.

What is the purpose of the study?

The retina is a structure at the back of the eye that is important for vision. It creates a picture that is sent to the brain via the optic nerve to produce the image that we see. It is made up of 'seeing cells' called rods and cones. The development of the retina is not completely understood and maybe affected by our genes and other eye conditions.

We wish to study the normal and abnormal development of the retina and optic nerve in infants and children and compare it to adults. We hope that the knowledge we gain from this research will lead to improved diagnosis, management and treatment of conditions affecting retinal development.

What will be involved if my child takes part in the study?

We will ask you some questions about your family and child's medical history including any problems they may have had with their eyes.

We will then perform eye examinations and special tests as described below. If we perform all the examinations it will take up to a maximum of 6 hours but we will spread out the tests over a number of visits and give you and your child sufficient time to rest. All these examinations are completely harmless.

Eye examination

We will examine how clearly your child can see (similar to the tests performed at the opticians), how well the eyes move in different directions and check for a squint. We will also use a special microscope to examine the front and back of the eye in detail.

This examination will be performed at the University Hospitals of Leicester NHS Trust in an ophthalmology clinic and should take no longer than an hour.

Optical Coherence Tomography (OCT)

We will take images of the back of the eye using a scanning light (OCT). To ensure the best quality pictures we may put drops into your child's eyes to dilate the pupil. The eye drops may sting when inserted and will blur his/her vision for 4-6 hours after they have been used. All the effects of the drops are temporary.

This examination will be performed at the University Hospitals of Leicester NHS Trust in an ophthalmology clinic and should take no longer than 30 minutes depending on how easily we can take the images.

Eye movement recordings

We may record your child's eye movements using infrared video cameras. This involves placing special small cameras in front of the eyes and asking him/her to follow a target on a screen that moves in different directions.

This examination will be performed at the University Hospitals of Leicester NHS Trust in an ophthalmology clinic and can take up to 30 minutes.

Photography/ Video recording

We may ask to take photographs and/or videos of the eyes in different positions to help us diagnose and monitor the eye condition.

This examination will be performed at the University Hospitals of Leicester NHS Trust in an ophthalmology clinic and can take up to 30 minutes.

Electrophysiology

We may ask to measure how well your child's eyes send electrical messages to the brain. It involves placing stickers (tape wires) around the eyes and recording the activity while your child looks at objects in the light and dark.

This examination will be performed at the University Hospitals of Leicester NHS Trust in the Medical Physics Department and can take up to 90 minutes. If successful this will be completed only once.

Repeat examinations

After your first visit, we may invite you and your child to attend further appointments to repeat the examinations.

The eye continues to develop throughout early childhood and our study aims to monitor these changes.

If you agree we may ask you to attend regular appointments:

- every 3 months until the age of 1 year
- every 6 months until 3 years of age
- yearly until 7 years of age.

This will be a maximum of 12 examinations over a period of 5 years however each examination is optional and you can choose which (if any) repeat reviews you would like.

Future appointments may include some or all of the examinations above depending on the diagnosis and age of your child. The repeat examinations may take between 30 minutes and 4 hours to complete and can be spread over a number of visits if you would prefer.

Why has my child been asked to participate?

Your child has been asked to participate in this study as he/she may have an eye condition that affects the development of the retina or optic nerve.

What is the benefit of this study to others and your child?

This study aims to improve our understanding of the development of the retina and optic nerve in people with and without eye anomalies. This may not lead to direct benefits for participants to the study, however increasing our knowledge of retinal development will hopefully lead to early diagnosis and treatment of patients in the future.

Will information obtained in the study be confidential?

Any personal information and individual results will be kept confidential. The tests will be recorded in your child's medical records and will be treated with the usual degree of confidentiality under the Data Protection Act. Your child will not be identified in any documents relating to the study. Any information will be accessible by research staff only and will be stored within the research department in a secure and locked location and/or on a password-protected database.

We will also write to your General Practitioner to inform them that your child has been included in this study.

What will happen to the data obtained in this study?

The data collected during this study may include clinical information, images and video recordings of your child's eye movements. As part of this process we will allocate a unique coding number to your data. This unique code and images may be given to collaborators. This is to ensure only those researchers that have a direct link to the project within this department will have access to personal data.

What if my child is harmed by the study?

All the tests within this study have minimal risk but if your child is harmed by taking part in this research project, there are no special compensation arrangements. If your child is harmed due to someone's negligence, then you may have grounds for a legal action but you may have to pay for it. Regardless of this, if you have any concerns about any aspect of the way you have been approached or treated during the course of this study, the normal National Health Service complaints mechanisms should be available to you. This can be done by contacting the NHS Patient Information and Liaison Service (PILS) on 0808178 8337 or by writing to:

The Chief Executive
Trust Headquarters
Gwendolen House
Gwendolen Road
Leicester, LE5 4QF

Who is organising and funding the research?

The project is being undertaken by the University of Leicester Ophthalmology Group. It is being sponsored by The University of Leicester and is being funded by the Medical Research Council.

Who has reviewed the study?

All research in the NHS is looked at by an independent group of people called a Research Ethics Committee to protect your safety, rights, wellbeing and dignity. This study has been reviewed and given favorable opinion by a Research Ethics Committee.

What happens if I do not want my child to participate in this study or if I want to withdraw from the study?

Your child is not under any obligation to participate in this study. If your child does enter the study and you subsequently wish to withdraw their participation please inform the Ophthalmology Group at the University of Leicester. You do not need to give a reason for doing so. Your child's medical care will not be affected if you decide not to participate in the study.

Will we receive out of pocket expenses for taking part in the study?

Return travel expenses from your home to the Leicester Royal Infirmary may be reimbursed if you come especially for the research.

What will happen to the results of the research study?

The clinical information and images that we take and analyses are for research purposes only, to help us investigate the development of the eye. This study may take over five years to complete and the results will be published in medical journals.

Who do I contact for further information?

Professor Irene Gottlob
Ophthalmology
The Robert Kilpatrick Clinical Sciences Building
PO Box 65, The Leicester Royal Infirmary
Leicester, LE2 7LX.

Tel: 0116 2586291
Fax: 0116 2558810

Thank you for reading this

Centre Number:
Study Number:
Patient Identification Number for this trial:

University Hospitals of Leicester **NHS**
NHS Trust

Leicester Royal Infirmary
Leicester
LE1 5WW

Tel: 0116 2541414
Fax: 0116 2585631
Minicom: 0116 2586878

CONSENT FORM FOR PARENTS/GUARDIANS OF CHILDREN WITH EYE PROBLEMS

Characterisation of normal and abnormal ocular development using ultra-high resolution optical coherence tomography (UHR-SD OCT)

Name of Researcher/Principal Investigator: Professor Irene Gottlob
Professor of Ophthalmology
Tel: 0116 2586291

Name of participant: _____

Address of participant: _____

DOB of participant: _____

This form shall be read in conjunction with the Information Leaflet for Parents/Guardians of Children With Eye Problems Version 2 dated 18th February 2013.

Please initial the following box(es):

- I confirm that I have read and understand the Information Leaflet for Parents/Guardians of Children With Eye Problems Version 2 dated 18th February 2013 for the above study and have had the opportunity to ask questions.
- I understand that I may withdraw my consent at any time without justifying my decision and without affecting my child's normal care and medical management.
- I understand that if my child's investigations produce information that has immediate clinical relevance to my child, I will be informed by my hospital consultant or GP and be given an opportunity to discuss the results.
- I understand that sections of any of my child's medical notes may be looked at by responsible individuals from the research team, [Ophthalmology, University of Leicester], Sponsor and NHS trust or from regulatory authorities where it is relevant to my child taking part in research. I give permission for these individuals to have access to his/her records.

OCT and ocular development
Consent Form for Parents/Guardians of Children With Eye Problems Version 2 dated 18/02/13

Centre Number:
Study Number:
Patient Identification Number for this trial:

5. I understand that images of my child may be transferred to non-commercial research partners of the University Hospitals of Leicester NHS Trust and Ophthalmology, University of Leicester but that the personal information will be removed prior to transfer.

6. I agree to my child taking part in the following eye examinations (tick):

- Eye examination
- Optical coherence tomography
- Eye movement recording
- Photography /Video recording
- Electrophysiology

7. I agree for any images/videos collected to be used for teaching purposes and/or publications

8. I agree to my child taking part in the above study

I agree for my child to take part in the above study.

Signature of parent/guardian : _____

(Name in BLOCK LETTERS): _____

Date: _____

I agree to take part in the above study (to be completed by child).

Signature of child (if applicable): _____

(Name in BLOCK LETTERS): _____

Date: _____

I confirm I have explained the nature of the Study, as detailed in the Information Leaflet for Parents/Guardians of Children With Eye Problems Version 2 dated 18th February 2013 in terms, which in my judgment are suited to the understanding of the adult.

Signature of investigator: _____

(Name in BLOCK LETTERS): _____

Date: _____

9.4 Awards and Conferences

9.4.1 Award

1. Young investigator travel fellowship of ISER (International Society of Eye Research, Belfast, Northern Ireland. (Title: ***Hand-held Spectral Domain Optical Coherence Tomography Measurements of Anterior Chamber Angle in Children with Congenital Glaucoma***).

9.4.2 Conferences

Posters and Presentations

In 2017

1. A poster (Title: ***Reproducibility of measurements of irido-corneal angle in children using hand-held spectral domain optical coherence tomography***) at ARVO (the Association for Research in Vision and Ophthalmology), Baltimore, USA.
2. Free paper talk (Title: ***Changes of Anterior Chamber Morphometry with Age in Children using Hand-held Spectral Domain Optical Coherence Tomography***) at EVER (European vision and eye research Conference), Nice, France.
3. A rapid fire talk and a poster (Title: ***Reproducibility of Angle Metrics in Children Using Hand-held Spectral Domain Optical Coherence Tomography: Intra-observer and Inter-observer variability***) at EVER (European vision and eye research Conference) Nice, France. My abstracts were considered of great values and high interest.
4. A free talk (Title: ***Development of Anterior Chamber angle in Children: A Hand-held Spectral Domain Optical Coherence Tomography study***) at Paediatric OCT course, University of Leicester.

In 2018

5. A free paper talk (Title: ***A Hand-held Spectral Domain Optical Coherence Tomography Study of Development of the Anterior Chamber Angle in Children***) at 22nd Nottingham Eye Symposium.
6. A poster (Title: ***Hand-held Spectral Domain Optical Coherence Tomography Measurements of Anterior Chamber Angle in Children with Congenital Glaucoma***) at ISER (International Society of Eye Research, Belfast, Northern Ireland.
7. A free paper talk (Title: ***Hand Held Spectral Domain Optical Coherence Tomography Measurement of Anterior Chamber Angle Development in Preterm and Full-term Children***) at BIPOSA, Manchester, UK.

10. Chapter ten: Bibliography

- ABU-AMERO, K. K. & EDWARD, D. P. 1993. Primary Congenital Glaucoma. In: ADAM, M. P., ARDINGER, H. H., PAGON, R. A., WALLACE, S. E., BEAN, L. J. H., MEFFORD, H. C., STEPHENS, K., AMEMIYA, A. & LEDBETTER, N. (eds.) *GeneReviews(R)*. Seattle (WA).
- AIELLO, L. P. 1996. Vascular endothelial growth factor and the eye. Past, present and future. *Arch Ophthalmol*, 114, 1252-4.
- AKHTER, K. & SALIM, S. 2014. Sturge-Weber Syndrome and Secondary Glaucoma. *EyeNet Magazine*. The American Academy of Ophthalmology.
- AKIL, H., DASTIRIDOU, A., MARION, K., FRANCIS, B. & CHOPRA, V. 2017a. Repeatability, reproducibility, agreement characteristics of 2 SD-OCT devices for anterior chamber angle measurements. *Can J Ophthalmol*, 52, 166-170.
- AKIL, H., MARION, K., DASTIRIDOU, A., JENKINS, D., KRAMER, B., FRANCIS, B. A. & CHOPRA, V. 2017b. Identification of anterior chamber angle parameters with a portable SD-OCT device compared to a non-portable SD-OCT. *Int Ophthalmol*, 37, 31-37.
- ALMOALLEM, B., BAUWENS, M., WALRAEDT, S., DELBEKE, P., DE ZAEYTIJD, J., KESTELYN, P., MEIRE, F., JANSSENS, S., VAN CAUWENBERGH, C., VERDIN, H., HOOGHE, S., KUMAR THAKUR, P., COPPIETERS, F., DE LEENEER, K., DEVRIENDT, K., LEROY, B. P. & DE BAERE, E. 2015. Novel FRMD7 Mutations and Genomic Rearrangement Expand the Molecular Pathogenesis of X-Linked Idiopathic Infantile Nystagmus. *Invest Ophthalmol Vis Sci*, 56, 1701-10.
- ALZUHAIRY, S., ABU-AMERO, K. K., AL-SAHWAN, S. & EDWARD, D. P. 2015. A novel CYP1B1 mutation with congenital glaucoma and total aniridia. *Ophthalmic Genet*, 36, 89-91.
- AMERASINGHE, N., FOSTER, P. J., WONG, T. Y., HTOON, H. M., HE, M., SHEN, S. Y., AUNG, H. T., SAW, S.-M. & AUNG, T. 2009a. Variation of Angle Parameters in Asians: An Anterior Segment Optical Coherence Tomography Study in a Population of Singapore Malays. *Investigative Ophthalmology & Visual Science*, 50, 2626-2631.
- AMERASINGHE, N., FOSTER, P. J., WONG, T. Y., HTOON, H. M., HE, M., SHEN, S. Y., AUNG, H. T., SAW, S. M. & AUNG, T. 2009b. Variation of angle parameters in asians: an anterior segment optical coherence tomography study in a population of singapore malays. *Invest Ophthalmol Vis Sci*, 50, 2626-31.
- AMINI, H., FAKHRAIE, G., ABOLMAALI, S., AMINI, N. & DANESHVAR, R. 2012. Central corneal thickness in Iranian congenital glaucoma patients. *Middle East Afr J Ophthalmol*, 19, 194-8.
- ANDERSON, D. R. 1981. The development of the trabecular meshwork and its abnormality in primary infantile glaucoma. *Trans Am Ophthalmol Soc*, 79, 458-85.

- ANDERSON, K. L., LEWIS, R. A., BEJJANI, B. A., BAIRD, L., OTTERUD, B., TOMEY, K. F., ASTLE, W. F., DUEKER, D. K., LEPPERT, M. & LUPSKI, J. R. 1996. A gene for primary congenital glaucoma is not linked to the locus on chromosome 1q for autosomal dominant juvenile-onset open angle glaucoma. *J Glaucoma*, 5, 416-21.
- ANG, M., CHONG, W., TAY, W. T., YUEN, L., WONG, T. Y., HE, M.-G., SAW, S. M., AUNG, T. & MEHTA, J. S. 2012. Anterior Segment Optical Coherence Tomography Study of the Cornea and Anterior Segment in Adult Ethnic South Asian Indian Eyes. *Investigative Ophthalmology & Visual Science*, 53, 120-125.
- ARNOLD, J. 1995. Ocular manifestations of congenital rubella. *Curr Opin Ophthalmol*, 6, 45-50.
- ASRANI, S., SARUNIC, M., SANTIAGO, C. & IZATT, J. 2008. Detailed visualization of the anterior segment using Fourier-domain optical coherence tomography. *Archives of Ophthalmology*, 126, 765-771.
- ATCHISON, D. A., PRITCHARD, N., SCHMID, K. L., SCOTT, D. H., JONES, C. E. & POPE, J. M. 2005. Shape of the retinal surface in emmetropia and myopia. *Invest Ophthalmol Vis Sci*, 46, 2698-707.
- AUTZEN, T. & BJORNSTROM, L. 1989. Central corneal thickness in full-term newborns. *Acta Ophthalmol (Copenh)*, 67, 719-20.
- AUTZEN, T. & BJORNSTROM, L. 1991. Central corneal thickness in premature babies. *Acta Ophthalmol (Copenh)*, 69, 251-2.
- AVTAR, R. & SRIVASTAVA, R. 2007. Modelling aqueous humor outflow through trabecular meshwork. *Applied Mathematics and Computation*, 189, 734-745.
- AYSE, Y. K., ONDER, U. & SUHEYLA, K. 2011. Accuracy of Plusoptix S04 in children and teens. *Canadian Journal of Ophthalmology-Journal Canadien D Ophtalmologie*, 46, 153-157.
- BAIKOFF, G., LUTUN, E., FERRAZ, C. & WEI, J. 2004. Static and dynamic analysis of the anterior segment with optical coherence tomography. *J Cataract Refract Surg*, 30, 1843-50.
- BAKER, P. S. & TASMAN, W. 2008. Myopia in adults with retinopathy of prematurity. *Am J Ophthalmol*, 145, 1090-4.
- BALD, M., LI, Y. & HUANG, D. 2012. Anterior chamber angle evaluation with fourier-domain optical coherence tomography. *J Ophthalmol*, 2012, 103704.
- BANERJEE, A., CHAKRABORTY, S., CHAKRABORTY, A., CHAKRABARTI, S. & RAY, K. 2016. Functional and Structural Analyses of CYP1B1 Variants Linked to Congenital and Adult-Onset Glaucoma to Investigate the Molecular Basis of These Diseases. *Plos One*, 11.
- BARISHAK, Y. R. 1992. Embryology of the eye and its adnexae. *Dev Ophthalmol*, 24, 1-142.

- BARKAN, O. 1947. Goniotomy for congenital glaucoma; urgent need for early diagnosis and operation. *J Am Med Assoc*, 133, 526-33.
- BARKAN, O. 1955. Pathogenesis of congenital glaucoma: gonioscopic and anatomic observation of the angle of the anterior chamber in the normal eye and in congenital glaucoma. *Am J Ophthalmol*, 40, 1-11.
- BARKANA, Y., DORAIRAJ, S. K., GERBER, Y., LIEBMANN, J. M. & RITCH, R. 2007. Agreement between gonioscopy and ultrasound biomicroscopy in detecting iridotrabecular apposition. *Archives of Ophthalmology*, 125, 1331-1335.
- BEJJANI, B. A., XU, L., ARMSTRONG, D., LUPSKI, J. R. & RENEKER, L. W. 2002. Expression patterns of cytochrome P4501B1 (Cyp1b1) in FVB/N mouse eyes. *Exp Eye Res*, 75, 249-57.
- BELOVAY, G. W., ALABDULJALIL, T., PAVLIN, C. J., HAMEL, P. & ALI, A. 2015. Plateau iris in children. *J AAPOS*, 19, 377-9.
- BHANDARI, R., FERRI, S., WHITTAKER, B., LIU, M. & LAZZARO, D. R. 2011. Peters anomaly: review of the literature. *Cornea*, 30, 939-44.
- BHARDWAJ, V. & RAJESHBHAI, G. P. 2013. Axial length, anterior chamber depth-a study in different age groups and refractive errors. *J Clin Diagn Res*, 7, 2211-2.
- BHATTI, S., PAYSSE, E. A., WEIKERT, M. P. & KONG, L. 2016. Evaluation of structural contributors in myopic eyes of preterm and full-term children. *Graefes Arch Clin Exp Ophthalmol*, 254, 957-62.
- BIRCH, E. E., CHENG, C., STAGER, D. R., WEAKLEY, D. R. & STAGER, D. R. 2009. The critical period for surgical treatment of dense congenital bilateral cataracts. *Journal of Aapos*, 13, 67-71.
- BOLZ, M., PRINZ, A., DREXLER, W. & FINDL, O. 2007. Linear relationship of refractive and biometric lenticular changes during accommodation in emmetropic and myopic eyes. *Br J Ophthalmol*, 91, 360-5.
- BRANDT, J. D., BEISER, J. A., KASS, M. A., GORDON, M. O. & STUD, O. H. T. 2001. Central corneal thickness in the Ocular Hypertension Treatment Study (OHTS). *Ophthalmology*, 108, 1779-1788.
- BROWN, N. P., KORETZ, J. F. & BRON, A. J. 1999. The development and maintenance of emmetropia. *Eye (Lond)*, 13 (Pt 1), 83-92.
- CAUDURO, R. S., FERRAZ CDO, A., MORALES, M. S., GARCIA, P. N., LOPES, Y. C., SOUZA, P. H. & ALLEMANN, N. 2012. Application of anterior segment optical coherence tomography in pediatric ophthalmology. *J Ophthalmol*, 2012, 313120.

- CERNICHIARO-ESPINOSA, L. A., GARCIA-HUERTA, M. M., GIORDANO, V. E., SALINAS-LONGORIA, S. M., ROMERO-VERA, R., GARCIA-AGUIRRE, G., SALCEDO-VILLANUEVA, G., QUIROZ-MERCADO, H. & MARTINEZ-CASTELLANOS, M. A. 2014. Comparison of iridocorneal angle in infants with retinopathy of prematurity and healthy infants using spectral domain optical coherence tomography. *J AAPOS*, 18, 344-6.
- CHAMBERS, D., WILSON, L., MADEN, M. & LUMSDEN, A. 2007. RALDH-independent generation of retinoic acid during vertebrate embryogenesis by CYP1B1. *Development*, 134, 1369-83.
- CHAN, W. H., BISWAS, S., ASHWORTH, J. L. & LLOYD, I. C. 2012. Educational paper Congenital and infantile cataract: aetiology and management. *European Journal of Pediatrics*, 171, 625-630.
- CHANG, M. S., HAN, J. C., LEE, J., KWUN, Y., HUH, R., KI, C. S., KEE, C., CHO, S. Y. & JIN, D. K. 2015. A novel splice site mutation in the PAX6 gene in a Korean family with isolated aniridia. *Ann Clin Lab Sci*, 45, 90-3.
- CHANG, S. H. L., LEE, Y. S., WU, S. C., SEE, L. C., CHUNG, C. C., YANG, M. L., LAI, C. C. & WU, W. C. 2017. Anterior Chamber Angle and Anterior Segment Structure of Eyes in Children With Early Stages of Retinopathy of Prematurity. *Am J Ophthalmol*, 179, 46-54.
- CHANG, T. C. & CAVUOTO, K. M. 2013. Surgical management in primary congenital glaucoma: four debates. *J Ophthalmol*, 2013, 612708.
- CHANG, T. C., SUMMERS, C. G., SCHIMMENTI, L. A. & GRAJEWSKI, A. L. 2012. Axenfeld-Rieger syndrome: new perspectives. *Br J Ophthalmol*, 96, 318-22.
- CHAU, F. Y., WALLACE, D., VAJARANANT, T., HERNDON, L., LEE, P., CHALLA, P., ALLINGHAM, R. & MAUMENE, I. 2014. Chapter 31 - Osteogenesis Imperfecta and the Eye. In: SHAPIRO, J. R., BYERS, P. H., GLORIEUX, F. H. & SPONSELLER, P. D. (eds.) *Osteogenesis Imperfecta*. San Diego: Academic Press.
- CHEN, H., LIN, H., LIN, Z., CHEN, J. & CHEN, W. 2016. Distribution of axial length, anterior chamber depth, and corneal curvature in an aged population in South China. *BMC Ophthalmol*, 16, 47.
- CHEN, R. I., BARBOSA, D. T., HSU, C. H., PORCO, T. C. & LIN, S. C. 2015. Ethnic differences in trabecular meshwork height by optical coherence tomography. *JAMA Ophthalmol*, 133, 437-41.
- CHEN, Z., SUN, J., LI, M., LIU, S., CHEN, L., JING, S., CAI, Z., XIANG, Y., SONG, Y., ZHANG, H. & WANG, J. 2018. Effect of age on the morphologies of the human Schlemm's canal and trabecular meshwork measured with swept-source optical coherence tomography. *Eye*.

- CHENG, J. W., ZONG, Y., ZENG, Y. Y. & WEI, R. L. 2014. The prevalence of primary angle closure glaucoma in adult Asians: a systematic review and meta-analysis. *PLoS One*, 9, e103222.
- CHEUNG, C. Y., LIU, S., WEINREB, R. N., LIU, J., LI, H., LEUNG, D. Y., DORAIRAJ, S., LIEBMANN, J., RITCH, R., LAM, D. S. & LEUNG, C. K. 2010. Dynamic analysis of iris configuration with anterior segment optical coherence tomography. *Invest Ophthalmol Vis Sci*, 51, 4040-6.
- CHEUNG, C. Y., ZHENG, C., HO, C.-L., TUN, T. A., KUMAR, R. S., EL SAYYAD, F., WONG, T. Y. & AUNG, T. 2011a. Novel anterior-chamber angle measurements by high-definition optical coherence tomography using the Schwalbe line as the landmark. *British Journal of Ophthalmology*, 95, 955-959.
- CHEUNG, C. Y., ZHENG, C., HO, C. L., TUN, T. A., KUMAR, R. S., EL SAYYAD, F., WONG, T. Y. & AUNG, T. 2011b. Novel anterior-chamber angle measurements by high-definition optical coherence tomography using the Schwalbe line as the landmark. *British Journal of Ophthalmology*, 95, 955-959.
- CHOUDHARI, N. S., GEORGE, R., SATHYAMANGALAM, R. V., RAJU, P., ASOKAN, R., VELUMURI, L. & VIJAYA, L. 2013. Long-term change in central corneal thickness from a glaucoma perspective. *Indian J Ophthalmol*, 61, 580-4.
- CHOUDHARY, D., JANSSON, I., REZAUL, K., HAN, D. K., SARFARAIZI, M. & SCHENKMAN, J. B. 2007. Cyp1b1 protein in the mouse eye during development: an immunohistochemical study. *Drug Metab Dispos*, 35, 987-94.
- CHOUITER, L. & NADIFI, S. 2017. Analysis of CYP1B1 Gene Mutations in Patients with Primary Congenital Glaucoma. *J Pediatr Genet*, 6, 205-214.
- CLINICALGATE. 2015. *Uvea* [Online]. Available: <https://clinicalgate.com/uvea/> [Accessed 28 Aug 2018].
- CONGDON, N. G., QI, Y. L., QUIGLEY, H., HUNG, P. T., WANG, T. H., HO, T. C. & TIELSCH, J. M. 1997. Biometry and primary angle-closure glaucoma among Chinese, white, and black populations. *Ophthalmology*, 104, 1489-1495.
- CONSOLE, J. W., SAKATA, L. M., AUNG, T., FRIEDMAN, D. S. & HE, M. 2008. Quantitative analysis of anterior segment optical coherence tomography images: the Zhongshan Angle Assessment Program. *British Journal of Ophthalmology*, 92, 1612-1616.
- COOK, A., WHITE, S., BATTERBURY, M. & CLARK, D. 2003. Ocular growth and refractive error development in premature infants without retinopathy of prematurity. *Invest Ophthalmol Vis Sci*, 44, 953-60.
- CRONEMBERGER, S., CALIXTO, N., AVELLAR MILHOMENS, T. G., GAMA, P. O., MILHOMENS, E. G., ROLIM, H. & MENDONCA, S. C. 2014. Effect of intraocular pressure control on

- central corneal thickness, horizontal corneal diameter, and axial length in primary congenital glaucoma. *J AAPOS*, 18, 433-6.
- CUI, Y., MENG, Q., GUO, H., ZENG, J., ZHANG, H., ZHANG, G., HUANG, Y. & LAN, J. 2014. Biometry and corneal astigmatism in cataract surgery candidates from Southern China. *J Cataract Refract Surg*, 40, 1661-9.
- CUMBA, R. J., RADHAKRISHNAN, S., BELL, N. P., NAGI, K. S., CHUANG, A. Z., LIN, S. C., MANKIEWICZ, K. A. & FELDMAN, R. M. 2012. Reproducibility of Scleral Spur Identification and Angle Measurements Using Fourier Domain Anterior Segment Optical Coherence Tomography. *Journal of Ophthalmology*.
- CVEKL, A. & TAMM, E. R. 2004. Anterior eye development and ocular mesenchyme: new insights from mouse models and human diseases. *Bioessays*, 26, 374-86.
- DACOSTA, S., FERNANDES, G., RAJENDRAN, B. & JANAKIRAMAN, P. 2008. Assessment of anterior segment parameters under photopic and scotopic conditions in Indian eyes using anterior segment optical coherence tomography. *Indian Journal of Ophthalmology*, 56, 17-22.
- DASCALESCU, D., CORBU, C., VASILE, P., IANCU, R., CRISTEA, M., IONESCU, C., RADU CONSTANTIN, C. & VOINEA, L. 2016. The importance of assessing corneal biomechanical properties in glaucoma patients care - a review. *Rom J Ophthalmol*, 60, 219-225.
- DE SILVA, D. J., KHAW, P. T. & BROOKES, J. L. 2011. Long-term outcome of primary congenital glaucoma. *J AAPOS*, 15, 148-52.
- DEFREYN, A., MAUGERY, J., CHABRIER, S. & COULLET, J. 2007. [Gillespie syndrome: an uncommon presentation of congenital aniridia]. *J Fr Ophthalmol*, 30, e1.
- DELLAPORTA, A. 1975. Historical notes on gonioscopy. *Surv Ophthalmol*, 20, 137-49.
- DELUISE, V. P. & ANDERSON, D. R. 1983. Primary infantile glaucoma (congenital glaucoma). *Surv Ophthalmol*, 28, 1-19.
- DEOL, M., TAYLOR, D. A. & RADCLIFFE, N. M. 2015. Corneal hysteresis and its relevance to glaucoma. *Curr Opin Ophthalmol*, 26, 96-102.
- DINC, U. A., GORGUN, E., ONCEL, B., YENEREL, M. N. & ALIMGIL, L. 2010. Assessment of anterior chamber depth using Visante optical coherence tomography, slitlamp optical coherence tomography, IOL Master, Pentacam and Orbscan IIz. *Ophthalmologica*, 224, 341-6.
- DOMINGUEZ-VICENT, A., MONSALVEZ-ROMIN, D., DEL AGUILA-CARRASCO, A. J., FERRER-BLASCO, T. & MONTES-MICO, R. 2014. Changes in the anterior chamber during accommodation assessed with a Scheimpflug system. *J Cataract Refract Surg*, 40, 1790-7.

- DOSHI, M., MARCUS, C., BEJJANI, B. A. & EDWARD, D. P. 2006. Immunolocalization of CYP1B1 in normal, human, fetal and adult eyes. *Exp Eye Res*, 82, 24-32.
- DU, C., SHEN, M., LI, M., ZHU, D., WANG, M. R. & WANG, J. 2012. Anterior segment biometry during accommodation imaged with ultralong scan depth optical coherence tomography. *Ophthalmology*, 119, 2479-85.
- DUBEY, S. K., MAHALAXMI, N., VIJAYALAKSHMI, P. & SUNDARESAN, P. 2015. Mutational analysis and genotype-phenotype correlations in southern Indian patients with sporadic and familial aniridia. *Mol Vis*, 21, 88-97.
- ECSEDY, M., KOVACS, I., MIHALTZ, K., RECSAN, Z., SZIGETI, A., JUHASZ, E., NEMETH, J. & NAGY, Z. Z. 2014. Scheimpflug imaging for long-term evaluation of optical components in Hungarian children with a history of preterm birth. *J Pediatr Ophthalmol Strabismus*, 51, 235-41.
- EHLERS, N., BRAMSEN, T. & SPERLING, S. 1975. Applanation tonometry and central corneal thickness. *Acta Ophthalmol (Copenh)*, 53, 34-43.
- EHLERS, N. & HJORTDAL, J. 2005. The Cornea: Epithelium and Stroma. In: FISCHBARG, J. (ed.) *Advances in Organ Biology*. Elsevier.
- EHLERS, N., SORENSEN, T., BRAMSEN, T. & POULSEN, E. H. 1976. Central corneal thickness in newborns and children. *Acta Ophthalmol (Copenh)*, 54, 285-90.
- EL SHAKANKIRI, N. M., BAYOUMI, N. H., ABDALLAH, A. H. & EL SAHN, M. M. 2009. Role of ultrasound and biomicroscopy in evaluation of anterior segment anatomy in congenital and developmental cataract cases. *J Cataract Refract Surg*, 35, 1893-905.
- ENGELS, B. F., DIETLEIN, T. S., JACOBI, P. C. & KRIEGLSTEIN, G. K. 1999. [Ultrasound biomicroscopy diagnosis of congenital glaucoma]. *Klin Monbl Augenheilkd*, 215, 338-41.
- EUGENE CHANG, J. V., SCOTT A. LARSON. 2014. *Peters Anomaly* [Online]. Department of Ophthalmology and Visual Sciences, University of Iowa,. : EyeRounds.org. Available: <http://webeye.ophth.uiowa.edu/eyeforum/cases/187-peters-anomaly.htm> [Accessed 30 Aug 2018].
- FAROUK, M. M., NAITO, T., SHINOMIYA, K., EGUCHI, H., SAYED, K. M., NAGASAWA, T., KATOME, T. & MITAMURA, Y. 2015. Optical Coherence Tomography Reveals New Insights into the Accommodation Mechanism. *Journal of Ophthalmology*.
- FAUL, F., ERDFELDER, E., LANG, A. G. & BUCHNER, A. 2007. G*Power 3: a flexible statistical power analysis program for the social, behavioral, and biomedical sciences. *Behav Res Methods*, 39, 175-91.

- FELTGEN, N., LEIFERT, D. & FUNK, J. 2001. Correlation between central corneal thickness, applanation tonometry, and direct intracameral IOP readings. *Br J Ophthalmol*, 85, 85-7.
- FERNANDEZ-VIGO, J. I., DE-PABLO-GOMEZ-DE-LIANO, L., FERNANDEZ-VIGO, C., ARCOS-VILLEGAS, G., FERNANDEZ-PEREZ, C., GARCIA-FEIJOO, J. & FERNANDEZ-VIGO, J. A. 2017. Anterior Chamber Angle and Trabecular Meshwork Measurements Made by Fourier-domain Optical Coherence Tomography in Healthy White Children. *J Glaucoma*, 26, 810-815.
- FERNANDEZ-VIGO, J. I., FERNANDEZ-VIGO, J. A., MACARRO-MERINO, A., FERNANDEZ-PEREZ, C., MARTINEZ-DE-LA-CASA, J. M. & GARCIA-FEIJOO, J. 2015a. Determinants of anterior chamber depth in a large Caucasian population and agreement between intra-ocular lens Master and Pentacam measurements of this variable. *Acta Ophthalmol*.
- FERNANDEZ-VIGO, J. I., GARCIA-FEIJOO, J., MARTINEZ-DE-LA-CASA, J. M., GARCIA-BELLA, J. & FERNANDEZ-VIGO, J. A. 2015b. Morphometry of the trabecular meshwork in vivo in a healthy population using fourier-domain optical coherence tomography. *Invest Ophthalmol Vis Sci*, 56, 1782-8.
- FERREIRA, C. C. M. & TAVARES, I. M. 2017. Intraocular pressure and central corneal thickness in full-term newborns. *Arq Bras Oftalmol*, 80, 313-316.
- FIESS, A., KOLB-KEERL, R., KNUF, M., KIRCHHOF, B., BLECHA, C., OBERACHER-VELTEN, I., MUETHER, P. S. & BAUER, J. 2017. Axial Length and Anterior Segment Alterations in Former Preterm Infants and Full-Term Neonates Analyzed With Scheimpflug Imaging. *Cornea*, 36, 821-827.
- FIRASAT, S., KAUL, H., ASHFAQ, U. A. & IDREES, S. 2017. In silico analysis of five missense mutations in CYP1B1 gene in Pakistani families affected with primary congenital glaucoma. *Int Ophthalmol*.
- FLEDELIUS, H. C. 1996. Pre-term delivery and subsequent ocular development. A 7-10 year follow-up of children screened 1982-84 for ROP. 4) Oculometric - and other metric considerations. *Acta Ophthalmol Scand*, 74, 301-5.
- FOLGAR, F. A., JAFFE, G. J., YING, G. S., MAGUIRE, M. G., TOTH, C. A. & DEG, C. A.-R. M. 2014. Comparison of Optical Coherence Tomography Assessments in the Comparison of Age-Related Macular Degeneration Treatments Trials. *Ophthalmology*, 121, 1956-+.
- FRIEDMAN, D. S., GAZZARD, G., MIN, C. B., BROMAN, A. T., QUIGLEY, H., TIELSCH, J., SEAH, S. & FOSTER, P. J. 2008. Age and sex variation in angle findings among normal Chinese subjects: a comparison of UBM, Scheimpflug, and gonioscopic assessment of the anterior chamber angle. *J Glaucoma*, 17, 5-10.
- FUCHSHOFER, R., STEPHAN, D. A., RUSSELL, P. & TAMM, E. R. 2009. Gene expression profiling of TGFbeta2- and/or BMP7-treated trabecular meshwork cells: Identification of Smad7 as a critical inhibitor of TGF-beta2 signaling. *Exp Eye Res*, 88, 1020-32.

- FUJIMOTO, J. G., PITRIS, C., BOPPART, S. A. & BREZINSKI, M. E. 2000. Optical coherence tomography: an emerging technology for biomedical imaging and optical biopsy. *Neoplasia*, 2, 9-25.
- GARCIA-ANTON, M. T., SALAZAR, J. J., DE HOZ, R., ROJAS, B., RAMIREZ, A. I., TRIVINO, A., AROCA-AGUILAR, J. D., GARCIA-FEIJOO, J., ESCRIBANO, J. & RAMIREZ, J. M. 2017. Goniodysgenesis variability and activity of CYP1B1 genotypes in primary congenital glaucoma. *PLoS One*, 12, e0176386.
- GATZIOUFAS, Z., LABIRIS, G., STACHS, O., HOVAKIMYAN, M., SCHNAIDT, A., VIESTENZ, A., KASMANN-KELLNER, B. & SEITZ, B. 2013. Biomechanical profile of the cornea in primary congenital glaucoma. *Acta Ophthalmol*, 91, e29-34.
- GENCIK, A., GENCIKOVA, A. & GERINEC, A. 1980. Genetic heterogeneity of congenital glaucoma. *Clin Genet*, 17, 241-8.
- GERTH, C., ZAWADZKI, R. J., HEON, E. & WERNER, J. S. 2009. High-resolution retinal imaging in young children using a handheld scanner and Fourier-domain optical coherence tomography. *J AAPOS*, 13, 72-4.
- GHASEMI, A. & ZAHEDIASL, S. 2012. Normality tests for statistical analysis: a guide for non-statisticians. *Int J Endocrinol Metab*, 10, 486-9.
- GOLDSMITH, J. A., LI, Y., CHALITA, M. R., WESTPHAL, V., PATIL, C. A., ROLLINS, A. M., IZATT, J. A. & HUANG, D. 2005a. Anterior chamber width measurement by high-speed optical coherence tomography. *Ophthalmology*, 112, 238-44.
- GOLDSMITH, J. A., LI, Y., CHALITA, M. R., WESTPHAL, V., PATIL, C. A., ROLLINS, A. M., IZATT, J. A. & HUANG, D. 2005b. Anterior chamber width measurement by high speed optical coherence tomography. *Ophthalmology*, 112, 238-244.
- GUNVANT, P., NEWCOMB, R. D., KIRSTEIN, E. M., MALINOVSKY, V. E., MADONNA, R. J. & MEETZ, R. E. 2010. Measuring accurate IOPs: Does correction factor help or hurt? *Clin Ophthalmol*, 4, 611-6.
- GUPTA, V., CHAURASIA, A. K., GUPTA, S., GORIMANIPALLI, B., SHARMA, A. & GUPTA, A. 2017. In Vivo Analysis of Angle Dysgenesis in Primary Congenital, Juvenile, and Adult-Onset Open Angle Glaucoma. *Invest Ophthalmol Vis Sci*, 58, 6000-6005.
- GUPTA, V., JHA, R., SRINIVASAN, G., DADA, T. & SIHOTA, R. 2007. Ultrasound biomicroscopic characteristics of the anterior segment in primary congenital glaucoma. *J AAPOS*, 11, 546-50.
- GUZMAN, C. P., GONG, T., NONGPIUR, M. E., PERERA, S. A., HOW, A. C., LEE, H. K., CHENG, L., HE, M., BASKARAN, M. & AUNG, T. 2013. Anterior segment optical coherence tomography parameters in subtypes of primary angle closure. *Invest Ophthalmol Vis Sci*, 54, 5281-6.

- HADDAD, M. A. O., SAMPAIO, M. W., OLTRORGGE, E. W., KARA-JOSÉ, N. & BETINJANE, A. J. 2009. Visual Impairment Secondary to Congenital Glaucoma in Children: Visual Responses, Optical Correction and Use of Low Vision Aids. *Clinics (Sao Paulo, Brazil)*, 64, 725-730.
- HASHEMI, H., ASGARI, S., EMAMIAN, M. H., MEHRAVARAN, S. & FOTOUHI, A. 2016. Five year changes in central and peripheral corneal thickness: The Shahroud Eye Cohort Study. *Cont Lens Anterior Eye*, 39, 331-5.
- HASHEMI, H., JAFARZADEHPUR, E., GHADERI, S., YEKTA, A., OSTADMOGHADDAM, H., NOROUZIRAD, R. & KHABAZKHOOB, M. 2015. Ocular components during the ages of ocular development. *Acta Ophthalmol*, 93, e74-81.
- HATA, M., MIYAMOTO, K., OISHI, A., MAKIYAMA, Y., GOTOH, N., KIMURA, Y., AKAGI, T. & YOSHIMURA, N. 2014. Comparison of Optic Disc Morphology of Optic Nerve Atrophy between Compressive Optic Neuropathy and Glucomatous Optic Neuropathy. *Plos One*, 9.
- HE, M., HUANG, W., ZHENG, Y., ALSBIRK, P. H. & FOSTER, P. J. 2008. Anterior chamber depth in elderly Chinese: the Liwan eye study. *Ophthalmology*, 115, 1286-90, 1290 e1-2.
- HEINZ, C., SCHLOTE, T., DIETLEIN, T. & PILLUNAT, L. 2007. [Glaucoma in childhood uveitis]. *Klin Monbl Augenheilkd*, 224, 511-5.
- HENDRICKSON, A. E. & YUODELIS, C. 1984. The morphological development of the human fovea. *Ophthalmology*, 91, 603-12.
- HENRIQUES, M. J., VESSANI, R. M., REIS, F. A., DE ALMEIDA, G. V., BETINJANE, A. J. & SUSANNA, R., JR. 2004. Corneal thickness in congenital glaucoma. *J Glaucoma*, 13, 185-8.
- HINGORANI, M., HANSON, I. & VAN HEYNINGEN, V. 2012. Aniridia. *European Journal Of Human Genetics*, 20, 1011.
- HIROSE, F., HATA, M., ITO, S., MATSUKI, T. & KURIMOTO, Y. 2013. Light-dark changes in iris thickness and anterior chamber angle width in eyes with occludable angles. *Graefes Archive for Clinical and Experimental Ophthalmology*, 251, 2395-2402.
- HOERAUF, H., SCHOLZ, C., KOCH, P., ENGELHARDT, R., LAQUA, H. & BIRNGRUBER, R. 2002a. Transscleral optical coherence tomography - A new imaging method for the anterior segment of the eye. *Archives of Ophthalmology*, 120, 816-819.
- HOERAUF, H., WINKLER, J., SCHOLZ, C., WIRBELAUER, C., GORDES, R. S., KOCH, P., ENGELHARDT, R., LAQUA, H. & BIRNGRUBER, R. 2002b. Transscleral optical coherence tomography - An experimental study in ex-vivo human eyes. *Lasers in Surgery and Medicine*, 30, 209-215.

- HOFFMANN, E. M., LAMPARTER, J., MIRSHAH, A., ELFLEIN, H., HOEHN, R., WOLFRAM, C., LORENZ, K., ADLER, M., WILD, P. S., SCHULZ, A., MATHES, B., BLETTNER, M. & PFEIFFER, N. 2013. Distribution of central corneal thickness and its association with ocular parameters in a large central European cohort: the Gutenberg health study. *PLoS One*, 8, e66158.
- HOLMSTROM, M., EL AZAZI, M. & KUGELBERG, U. 1998. Ophthalmological long-term follow up of preterm infants: a population based, prospective study of the refraction and its development. *Br J Ophthalmol*, 82, 1265-71.
- HUANG, B. & HE, W. 2010. Molecular characteristics of inherited congenital cataracts. *Eur J Med Genet*, 53, 347-57.
- HUANG, D. 2009. *OCT Terminology - Demystified* [Online]. Ophthalmology Management. Available: <https://www.ophthalmologymanagement.com/issues/2009/april-2009/oct-terminology-demystified!> [Accessed 2018].
- HUANG, D., SWANSON, E. A., LIN, C. P., SCHUMAN, J. S., STINSON, W. G., CHANG, W., HEE, M. R., FLOTTE, T., GREGORY, K., PULIAFITO, C. A. & ET AL. 1991. Optical coherence tomography. *Science*, 254, 1178-81.
- HUANG, L., COUTO, J. A., PINTO, A., ALEXANDRESCU, S., MADSEN, J. R., GREENE, A. K., SAHIN, M. & BISCHOFF, J. 2017. Somatic GNAQ Mutation is Enriched in Brain Endothelial Cells in Sturge-Weber Syndrome. *Pediatric Neurology*, 67, 59-63.
- HUANG, W., GAO, X., LI, X., WANG, J., CHEN, S., WANG, W., DU, S., HE, M. & ZHANG, X. 2015a. Anterior and posterior ocular biometry in healthy Chinese subjects: data based on AS-OCT and SS-OCT. *PLoS One*, 10, e0121740.
- HUANG, W. B., GAO, X. B., LI, X. Y., WANG, J. W., CHEN, S. D., WANG, W., DU, S. L., HE, M. G. & ZHANG, X. L. 2015b. Anterior and Posterior Ocular Biometry in Healthy Chinese Subjects: Data Based on AS-OCT and SS-OCT. *Plos One*, 10.
- HUSSAIN, R. N., SHAHID, F. & WOODRUFF, G. 2014. Axial length in apparently normal pediatric eyes. *Eur J Ophthalmol*, 24, 120-3.
- HUSSEIN, T. R., SHALABY, S. M., ELBAKARY, M. A., ELSEHT, R. M. & GAD, R. E. 2014. Ultrasound biomicroscopy as a diagnostic tool in infants with primary congenital glaucoma. *Clinical Ophthalmology (Auckland, N.Z.)*, 8, 1725-1730.
- INFANT APHAKIA TREATMENT STUDY, G., LAMBERT, S. R., LYNN, M. J., HARTMANN, E. E., DUBOIS, L., DREWS-BOTSCH, C., FREEDMAN, S. F., PLAGER, D. A., BUCKLEY, E. G. & WILSON, M. E. 2014. Comparison of contact lens and intraocular lens correction of monocular aphakia during infancy: a randomized clinical trial of HOTV optotype acuity at age 4.5 years and clinical findings at age 5 years. *JAMA Ophthalmol*, 132, 676-82.

- ISHII, K., IWATA, H. & OSHIKA, T. 2011. Quantitative evaluation of changes in eyeball shape in emmetropization and myopic changes based on elliptic fourier descriptors. *Invest Ophthalmol Vis Sci*, 52, 8585-91.
- ISHIKAWA, H., ESAKI, K., LIEBMANN, J. M., UJI, Y. & RITCH, R. 1999. Ultrasound biomicroscopy dark room provocative testing: A quantitative method for estimating anterior chamber angle width. *Japanese Journal of Ophthalmology*, 43, 526-534.
- ISHIKAWA, H., LIEBMANN, J. M. & RITCH, R. 2000. Quantitative assessment of the anterior segment using ultrasound biomicroscopy. *Curr Opin Ophthalmol*, 11, 133-9.
- IZATT, J. A., HEE, M. R., SWANSON, E. A., LIN, C. P., HUANG, D., SCHUMAN, J. S., PULIAFITO, C. A. & FUJIMOTO, J. G. 1994. Micrometer-Scale Resolution Imaging of the Anterior Eye in-Vivo with Optical Coherence Tomography. *Archives of Ophthalmology*, 112, 1584-1589.
- JETHANI, J., DAVE, P., JETHANI, M., DESAI, Y. & PATEL, P. 2016. The applicability of correction factor for corneal thickness on non-contact tonometer measured intraocular pressure in LASIK treated eyes. *Saudi J Ophthalmol*, 30, 25-8.
- JOHNSON, M. C. & KAMM, R. D. 1983. The role of Schlemm's canal in aqueous outflow from the human eye. *Invest Ophthalmol Vis Sci*, 24, 320-5.
- KAGEMANN, L., WOLLSTEIN, G., ISHIKAWA, H., BILONICK, R. A., BRENNEN, P. M., FOLIO, L. S., GABRIELE, M. L. & SCHUMAN, J. S. 2010. Identification and assessment of Schlemm's canal by spectral-domain optical coherence tomography. *Invest Ophthalmol Vis Sci*, 51, 4054-9.
- KALUZNY, B. J. 2007. Anterior movement of the crystalline lens in the process of accommodation in children. *Eur J Ophthalmol*, 17, 515-20.
- KANDASAMY, Y., HARTLEY, L., RUDD, D. & SMITH, R. 2017. The association between systemic vascular endothelial growth factor and retinopathy of prematurity in premature infants: a systematic review. *Br J Ophthalmol*, 101, 21-24.
- KARAHAN, E., ZENGİN, M. O., TUNCER, I. & ZENGİN, N. 2015. Correlation of intraocular pressure with central corneal thickness in premature and full-term newborns. *Eur J Ophthalmol*, 25, 14-7.
- KAUSHIK, S. & PANDAV, S. S. 2012. Ocular Response Analyzer. *J Curr Glaucoma Pract*, 6, 17-19.
- KIEFER, G., SCHWENN, O. & GREHN, F. 2001. Correlation of postoperative axial length growth and intraocular pressure in congenital glaucoma--a retrospective study in trabeculotomy and goniotomy. *Graefes Arch Clin Exp Ophthalmol*, 239, 893-9.
- KIERNAN, D. F., MIELER, W. F. & HARIPRASAD, S. M. 2010. Spectral-Domain Optical Coherence Tomography: A Comparison of Modern High-Resolution Retinal Imaging Systems. *American Journal of Ophthalmology*, 149, 18-31.

- KIM, D. Y., SUNG, K. R., KANG, S. Y., CHO, J. W., LEE, K. S., PARK, S. B., KIM, S. T. & KOOK, M. S. 2011. Characteristics and reproducibility of anterior chamber angle assessment by anterior-segment optical coherence tomography. *Acta Ophthalmologica*, 89, 435-441.
- KISKIS, A. A., MARKOWITZ, S. N. & MORIN, J. D. 1985. Corneal diameter and axial length in congenital glaucoma. *Can J Ophthalmol*, 20, 93-7.
- KOBAYASHI, H., KIRYU, J., KOBAYASHI, K. & KONDO, T. 1997. Ultrasound biomicroscopic measurement of anterior chamber angle in premature infants. *Br J Ophthalmol*, 81, 460-4.
- KOBAYASHI, H., ONO, H., KIRYU, J., KOBAYASHI, K. & KONDO, T. 1999. Ultrasound biomicroscopic measurement of development of anterior chamber angle. *Br J Ophthalmol*, 83, 559-62.
- KOHLHAAS, M., BOEHM, A. G., SPOERL, E., PURSTEN, A., GREIN, H. J. & PILLUNAT, L. E. 2006. Effect of central corneal thickness, corneal curvature, and axial length on applanation tonometry. *Arch Ophthalmol*, 124, 471-6.
- KOHNNEN, T., THOMALA, M. C., CICHOCKI, M. & STRENGER, A. 2006. Internal anterior chamber diameter using optical coherence tomography compared with white-to-white distances using automated measurements. *Journal of Cataract and Refractive Surgery*, 32, 1809-1813.
- KOKTEKIR, B. E., GONUL, S., BAKBAK, B., GEDIK, S. & DOGAN, O. K. 2014. The Effect of Room Illumination on the Measurement of Anterior Segment Parameters. *Eye & Contact Lens-Science and Clinical Practice*, 40, 181-184.
- KOO, T. K. & LI, M. Y. 2016. A Guideline of Selecting and Reporting Intraclass Correlation Coefficients for Reliability Research. *J Chiropr Med*, 15, 155-63.
- LAMBERT, S. R., LYNN, M., DREWS-BOTSCH, C., DUBOIS, L., WILSON, M. E., PLAGER, D. A., WHEELER, D. T., CHRISTIANSEN, S. P., CROUCH, E. R., BUCKLEY, E. G., STAGER, D., JR. & DONAHUE, S. P. 2003. Intraocular lens implantation during infancy: perceptions of parents and the American Association for Pediatric Ophthalmology and Strabismus members. *J AAPOS*, 7, 400-5.
- LAVANYA, R., WONG, T. Y., FRIEDMAN, D. S., AUNG, H. T., ALFRED, T., GAO, H., SEAH, S. K., KASHIWAGI, K., FOSTER, P. J. & AUNG, T. 2008. Determinants of angle closure in older Singaporeans. *Arch Ophthalmol*, 126, 686-91.
- LEE, H. 2014. *Investigation of the normal and pathological development of the macula of the infant human eye using high resolution Optical Coherence Tomography (OCT)*. PhD, University of Leicester.
- LEE, H., PROUDLOCK, F. & GOTTLÖB, I. 2013a. Is handheld optical coherence tomography reliable in infants and young children with and without nystagmus? *Invest Ophthalmol Vis Sci*, 54, 8152-9.

- LEE, H., PUROHIT, R., PATEL, A., PAPAGEORGIOU, E., SHETH, V., MACONACHIE, G., PILAT, A., MCLEAN, R. J., PROUDLOCK, F. A. & GOTTLÖB, I. 2015. In Vivo Foveal Development Using Optical Coherence Tomography. *Invest Ophthalmol Vis Sci*, 56, 4537-45.
- LEE, H., SHETH, V., BIBI, M., MACONACHIE, G., PATEL, A., MCLEAN, R. J., MICHAELIDES, M., THOMAS, M. G., PROUDLOCK, F. A. & GOTTLÖB, I. 2013b. Potential of handheld optical coherence tomography to determine cause of infantile nystagmus in children by using foveal morphology. *Ophthalmology*, 120, 2714-24.
- LEE, R. Y., LIN, S. C., CHEN, R. I., BARBOSA, D. T. & LIN, S. C. 2016. Association Between Trabecular Meshwork Anteroposterior Length and Anterior Chamber Angle Width. *American Journal of Ophthalmology*, 162, 53-58.
- LESNIK OBERSTEIN, S. A. J., RUIVENKAMP, C. A. L. & HENNEKAM, R. C. 1993. Peters Plus Syndrome. In: ADAM, M. P., ARDINGER, H. H., PAGON, R. A., WALLACE, S. E., BEAN, L. J. H., STEPHENS, K. & AMEMIYA, A. (eds.) *GeneReviews(R)*. Seattle (WA).
- LEUNG, C. K.-S., CHEUNG, C. Y. L., LI, H., DORAIRAJ, S., YIU, C. K. F., WONG, A. L., LIEBMANN, J., RITCH, R., WEINREB, R. & LAM, D. S. C. 2007. Dynamic analysis of dark-light changes of the anterior chamber angle with anterior segment OCT. *Investigative Ophthalmology & Visual Science*, 48, 4116-4122.
- LEUNG, C. K., PALMIERO, P. M., WEINREB, R. N., LI, H., SBEITY, Z., DORAIRAJ, S., LEUNG, D., LIU, S., LIEBMANN, J. M., CONGDON, N., LAM, D. S. & RITCH, R. 2010. Comparisons of anterior segment biometry between Chinese and Caucasians using anterior segment optical coherence tomography. *Br J Ophthalmol*, 94, 1184-9.
- LEUNG, C. K. & WEINREB, R. N. 2011. Anterior chamber angle imaging with optical coherence tomography. *Eye (Lond)*, 25, 261-7.
- LEUNG, C. K. S., LI, H. T., WEINREB, R. N., LIU, J., CHEUNG, C. Y. L., LAI, R. Y. K., PANG, C. P. & LAM, D. S. C. 2008. Anterior chamber angle measurement with anterior segment optical coherence tomography: A comparison between slit lamp OCT and Visante OCT. *Investigative Ophthalmology & Visual Science*, 49, 3469-3474.
- LEWIS, C. J., HEDBERG-BUENZ, A., DELUCA, A. P., STONE, E. M., ALWARD, W. L. M. & FINGERT, J. H. 2017. Primary congenital and developmental glaucomas. *Human Molecular Genetics*, 26, R28-R36.
- LI, H., LEUNG, C. K., CHEUNG, C. Y., WONG, L., PANG, C. P., WEINREB, R. N. & LAM, D. S. 2007. Repeatability and reproducibility of anterior chamber angle measurement with anterior segment optical coherence tomography. *Br J Ophthalmol*, 91, 1490-2.
- LI, H., LEUNG, C. K. S., WONG, L., CHEUNG, C. Y. L., PANG, C. P., WEINREB, R. N. & LAM, D. S. C. 2008. Comparative study of central corneal thickness measurement with slit-lamp optical coherence tomography and visante optical coherence tomography. *Ophthalmology*, 115, 796-801.

- LI, N., ZHOU, Y., DU, L., WEI, M. & CHEN, X. 2011. Overview of Cytochrome P450 1B1 gene mutations in patients with primary congenital glaucoma. *Exp Eye Res*, 93, 572-9.
- LIBBY, R. T., SMITH, R. S., SAVINOVA, O. V., ZABAleta, A., MARTIN, J. E., GONZALEZ, F. J. & JOHN, S. W. 2003. Modification of ocular defects in mouse developmental glaucoma models by tyrosinase. *Science*, 299, 1578-81.
- LIM, H. T., KIM, D. H. & KIM, H. 2017a. PAX6 aniridia syndrome: clinics, genetics, and therapeutics. *Curr Opin Ophthalmol*, 28, 436-447.
- LIM, L. S., CHEUNG, G. & LEE, S. Y. 2014. Comparison of spectral domain and swept-source optical coherence tomography in pathological myopia. *Eye*, 28, 488-491.
- LIM, M. E., BUCKLEY, E. G. & PRAKALAPAKORN, S. G. 2017b. Update on congenital cataract surgery management. *Curr Opin Ophthalmol*, 28, 87-92.
- LIU, S., LI, H., DORAIRAJ, S., CHEUNG, C. Y., ROUSSO, J., LIEBMANN, J., RITCH, R., LAM, D. S. & LEUNG, C. K. 2010. Assessment of scleral spur visibility with anterior segment optical coherence tomography. *J Glaucoma*, 19, 132-5.
- LIU, S., YU, M., YE, C., LAM, D. S. C. & LEUNG, C. K. S. 2011. Anterior Chamber Angle Imaging with Swept-Source Optical Coherence Tomography: An Investigation on Variability of Angle Measurement. *Investigative Ophthalmology & Visual Science*, 52, 8598-8603.
- LLEO, A., MARCOS, A., CALATAYUD, M., ALONSO, L., RAHHAL, S. M. & SANCHIS-GIMENO, J. A. 2003. The relationship between central corneal thickness and Goldmann applanation tonometry. *Clin Exp Optom*, 86, 104-8.
- LLOBET, A., GASULL, X. & GUAL, A. 2003. Understanding trabecular meshwork physiology: a key to the control of intraocular pressure? *News Physiol Sci*, 18, 205-9.
- LOGAN, N. S., GILMARTIN, B., WILDSOET, C. F. & DUNNE, M. C. 2004. Posterior retinal contour in adult human anisomyopia. *Invest Ophthalmol Vis Sci*, 45, 2152-62.
- LUMLEY, T., DIEHR, P., EMERSON, S. & CHEN, L. 2002. The importance of the normality assumption in large public health data sets. *Annu Rev Public Health*, 23, 151-69.
- MAJANDER, A. S., LINDAHL, P. M., VASARA, L. K. & KROOTILA, K. 2012. Anterior segment optical coherence tomography in congenital corneal opacities. *Ophthalmology*, 119, 2450-7.
- MAK, H., XU, G. & LEUNG, C. K. 2013. Imaging the iris with swept-source optical coherence tomography: relationship between iris volume and primary angle closure. *Ophthalmology*, 120, 2517-24.
- MALDONADO, R. S., IZATT, J. A., SARIN, N., WALLACE, D. K., FREEDMAN, S., COTTEN, C. M. & TOTH, C. A. 2010. Optimizing hand-held spectral domain optical coherence

- tomography imaging for neonates, infants, and children. *Invest Ophthalmol Vis Sci*, 51, 2678-85.
- MANDAL, A. K. & CHAKRABARTI, D. 2011. Update on congenital glaucoma. *Indian J Ophthalmol*, 59 Suppl, S148-57.
- MANSOORI, T. & BALAKRISHNA, N. 2018. Effect of central corneal thickness on intraocular pressure and comparison of Topcon CT-80 non-contact tonometry with Goldmann applanation tonometry. *Clin Exp Optom*, 101, 206-212.
- MANTELLI, F., BRUSCOLINI, A., LA CAVA, M., ABDOLRAHIMZADEH, S. & LAMBIASE, A. 2016. Ocular manifestations of Sturge-Weber syndrome: pathogenesis, diagnosis, and management. *Clin Ophthalmol*, 10, 871-8.
- MARAM, J., PAN, X., SADDA, S., FRANCIS, B., MARION, K. & CHOPRA, V. 2015a. Reproducibility of angle metrics using the time-domain anterior segment optical coherence tomography: intra-observer and inter-observer variability. *Curr Eye Res*, 40, 496-500.
- MARAM, J., PAN, X. J., SADDA, S., FRANCIS, B., MARION, K. & CHOPRA, V. 2015b. Reproducibility of Angle Metrics Using the Time-Domain Anterior Segment Optical Coherence Tomography: Intra-Observer and Inter-Observer Variability. *Current Eye Research*, 40, 496-500.
- MARION, K. M., MARAM, J., PAN, X., DASTIRIDOU, A., ZHANG, Z., HO, A., FRANCIS, B. A., SADDA, S. R. & CHOPRA, V. 2015. Reproducibility and Agreement Between 2 Spectral Domain Optical Coherence Tomography Devices for Anterior Chamber Angle Measurements. *J Glaucoma*.
- MARTIN, H., GUTHOFF, R., TERWEE, T. & SCHMITZ, K. P. 2005. Comparison of the accommodation theories of Coleman and of Helmholtz by finite element simulations. *Vision Research*, 45, 2910-2915.
- MASOODI, H., JAFARZADEHPUR, E., ESMAEILI, A., ABOLBASHARI, F. & HOSSEINI, S. M. A. 2014. Evaluation of anterior chamber angle under dark and light conditions in angle closure glaucoma: An anterior segment OCT study. *Contact Lens & Anterior Eye*, 37, 300-304.
- MAUMENE, A. E. 1958. The pathogenesis of congenital glaucoma: a new theory. *Trans Am Ophthalmol Soc*, 56, 507-70.
- MAUMENE, A. E. 1959. The pathogenesis of congenital glaucoma; a new theory. *Am J Ophthalmol*, 47, 827-58.
- MAUMENE, A. E. 1963. Further observations on the pathogenesis of congenital glaucoma. *Am J Ophthalmol*, 55, 1163-76.
- MCKEE, H., YE, C., YU, M., LIU, S., LAM, D. S. C. & LEUNG, C. K. S. 2013. Anterior Chamber Angle Imaging With Swept-Source Optical Coherence Tomography: Detecting the Scleral Spur, Schwalbe's Line, and Schlemm's Canal. *Journal of Glaucoma*, 22, 468-472.

- MCMENAMIN, P. G. 1989. A Morphological-Study of the Inner Surface of the Anterior-Chamber Angle in Prenatal and Postnatal Human Eyes. *Current Eye Research*, 8, 727-739.
- MCMENAMIN, P. G. 1991. A Quantitative Study of the Prenatal Development of the Aqueous Outflow System in the Human Eye. *Experimental Eye Research*, 53, 507-517.
- MEGHPARA, B., LI, X., NAKAMURA, H., KHAN, A., BEJJANI, B. A., LIN, S. & EDWARD, D. P. 2008. Human anterior chamber angle development without cell death or macrophage involvement. *Molecular Vision*, 14, 2492-2498.
- MICHEAL, S., AYUB, H., ZAFAR, S. N., BAKKER, B., ALI, M., AKHTAR, F., ISLAM, F., KHAN, M. I., QAMAR, R. & DEN HOLLANDER, A. I. 2015. Identification of novel CYP1B1 gene mutations in patients with primary congenital and primary open-angle glaucoma. *Clin Exp Ophthalmol*, 43, 31-9.
- MODRZEJEWSKA, M., GRZESIAK, W., KARCZEWCZ, D. & ZABORSKI, D. 2010. Refractive status and ocular axial length in preterm infants without retinopathy of prematurity with regard to birth weight and gestational age. *J Perinat Med*, 38, 327-31.
- MONSALVEZ-ROMIN, D., DEL AGUILA-CARRASCO, A., FERRER-BLASCO, T., ESTEVE-TABOADA, J. J. & MONTES-MICO, R. 2017. Evaluation of the iridocorneal angle with accommodation using optical coherence tomography. *Int J Ophthalmol*, 10, 1614-1616.
- MOOKHERJEE, S., ACHARYA, M., BANERJEE, D., BHATTACHARJEE, A. & RAY, K. 2012. Molecular Basis for Involvement of CYP1B1 in MYOC Upregulation and Its Potential Implication in Glaucoma Pathogenesis. *Plos One*, 7.
- MUELLER, M., SCHULZ-WACKERBARTH, C., STEVEN, P., LANKENAU, E., BONIN, T., MUELLER, H., BRUEGGEMANN, A., BIRNGRUBER, R., GRISANTI, S. & HUETTMANN, G. 2010. Slit-Lamp-Adapted Fourier-Domain OCT for Anterior and Posterior Segments: Preliminary Results and Comparison to Time-Domain OCT. *Current Eye Research*, 35, 722-732.
- MUNI, R. H., KOHLY, R. P., SOHN, E. H. & LEE, T. C. 2010. Hand-held spectral domain optical coherence tomography finding in shaken-baby syndrome. *Retina*, 30, S45-50.
- MUNOZ DE ESCALONA ROJAS, J. E., QUEREDA CASTANEDA, A. & GARCIA GARCIA, O. 2016. Utility of optical coherence tomography in a case of bilateral congenital macular coloboma. *Indian J Ophthalmol*, 64, 683-685.
- MUNRO, R. J., FULTON, A. B., CHUI, T. Y., MOSKOWITZ, A., RAMAMIRTHAM, R., HANSEN, R. M., PRABHU, S. P. & AKULA, J. D. 2015. Eye growth in term- and preterm-born eyes modeled from magnetic resonance images. *Invest Ophthalmol Vis Sci*, 56, 3121-31.
- MURTHY, R. K., HAJI, S., SAMBHAV, K., GROVER, S. & CHALAM, K. V. 2016. Clinical applications of spectral domain optical coherence tomography in retinal diseases. *Biomed J*, 39, 107-20.

- MUTTI, D. O., MITCHELL, G. L., JONES, L. A., FRIEDMAN, N. E., FRANE, S. L., LIN, W. K., MOESCHBERGER, M. L. & ZADNIK, K. 2005. Axial growth and changes in lenticular and corneal power during emmetropization in infants. *Invest Ophthalmol Vis Sci*, 46, 3074-80.
- MWANZA, J. C., TULENKO, S. E., BUDENZ, D. L., MATHENGE, E., HERNDON, L. H., KIM, H. Y., HALL, A., HAY-SMITH, G., SPRATT, A. & BARTON, K. 2018. Longitudinal Change in Central Corneal Thickness in the Tema Eye Survey. *Am J Ophthalmol*, 186, 10-18.
- NARAYANASWAMY, A., SAKATA, L. M., HE, M. G., FRIEDMAN, D. S., CHAN, Y. H., LAVANYA, R., BASKARAN, M., FOSTER, P. J. & AUNG, T. 2010a. Diagnostic Performance of Anterior Chamber Angle Measurements for Detecting Eyes With Narrow Angles An Anterior Segment OCT Study. *Archives of Ophthalmology*, 128, 1321-1327.
- NARAYANASWAMY, A., SAKATA, L. M., HE, M. G., FRIEDMAN, D. S., CHAN, Y. H., LAVANYA, R., BASKARAN, M., FOSTER, P. J. & AUNG, T. 2010b. Diagnostic performance of anterior chamber angle measurements for detecting eyes with narrow angles: an anterior segment OCT study. *Arch Ophthalmol*, 128, 1321-7.
- NARAYANASWAMY, A., VIJAYA, L., SHANCHA, B., BASKARAN, M., SATHIDEVI, A. V. & BALUSWAMY, S. 2004. Anterior chamber angle assessment using gonioscopy and ultrasound biomicroscopy. *Japanese Journal of Ophthalmology*, 48, 44-49.
- NEUSTEIN, R. F. & BECK, A. D. 2017. Circumferential Trabeculotomy Versus Conventional Angle Surgery: Comparing Long-term Surgical Success and Clinical Outcomes in Children With Primary Congenital Glaucoma. *Am J Ophthalmol*, 183, 17-24.
- NONGPIUR, M. E., GONG, T., LEE, H. K., PERERA, S. A., CHENG, L., FOO, L. L., HE, M., FRIEDMAN, D. S. & AUNG, T. 2013. Subgrouping of primary angle-closure suspects based on anterior segment optical coherence tomography parameters. *Ophthalmology*, 120, 2525-31.
- NONGPIUR, M. E., HE, M., AMERASINGHE, N., FRIEDMAN, D. S., TAY, W.-T., BASKARAN, M., SMITH, S. D., WONG, T. Y. & AUNG, T. 2011a. Lens Vault, Thickness, and Position in Chinese Subjects with Angle Closure. *Ophthalmology*, 118, 474-479.
- NONGPIUR, M. E., HE, M. G., AMERASINGHE, N., FRIEDMAN, D. S., TAY, W. T., BASKARAN, M., SMITH, S. D., WONG, T. Y. & AUNG, T. 2011b. Lens Vault, Thickness, and Position in Chinese Subjects with Angle Closure. *Ophthalmology*, 118, 474-479.
- NONGPIUR, M. E., SAKATA, L. M., FRIEDMAN, D. S., HE, M., CHAN, Y. H., LAVANYA, R., WONG, T. Y. & AUNG, T. 2010a. Novel association of smaller anterior chamber width with angle closure in Singaporeans. *Ophthalmology*, 117, 1967-73.
- NONGPIUR, M. E., SAKATA, L. M., FRIEDMAN, D. S., HE, M. G., CHAN, Y. H., LAVANYA, R., WONG, T. Y. & AUNG, T. 2010b. Novel Association of Smaller Anterior Chamber Width with Angle Closure in Singaporeans. *Ophthalmology*, 117, 1967-1973.

- O'DONNELL, C., HARTWIG, A. & RADHAKRISHNAN, H. 2011. Correlations between refractive error and biometric parameters in human eyes using the LenStar 900. *Cont Lens Anterior Eye*, 34, 26-31.
- OBERACHER-VELTEN, I., PRASSER, C. & LORENZ, B. 2008. Evolution of central corneal thickness in children with congenital glaucoma requiring glaucoma surgery. *Graefes Arch Clin Exp Ophthalmol*, 246, 397-403.
- OPTICIAN ONLINE. 2018. *Inflammatory disease of the posterior chamber* [Online]. www.opticianonline.net: MA Healthcare. Available: <https://www.opticianonline.net/cet-archive/4744> [Accessed 30 Aug 2018].
- ORAWIEC, B., MLYNARSKI, W., BUDZINSKA-MIKURENDA, M., GRALEK, M., SZEWCZYK-ZALEWSKA, B. & NIWALD, A. 2010. [Sporadic aniridia and Wilm's tumor--a case report and review of recommendation for diagnostic approach in WAGR's syndrome]. *Klin Oczna*, 112, 321-3.
- ORUCOGLU, F., AKMAN, M. & ONAL, S. 2015. Analysis of age, refractive error and gender related changes of the cornea and the anterior segment of the eye with Scheimpflug imaging. *Cont Lens Anterior Eye*.
- PAFF, T., OUDESLUYS-MURPHY, A. M., WOLTERBEEK, R., SWART-VAN DEN BERG, M., DE NIE, J. M., TIJSSEN, E. & SCHALIJ-DELFS, N. E. 2010. Screening for refractive errors in children: The plusoptix S08 and the Retinomax K-plus2 performed by a lay screener compared to cycloplegic retinoscopy. *Journal of Aapos*, 14, 478-483.
- PALETTA GUEDES, R. A., PENA, A. B., PALETTA GUEDES, V. M. & CHAOUBAH, A. 2016. Longitudinal evaluation of central corneal thickness in congenital glaucoma. *J Fr Ophthalmol*, 39, 706-710.
- PAN, X. J., MARION, K., MARAM, J., ZHANG, Z. Y., FRANCIS, B. A., NITTALA, M. G., SADDA, S. R. & CHOPRA, V. 2015. Reproducibility of Anterior Segment Angle Metrics Measurements Derived From Cirrus Spectral Domain Optical Coherence Tomography. *Journal of Glaucoma*, 24, e47-e51.
- PATEL, A., PUROHIT, R., LEE, H., SHETH, V., MACONACHIE, G., PAPAGEORGIOU, E., MCLEAN, R. J., GOTTLÖB, I. & PROUDLOCK, F. A. 2016. Optic Nerve Head Development in Healthy Infants and Children Using Handheld Spectral-Domain Optical Coherence Tomography. *Ophthalmology*, 123, 2147-57.
- PAVLIN, C. J., HARASIEWICZ, K. & FOSTER, F. S. 1992. Ultrasound Biomicroscopy of Anterior Segment Structures in Normal and Glaucomatous Eyes. *American Journal of Ophthalmology*, 113, 381-389.
- PAVLIN, C. J., HARASIEWICZ, K., SHERAR, M. D. & FOSTER, E. S. 1991. Clinical Use of Ultrasound Biomicroscopy. *Ophthalmology*, 98, 287-295.

- PENNIE, F. C., WOOD, I. C., OLSEN, C., WHITE, S. & CHARMAN, W. N. 2001. A longitudinal study of the biometric and refractive changes in full-term infants during the first year of life. *Vision Res*, 41, 2799-810.
- PETERSEIM, M. M. W., PAPA, C. E., WILSON, M. E., CHEESEMAN, E. W., WOLF, B. J., DAVIDSON, J. D. & TRIVEDI, R. H. 2014. Photoscreeners in the Pediatric Eye Office: Compared Testability and Refractions on High-Risk Children. *American Journal of Ophthalmology*, 158, 932-938.
- PHAT, N. 2016. *Gonioscopy and Other Techniques for Assessing the Anterior Segment* [Online]. Available: <https://entokey.com/3-2/> [Accessed 28 Aug 2018].
- PHELPS, C. D. 1978. The pathogenesis of glaucoma in Sturge-Weber syndrome. *Ophthalmology*, 85, 276-86.
- PI, L. H., CHEN, L., LIU, Q., KE, N., FANG, J., ZHANG, S., XIAO, J., YE, W. J., XIONG, Y., SHI, H., ZHOU, X. Y. & YIN, Z. Q. 2012. Prevalence of eye diseases and causes of visual impairment in school-aged children in Western China. *J Epidemiol*, 22, 37-44.
- PILAT, A. V., SHETH, V., PUROHIT, R., PROUDLOCK, F. A., ANWAR, S. & GOTTLÖB, I. 2017. Hand-held optical coherence tomography imaging in children with anterior segment dysgenesis. *Acta Ophthalmol*, 95, 537-541.
- POMELLA, K. M. & WAGNER, H. 1998. Unilateral Peters' anomaly complicated by a corneal tattoo. *Optometry and Vision Science*, 75, 635-639.
- PORTELLINHA, W. & BELFORT, R., JR. 1991. Central and peripheral corneal thickness in newborns. *Acta Ophthalmol (Copenh)*, 69, 247-50.
- PROST, M. E. & OLESZCZYNSKA-PROST, E. 2005. [Central corneal thickness in children with congenital glaucoma]. *Klin Oczna*, 107, 445-7.
- PUVANACHANDRA, N. & LYONS, C. J. 2009. Rapid measurement of corneal diameter in children: validation of a clinic-based digital photographic technique. *J AAPOS*, 13, 287-8.
- QIN, B., FRANCIS, B. A., LI, Y., TANG, M. L., ZHANG, X. B., JIANG, C. H., CLEARY, C. & HUANG, D. 2013. Anterior Chamber Angle Measurements Using Schwalbe's Line With High-resolution Fourier-Domain Optical Coherence Tomography. *Journal of Glaucoma*, 22, 684-688.
- QIN, B., TANG, M., LI, Y., ZHANG, X., CHU, R. & HUANG, D. 2012. Anterior segment dimensions in Asian and Caucasian eyes measured by optical coherence tomography. *Ophthalmic Surg Lasers Imaging*, 43, 135-42.
- QUEK, D. T., NARAYANASWAMY, A. K., TUN, T. A., HTOON, H. M., BASKARAN, M., PERERA, S. A. & AUNG, T. 2012a. Comparison of Two Spectral Domain Optical Coherence

Tomography Devices for Angle-Closure Assessment. *Investigative Ophthalmology & Visual Science*, 53, 5131-5136.

- QUEK, D. T., NARAYANASWAMY, A. K., TUN, T. A., HTOON, H. M., BASKARAN, M., PERERA, S. A. & AUNG, T. 2012b. Comparison of two spectral domain optical coherence tomography devices for angle-closure assessment. *Invest Ophthalmol Vis Sci*, 53, 5131-6.
- QUERQUES, G., BUX, A. V., IACULLI, C. & DELLE NOCI, N. 2008. Isolated foveal hypoplasia. *Retina*, 28, 1552-3.
- RADHAKRISHNAN, S., GOLDSMITH, J., HUANG, D., WESTPHAL, V., DUEKER, D. K., ROLLINS, A. M., IZATT, J. A. & SMITH, S. D. 2005a. Comparison of optical coherence tomography and ultrasound biomicroscopy for detection of narrow anterior chamber angles. *Archives of Ophthalmology*, 123, 1053-1059.
- RADHAKRISHNAN, S., HUANG, D. & SMITH, S. D. 2005b. Optical coherence tomography imaging of the anterior chamber angle. *Ophthalmol Clin North Am*, 18, 375-81, vi.
- RADHAKRISHNAN, S., ROLLINS, A. M., ROTH, J. E., YAZDANFAR, S., WESTPHAL, V., BARDENSTEIN, D. S. & IZATT, J. A. 2001. Real-time optical coherence tomography of the anterior segment at 1310 nm. *Arch Ophthalmol*, 119, 1179-85.
- RAMOS, J. L. B., LI, Y. & HUANG, D. 2009. Clinical and research applications of anterior segment optical coherence tomography - a review. *Clinical and Experimental Ophthalmology*, 37, 81-89.
- READ, S. A., ALONSO-CANEIRO, D., VINCENT, S. J., BREMNER, A., FOTHERGILL, A., ISMAIL, B., MCGRAW, R., QUIRK, C. J. & WRIGLEY, E. 2016. Anterior eye tissue morphology: Scleral and conjunctival thickness in children and young adults. *Scientific Reports*, 6.
- READ, S. A., COLLINS, M. J., BECKER, H., CUTTING, J., ROSS, D., SAVILL, A. K. & TREVOR, B. 2010a. Changes in intraocular pressure and ocular pulse amplitude with accommodation. *Br J Ophthalmol*, 94, 332-5.
- READ, S. A., COLLINS, M. J., WOODMAN, E. C. & CHEONG, S. H. 2010b. Axial length changes during accommodation in myopes and emmetropes. *Optom Vis Sci*, 87, 656-62.
- REIS, L. M., TYLER, R. C., VOLKMANN KLOSS, B. A., SCHILTER, K. F., LEVIN, A. V., LOWRY, R. B., ZWIJNENBURG, P. J., STROH, E., BROECKEL, U., MURRAY, J. C. & SEMINA, E. V. 2012. PITX2 and FOXC1 spectrum of mutations in ocular syndromes. *Eur J Hum Genet*, 20, 1224-33.
- REIS, L. M., TYLER, R. C., WEH, E., HENDEE, K. E., KARIMINEJAD, A., ABDUL-RAHMAN, O., BEN-OMRAN, T., MANNING, M. A., YESILYURT, A., MCCARTY, C. A., KITCHNER, T. E., COSTAKOS, D. & SEMINA, E. V. 2016. Analysis of CYP1B1 in pediatric and adult glaucoma and other ocular phenotypes. *Mol Vis*, 22, 1229-1238.

- REIS, L. M., TYLER, R. C., ZORI, R., BURGESS, J., MUELLER, J. & SEMINA, E. V. 2015. A case of 22q11.2 deletion syndrome with Peters anomaly, congenital glaucoma, and heterozygous mutation in CYP1B1. *Ophthalmic Genet*, 36, 92-4.
- REME, C. & D'EPINAY, S. L. 1981. Periods of development of the normal human chamber angle. *Doc Ophthalmol*, 51, 241-68.
- REME, C. & DEPINAY, S. L. 1981. Periods of Development of the Normal Human Chamber Angle. *Documenta Ophthalmologica*, 51, 241-268.
- REME, C., URNER, U. & AEBERHARD, B. 1983. The Occurrence of Cell-Death during the Remodeling of the Chamber Angle Recess in the Developing Rat Eye. *Graefes Archive for Clinical and Experimental Ophthalmology*, 221, 113-121.
- REMON, L., CRISTOBAL, J. A., CASTILLO, J., PALOMAR, T., PALOMAR, A. & PEREZ, J. 1992. Central and peripheral corneal thickness in full-term newborns by ultrasonic pachymetry. *Invest Ophthalmol Vis Sci*, 33, 3080-3.
- RICCI, B. 1999. Intraocular pressure in premature babies in the first month of life. *J AAPOS*, 3, 125-7.
- RICHARDSON, T. M., MARKS, M. S., AUSPRUNK, D. H. & MILLER, M. 1985. A Morphologic and Morphometric Analysis of the Aqueous Outflow System of the Developing Cat Eye. *Experimental Eye Research*, 41, 31-51.
- RITCH, R., CHANG, B. M. & LIEBMANN, J. M. 2003. Angle closure in younger patients. *Ophthalmology*, 110, 1880-9.
- ROBINSON, J., CHEUNG, A. Y., NUDLEMAN, E., TRESE, M. T., CAPONE, A., DRENSEN, K. A. & WILLIAMS, G. A. 2018. Ocular Hypertension in Adults with a History of Prematurity. *Ophthalmology Retina*, 2, 629-635.
- ROJAS, B., RAMIREZ, A. I., DE-HOZ, R., SALAZAR, J. J., REMIREZ, J. M. & TRIVINO, A. 2006. [Structural changes of the anterior chamber angle in primary congenital glaucoma with respect to normal development]. *Arch Soc Esp Oftalmol*, 81, 65-71.
- RUFER, F., SCHRODER, A., KLETTNER, A., FRIMPONG-BOATENG, A., ROIDER, J. B. & ERB, C. 2010. Anterior chamber depth and iridocorneal angle in healthy White subjects: effects of age, gender and refraction. *Acta Ophthalmol*, 88, 885-90.
- SAKATA, L. M., LAVANYA, R., FRIEDMAN, D. S., AUNG, H. T., GAO, H., KUMAR, R. S., FOSTER, P. J. & AUNG, T. 2008a. Comparison of gonioscopy and anterior segment ocular coherence tomography in detecting angle closure in different quadrants of the anterior chamber angle. *Ophthalmology*, 115, 769-774.
- SAKATA, L. M., LAVANYA, R., FRIEDMAN, D. S., AUNG, H. T., SEAH, S. K., FOSTER, P. J. & AUNG, T. 2008b. Assessment of the scleral spur in anterior segment optical coherence tomography images. *Arch Ophthalmol*, 126, 181-5.

- SAKATA, L. M., LAVANYA, R., FRIEDMAN, D. S., AUNG, H. T., SEAH, S. K., FOSTER, P. J. & AUNG, T. 2008c. Assessment of the scleral spur in anterior segment optical coherence tomography images. *Archives of Ophthalmology*, 126, 181-185.
- SAMPAOLESI, R. & CARUSO, R. 1982. Ocular echometry in the diagnosis of congenital glaucoma. *Arch Ophthalmol*, 100, 574-7.
- SANCHEZ-PARRA, L., PARDHAN, S., BUCKLEY, R. J., PARKER, M. & BOURNE, R. R. A. 2015. Diurnal Intraocular Pressure and the Relationship With Swept-Source OCT-Derived Anterior Chamber Dimensions in Angle Closure: The IMPACT Study. *Investigative Ophthalmology & Visual Science*, 56, 2943-2949.
- SAYED, K. M. & ALSAMMAN, A. H. 2015. Interchangeability between Pentacam and IOLMaster in phakic intraocular lens calculation. *Eur J Ophthalmol*, 25, 202-7.
- SCHMITT, J. M. 1999. Optical coherence tomography (OCT): A review. *Ieee Journal of Selected Topics in Quantum Electronics*, 5, 1205-1215.
- SCHNEIDER, P., DROUIN-GARRAUD, V., BACHY, B., BRASSEUR, G., LAHSINAT, K., HEMET, J., VANNIER, J. P. & TRON, P. 1996. [Aniridia and Wilms tumor: 2 cases of fetal rhabdomyomatous nephroblastoma]. *Arch Pediatr*, 3, 1243-7.
- SCHUSTER, A. K., FISCHER, J. E. & VOSSMERBAEUMER, U. 2016. Central Corneal Thickness in Spectral-Domain OCT and Associations with Ocular and Systemic Parameters. *J Ophthalmol*, 2016, 2596956.
- SCOTT, A. W., FARSIU, S., ENYEDI, L. B., WALLACE, D. K. & TOTH, C. A. 2009. Imaging the Infant Retina with a Hand-held Spectral-Domain Optical Coherence Tomography Device. *American Journal of Ophthalmology*, 147, 364-373.
- SCUDERI, G., IACOVELLO, D., PRANNO, F., PLATEROTI, P. & SCUDERI, L. 2015. Pediatric Glaucoma: A Literature's Review and Analysis of Surgical Results. *Biomed Res Int*, 2015, 393670.
- SEIFI, M. & WALTER, M. A. 2018. Axenfeld-Rieger syndrome. *Clin Genet*, 93, 1123-1130.
- SEKEROGLU, M. A., HEKIMOGLU, E., PETRICLI, I. S., KARAKAYA, J., OZCAN, B., YUCEL, H., KAVURT, A. S. & BAS, A. Y. 2015. Central corneal thickness and intraocular pressure in premature infants. *Int Ophthalmol*, 35, 847-51.
- SERRA, A. & LEIGH, R. J. 2002. Diagnostic value of nystagmus: spontaneous and induced ocular oscillations. *J Neurol Neurosurg Psychiatry*, 73, 615-8.
- SHARMA, R., SHARMA, A., ARORA, T., SHARMA, S., SOBTI, A., JHA, B., CHATURVEDI, N. & DADA, T. 2014. Application of anterior segment optical coherence tomography in glaucoma. *Surv Ophthalmol*, 59, 311-27.

- SHETH, V., GOTTLÖB, I., MOHAMMAD, S., MCLEAN, R. J., MACONACHIE, G. D., KUMAR, A., DEGG, C. & PROUDLOCK, F. A. 2013. Diagnostic potential of iris cross-sectional imaging in albinism using optical coherence tomography. *Ophthalmology*, 120, 2082-90.
- SHI, Y., WANG, H., YIN, J., ZHANG, X., LI, M., XIN, C., CHEN, X. & WANG, N. 2017. Outcomes of microcatheter-assisted trabeculotomy following failed angle surgeries in primary congenital glaucoma. *Eye (Lond)*, 31, 132-139.
- SHIMIZU, Y., NAKAKURA, S., NAGASAWA, T., OKAMOTO, A., TABUCHI, H. & KIUCHI, Y. 2017. Comparison of the anterior chamber angle structure between children and adults. *J AAPOS*, 21, 57-62.
- SHOHDY, K. S., RASHAD, W. A., FARGOUN, M. K. & URBAN, P. 2017. The morphogen behind primary congenital glaucoma and the dream of targeting. *Rom J Morphol Embryol*, 58, 351-361.
- SILVERTHORN, D. U., JOHNSON, B. R., OBER, W. C., OBER, C. E. & SILVERTHORN, A. C. 2016. *Human physiology : an integrated approach*.
- SINGH, K. D., LOGAN, N. S. & GILMARTIN, B. 2006. Three-dimensional modeling of the human eye based on magnetic resonance imaging. *Invest Ophthalmol Vis Sci*, 47, 2272-9.
- SKALICKY, S. E. 2016. The Ciliary Body and Aqueous Fluid Formation and Drainage. *Ocular and Visual Physiology: Clinical Application*. Singapore: Springer Singapore.
- SKARMOOTSOS, F., SANDHU, S. S., VOROS, G. M. & SHAFIQ, A. 2006. The use of optical coherence tomography in the management of cystoid macular edema in pediatric uveitis. *J AAPOS*, 10, 173-4.
- SNG, C. C., ALLEN, J. C., NONGPIUR, M. E., FOO, L. L., ZHENG, Y., CHEUNG, C. Y., HE, M., FRIEDMAN, D. S., WONG, T. Y. & AUNG, T. 2013. Associations of Iris Structural Measurements in a Chinese Population: The Singapore Chinese Eye Study. *Investigative Ophthalmology & Visual Science*, 54, 2829-2835.
- SNG, C. C., FOO, L. L., CHENG, C. Y., ALLEN, J. C., JR., HE, M., KRISHNASWAMY, G., NONGPIUR, M. E., FRIEDMAN, D. S., WONG, T. Y. & AUNG, T. 2012. Determinants of anterior chamber depth: the Singapore Chinese Eye Study. *Ophthalmology*, 119, 1143-50.
- SNIR, M., FRILING, R., WEINBERGER, D., SHERF, I. & AXER-SIEGEL, R. 2004. Refraction and keratometry in 40 week old premature (corrected age) and term infants. *Br J Ophthalmol*, 88, 900-4.
- SOLEBO, A. L., RUSSELL-EGGITT, I., CUMBERLAND, P. M., RAHI, J. S. & BRITISH ISLES CONGENITAL CATARACT INTEREST, G. 2015. Risks and outcomes associated with primary intraocular lens implantation in children under 2 years of age: the IoLunder2 cohort study. *Br J Ophthalmol*, 99, 1471-6.

- SOOD, D., RATHORE, A., SOOD, I., SINGH, G. & SOOD, N. N. 2018. Long-term outcome of combined trabeculotomy-trabeculectomy by a single surgeon in patients with primary congenital glaucoma. *Eye (Lond)*, 32, 426-432.
- SOUZEAU, E. 2018. Biallelic CPAMD8 Variants Associated with Congenital Glaucoma and Anterior Segment Dysgenesis. *International Society of Eye Research*. Belfast, Northren Ireland.
- STANFORDMEDINE25. 2018. *Fundoscopic / Ophthalmoscopic Exam* [Online]. Stanford University School of Medicine. Available: <https://stanfordmedicine25.stanford.edu/the25/fundoscopic.html> [Accessed 08 Oct 2018].
- STEGMAN, Z., SOKOL, J., LIEBMANN, J. M., COHEN, H., TELLO, C. & RITCH, R. 1996. Reduced trabecular meshwork height in juvenile primary open-angle glaucoma. *Arch Ophthalmol*, 114, 660-3.
- STEMCELLREFERENCE. 2018. *Retinopathy of Prematurity* [Online]. Stem Cell Reference. Available: <https://stemcellreference.com/retinopathy-of-prematurity/> [Accessed 06 Oct 2018].
- SUN, J. H., SUNG, K. R., YUN, S. C., CHEON, M. H., TCHAH, H. W., KIM, M. J. & KIM, J. Y. 2012. Factors associated with anterior chamber narrowing with age: an optical coherence tomography study. *Invest Ophthalmol Vis Sci*, 53, 2607-10.
- SUN, X. H., DAI, Y., CHEN, Y. H., YU, D. Y., CRINGLE, S. J., CHEN, J. Y., KONG, X. M., WANG, X. L. & JIANG, C. H. 2017. Primary angle closure glaucoma: What we know and what we don't know. *Progress in Retinal and Eye Research*, 57, 26-45.
- SURI, F., YAZDANI, S., NAROOIE-NEJHAD, M., ZARGAR, S. J., PAYLAKHI, S. H., ZEINALI, S., PAKRAVAN, M. & ELAHI, E. 2009. Variable Expressivity and High Penetrance of CYP1B1 Mutations Associated with Primary Congenital Glaucoma. *Ophthalmology*, 116, 2101-2109.
- SUZUKI, A., KONDO, N. & TERASAKI, H. 2005. High resolution ultrasonography in eyes with angle-closure glaucoma associated with the cicatricial stage of retinopathy of prematurity. *Jpn J Ophthalmol*, 49, 312-4.
- TAMM, E. R. 2009. The trabecular meshwork outflow pathways: structural and functional aspects. *Exp Eye Res*, 88, 648-55.
- TAMM, E. R. 2011. [Development of the iridocorneal angle and congenital glaucoma]. *Ophthalmologe*, 108, 610-4, 616-7.
- TAN, A. N., SAUREN, L. D., DE BRABANDER, J., BERENDSCHOT, T. T., PASSOS, V. L., WEBERS, C. A., NUIJTS, R. M. & BECKERS, H. J. 2011. Reproducibility of anterior chamber angle measurements with anterior segment optical coherence tomography. *Invest Ophthalmol Vis Sci*, 52, 2095-9.

TARPEY, P., THOMAS, S., SARVANANTHAN, N., MALLYA, U., LISGO, S., TALBOT, C. J., ROBERTS, E. O., AWAN, M., SURENDRAN, M., MCLEAN, R. J., REINECKE, R. D., LANGMANN, A., LINDNER, S., KOCH, M., JAIN, S., WOODRUFF, G., GALE, R. P., BASTAWROUS, A., DEGG, C., DROUTSAS, K., ASPROUDIS, I., ZUBCOV, A. A., PIEH, C., VEAL, C. D., MACHADO, R. D., BACKHOUSE, O. C., BAUMBER, L., CONSTANTINESCU, C. S., BRODSKY, M. C., HUNTER, D. G., HERTLE, R. W., READ, R. J., EDKINS, S., O'MEARA, S., PARKER, A., STEVENS, C., TEAGUE, J., WOOSTER, R., FUTREAL, P. A., TREMBATH, R. C., STRATTON, M. R., RAYMOND, F. L. & GOTTLÖB, I. 2006. Mutations in FRMD7, a newly identified member of the FERM family, cause X-linked idiopathic congenital nystagmus. *Nat Genet*, 38, 1242-4.

TEIXEIRA, L. B., ZHAO, Y., DUBIELZIG, R. R., SORENSEN, C. M. & SHEIBANI, N. 2015. Ultrastructural abnormalities of the trabecular meshwork extracellular matrix in Cyp1b1-deficient mice. *Vet Pathol*, 52, 397-403.

TELLO, C., LIEBMANN, J., POTASH, S. D., COHEN, H. & RITCH, R. 1994. Measurement of Ultrasound Biomicroscopy Images - Intraobserver and Interobserver Reliability. *Investigative Ophthalmology & Visual Science*, 35, 3549-3552.

THOMAS, M. G., CROSIER, M., LINDSAY, S., KUMAR, A., ARAKI, M., LEROY, B. P., MCLEAN, R. J., SHETH, V., MACONACHIE, G., THOMAS, S., MOORE, A. T. & GOTTLÖB, I. 2014. Abnormal retinal development associated with FRMD7 mutations. *Hum Mol Genet*, 23, 4086-93.

THOMAS, S., PROUDLOCK, F. A., SARVANANTHAN, N., ROBERTS, E. O., AWAN, M., MCLEAN, R., SURENDRAN, M., KUMAR, A. S., FAROOQ, S. J., DEGG, C., GALE, R. P., REINECKE, R. D., WOODRUFF, G., LANGMANN, A., LINDNER, S., JAIN, S., TARPEY, P., RAYMOND, F. L. & GOTTLÖB, I. 2008. Phenotypical characteristics of idiopathic infantile nystagmus with and without mutations in FRMD7. *Brain*, 131, 1259-67.

TIAN, J., MARZILIANO, P., BASKARAN, M., WONG, H.-T. & AUNG, T. 2011. Automatic Anterior Chamber Angle Assessment for HD-OCT Images.

TIAN, M., ZHOU, L., LUO, Q., YE, M. & XU, Y. 2015. [A study of refractive state in premature infants without retinopathy of prematurity and full-term children at the age of 0 to 6]. *Zhonghua Yan Ke Za Zhi*, 51, 505-9.

TRIVEDI, R. H., LAMBERT, S. R., LYNN, M. J., WILSON, M. E. & INFANT APHAKIA TREATMENT STUDY, G. 2014. The role of preoperative biometry in selecting initial contact lens power in the Infant Aphakia Treatment Study. *J AAPOS*, 18, 251-4.

TUMER, Z. & BACH-HOLM, D. 2009. Axenfeld-Rieger syndrome and spectrum of PITX2 and FOXC1 mutations. *Eur J Hum Genet*, 17, 1527-39.

TUN, T. A., BASKARAN, M., TAN, S. S., PERERA, S. A., AUNG, T. & HUSAIN, R. 2017. Evaluation of the Anterior Segment Angle-to-Angle Scan of Cirrus High-Definition Optical Coherence Tomography and Comparison With Gonioscopy and With the Visante OCT. *Invest Ophthalmol Vis Sci*, 58, 59-64.

- TUN, T. A., BASKARAN, M., ZHENG, C., SAKATA, L. M., PERERA, S. A., CHAN, A. S., FRIEDMAN, D. S., CHEUNG, C. Y. & AUNG, T. 2013a. Assessment of trabecular meshwork width using swept source optical coherence tomography. *Graefes Archive for Clinical and Experimental Ophthalmology*, 251, 1587-1592.
- TUN, T. A., BASKARAN, M., ZHENG, C., SAKATA, L. M., PERERA, S. A., CHAN, A. S., FRIEDMAN, D. S., CHEUNG, C. Y. & AUNG, T. 2013b. Assessment of trabecular meshwork width using swept source optical coherence tomography. *Graefes Arch Clin Exp Ophthalmol*, 251, 1587-92.
- TWELKER, J. D., MITCHELL, G. L., MESSER, D. H., BHAKTA, R., JONES, L. A., MUTTI, D. O., COTTER, S. A., KLENSTEIN, R. N., MANNY, R. E., ZADNIK, K. & GROUP, C. S. 2009. Children's Ocular Components and Age, Gender, and Ethnicity. *Optom Vis Sci*, 86, 918-35.
- URBAK, S. E., PEDERSEN, J. K. & THORSEN, T. T. 1998. Ultrasound biomicroscopy. II. Intraobserver and interobserver reproducibility of measurements. *Acta Ophthalmologica Scandinavica*, 76, 546-549.
- USUI, T., TOMIDOKORO, A., MISHIMA, K., MATAKI, N., MAYAMA, C., HONDA, N., AMANO, S. & ARAIE, M. 2011. Identification of Schlemm's Canal and Its Surrounding Tissues by Anterior Segment Fourier Domain Optical Coherence Tomography. *Investigative Ophthalmology & Visual Science*, 52, 6934-6939.
- UTINE, C. A., ALTIN, F., CAKIR, H. & PERENTE, I. 2009. Comparison of anterior chamber depth measurements taken with the Pentacam, Orbscan IIz and IOLMaster in myopic and emmetropic eyes. *Acta Ophthalmol*, 87, 386-91.
- UVA, M. G., REIBALDI, M., LONGO, A., AVITABILE, T., GAGLIANO, C., SCOLLO, D., LIONETTI, E. & REIBALDI, A. 2011. Intraocular pressure and central corneal thickness in premature and full-term newborns. *Journal of Aapos*, 15, 367-369.
- VARGHESE, R. M., SREENIVAS, V., PULIYEL, J. M. & VARUGHESE, S. 2009. Refractive status at birth: its relation to newborn physical parameters at birth and gestational age. *PLoS One*, 4, e4469.
- VARUGHESE, S., VARGHESE, R. M., GUPTA, N., OJHA, R., SREENIVAS, V. & PULIYEL, J. M. 2005. Refractive error at birth and its relation to gestational age. *Curr Eye Res*, 30, 423-8.
- VIESTENZ, A., VOGT, S., LANGENBUCHER, A., VIESTENZ, A., WALTER, S. & BEHRENS-BAUMANN, W. 2009. Biometry of the anterior segment using optical coherence tomography. Evaluation of different devices and analysis programs. *Ophthalmologe*, 106, 723-728.
- VOLKMANN, B. A., ZINKEVICH, N. S., MUSTONEN, A., SCHILTER, K. F., BOSENKO, D. V., REIS, L. M., BROECKEL, U., LINK, B. A. & SEMINA, E. V. 2011. Potential novel mechanism for Axenfeld-Rieger syndrome: deletion of a distant region containing regulatory elements of PITX2. *Invest Ophthalmol Vis Sci*, 52, 1450-9.

- VOSSMERBAEUMER, U., SCHUSTER, A. K. & FISCHER, J. E. 2013. Width of anterior chamber angle determined by OCT, and correlation to refraction and age in a German working population: the MIPH Eye&Health Study. *Graefes Arch Clin Exp Ophthalmol*, 251, 2741-6.
- WALKER, T. W. & MUTTI, D. O. 2002. The effect of accommodation on ocular shape. *Optom Vis Sci*, 79, 424-30.
- WALTON, D. S. & KATSAVOUNIDOU, G. 2005. Newborn primary congenital glaucoma: 2005 update. *Journal of Pediatric Ophthalmology & Strabismus*, 42, 333-341.
- WAN, M. J. & VANDERVEEN, D. K. 2015. Eye disorders in newborn infants (excluding retinopathy of prematurity). *Arch Dis Child Fetal Neonatal Ed*, 100, F264-9.
- WANG, B. S., SAKATA, L. M., FRIEDMAN, D. S., CHAN, Y. H., HE, M. G., LAVANYA, R., WONG, T. Y. & AUNG, T. 2010. Quantitative Iris Parameters and Association with Narrow Angles. *Ophthalmology*, 117, 11-17.
- WANG, D., QI, M., HE, M., WU, L. & LIN, S. 2012. Ethnic difference of the anterior chamber area and volume and its association with angle width. *Invest Ophthalmol Vis Sci*, 53, 3139-44.
- WANG, F. R., ZHOU, X. D. & ZHOU, S. Z. 1994. [A CT study of the relation between ocular axial biometry and refraction]. *Zhonghua Yan Ke Za Zhi*, 30, 39-40.
- WANG, J., HE, X., XIONG, S., ZHOU, M., WANG, M., ZOU, H. & XU, X. 2018. Distribution of Anterior Chamber Parameters in Normal Chinese Children and the Associated Factors. *J Glaucoma*.
- WANG, N. G., WANG, B. S., ZHAI, G. S., LEI, K., WANG, L. & CONGDON, N. 2007. A method of measuring anterior chamber volume using the anterior segment optical coherence tomographer and specialized software. *American Journal of Ophthalmology*, 143, 879-881.
- WEINREB, R. N. & KHAW, P. T. 2004. Primary open-angle glaucoma. *Lancet*, 363, 1711-20.
- WIRBELAUER, C., THANNHAUSER, C. L. & PHAM, D. T. 2009. Influence of Corneal Curvature on Central and Paracentral Pachymetry With Optical Coherence Tomography. *Cornea*, 28, 254-260.
- WONG, H. T., LIM, M. C., SAKATA, L. M., AUNG, H. T., AMERASINGHE, N., FRIEDMAN, D. S. & AUNG, T. 2009. High-definition optical coherence tomography imaging of the iridocorneal angle of the eye. *Arch Ophthalmol*, 127, 256-60.
- WOO, E. K., PAVLIN, C. J., SLOMOVIC, A., TABACK, N. & BUYS, Y. M. 1999. Ultrasound biomicroscopic quantitative analysis of light-dark changes associated with pupillary block. *American Journal of Ophthalmology*, 127, 43-47.

- WORST, J. G. 1968. The development of the angle of the anterior chamber. *Ophthalmologica*, 155, 330-1.
- WU, R. Y., NONGPIUR, M. E., HE, M. G., SAKATA, L. M., FRIEDMAN, D. S., CHAN, Y. H., LAVANYA, R., WONG, T. Y. & AUNG, T. 2011. Association of narrow angles with anterior chamber area and volume measured with anterior-segment optical coherence tomography. *Arch Ophthalmol*, 129, 569-74.
- WU, S. C., LEE, Y. S., WU, W. C. & CHANG, S. H. L. 2015. Acute angle-closure glaucoma in retinopathy of prematurity following pupil dilation. *Bmc Ophthalmology*, 15.
- WYGNANSKI-JAFFE, T. & BAREQUET, I. S. 2006. Central corneal thickness in congenital glaucoma. *Cornea*, 25, 923-5.
- WYLEGALA, E., TEPER, S., NOWINSKA, A. K., MILKA, M. & DOBROWOLSKI, D. 2009. Anterior segment imaging: Fourier-domain optical coherence tomography versus time-domain optical coherence tomography. *J Cataract Refract Surg*, 35, 1410-4.
- XU, B. Y., MAI, D. D., PENTEADO, R. C., SAUNDERS, L. & WEINREB, R. N. 2017. Reproducibility and Agreement of Anterior Segment Parameter Measurements Obtained Using the CASIA2 and Spectralis OCT2 Optical Coherence Tomography Devices. *J Glaucoma*, 26, 974-979.
- XU, L., CAO, W. F., WANG, Y. X., CHEN, C. X. & JONAS, J. B. 2008. Anterior chamber depth and chamber angle and their associations with ocular and general parameters: The Beijing eye study. *American Journal of Ophthalmology*, 145, 929-936.
- YAN, P. S., LIN, H. T., WANG, Q. L. & ZHANG, Z. P. 2010. Anterior segment variations with age and accommodation demonstrated by slit-lamp-adapted optical coherence tomography. *Ophthalmology*, 117, 2301-7.
- YANG, Y., ZHANG, L., LI, S., ZHU, X. & SUNDARESAN, P. 2017. Candidate Gene Analysis Identifies Mutations in CYP1B1 and LTBP2 in Indian Families with Primary Congenital Glaucoma. *Genet Test Mol Biomarkers*, 21, 252-258.
- YANG, Y. J., HONG, J. X., DENG, S. X. & XU, J. J. 2014. Age-Related Changes in Human Corneal Epithelial Thickness Measured With Anterior Segment Optical Coherence Tomography. *Investigative Ophthalmology & Visual Science*, 55, 5032-5038.
- YASSIN, S. A. 2017. Long-term visual outcomes in children with primary congenital glaucoma. *Eur J Ophthalmol*, 0.
- YEUNG, H. H. 2017. "My Baby's Glaucoma Operations Have Failed...". *J Pediatr Ophthalmol Strabismus*, 54, 266.
- YOO, C., EOM, Y. S., SUH, Y. W. & KIM, Y. Y. 2011. Central Corneal Thickness and Anterior Scleral Thickness in Korean Patients With Open-angle Glaucoma: An Anterior Segment Optical Coherence Tomography Study. *Journal of Glaucoma*, 20, 95-99.

- YUEN, L. H., HE, M. G., AUNG, T., HTOON, H. M., TAN, D. T. & MEHTA, J. S. 2010. Biometry of the Cornea and Anterior Chamber in Chinese Eyes: An Anterior Segment Optical Coherence Tomography Study. *Investigative Ophthalmology & Visual Science*, 51, 3433-3440.
- YÜKSEL, Z. & KARAER, K. 2013. *Iris coloboma: A New Finding Of Waardenburg Syndromes ?*
- ZADNIK, K., MUTTI, D. O., FUSARO, R. E. & ADAMS, A. J. 1995. Longitudinal Evidence of Crystalline Lens Thinning in Children. *Investigative Ophthalmology & Visual Science*, 36, 1581-1587.
- ZAHN, J. R. 1978. Incidence and characteristics of voluntary nystagmus. *J Neurol Neurosurg Psychiatry*, 41, 617-23.
- ZHA, Y., ZHU, G., ZHUANG, J., ZHENG, H., CAI, J. & FENG, W. 2017a. Axial Length and Ocular Development of Premature Infants without ROP. *J Ophthalmol*, 2017, 6823965.
- ZHA, Y., ZHU, G. D., ZHUANG, J. F., ZHENG, H. H., CAI, J. Q. & FENG, W. Q. 2017b. Axial Length and Ocular Development of Premature Infants without ROP. *Journal of Ophthalmology*.
- ZHAO, Y., SORENSEN, C. M. & SHEIBANI, N. 2015. Cytochrome P450 1B1 and Primary Congenital Glaucoma. *J Ophthalmic Vis Res*, 10, 60-7.
- ZHAO, Y., WANG, S., SORENSEN, C. M., TEIXEIRA, L., DUBIELZIG, R. R., PETERS, D. M., CONWAY, S. J., JEFCOATE, C. R. & SHEIBANI, N. 2013. Cyp1b1 mediates periostin regulation of trabecular meshwork development by suppression of oxidative stress. *Mol Cell Biol*, 33, 4225-40.
- ZIEMSSEN, F., ADAM, H., BARTZ-SCHMIDT, K. U. & SCHLOTE, T. 2004. Late-onset angle-closure glaucoma in association with relative anterior microphthalmus (RAM) after retinopathy of prematurity (ROP). *Klinische Monatsblatter Fur Augenheilkunde*, 221, 503-508.